

**Metal-Foam Interface Stability**  
**During the Filling of Lost Foam Moulds**  
**with Aluminium Alloys**

By

Mark Jonathan Ainsworth

A thesis submitted to the Faculty of Engineering of  
The University of Birmingham  
For the degree of  
Doctor of Philosophy

School of Metallurgy and Materials  
College of Engineering & Physical Sciences  
University of Birmingham  
Birmingham B15 2TT  
United Kingdom

September 2010

UNIVERSITY OF  
BIRMINGHAM

**University of Birmingham Research Archive**

**e-theses repository**

This unpublished thesis/dissertation is copyright of the author and/or third parties. The intellectual property rights of the author or third parties in respect of this work are as defined by The Copyright Designs and Patents Act 1988 or as modified by any successor legislation.

Any use made of information contained in this thesis/dissertation must be in accordance with that legislation and must be properly acknowledged. Further distribution or reproduction in any format is prohibited without the permission of the copyright holder.

## ABSTRACT

Counter-gravity mould filling has been developed to prevent the entrainment of deleterious oxide films into the liquid metal by eliminating turbulence at the metal surface. However, its application to the Lost Foam process has not been studied in detail. In this research, aluminium Lost Foam castings were made using gravity and counter-gravity filling techniques and the velocity of the metal fronts was estimated from timing electrodes and real time X-ray radiography. The latter technique was also used to study the morphology of the metal fronts as they progressed through the moulds. Casting quality was evaluated by means of tensile strength testing and SEM and EDX studies of the fracture surfaces of the tensile test bars. A room temperature analogue, which accelerated a Hg-glucose interface vertically upwards, was constructed to understand the mechanisms that might have controlled the shape of the metal front and the viscosity of liquid polystyrene, in its untreated and Br-treated forms, was determined from its molecular weight. Finally, the influence of viscosity on metal front morphology was assessed by casting an untreated and a Br-treated pattern plate under the same filling conditions and comparing tensile strength data and metal front profiles from each.

The metal fronts observed during gravity casting were unstable and associated with a number of fingers that protruded into the pattern from the main body of metal. Casting quality was very poor and unaffected by ingate location, even though filling velocity was marginally reduced by bottom gating. Casting in a counter-gravity fashion provided control of the filling velocity and this influenced the shape of the metal front such that it was planar at low velocities and became unstable as the speed of the interface increased. The quality of the castings made under stable filling conditions, measured by tensile strength variation, was markedly better than those where a non-planar front had been observed. However, a low filling velocity tended to promote premature freezing which manifested itself as a misrun defect at the top of the casting. Where an instability was present during casting, its severity was unrelated to casting quality. The SEM and EDX studies revealed small irregular pores on all the fracture surfaces with larger more spherical pores also being found within the castings where the metal front had been unstable. Carbon was found in every pore that was analysed and this suggested that their formation was the result of polymer entrapment.

As the velocity of the Hg in the analogue increased, the interface became unstable and a number of fingers developed. It was found that the velocity necessary to bring about the onset of such an instability increased with decreasing glucose viscosity. Liquid polystyrene viscosity was found to decrease with increasing temperature, increasing exposure to heat and in the presence of a Br additive. The planar interface present during the filling of a Br-treated pattern contrasted sharply with the unstable one that was seen when an untreated pattern was cast under the same conditions of temperature and velocity. The velocity at which the interface became unstable correlated well with predictions made using the Saffman-Taylor equation and was therefore probably of this type.

This research provided a better understanding of the interaction of liquid aluminium with polystyrene degradation products as well as the benefits of controlled counter-gravity filling in making Lost Foam castings. It forms the basis for other researchers to pursue techniques and materials that permit an increase in the filling velocity without promoting an instability in order to improve process flexibility and eliminate surface defects such as misruns.

to Jan van Gemert,

for your unwavering support through times of adversity.

## **ACKNOWLEDGEMENTS**

I would like to extend my sincerest gratitude to my supervisor, Dr. W. D. Griffiths, for his excellent supervision and tenacious encouragement. It would not have been possible to produce this work without his help and guidance and I was privileged to have worked under his supervision.

I would also like to thank my employer, Gemco Cast Metal Technology B.V., for providing financial support and the use of its casting facilities for the duration of the course.

Additionally, Mr Adrian Caden deserves significant recognition for his technical support throughout this program. Without his assistance much of the experimental work would not have been possible. In this regard I would also like to express my thanks to Mr. Mick Wickins, Mr. Paul Stanley and other technical staff at the School of Metallurgy and Materials.

I would also like to thank Dr Paul Davies and Professor John Campbell with whom I had many discussions and whose opinions and assistance proved invaluable.

Finally, I would like to express my deepest thanks to my wife and children for their devotion and patience throughout the course of this research.

# CONTENTS

<b>1</b>	<b>INTRODUCTION</b> .....	<b>3</b>
<b>2</b>	<b>LITERATURE REVIEW</b> .....	<b>7</b>
<b>2.1</b>	<b>GRAVITY FILLING OF LOST FOAM CASTINGS</b> .....	<b>8</b>
2.1.1	Pattern Degradation .....	8
2.1.2	Removal of Degradation Products .....	17
2.1.3	Influence of the Filling Velocity .....	25
2.1.4	Influence of the Coating .....	28
2.1.5	Influence of the Gating System .....	33
2.1.6	Influence of Pouring Temperature .....	35
2.1.7	Effects of Temperature Gradients .....	39
<b>2.2</b>	<b>CASTING DEFECTS</b> .....	<b>41</b>
2.2.1	Porosity .....	42
2.2.2	Folds .....	43
2.2.3	Surface Roughness and Staining .....	47
2.2.4	Effect on Mechanical Properties .....	48
<b>2.3</b>	<b>COUNTER-GRAVITY FILLING OF LOST FOAM CASTINGS</b> .....	<b>51</b>
<b>2.4</b>	<b>FOAM-METAL INTERFACE PHENOMENA</b> .....	<b>54</b>
2.4.1	Hydrodynamic Instabilities .....	54
2.4.1.1	The Rayleigh-Taylor Instability .....	55
2.4.1.2	The Saffman-Taylor Instability .....	57
2.4.1.3	Kelvin-Helmholtz Instability .....	62
2.4.2	Viscosity of Liquid Polystyrene .....	65
<b>2.5</b>	<b>ALTERNATIVE PATTERN MATERIALS</b> .....	<b>70</b>
2.5.1	Polymethyl Methacrylate .....	70
2.5.2	Bromine-based Additives .....	72
<b>2.6</b>	<b>TECHNIQUES FOR MONITORING FILLING BEHAVIOUR</b> .....	<b>73</b>
<b>2.7</b>	<b>STATISTICAL ANALYSIS OF THE PROPERTIES OF CASTINGS</b> .....	<b>77</b>
<b>2.8</b>	<b>SUMMARY</b> .....	<b>80</b>
<b>3</b>	<b>EXPERIMENTAL PROCEDURE</b> .....	<b>82</b>
<b>3.1</b>	<b>GRAVITY FILLING OF LOST FOAM CASTINGS</b> .....	<b>82</b>
3.1.1	Mould Filling Observations .....	82
3.1.1.1	Datalogger Method .....	82
3.1.1.2	Real Time X-ray Method .....	87
3.1.2	Tensile Strength Testing .....	89
3.1.3	Examination of Fracture Surfaces .....	90
<b>3.2</b>	<b>COUNTER-GRAVITY FILLING OF LOST FOAM CASTINGS</b> .....	<b>91</b>
3.2.1	Mould Filling Observations .....	92
3.2.2	Tensile Testing .....	95
3.2.3	Determination of Hydrogen Pick-up .....	96
<b>3.3</b>	<b>ACCELERATED LIQUID-LIQUID INTERFACE EXPERIMENTS</b> .....	<b>97</b>
<b>3.4</b>	<b>APPROXIMATION OF THE VISCOSITY OF LIQUID POLYSTYRENE</b> .....	<b>100</b>

<b>4</b>	<b>RESULTS</b>	<b>104</b>
4.1	<b>CLUSTER CHARACTERISTICS</b>	<b>104</b>
4.1.1	Pattern Density Variations	104
4.1.2	Coating Permeability and Coating Thickness	107
4.2	<b>GRAVITY FILLING</b>	<b>108</b>
4.2.1	Metal Flow Characteristics Through Plate Patterns	108
4.2.2	Metal Flow Characteristics Through Frame Patterns	119
4.3	<b>PROPERTIES OF GRAVITY FILLED CASTINGS</b>	<b>128</b>
4.3.1	Tensile Strength Variation in the Castings	128
4.3.2	Fracture Surface Defects	136
4.4	<b>COUNTER-GRAVITY FILLING</b>	<b>138</b>
4.5	<b>PROPERTIES OF COUNTER-GRAVITY FILLED CASTINGS</b>	<b>147</b>
4.5.1	Tensile Strength Variation in the Castings	148
4.5.2	Hydrogen Pick-up During Mould Filling	153
4.5.3	Fracture Surface Defects	156
4.6	<b>ACCELERATED LIQUID-LIQUID INTERFACE MODELLING</b>	<b>162</b>
4.6.1	Glucose Syrup Viscosity	162
4.6.2	Interfacial Observations During Model Operation	165
4.7	<b>PROPERTIES OF POLYSTYRENE DEGRADATION PRODUCTS</b>	<b>170</b>
4.7.1	The Molecular Weight of Liquid Polystyrene	170
4.7.2	The Viscosity of Liquid Polystyrene	174
4.8	<b>CASTING OF PATTERNS CONTAINING A BROMINE COMPOUND</b>	<b>176</b>
4.8.1	Mould Filling Observations	176
4.8.2	Tensile Strength Variation in the Castings	189
4.9	<b>SUMMARY</b>	<b>191</b>
<b>5</b>	<b>DISCUSSION</b>	<b>195</b>
5.1	<b>MECHANICAL PROPERTIES OF GRAVITY FILLED CASTINGS</b>	<b>196</b>
5.2	<b>MECHANICAL PROPERTIES OF COUNTER-GRAVITY FILLED CASTINGS</b>	<b>200</b>
5.3	<b>INTERFACIAL INSTABILITY DURING MOULD FILLING</b>	<b>202</b>
5.3.1	The Nature of the Liquid Metal – Pattern Interface	202
5.3.2	Saffman-Taylor Instability and Lost Foam Casting	204
5.3.3	Mechanical Properties and the Metal – Pattern Interfacial Instability	213
5.4	<b>PRACTICAL IMPLICATIONS</b>	<b>214</b>
<b>6</b>	<b>CONCLUSIONS</b>	<b>218</b>
<b>7</b>	<b>FURTHER WORK</b>	<b>220</b>
	<b>APPENDIX I: VIDEO RECORDINGS OF THE MOULD FILLING &amp; LIQUID-LIQUID</b>	
	<b>INTERFACE EXPERIMENTS</b>	<b>221</b>
	<b>APPENDIX II: CONFERENCE PAPERS</b>	<b>222</b>
	<b>LIST OF REFERENCES</b>	<b>258</b>

# 1 INTRODUCTION

The Lost Foam casting process is characterized by the use of one or more expendable patterns made usually of expanded polystyrene foam. These are manufactured either in sections or complete, depending upon their complexity, and assembled by means of hot-melt glue that is applied on all pattern interfaces immediately prior to joining. The complete assembly is then attached to a gating system of identical material using the same fixing method.

The complete assembly, known as a cluster, is coated with a permeable, water based, ceramic slurry. This acts as a barrier between the loose sand mass and the advancing metal front during the casting stage of the process. The water in the coating acts as a carrier fluid that facilitates total and even coating of the cluster and is subsequently removed, prior to moulding, by means of a drying oven operating at a temperature of around 60°C. Figure 1.1 illustrates the steps required to manufacture complete cluster assemblies to a level that the moulding media can be consolidated around them. This set of steps is known collectively as “White Side Production”.

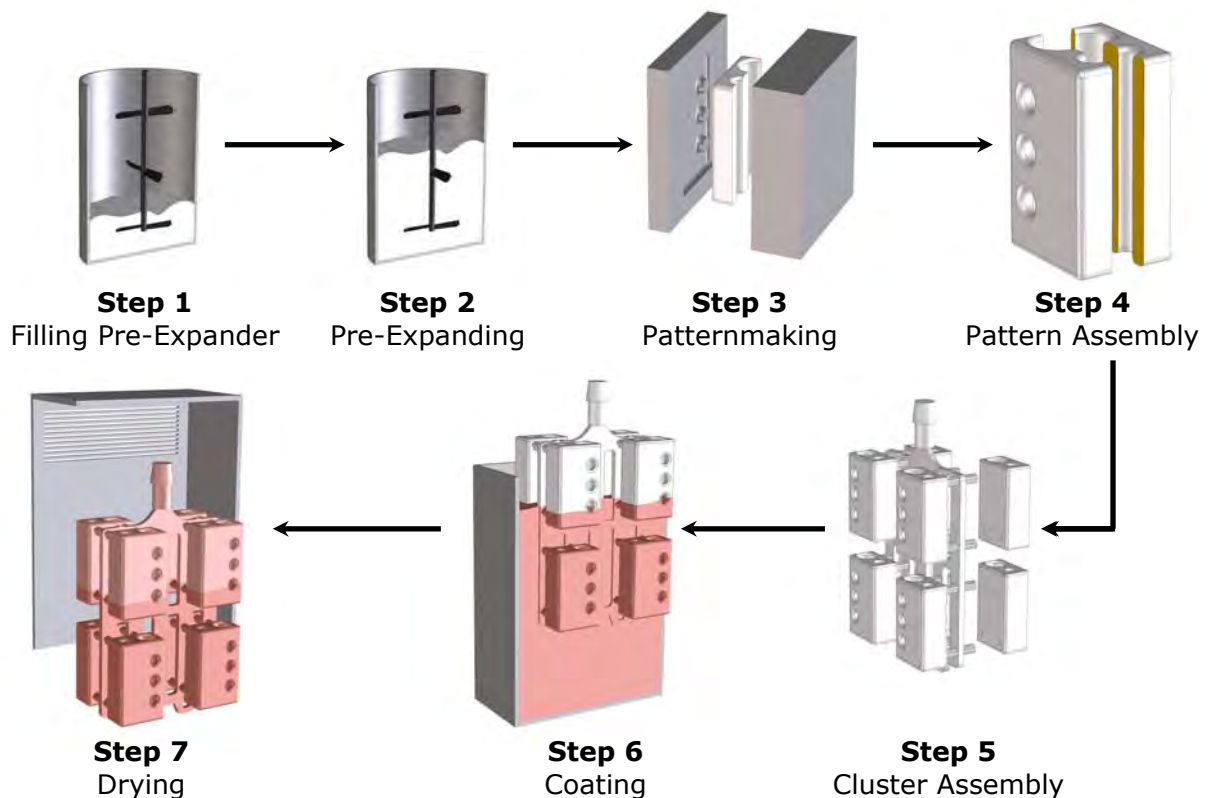


Figure 1.1: Main steps in complete pattern (cluster) manufacture.

The coated and dried clusters are transferred to the moulding line where they are placed into empty moulding flasks. Correct positioning of the cluster is usually accomplished by means of a simple jig known as a spider. The free volume remaining in the flask is taken up by adding loose, dry, unbonded sand that is consolidated around the cluster by application of an externally located vibration source.

Liquid metal is poured, or in a very limited number of cases pumped, onto that part of the polystyrene cluster emerging from the face of the mould. The heat energy in the metal causes the foam to undergo a series of physical changes, which culminates in decomposition. The permeable nature of the cluster coating and the moulding sand allows the products of decomposition to escape and, in so doing, allows the advancing liquid metal to flow into the resultant cavity. After complete filling has been achieved the mould and its contents are allowed to cool naturally prior to removal of the casting from the mould. This part of the process is referred to as the “Black Side Production” and is illustrated in Figure 1.2.

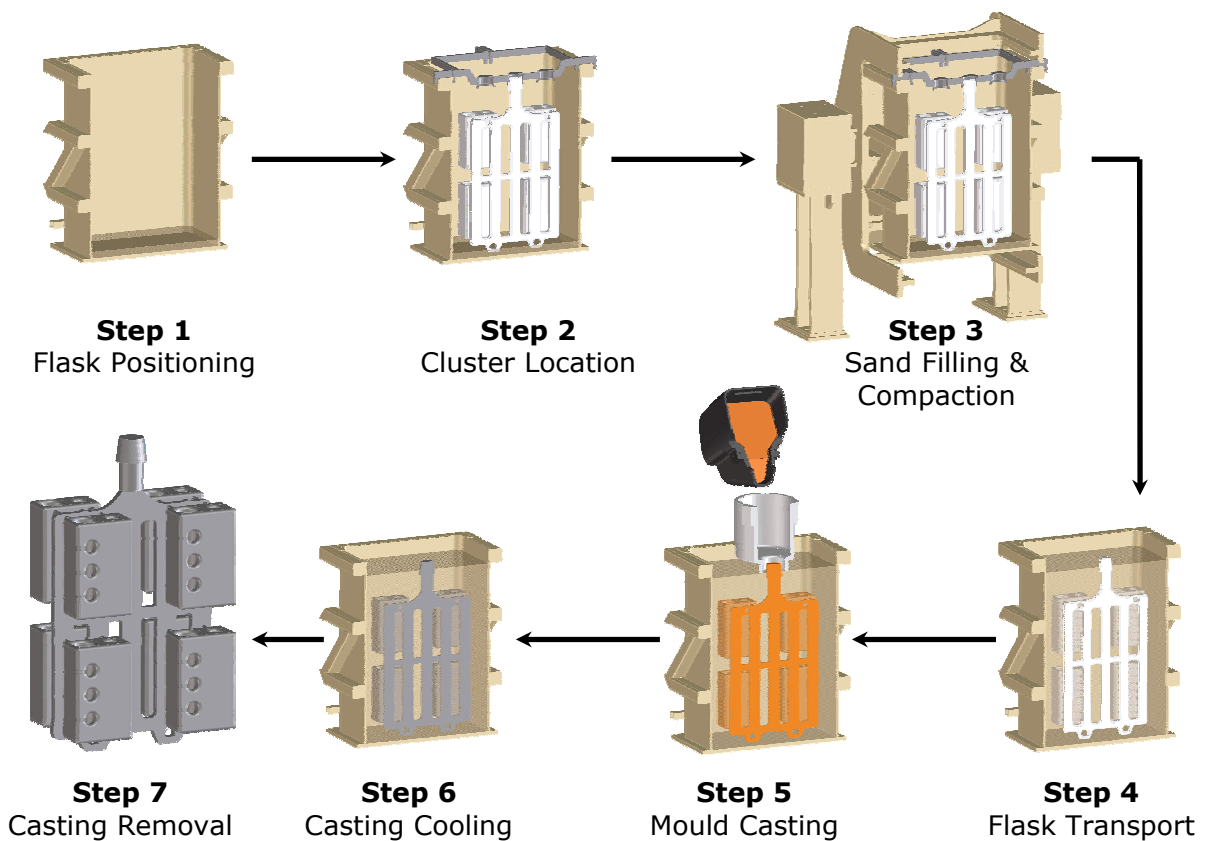


Figure 1.2: Main steps in Lost Foam moulding and casting.

The process has been successful in producing castings in aluminium, brass, bronze, cast iron and steel. However, application with some ferrous grades of material has necessitated that the polystyrene pattern material be substituted by a copolymer of polystyrene and polymethylmethacrylate in order to eliminate carbon film defects.

The Lost Foam process offers significant benefits in terms of improved dimensional accuracy, elimination of cores and consolidation of parts into a single component. However, castings produced by this technique suffer from classes of defect inherent in the casting method. The advancing metal front provides the heat needed to degrade the polystyrene pattern and this can result in misrun defects due to premature freezing. Additionally, seemingly well-formed castings can contain entrainment and entrapment defects. Entrapment defects are caused by the degradation products being trapped within the liquid metal and entrainment defects are caused by the meeting of two advancing metal fronts.

It has been widely suggested that the velocity of the liquid metal front during filling is critical in producing castings of high quality. However, in contrast to open-channel casting processes, the gating system has not been considered significant in controlling this variable. Instead, liquid metal flow has been controlled through variation of pattern and coating properties. This is an indirect way of controlling the critical variable, i.e., liquid metal filling velocity and is far from ideal because it is inflexible, costly to operate and has a high potential for failure.

Counter-gravity filling of aluminium into open channel moulds has previously been used to control liquid metal filling velocities independently of other variables such as mould permeability or runner system design. The castings produced were of a significantly higher quality than when cast in a gravity fashion.

The objective of this research has been to determine whether the application of this technique has a similar effect on the quality of aluminium Lost Foam castings. Castings have been made using both gravity and counter-gravity filling techniques and the morphology of the metal fronts observed in real time, using X-ray radiography as they progressed through the moulds. The quality of the resultant castings was determined by means of tensile testing and casting defect analysis, and the interface between the advancing metal front and the polystyrene

pattern was examined to determine any correlation between metal front morphology and casting quality.

Based on the outcome of these experiments, predictions were made to determine the maximum speed of filling that could be achieved without loss of casting quality. These predictions were confirmed by the manufacture and subsequent evaluation of a further set of castings that were filled at a velocity in accordance with predictions.

## 2 LITERATURE REVIEW

The Lost Foam casting process originated in 1958 when Shroyer [1] was granted a patent for a cavityless casting method that used a polystyrene foam pattern embedded in bonded sand. He suggested that, as castings became more and more complex in design, the application of conventional casting processes became less and less practical because of the necessity to apply multiple parting lines and complex core assemblies to the construction of the mould. Using a disposable pattern that did not need to be removed from the mould prior to filling with liquid metal, but that decomposed and was replaced by this metal, overcame these limitations.

The original patent [1] specified greensand as the moulding medium. However, this material contains considerable amounts of clay and water that not only reduced the flowability of the mix during mould consolidation but also restricted the escape of pattern degradation products from the mould during the filling process. Although some attempts were made to overcome the problem by applying gas vents to the mould this procedure was both time consuming and awkward and detracted somewhat from the original process concept.

In 1964 Smith [2] patented the use of dry, unbonded sand as a substitute for greensand. The absence of both the bonding medium and associated water had a two-fold beneficial effect. Firstly, the permeability of the mould was increased significantly and this allowed the pattern degradation products to leave the mould in a much less restricted fashion. The second effect was to maximise the flowability of the moulding medium. With no bonding material to lock grains of sand together, vibration could be applied to encourage flow of sand into the most intricate of cavities in the pattern and consolidate it effectively to provide maximum support during casting.

Introduction of free-flowing, unbonded sand was undoubtedly a significant improvement to the original process but its use meant that a coating had to be applied to all surfaces of the pattern prior to forming a mould around it. Initially, these coatings were zircon based [3] and acted as a barrier between the polystyrene pattern and the unbonded sand mould. Early coatings were used to prevent sand collapse into the cavity left through degradation of the pattern before it could be replaced by the advancing metal front and to improve the surface

finish of the casting produced [3]. However, over the last 25 years, coatings have been developed to act also as a control mechanism for the escape of degradation products [4-6] and hence influence the rate at which the liquid metal travels within the mould during the filling process.

## **2.1 GRAVITY FILLING OF LOST FOAM CASTINGS**

Open-cavity casting involves the introduction of liquid metal through a series of interconnected channels, which are collectively known as the running and gating system, into one or more empty cavities contained within a mould. Conversely, the pattern used in the Lost Foam process is linked to the surface of the mould by a running and gating system that is usually made of the same, solid material as the pattern, although hollow sections and pre-formed fibre downsprues are also used on occasions. The complete assembly remains in the mould until it is degraded during the filling operation and therefore a Lost Foam mould has limited or no open channels through which the liquid metal travels during casting.

### **2.1.1 Pattern Degradation**

Upon thermal decomposition, polystyrene yields the styrene monomer and various saturated and unsaturated fragments, with the styrene monomer the major product among the decomposition components when complete depolymerisation takes place below 500 °C [7]. At temperatures above 500 °C, the oligomers undergo further defragmentation and form low molecular weight gaseous fractions, including toluene, benzene and significant amounts of partially depolymerised viscous residue [8]. The ratio of gaseous to liquid products increases at temperatures above 750 °C, implying degradation into the gaseous phase at those temperatures as the exposure time increases [9]. The degradation of polystyrene occurs by a radical chain process characterized by three consecutive steps: (i) initiation, (ii) propagation and (iii) termination. Since most of these reactions involve a C–C bond cleavage, the thermal stability of polystyrene depends on the strength of its C–C bond. Initiation reactions can either occur by random scission or by C–C bond chain-end cleavage resulting in the production of radicals. Propagation reactions consist of the sequence of H-abstraction and  $\beta$ -decomposition or unzipping reactions as shown in Figure 2.1.



site to the surroundings, temperature losses in the liquid metal due to heat transfer, permeability of the refractory coating, and sand and metal flow behaviour.

Yang et al. [14] suggested that during mould filling a transformation zone forms between the advancing metal front and the polystyrene pattern, consisting of a melt zone and a thermally affected (TA) zone.

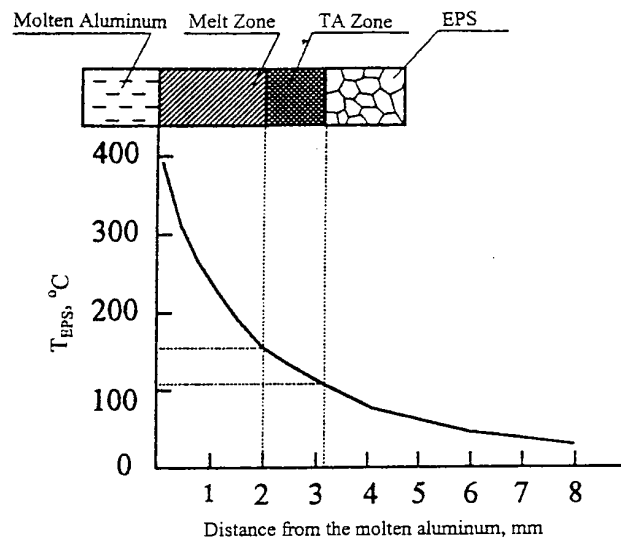


Figure 2.2: Effect of molten aluminium on an EPS pattern at a specific moment during mould filling [14].

The melt zone consists of partially decomposed liquid polymer and some gas whereas the thermally affected (TA) zone consists of shrinking polymer. Temperatures measured within plate patterns during the mould filling process suggested that the transformation zone was just over 3 mm thick, as illustrated in Figure 2.2. Additionally, Yang et al. applied sensors to measure gas pressures when pouring aluminium and iron in EPS patterns coated with a low-permeability coating and obtained values of 200-500 Pa and 11,000-26,000 Pa respectively. The authors concluded that very little gas was produced when pouring aluminium, and that the gas pressure measured in their experiments was mainly from the air originating in the polystyrene pattern.

Zhao et al. [15] agreed with Yang et al. in proposing the presence of an organic gas-liquid phase between the advancing liquid metal and the retreating solid foam pattern. Zhao et al.

proposed that, when the molten metal is poured on to the foam pattern, direct contact between the metal and the solid foam occurs. Due to the highly endothermic nature of the degradation process, a significant amount of heat flux occurs during the initial contact phase resulting in immediate gasification of the foam. But, during casting, the contact time is very small and heat transfer by direct contact is predominant only in the early stages of the fill [16]. As the process proceeds, radiation becomes the dominant mode of heat transfer because of an increase in the thickness of the gas layer. The radiant heat softens, collapses and melts the foam, which flows outward, away from the advancing liquid metal front towards the coating/sand interface, where it coalesces and adheres to the coating surfaces. The advancing metal envelopes the coalesced foam products (referred to as “plastic globs” by Zhao et al. [15]). The thermal conductivity of polystyrene is very low; hence, large temperature gradients exist across the plastic globs. Zhao’s infrared imaging of the filling of a coated polystyrene plate, through a glass window in the mould, indicated that the temperature at the coating substrate was less than 150 °C whereas that at the plastic/melt interface was around 440 °C. Based on these data, it seems that gasification occurs at the melt/plastic interface, and this reduces the size of the plastic globs.

A schematic of the physical model of foam degradation proposed by Molibog et al. [16] is shown in Figure 2.3. Explanations concerning the formation and elimination of degradation products were similar to Zhao’s physical model [15]. According to Molibog et al., a three-phase kinetic zone comprising the solid polymer, liquid polymer and the gaseous products of foam pyrolysis is formed between the metal and the pattern. It was argued that the width of this kinetic zone and the shape of the metal front dictated the rate of formation of the pyrolysis products.

Depending on the width of the kinetic zone, the heat transfer from the metal to the pattern varies, consequently varying the amount of energy supplied to the foam. As the width increases, the rate of heat transfer decreases and the gas layer starts to build up. Due to this decrease in heat transfer, the rate of gas generation also decreases until the gaseous products escape from the kinetic zone, thus starting the cycle again.

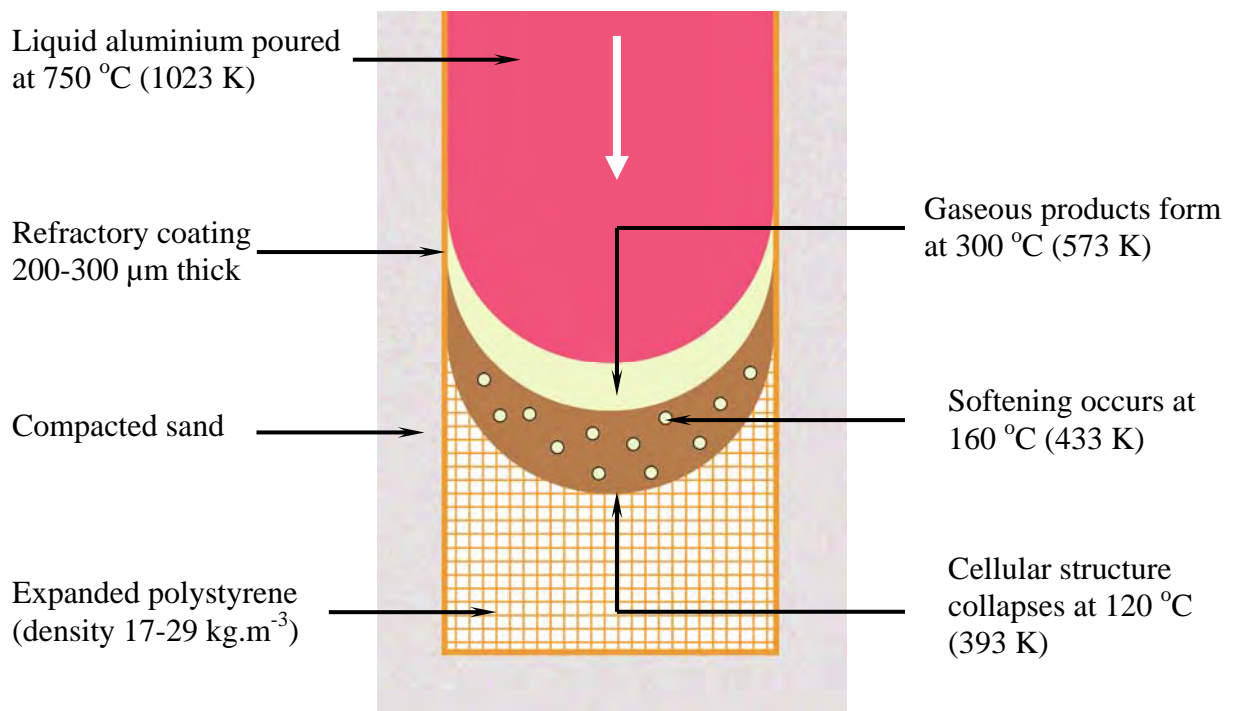


Figure 2.3: Schematic of the foam degradation process [16].

More recent interpretations of the mechanisms of foam degradation have been published by Barone and Caulk [17] and by Caulk [18-20]. When the polystyrene pattern comes into direct contact with liquid metal foam ablation occurs, a condition that applies at the start of almost all Lost Foam mould filling cycles. Barone and Caulk [17] refer to this as the contact mode of decomposition. When this condition is satisfied, the molten metal becomes separated from the solid pattern by a small layer of liquid foam between 100 and 200 microns thick. The authors refer to this zone as the decomposition layer and suggest that foam cells adjacent to it melt continually as a result of heat flow from the liquid metal (Figure 2.4).

The newly liquefied cells join the decomposition layer and replace some of the layer material that is drawn towards the porous coating where it gasifies and escapes into the surrounding sand mass.

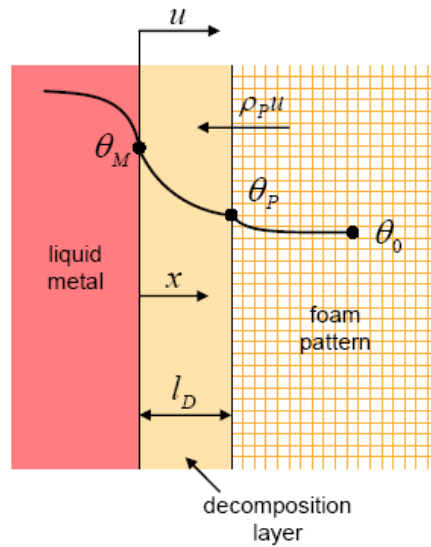


Figure 2.4: Schematic of a decomposition layer between liquid metal and receding foam [17].

Key to Figure 2.4:  $u$  = velocity of the liquid metal,  $\theta_M$  = temperature at the surface of the metal,  $\theta_0$  = the initial temperature of the pattern,  $\theta_P$  = pattern melting temperature,  $l_D$  = the thickness of the decomposition layer, and  $\rho_P u$  = the normal mass flux entering the decomposition layer from the decomposing foam.

For a foam pattern to degrade by melting, Caulk [18] suggested that a vapour gap must form between the liquid metal and the receding foam. This gap is initiated by polymer vapour bubbling through the liquid metal from some other region of the mould cavity. When these bubbles reach an upward-facing flow front, they accumulate and form a vapour layer that separates the metal from the foam. This interrupts the foam ablation process in contact mode and replaces it by the slower process of foam melting across a finite gap. Caulk calls this mechanism of foam degradation the gap mode, shown in Figure 2.5.

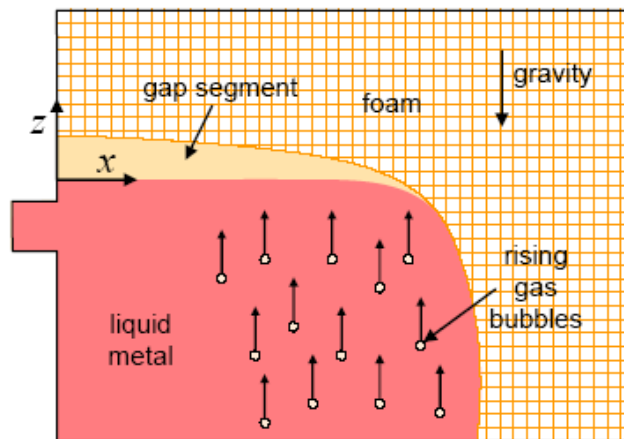


Figure 2.5: Schematic of the mechanism responsible for initiating gap mode during side-filling of a uniform plate pattern [18].

In contact and gap modes filling speeds are reported to increase with metal pressure and are insensitive to pattern thickness [17,18]. However, the rate of filling when a gap is present between the liquid metal and the solid foam pattern is influenced significantly by metal temperature.

The third mechanism put forward by Caulk for pattern degradation by the liquid metal is that of foam collapse [19]. Polystyrene bead expansion in the pattern moulding process, which occurs immediately after blowing of the pre-expanded material into the tooling cavity, can have a high degree of variability in soundness of the final foam pattern. Sun et al. [21-22] referred to this condition as poorly fused foam, and Littleton et al. [23] characterised it as foam with too great a permeability.

During mould filling, Barone and Caulk [17] proposed that the smooth process of foam ablation can be suddenly interrupted if the liquid metal encounters a region in the pattern that contains low density, unsound foam [19], as illustrated in Figure 2.6. If a polystyrene pattern has been manufactured in such a way that it contains a region of inter-bead porosity that extends to its surface, this fissure provides an alternative means for the air in the foam to escape during casting. Caulk proposes that if the fissure is sufficiently permeable to gas diffusion, then foam beads within it can collapse and expel their air directly into the fissure itself. Liquid metal fills the space left by the collapsing beads and forces the air down the fissure and out through the coating at the opposite end. This causes the metal to shoot forward

quite suddenly into the empty void forming a protrusion or a finger. The phenomenon has been reported by Sun et al. [21] who observed an irregular metal filling pattern during the casting of an 8mm thick plate at filling velocities of approximately 55 mm/s.

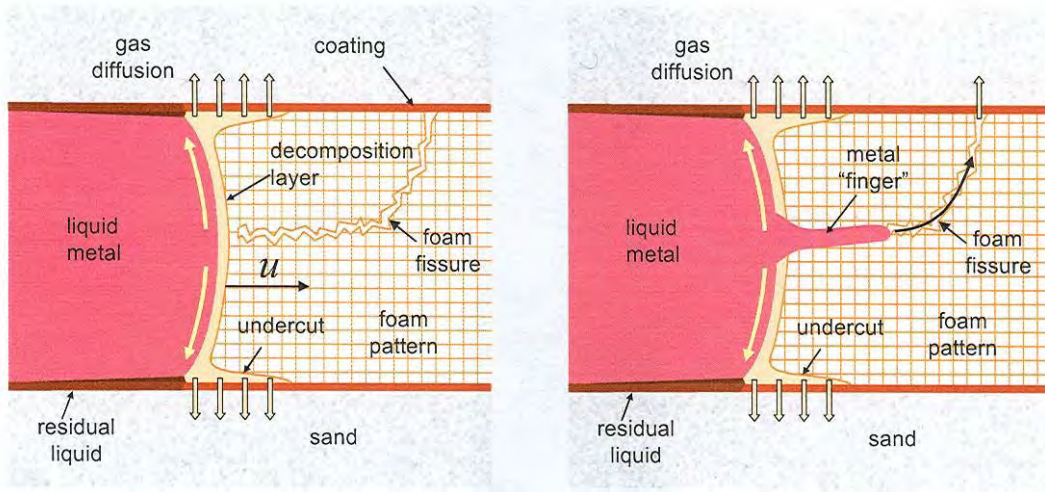


Figure 2.6: Schematic of the mechanism responsible for initiating the collapse mode of pattern degradation during filling of a lost foam mould [19].

Foam engulfment [20] is the fourth and final mechanism that Caulk proposes for pattern degradation. For this to occur in preference to foam ablation, melting or collapse, the advancing metal front must have a concave profile. As a metal front becomes increasingly concave, it surrounds a region of foam on two sides as depicted in Figure 2.7. If there is a sudden agitation in the flow of the liquid metal, or there is a random fissure in the foam, some part of the pattern may break away. When this happens the liquid metal quickly surrounds the detached piece of foam causing it to liquefy very quickly and then vaporise.

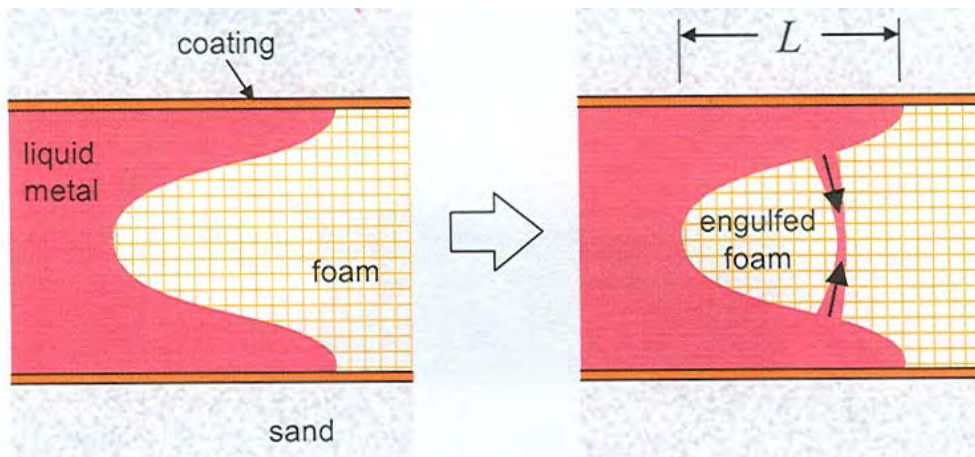


Figure 2.7: Development of a foam core inside the hollow of a concave flow front (a) before and (b) after the foam core breaks off, allowing the metal to engulf a piece of foam [20].

Because the polymer vapour cannot escape readily, it forms a relatively large bubble within the metal stream that may ultimately rise to the surface of the liquid metal or lodge somewhere in the mould cavity. Caulk [20] suggests that this mode of mould filling proceeds in a pulse-like fashion so that, immediately after a piece of foam has been engulfed, the metal front profile flattens out somewhat before it begins to redevelop its concave shape and envelope yet another piece of foam. This pulse-like filling has been observed by Wang et al. [25] when casting thin aluminium plates at various velocities.

In addition to the physical models discussed so far, a few researchers have tried to estimate the rate of formation of the pattern decomposition products. Molibog et al. [16] determined gas fractions by pushing bars of polystyrene pattern material through a strip heater, (with temperatures ranging from 580 °C to 910 °C), at controlled velocities and pressures. Using polystyrene with a nominal density of  $19.6 \text{ kg.m}^{-3}$  and two different driving pressures of 10.3 kPa and 27.6 kPa, the gas fraction was observed to increase steadily from 20-25% at 600 °C to 33-43% at 900 °C (Figure 2.8). This was probably due to more heat energy being available to decompose the polymer to gas, rather than to liquid residue.

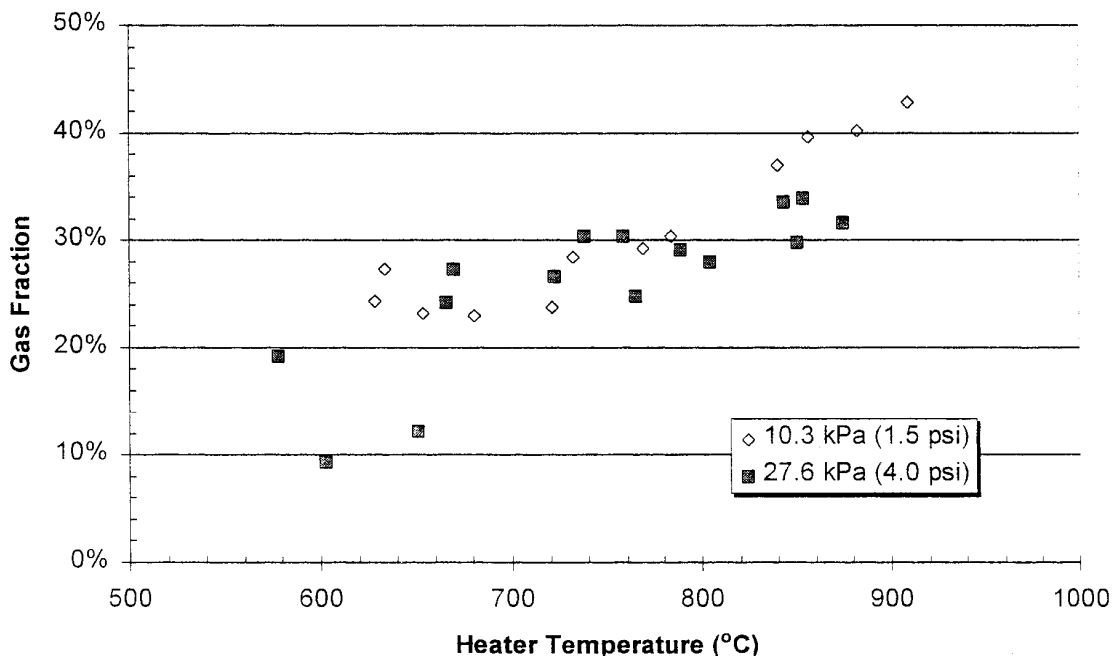


Figure 2.8: Gas fraction vs. heater temperature at driving pressures of 10.3 kPa and 27.6 kPa for  $19.6 \text{ kg.m}^{-3}$  density expanded polystyrene [16].

According to Molibog et al. [16], the specific energy of decomposition of expanded polystyrene can be estimated using the energy balance approach:

$$\Delta H_{degr} = \Delta H_{sens} + \Delta H_{depol} + F_{gas}\Delta H_{vapor} \quad \text{Equation 2.1}$$

where  $\Delta H_{degr}$  is the specific energy of degradation of the polymer to a gas fraction of  $F_{gas}$  and a liquid fraction of  $(1-F_{gas})$ ;  $\Delta H_{sens}$  is the sensible heat involved in heating the polymer from room temperature (25 °C) to the temperature of the liquid residue,  $\Delta H_{depol}$  is the heat of depolymerisation of the polymer to the main constituent of the liquid residue.  $\Delta H_{vapor}$  is the heat of vaporisation of the liquid fraction, which includes the heat of depolymerisation of the main constituent of the liquid fraction to the main constituent of the gas fraction and heating the gas from the liquid fraction temperature to the temperature of the gaseous fraction [16].

Molibog et al. [16] then calculated that, for a liquid fraction of 65% and a gas fraction of 35%, at a metal temperature of 650 °C, the energy of decomposition would be 965 J.g<sup>-1</sup>, which compared well with an experimentally determined value of 1075 J.g<sup>-1</sup>. “T” grade beads, which have a diameter of only 0.4 mm and a high potential for producing dense, uniform Lost Foam patterns, have been estimated by Mehta et al. [12] to have an average heat of decomposition of 912 J.g<sup>-1</sup>, as determined by Differential Scanning Calorimetry (DSC).

### 2.1.2 Removal of Degradation Products

For the mould to fill fully with liquid metal, degradation products need to be removed through the coating and into the sand mould [9]. Although coatings are permeable [26,27] gases can only escape through areas where the coating is not in contact with the virgin polystyrene pattern, liquid residues or molten metal. It is therefore very important that the exposed coating occurs at a suitable time and location ahead of the metal-foam interface [28]. The simplest model for determining how much of the coating is available for gas diffusion is shown in Figure 2.9 [17] and has been replicated by numerous authors over the past 40 years [16,21,29,30-33].

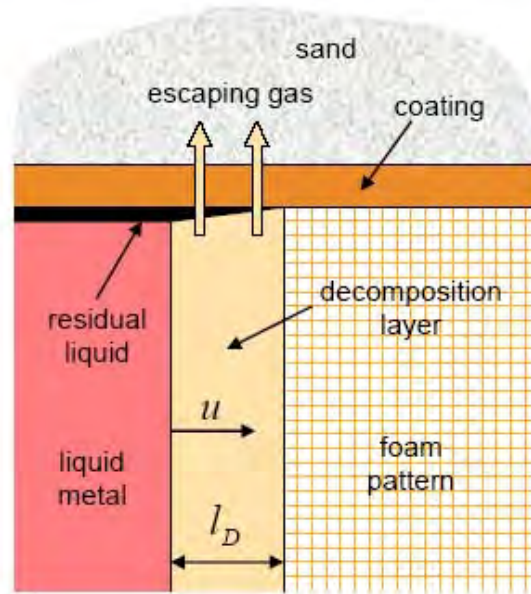


Figure 2.9: Traditional model of gas escaping from the decomposition layer [17].

This model assumes that gas escapes from the mould cavity through the area of coating between the liquid metal and the unmelted foam,  $l_D$ . The filling speed  $u$  and thickness  $l_D$  adjust in opposite directions so that gas escapes at the same rate as it is formed [17]. Although this concurs with previous experimental results, Barone and Caulk [17] suggest that it is unable to predict associated filling speeds with any accuracy. In fact, they calculate that the application of this model alone produces filling speed data that are approximately ten times slower than actually observed [21,34,35]. In an attempt to explain this disparity, Barone and Caulk [17] propose that a coating undercut exists at the pattern boundary, adjacent to the coating just ahead of the decomposition zone, as shown in Figure 2.10.

The products of decomposition from foam cells in the interior of the pattern enter the decomposition layer and flow parallel to the liquid metal front until they reach the coating and escape. However, the cells in the boundary layers of the pattern collapse through heating and expel air directly through the coating without first entering the decomposition layer. The resultant void is filled with liquid degradation products from the decomposition layer that heats the next cell and causes the mechanism to repeat. In so doing, a narrow *undercut* is formed between pattern and coating as illustrated in Figure 2.11. The length of the undercut  $l_C$  is determined by a balance between the heat flux in the foam and the rate that energy is

expended in causing the foam to collapse at its leading edge. Under these circumstances, there is a certain level of porosity between the beads that make up the polystyrene pattern. This porosity allows some of the air within the beads to pass between them and escape through the coating ahead of the metal front [23,24].

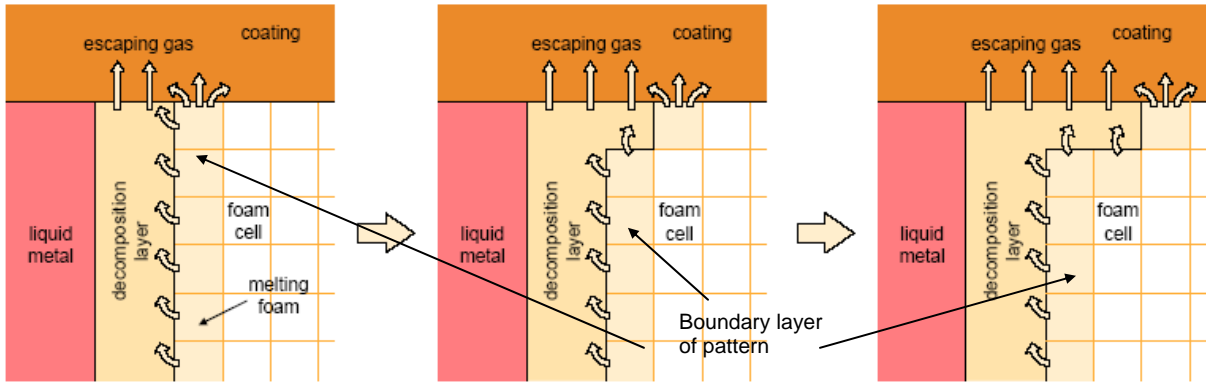


Figure 2.10: Schematic representation of foam collapse in cells adjacent to the coating, leading to the formation of an undercut [17].

A further phenomenon suggested by Barone and Caulk [17] and illustrated in Figure 2.11 is that liquid residues do not adhere to the inside surface of the coating, along the length of the undercut, because the coating has not yet achieved a sufficiently high temperature for this liquid to wet its surface [6]. Instead, as the gas loses heat to the coating during its escape into the sand, some of it condenses on the foam on the other side of the undercut and begins to melt it whilst some collects in isolated globules on the inside of the coating. This leaves most of the coating surface exposed and capable of permitting gas escape.

As the liquid metal fills the mould, it overtakes the globules of liquid residue. These globules then begin to vaporise and create gas bubbles within the liquid metal itself. Some of this gas diffuses through the coating as it rises through the metal and the rest ultimately reaches the surface and adds to that gas already within the gap as shown in Figure 2.12. Caulk argues that the gap sustains itself by continually generating excess quantities of liquid degradation products that vaporise and emerge in the gap region. In this mechanism of degradation product removal from the mould, it is assumed that all the air within the foam initially enters the gap. The same is also assumed with respect to polymer vapour. These assumptions are predominantly dependant upon the quality of the moulded foam [23,24].

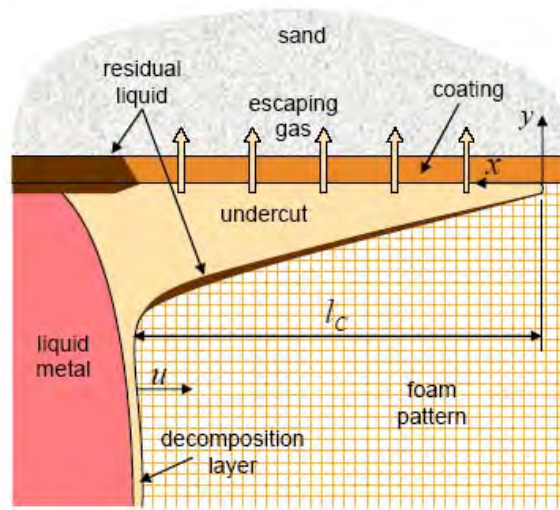


Figure 2.11: Schematic of the undercut as proposed by Barone and Caulk [17].

Fu et al. [36] collected time-temperature data in the sand mould at various distances from the metal – mould interface during and after casting of open cavity and Lost Foam moulds with aluminium. The results showed that, in a Lost Foam casting, the sand near the metal – mould interface stabilised at approximately 150 °C for about a minute before continuing to rise at a slower rate up to its peak temperature. At a distance of 1 mm from the metal – mould interface the peak temperature was recorded at 440 °C and a further 14 mm into the mould reached 260 °C.

Although the curves relating to open cavity moulds exhibited the same general profiles as those obtained from Lost Foam moulds, no temperature plateau was observed. Fu et al. [36] concluded that this phenomenon was caused by gaseous polystyrene degradation products condensing in the cooler sand in the vicinity of the metal – mould interface and, in so doing, reducing the permeability in that region. As the temperature of the sand increased by heat transfer from the metal, the condensed gases re-vaporised and travelled further into the sand [8,37]. This sequence of vaporisation-condensation-vaporisation continued even after the mould had been filled. Fu et al. [36] did not consider the transport of liquid polystyrene through the sand, yet this may also be important if the liquid polymer is transported through the coating.

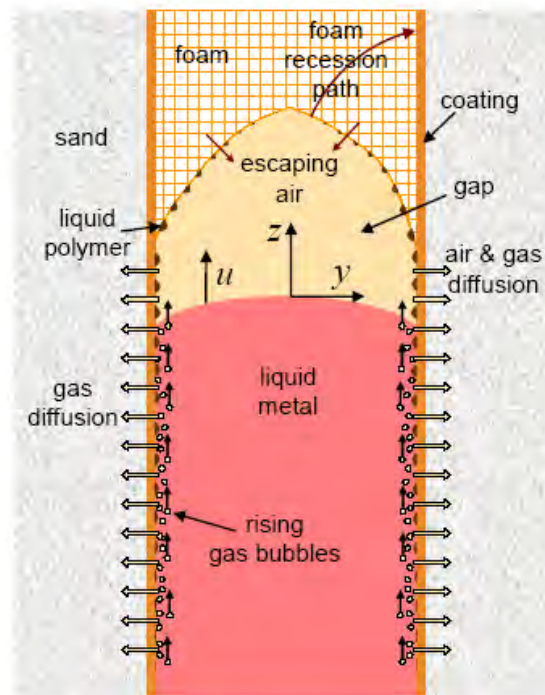


Figure 2.12: Schematic of the air and gas diffusion through the coating where a distinct vapour gap is present between liquid metal and solid foam [18].

Wetting and wicking have been put forward as mechanisms for the elimination of the liquid degradation products from the mould [6,38]. Sun et al. [6] proposed that it was unrealistic to assume that all the liquid polymer would vaporise and escape the mould cavity as a gas, but would instead be displaced to and accumulate at the metal-coating interface. The characteristics of the coating would then determine the mechanism and extent that liquid polymer would be removed from the mould cavity. They suggested that “wetting” and “wicking” may play a part in the transport of liquid polymer through the coating and into the surrounding sand. Wetting is described as the “the affinity of a liquid for a solid surface” [6]. In other words, when a liquid spreads spontaneously along a solid surface, it is said to wet the surface. Wicking, on the other hand, involves the infiltration of the liquid polymer into the porous coating material by means of capillary action.

Sun et al. [6] carried out a series of experiments to determine the critical combination of coating and liquid polystyrene temperatures needed for liquid polystyrene to wet and wick coating samples. Where either the coating or the polystyrene temperature had been towards the lower end of the experimental range, a discontinuous layer of polystyrene was observed on

the coating samples. The authors suggested that this was a result of the coating quenching the liquid polystyrene, even if the coating temperature was high and the polymer temperature was low. As the temperature of both components was increased, the liquid polystyrene was able to wet the coating surface, but no absorption or “wicking” was observed. As the temperature of both the polymer and the coating were increased further, liquid polystyrene was absorbed by all coating samples, and it was found that the critical temperature for wicking was between 325 °C and 400 °C, depending on the coating composition.

Alumina coatings were more capable of wetting and wicking liquid polystyrene at lower temperatures than mica or silica coatings. The authors suggested that the affinity of the base materials for liquid polystyrene was the decisive factor in controlling wetting. However, wicking was controlled by the shape, size, and size distribution of coating particles. This phenomenon is illustrated in Figure 2.13.

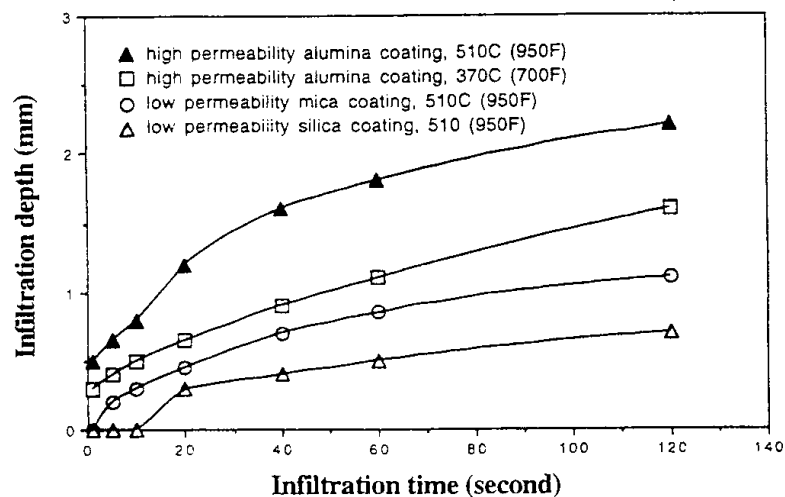


Figure 2.13: The effect of immersion time on liquid polystyrene infiltration depth at a liquid polystyrene temperature 370 °C [6].

Based on these results Sun et al. [6] developed a model for the removal of liquid polystyrene residue during aluminium casting, which is shown schematically in Figure 2.14. As liquid metal advances through the mould, the foam pattern is decomposed to liquid polystyrene with little gasification. The liquid polystyrene is then pushed toward the coating where it spreads across the coating surface and wicking into the coating and sand starts when both the coating and liquid polystyrene are heated to a critical temperature of between 275 to 300 °C [12],

where the polymer begins to decompose such that the liquid fraction begins to reduce in viscosity [39].

While the literature provides clear evidence that pattern coatings can absorb liquid polystyrene under certain conditions, Zhao et al. [38] argued that liquid polystyrene would not maintain direct contact with the liquid metal but would be separated by a film of vapour from the gaseous degradation products. The authors developed a technique that allowed them to interrupt mould filling and study decomposing polystyrene mass transfer behaviour, and the role of polymer vapour in foam removal from the mould cavity.

Using counter gravity casting equipment, liquid aluminium was drawn into a mould by the application of a vacuum. After a preset time the reduced pressure was removed causing the liquid aluminium to flow back into the crucible. At the same time air was fed into the mould cavity to cool the mould and any retained polymer residue as quickly as possible. Coating samples were then removed from the mould and examined using optical and scanning electron microscopy.

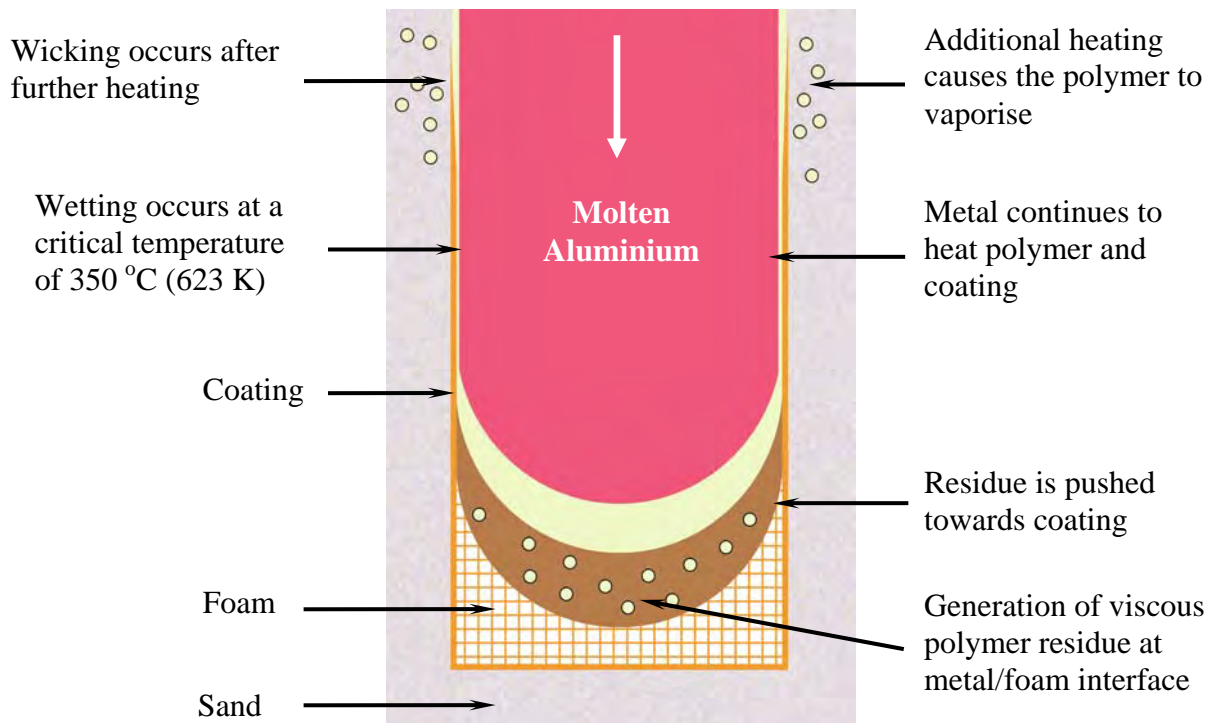


Figure 2.14: Model for wetting and wicking of liquid polystyrene during aluminium Lost Foam casting. Re-drawn from Sun et al. [6].

The experiments produced many coalesced liquid polystyrene globs on the inside of the pattern coating instead of a uniform liquid film. As the melt contact times increased these globs became smaller. The globs were analysed by gas chromatography and were found to have an average molecular weight of  $178,000 \text{ g.mol}^{-1}$ . Interestingly, a lower molecular weight was detected near the outer surface of the glob and a heavier molecular weight near the coating substrate (although specific values were not reported). This indicated a non-uniform temperature distribution across each plastic globule, which Zhao et al. [38] claimed made capillary driven liquid transfer kinetically unfavourable. Furthermore, the size reduction of plastic globs in all three dimensions indicated that the polymer was removed by an interface-controlled mechanism, as shown in Figure 2.15.

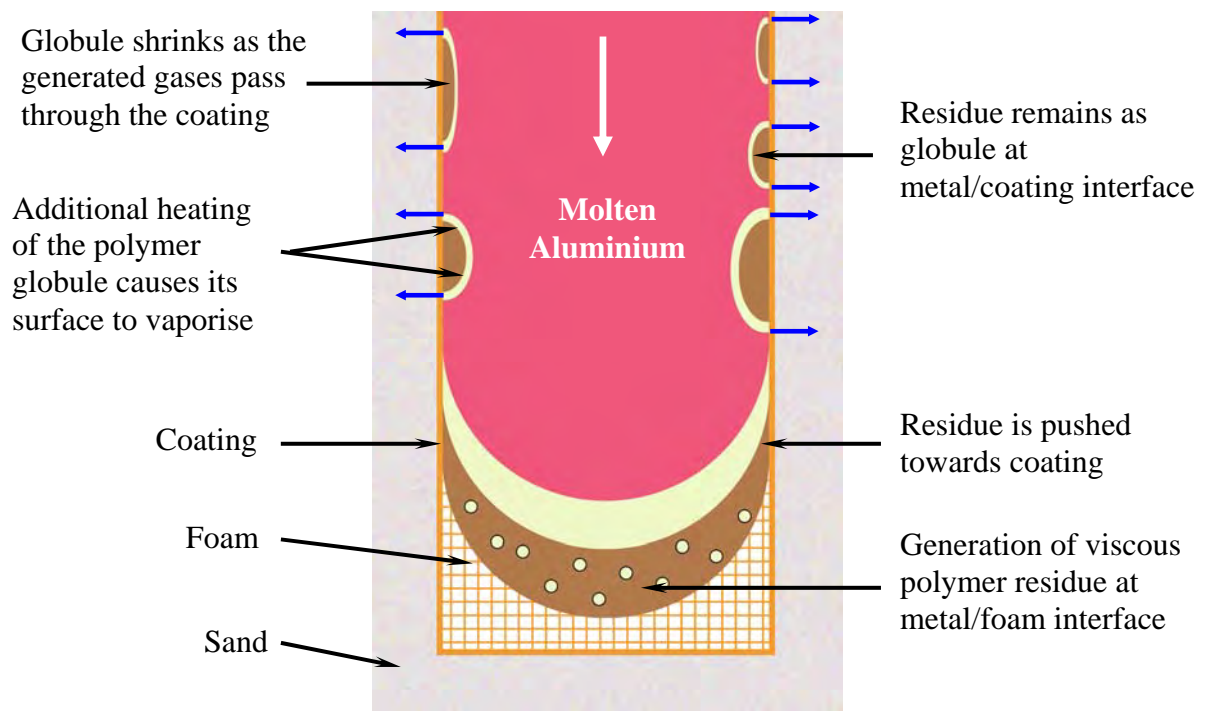


Figure 2.15: Gasification-driven foam removal mechanism. Re-drawn from Zhao et al [38].

Three distinct zones were observed on the outer coating surface, which the authors explained were due to liquid metal, liquid polymer and gas, contacting the inner coating surface. The coating directly under a glob of liquid polymer exhibited no change in its appearance and showed no sign of having absorbed any polymer. This was attributed to the polymer having insulated the coating from the liquid metal. However, around this central zone there was a region of coating that had become light grey in colour and that was a result of complete metal-

coating contact. Between these two zones a dark brown region of coating was observed and this was interpreted as being the area where gas had escaped through the coating.

It is possible that no absorbed polymer was found in the coating because the liquid metal was only in the mould for a few seconds. Therefore it is possible that neither the polymer nor the coating had reached the critical temperature proposed by Sun et al. [6] that was required for the liquid polystyrene to be absorbed into the coating. In experiments where the metal was allowed to cool and solidify in the mould, evidence of liquid polystyrene absorption was found [15]. To explain this it was suggested that the liquid polymer had been pushed into the coating by a combined increase in gas and metallostatic pressure that had built up between the non-permeable metal skin and the entrapped polymer glob. However, once the metal had formed a solid skin and the polymer globule continued to shrink, a larger area of exposed coating would have become available for the evolved gases to flow through. A significant build-up of gas pressure could therefore only have occurred if the coating pores had become blocked by polystyrene condensates.

### **2.1.3 Influence of the Filling Velocity**

In open cavity casting processes, the total time required for a mould cavity to fill is related to the quality of the casting. If filling times are too long, problems such as misrun or cold shuts may be observed. Filling times that are too short cause turbulence on the metal surface, erosion of the mould, introduction of inclusions, metal-mould reactions and a variety of other casting defects.

In the Lost Foam casting process, mould filling times and hence filling velocities are also important in preventing and controlling casting defects. A low filling velocity has often been reported as the cause of misrun, cold lap and sand collapse defects. Misruns occur when the liquid metal freezes before the pattern is completely filled [40]. When the metal stalls due to the loss of fluidity, it usually exhibits a smooth and rounded surface appearance. Although metal velocity is a significant factor in the formation and degree of severity of this defect, metal front temperature and the rate of removal of pattern decomposition products have also been reported as being factors [40,41].

Laps or folds form when two streams of molten metal meet and a thin layer of oxides and pattern decomposition products covering the metal fronts prevent the two streams of metal from fusing [40]. The defect appears as a distinct linear recess on the surface of the casting. The space between the folding surfaces can be between microns and millimetres in size, and is visible as a distinct line on the casting surface [15,41]. Cold lap defects are produced as a direct result of excessive, conductive heat loss from the metal to the sand and the foam.

Sand collapse is rarely mentioned in Lost Foam casting literature published within the past 10 years. However, Monroe [43] makes reference to it as a phenomenon that can be prevented by a coating with suitable mechanical strength. The only region of the mould into which sand can ingress is the void or “gap” that is formed between the advancing liquid metal front and the receding polystyrene pattern during mould filling. A slow filling velocity encourages a large vapour gap to form and a high permeability coating ensures that vapour degradation products can escape easily into the sand. The formation of a relatively large gap that has little or no positive pressure in comparison to the surrounding sand mass provides the optimum conditions for sand ingress. Hill et al [40] poured simple flange patterns using A356 aluminium alloy, and determined the significance of five variables on metal velocity and defect formation. Misrun and sand collapse was observed on castings filled below  $8 \text{ mm.s}^{-1}$  with the latter defect being reported until filling velocity exceeded  $14 \text{ mm.s}^{-1}$ .

As the filling velocity increases another group of defects becomes prevalent. These defects are formed primarily as a result of liquid or gaseous degradation products becoming entrapped within the liquid metal and result in the appearance of pores, rough surfaces, blisters, laps and folds. Examining thin aluminium castings, Wang et al. [25] observed internal pores only when the velocity of the liquid metal had exceeded  $23 \text{ mm.s}^{-1}$ . An unstable metal front profile, generated at a high filling velocity, was thought to be responsible for the trapped foam and pores. Hill et al. [40] observed rough surfaces on most castings that had been filled with a high velocity and suggested that this defect was caused by liquid polymer being pushed to the top surface of the mould cavity, but not having sufficient time to pyrolyse and escape prior to casting solidification. A similar explanation was offered by Liu et al. [42] who had observed rough surfaces on the upper ends of castings poured with aluminium alloy A319. Again, these were only found where the mould had filled at a high velocity.

Blisters are another form of surface defect and are the result of a thin layer of polystyrene residue trapped just beneath a solidified skin of metal [40]. Bennett et al. [34] suggested that blisters may form when a concave metal front permits liquid metal to flow rapidly along the foam pattern-coating interface. The thin film of metal may then solidify and trap liquid polymer just beneath the solidified skin.

Hill et al. [40] summarised the effects of filling velocity on the type and incidence of defects as illustrated in Figure 2.16. They determined that there was a narrow velocity window, between  $14 \text{ mm.s}^{-1}$  and  $18 \text{ mm.s}^{-1}$ , where no defects were observed. Above  $18 \text{ mm.s}^{-1}$ , porosity, folds and surface defects occurred, while misruns and sand collapse occurred below  $14 \text{ mm.s}^{-1}$ .

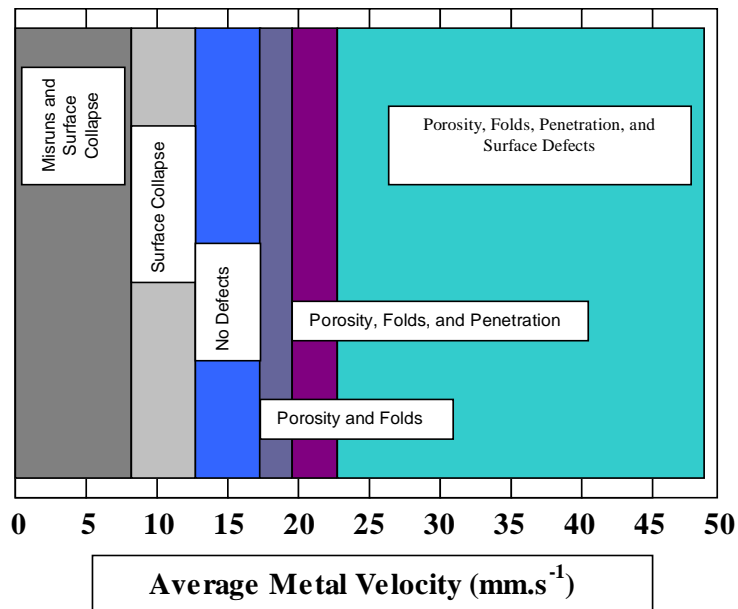


Figure 2.16: Summary of defects vs. average metal velocity, when casting A356 alloy [40].

In contradiction to the above findings, Hess [44] found no correlation between defect area and metal velocity when pouring A319, A356 and A206 aluminium alloys into coated EPS patterns. In fact, the highest incidence of defects was found at a velocity reported previously by Hill [40] to be optimum for reducing defects. Hess suggested that maintaining the desired filling velocity during mould filling was not sufficient to ensure good castings. He argued that the same factors that can be used to adjust metal velocity also impact on defect formation and that these factors should be optimised as a system in order to achieve a filling profile such that

liquid decomposition products do not become entrapped in the progressing metal front and enough time is available for decomposition products to exit the system through the coating.

Mould filling velocity, amongst other variables, has also been reported to influence metal front shape. Molibog et al. [16] hypothesised that using a pattern with a higher density towards the surface in conjunction with a low filling velocity would encourage the formation of an “arrow pointed” convex metal front. They also believed that the shape of the metal front has a strong effect on the rate of removal of pyrolysis products from the kinetic zone. A convex metal front would assist the highly viscous residue to move towards the coating from the centre and escape from the kinetic zone. Warner et al. [32] observed metal front profiles and measured metal front velocities as part of their aluminium casting experiments to study the effects of coating type, coating permeability and pattern geometry on pyrolysis related casting defects. They noted that the metal front profile had a tendency to become increasingly concave as both filling velocity and coating permeability increased.

#### **2.1.4 Influence of the Coating**

The thin refractory pattern coating controls the rate at which pattern decomposition products are eliminated from the mould cavity and the rate at which heat is lost from the liquid metal to the sand. Both of these factors influence filling behaviour and defect formation. Coating permeability varies with the size and shape of the refractory particles in the slurry and the thickness of the coating layer [26,27]. Inconsistencies in coating permeability are reported to be directly related to inconsistencies in casting quality by causing variations in the rate at which foam decomposition products can be removed from the mould during filling [4,28,45,46].

Kocan [47] and Littleton [46] developed two different types of apparatus for measuring coating permeability. The apparatus developed by Kocan [47] used a machine that had been originally designed for determining the permeability of sand mixes in conjunction with a modified sample tube that supported the coating sample. An exploded view of the sample tube assembly is shown in Figure 2.17.

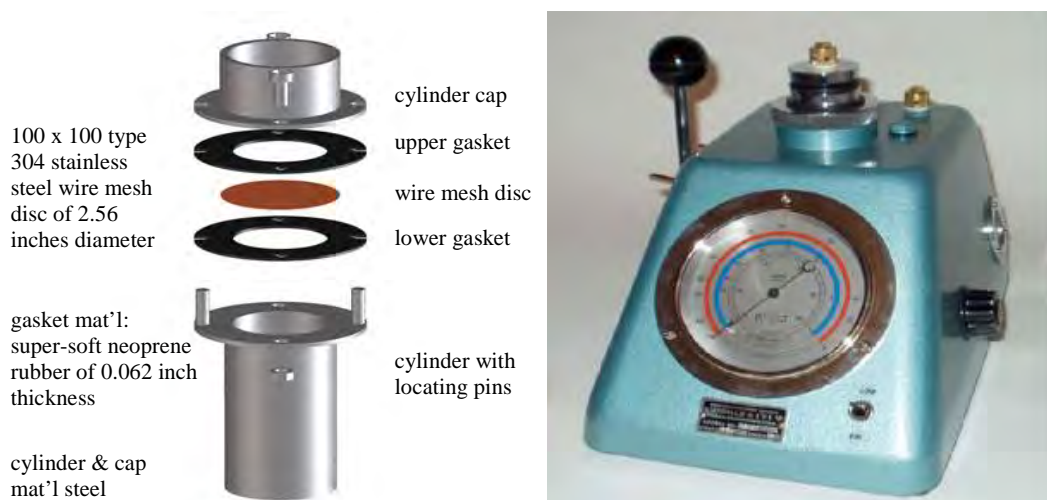


Figure 2.17: Modified foundry equipment for determining coating permeability [47].

A schematic of Littleton's apparatus [46] is shown in Figure 2.18. In this apparatus a disc of coating is clamped between two silicone gaskets and air is forced through the coating at a controlled pressure (typically between 7 and 20 kPa). Littleton gave no information regarding the size or thickness of the coating samples, or how the samples were obtained.

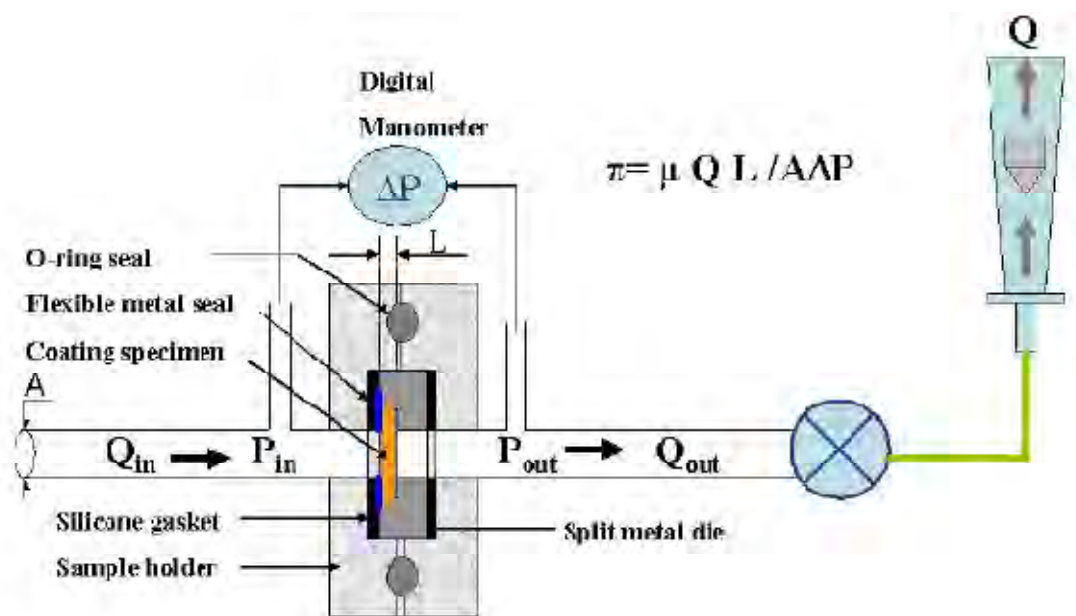


Figure 2.18: Schematic of apparatus for measuring air flow through coatings [46].

In a more recent paper Zhao et al. [48] described coating samples of 12 mm diameter and 1 mm thickness that were slip cast in aluminium moulds. The coating samples were ground to

different degrees in order to obtain a range of coating thickness for subsequent permeability measurements. However, the author failed to mention if a ground coating varied in structure from those that had been applied by dipping. Furthermore, in grinding the coating samples the authors may have inadvertently blocked some of the pores of the coating, and this would have resulted in lower airflow rates through the coating samples.

In Littleton's apparatus, airflow rates and the pressure differences across prepared coating discs were measured and the permeability of the coating calculated by application of Darcy's Law for the permeability of a porous medium (see Equation 2.2) [49-52]. For laminar viscous flow through a macroscopically homogeneous porous material, Darcy's law reads:

$$\frac{\Delta P}{L} = \frac{\mu}{k_1} U \quad \text{Equation 2.2}$$

where  $\Delta P$  is the total pressure drop across a medium of length  $L$  and specific permeability  $k_1$ .  $U$  is the superficial velocity of the fluid (with viscosity  $\mu$ ), and is uniform in the medium [49].

$$U = \frac{\Delta Q}{A} \quad \text{Equation 2.3}$$

where  $\Delta Q$  is the measured flow rate through the medium and  $A$  is the cross-sectional area [50].

Although Forchheimer's equation [53] has been accepted in the literature as giving more reliable information than Darcy's Law on the permeability of highly porous structures where fluid velocities are very high, for example in ceramic foam filters used in metal filtration, Darcy's Law is considered to be valid for lost foam coatings because of the low rates of fluid flow occurring within the coatings [17,48].

When pouring several aluminium plate castings at 800 °C, Hill et al. [40] observed that when the permeability of the coating was "high", rapid filling produced an unstable metal front that trapped liquid polystyrene. However, when the permeability of the coating was "low", the metal front became more convex, pushing the decomposition products to the metal-coating

interface. Liu et al. [42] made similar observations when pouring simple plate castings at 800 °C.

Hess et al. also found that more defects formed when a high permeability coating was used [4]. The sum of the area of all the defects (folds and blisters) that could be imaged and found in one casting (using an image analysis program) was defined as the total defect surface area for that casting. The total defect area for castings made using a high-permeability coating was at least twice the total defect area found in castings produced with a low permeability coating.

High permeability coatings allow air and gaseous pattern decomposition products to escape quickly from the metal-foam interface. This leads to a better contact between the metal and the foam which accelerates foam decomposition. As foam can decompose and leave the mould more rapidly, the metal front velocity also increases. Based upon Caulk's theory [19,20] a velocity increase can result in the pattern decomposing according to the engulf or collapse mode and ultimately encourage the formation of casting defects.

Under certain circumstances a pattern coating has the ability to remove liquid degradation products from the mould cavity by either wetting or wicking. Littleton [46] developed an apparatus for measuring the wicking capability of lost foam coatings by measuring the real-time weight of a liquid absorbed into the coating by means of an externally applied pressure and capillary pressure. In order for room temperature measurements to be made, olive oil was chosen to simulate the liquid degradation products of the polystyrene pattern but Littleton et al. [46] offered no explanation of the suitability of this choice. Although it is reasonable to see how this apparatus may be used as a routine check for coating consistency, the arbitrary use of olive oil at room temperature does not emulate the process of wicking in the Lost Foam process as described by various authors in Section 2.1.2. On the contrary, Sun et al. [6] considered that the crucial factor in controlling the wetting and wicking of a liquid polymer was the temperature - viscosity relationship of the polymer during mould filling and not its composition. Therefore, this apparatus has no direct application in determining a coating's propensity for removal of liquid polymer from the mould cavity by wicking.

Davies [54], however, considered that coating permeability was of more importance than its ability to absorb liquid polymer. This is because, in order to improve a coating's ability to absorb liquid polystyrene, its pores must increase in size. As a consequence, the permeability of the coating and the mould filling speed are increased. Higher metal front velocities have been consistently reported to affect casting quality in an adverse fashion [20,40,42] and therefore promotion of a coating with good wicking properties can be counter-productive.

The insulating properties of the pattern coating can also play an important part in the integrity of the castings produced. Tan et al. [55] studied the fluidity of liquid aluminium when cast into Lost Foam moulds in which patterns had been coated with either high conductivity silica-based, or low conductivity potassium aluminium silicate-based coatings. Square bars (cross section of 30 mm by 30 mm, and 254 mm in length), filled completely regardless of the coating used. However, thinner bars (30 mm wide by 3.3 mm thick and 254 mm long) only filled on average 59% of the total length when cast with the insulating coating, and not at all when silica based coatings were used.

When a coating with high thermal conductivity is used, heat transfer from the liquid metal into the mould occurs more quickly than with an insulating coating. Rapid heat loss may cause the liquid metal at the coating interface to solidify quickly, thereby resulting in misrun defects. Additionally, premature solidification at the interface may block the escape of pattern decomposition products and result in the formation of entrapment defects [56]. On the other hand, highly insulating coatings such as those containing mica, encourage the liquid metal at the metal-coating interface to remain molten for a longer period of time. The additional time available for pattern degradation products to escape through the coating into the mould may be necessary to render the casting "defect free". The mechanism by which mica improves the insulation properties of a coating has been explained by Zhao et al. [48]. They report that such particles tend to orientate themselves parallel to the free surfaces, which creates loosely packed layers of granular structures that significantly lower the heat and mass transfer rates of the coatings.

### **2.1.5 Influence of the Gating System**

In conventional, open cavity-type casting, the main aim of the gating system is to control the flow of liquid metal through the channels leading to the mould cavity so that flow is conducted in a controlled fashion devoid of surface turbulence. As long as all other variables are suitably controlled, a properly designed gating system should produce a casting that is free of defects deleterious to its function. Unfortunately, in the Lost Foam process the gating system cannot be relied upon to carry out this task because a number of other factors such as the foam degradation mechanism and removal rate of the degradation products from the mould are much more influential. Hence, the main requirements of a Lost Foam gating system are to provide mechanical support for the cluster, control the direction of flow of the liquid metal, and help to provide feed metal to compensate for solidification shrinkage.

Hill et al. [57] suggested that although the above was essentially true, “there must logically be some critical gate size below which restriction of fluid flow becomes more important than the rate of foam decomposition or transport of foam decomposition products”. A series of plates was cast, each coated with a high or low permeability coating, and with varying gate sizes of between 0.02 in.<sup>2</sup> and 0.5 in.<sup>2</sup>. It was found that gate areas above 0.05 in.<sup>2</sup> had no effect on mould filling times when used in conjunction with high permeability coatings. For low permeability coatings, where removal of degradation products proceeded at a slower rate, the critical gate area fell to 0.03 in.<sup>2</sup>. The authors concluded that, to avoid collapse of the pattern and surrounding sand during filling, the region between the advancing metal front and the solid polystyrene pattern must be pressurised, either due to contact or near contact between the liquid metal and the decomposing foam, or due to a high gas back pressure. If the gate was to act as the choke, these conditions could not be met and a sound casting could not be produced. This statement is supported by a number of authors [18,58,59] who agree that the only practical influence that the gating system can have on metal velocity is the level of metallostatic pressure applied throughout mould filling.

Although gate area may not be significant in determining the quality of the castings made by the Lost Foam process, the location and number of gates used has some effect. Lawrence et al. [59] stated that the minimum number of gates should be used to avoid impinging metal

streams, and that gates should be located near the bottom of the pattern to eliminate any surface turbulence at the metal front and encourage a smooth metal-pattern interface. They also suggested that the path of the metal front can be designed, by an appropriate gating system, to direct residual decomposition products that cannot be handled by the coating into the gating system, rather than being trapped in the casting. Sun et al. [60] made 30 mm diameter bars by casting A356 aluminium alloy into Lost Foam moulds. Patterns were gated from the top, bottom, one side or both sides, and the authors reported that defects encountered in top- or bottom-gated castings were not as severe as those observed where one or more side gates had been used. They concluded that this was because top and bottom gates more evenly distributed liquid polystyrene to the coating-metal interface.

To assemble Lost Foam patterns hot-melt adhesives are commonly used, which have amorphous properties, i.e., they are solid at room temperature and experience a decrease in viscosity as the temperature rises [61]. The glue adhesive has a relatively high density of approximately  $960 \text{ kg/m}^3$ , when compared to an average foam pattern of only  $24 \text{ kg/m}^3$ , and therefore requires more energy in degradation. When the liquid metal front reaches a joint in the cluster additional heat is lost in degrading the glue [62], and this may cause the metal front to stall momentarily.

Sun and Littleton [63] used a real time X-ray apparatus to view the influence of glue joints on the advancing metal front. They reported that when the metal stream reached the joint, its forward progress was halted for between 0.8 and 1 s. During this time the metal started to build up along the joint until it managed to break through at various locations. Mould filling then continued by means of multiple metal streams passing through the joint. The authors concluded that glue joints contributed significantly to the formation and subsequent convergence of multiple metal fronts which encouraged the creation of fold defects. Under these circumstances, a gating system with the minimum of glued joints should maximise casting quality.

### **2.1.6 Influence of Pouring Temperature**

The temperature of the metal provides heat to decompose the polystyrene pattern and fluidity for the liquid metal to fill the resultant cavity. A high temperature increases metal fluidity as in conventional casting processes, but published literature is inconsistent in reporting its influence on the filling speed of a Lost Foam mould. A number of authors [58,64,65] suggest that pouring temperature does not play a significant role whilst others [25,34,44] have observed the opposite.

Fu et al. [66] produced a number of clusters each made up of a gating system and four plates, each being 0.125 inches (3.17 mm) thick. Two of the four plates were oriented in the vertical plane and two in the horizontal plane. Each cluster was coated with either a high permeability, alumina-based coating, or a low permeability silica-based coating. The clusters were cast with a hypoeutectic A319 aluminium alloy at temperatures ranging between 660 °C and 900 °C, and it was found that in the lower range of pouring temperature fluidity increased rapidly with increased superheat, but improved little between 740 °C and 780 °C. As pouring temperature was raised further, fluidity again began to increase rapidly with increasing superheat. At a temperature of 860 °C and above all patterns, irrespective of coating or orientation, were fully filled.

The authors proposed that, at low pouring temperatures, the pattern degradation products were nearly all liquid and were removed into and through the coating by wetting and wicking. They suggested that, at these low temperatures, the coating temperature would also be relatively low and would not encourage the liquid polystyrene to decompose into gases and escape into the sand. Under these circumstances the coating might have become saturated with liquid residues and the permeability reduced. They hypothesised that, as the pouring temperature increased to 700 °C, more gas was evolved while at the same time enough liquid polystyrene produced to block the pores in the coating, thereby accounting for the levelling off in fluidity results observed between 740 °C and 780 °C. At even higher temperatures the ratio between liquid and gaseous degradation products fell even further which promoted more rapid removal of both through the coating.

Caulk [17,18] explained the apparent disparities in the published literature by suggesting that the mode of pattern decomposition influences the effect that pouring temperature has on filling times. Together with Barone [17], he calculated that, in contact mode, filling speed was essentially unaffected by metal temperature because any increase in heat flux into the foam was offset by an increase in the rate of vaporisation of the polymer liquid and the two trends balanced each other. This is illustrated in Figure 2.19 where the filling speed at a constant metal pressure equivalent to a 0.5 m head of aluminium was almost unaffected by the temperature at which the metal was cast. Interestingly, the graph also showed that the polystyrene pattern which had been treated with a compound of bromine was slightly less sensitive to metal temperature than the untreated one. The authors suggested that this was because the presence of bromine had reduced its activation energy by approximately 40%.

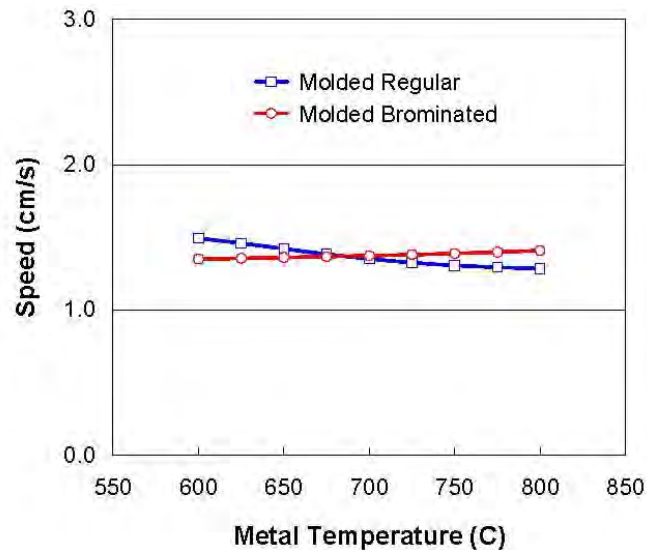


Figure 2.19: Filling speed in contact mode as a function of metal temperature for regular and brominated polystyrene foam with a metal pressure corresponding to 0.5 metres of aluminium [17].

However, when the method of pattern decomposition changed from contact into gap mode [18], the effect of pouring temperature on fill rate increased significantly. In the gap mode of filling, radiation is responsible for the majority of the heat flux used to decompose the polystyrene foam. Conversely the heat flux from conduction stays almost constant because gap width increases as the temperature rises, thus reducing heat transfer by conduction, and this offsets any difference across the gap.

The effect of metal temperature on the filling speed when the gap mode of pattern decomposition is apparent is shown in Figure 2.20 for four pattern thicknesses. Although the absolute speeds are relatively small, the percentage increase between 600 °C and 800 °C is approximately 50%.

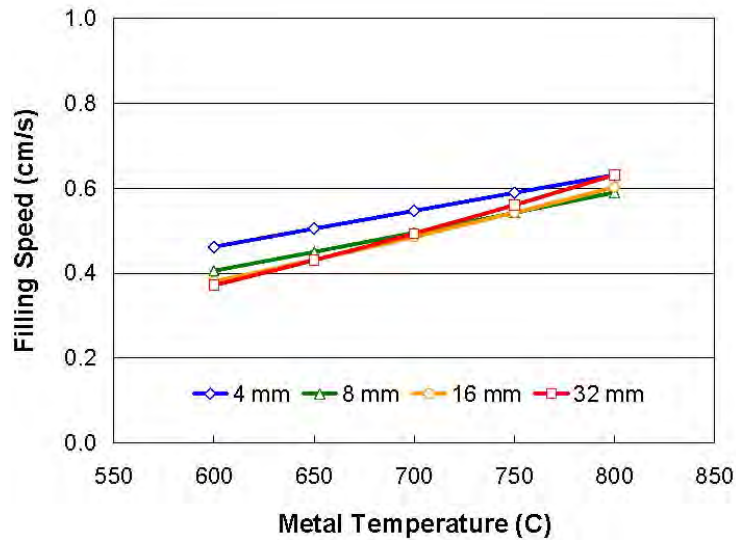


Figure 2.20: Filling speed in gap mode as a function of metal temperature for several values of pattern thickness and a metal pressure corresponding to 0.5 metres of aluminium [18].

The temperature at which a Lost Foam mould is poured has also been reported to contribute to the presence of a range of defects in the finished castings. High pouring temperatures have been associated with the presence of blisters [34], whilst low pouring temperatures have produced internal pores and folds [67]. Blisters have been found most commonly near ingates where metal temperatures were relatively high whereas internal pores and folds, on the other hand, have been associated with areas of the casting that filled towards the end of the pour and hence have been related to low metal temperatures and rapid solidification [34].

Bennett et al. [68] used the Lost Foam process to manufacture a number of flange-type castings in A356 aluminium alloy. To measure the liquid metal front temperature during filling they attached thermocouples to the patterns at the ingate, and at 90° and at 180° around the flange from the ingate. No defects were observed in the vicinity to the ingate where metal temperatures remained high throughout the mould filling cycle. Internal pores and folds congregated primarily in the region of the casting furthest from the ingate, and blisters were found exclusively in the region between. These findings corresponded well with earlier

research [69] and suggested that the temperature of the liquid metal during mould filling not only influenced the occurrence of casting defects but also their location and form.

Gas porosity is also associated with the use of high pouring temperatures in the casting of aluminium [70,71]. The solubility of hydrogen in aluminium at atmospheric pressure increases dramatically at the melting point and it is this difference in solubility between liquid and solid aluminium that causes gas porosity in the solidifying casting. In order to examine hydrogen gas pick-up, Shin et al. [70] cast a number of Lost Foam moulds, each containing a polystyrene pattern that had a 7 mm, an 11 mm and a 17 mm thick leg. The clusters were embedded in their own moulds and cast in aluminium at 670 °C, 750 °C or 830 °C under atmospheric or reduced pressure conditions of 710 mmHg. Where moulds were cast at reduced pressure, this under pressure was maintained until solidification was complete.

As the thickness of the leg increased, the level of porosity in the area of the casting nearest the sprue also increased. Conversely, porosity at the opposite end of the legs increased as thickness decreased. A pouring temperature of 750 °C was observed to produce the best results in legs of 17 mm and 11 mm whilst the lowest porosity results recorded in the thinnest legs occurred when cast at 800 °C. The application of a reduced pressure during mould filling also had the effect of reducing the level of porosity in all samples by about 0.4 percentage points.

The authors suggested that there was an optimum metal front temperature at which the lowest levels of gas porosity are achieved. Too high a pouring temperature will increase hydrogen pick-up and prolong solidification time, whereas a low temperature will produce a greater amount of liquid degradation products that may become entrapped and result in large pores.

Energy dispersive X-ray analysis (EDS) was performed in gas pores to determine the level of carbon present. The absence of carbon in a pore indicated that it was formed by precipitation of hydrogen whereas a pore that contained carbon was formed by entrapment of some decomposition products of polystyrene. Where both carbon and hydrogen were found in the same pore, the mechanism of formation was by foam entrapment with diffusion of hydrogen into it taking place during subsequent growth. The thicker 17 mm legs exhibited carbon levels of around 8 wt.% in samples cast at 700 °C and this fell to around 3 wt.% at pouring

temperatures between 750 °C and 830 °C. The flow tips of 7 and 11 mm legs contained pores with carbon contents as high as 10 and 13%. From these results the authors concluded that not only can pores form through capture of liquid or gaseous decomposition products, but also from supersaturated hydrogen gas which originates from the initial melt or from reaction with decomposed polystyrene.

### **2.1.7 Effects of Temperature Gradients**

Temperature gradients experienced within the metal during the filling and solidification phases of the Lost Foam casting process are considerably greater than those encountered in conventional, open-channel sand casting [67]. This is because liquid metal poured into a Lost Foam mould has the additional task of thermally decomposing an expendable polystyrene pattern in order to occupy the void so produced. In order to prevent the metal front from stalling during the filling process, casting temperatures are usually higher than those employed in conventional casting.

The higher temperature gradients present in the Lost Foam process can have both positive and negative consequences on casting quality. When a Lost Foam pattern is gravity filled from the top, the positive temperature gradient that results between the metal front and the ingate promotes directional solidification and therefore reduces the possibility of solidification shrinkage. However, a number of researchers [72-74] have applied the technique of counter-gravity casting to the Lost Foam process in order to achieve greater control over the filling of the mould. In this case, the downsprue is eliminated altogether and the complete running system and liquid metal reservoir are located below the casting. This produces a negative temperature gradient throughout the casting during filling and subsequent solidification. Unless the driving force used to generate a metal flow in the opposite direction to the gravity vector continues to be applied after the mould has been filled, feed metal may not be present, or have sufficient potential energy, to offset the shrinkage that occurs during solidification.

A higher pouring temperature also means that the various regions of the casting solidify at different rates [67,75]. Chen and Ravindran [75] made a series of stepped aluminium castings in the Lost Foam process. Thermocouples were inserted at the centre of each of the steps and

the metal was cast at varying levels of dissolved hydrogen, (between 0.149 and 0.409 cc/100g). Shrinkage was absent from all but the thinnest sections of the castings and even then, a high level of dissolved hydrogen (0.41 cc/100 g) suppressed this defect. Gas pores, however, were observed in every section of every casting with their size being related to solidification time. Where a solidification time of 5 minutes had been recorded the associated pore diameter was between 150 – 200  $\mu\text{m}$  but where it had taken 20 minutes for solidification the pores were between 400 – 900  $\mu\text{m}$  in diameter. The level of dissolved hydrogen in the sections that had taken longer to freeze was also influential on the pore size found. Generally, 400  $\mu\text{m}$  diameter pores were observed in castings where the dissolved hydrogen was 0.15 cc/100 g and the largest pores occurred where the hydrogen level had been measured at 0.41 cc/100 g. Therefore, whilst counteracting the potentially negative effects of solidification shrinkage, a high temperature gradient can encourage the formation of hydrogen gas porosity in the finished castings. Interestingly, the authors did not investigate if any of the pores contained carbon and therefore could not be sure that hydrogen was the cause of the defects.

Temperature gradients also exist between the metal, pattern coating and moulding media during mould filling, solidification and subsequent cooling, which affect the quality of the castings produced. Khan et al. [76] measured interfacial heat transfer coefficients in Lost Foam casting of aluminium alloys, for two thicknesses of pattern coating. Values were calculated based on solidified metal temperature measurements via an inverse heat conduction method and varied between 200 – 1800  $\text{W}/\text{m}^2\text{K}$  for a 1.0 mm coating thickness and 200 – 1000  $\text{W}/\text{m}^2\text{K}$  for a 2.5 mm coating thickness.

Subsequently, Khan et al. [77] remeasured the interfacial heat transfer coefficient across the metal-coating-mould interface using a modified technique to minimise possible convective heat transfer by gaseous decomposition products. A temperature dependant value for the coefficient varying from 150  $\text{W}/\text{m}^2\text{K}$  at the A356 aluminium alloy eutectic temperature (577  $^{\circ}\text{C}$ ) to about 80  $\text{W}/\text{m}^2\text{K}$  around 350  $^{\circ}\text{C}$  was reported. To estimate the effects of the coating, Khan et al. [77] proposed a model of the interfacial heat transfer coefficient based on thermal resistances; Equation 2.4.

$$h_{Total} = \frac{1}{\frac{1}{h_{M/C}} + \frac{l_C}{k_C} + \frac{1}{h_{C/S}}} \quad \text{Equation 2.4}$$

where  $h_{M/C}$  and  $h_{C/S}$  are the metal-coating and the coating/sand interface heat transfer coefficients, and  $l_C$  and  $k_C$  are the coating thickness and the coating thermal conductivity, respectively.

In more recent work, Zhao et al. [78] reviewed the effects of the pattern coating on heat transfer in the Lost Foam casting of aluminium with a view to preventing fold defects. They postulated that a minimum liquid metal cooling time is needed to allow complete foam removal from the mould cavity and prevent fold formation. Clusters were cast in an aluminium alloy in an uncoated condition, or after a single or double layer of coating had been applied. Unbonded silica sand was used as the moulding media in two moulds, while a third utilised steel shot, and a cluster with a single layer of coating.

Thinner bars filled more completely as the pattern coating thickness increased, which suggested a higher heat loss rate across the metal/sand interface where there was a limited coating or no coating at all. As casting thickness increased, the incidence of misrun and variation in dendrite cell spacing between castings was reduced until a point was reached where there was no difference with coating thickness. Interestingly, the authors reported that although steel shot had a slight effect on refining the structure in thin walled parts, its influence decreased as section size increased to such an extent that the moulding media played no part in the spacing of the dendrites in the thickest bars. Additionally, steel shot was not found to have any effect on the duration of mould filling.

## 2.2 CASTING DEFECTS

Defects associated with mould filling can manifest themselves in a number of different forms and many researchers [14,24,40,45,58,59,64,66,67,79] have found that the factors affecting mould filling are also closely related to formation of defects. These include (i) mechanical and chemical properties of the polystyrene pattern, (ii) morphology, size and compaction of the

moulding media, (iii) thickness, viscosity and permeability of the pattern coating, and (iv) pouring temperature, metal front velocity and profile, and the design of the gating system.

### 2.2.1 Porosity

Internal porosity is probably the most widely reported defect encountered in the production of aluminium castings. Although similar bulk density porosity levels of between 1.0% and 1.5% have been found in identical aluminium castings made in both the Lost Foam and the greensand processes [80], a considerable difference has been observed in pore morphology. Whilst interdendritic porosity and spherical gas bubbles are present in Lost Foam castings, only interdendritic cavities are observed in greensand samples. Figures 2.21 and 2.22 illustrate interdendritic and gas-type pore defects respectively.

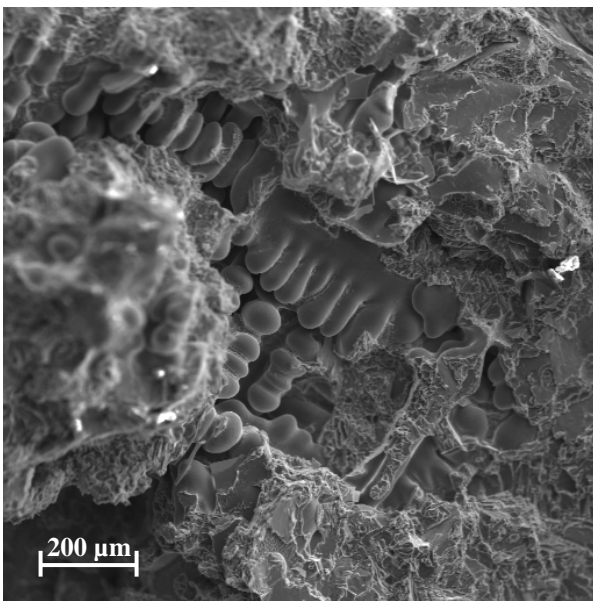


Figure 2.21: Interdendritic pore (characterised by predominant dendrite arms and an irregular pore surface)

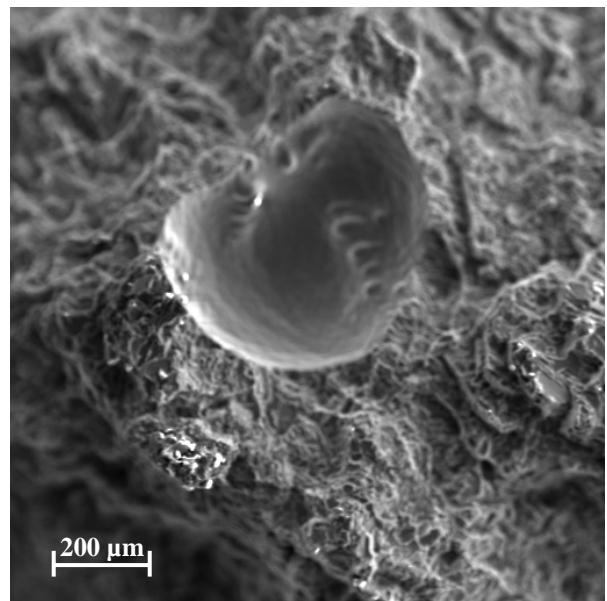


Figure 2.22: Gas pore (characterised by a smooth, rounded pore surface)

Shrinkage defects in aluminium castings occur during solidification as a result of volumetric differences between liquid and solid states. Interdendritic shrinkage porosity is most widely associated with aluminium containing significant quantities of magnesium or copper. These elements not only increase the freezing range of the alloy but also provide elevated temperature strength to the skin of the casting which is normally the first region to solidify.

With surface collapse unlikely and the progressive development of a primary dendrite network, resistance to the flow of the remaining, near eutectic liquid, increases to a point at which the pressure at the solidification front reaches zero and where interdendritic shrinkage forms. The phenomenon is found in all casting processes, especially those where a sand mould is used because the rate of solidification is relatively slow and non-uniform.

Apart from shrinkage, Shin et al. [70] suggested that pores form by three different mechanisms in Lost Foam casting. The first is by gasification of liquid polystyrene products that have been captured within the liquid metal as it flows through the mould during the filling process. The second is similar to the first but this time involves the entrapment of gaseous decomposition products directly rather than gasification after capture. The third mechanism is by supersaturated hydrogen gas contained within the melt that can originate from the melt itself or through reaction with decomposed polystyrene.

Based on the results of their experiments, they suggested that the different mechanisms of pore formation would result in a variation in the carbon content found within the pore cavity. The highest carbon contents should be associated with entrapped liquid polystyrene that subsequently forms a gas whereas the lowest values would be found in pores related to hydrogen precipitation. Carbon contents associated with pores found in the thicker 17 mm plates ranged from 0% to 4% when casting temperatures of 750 °C or above were used. As the plate thickness reduced to 11 mm and 7 mm the carbon levels associated with the pores rose, in some instances to 8% and 12% respectively. Lower casting temperatures, of below 750 °C, also produced higher carbon levels in pores. These results indicate that casting geometry and pouring temperature influence pore formation mechanisms.

### **2.2.2 Folds**

Folds are a group of defects exclusively found in aluminium and magnesium castings produced by the Lost Foam process. Zhao et al. [15] categorised this type of defect into a number of sub-categories depending on the morphology and location in which they are found. Folds connected to downward facing casting surfaces or the lowermost faces of the mould are termed “bubble-trail” defects, whilst those associated with converging metal fronts or the last

areas of the casting to fill are called “misruns” or “cold laps”. “Blisters” are another form of fold defect that are found on upward facing casting surfaces. These defects are usually accompanied by a severe distortion of the immediate casting surface.

They also suggested that, in some cases, internal pores can be classified as fold-type defects and reasoned that, because Auger depth profiling [81] and X-ray photoelectron spectroscopy [15] data published for bubble folds, bubble-trail folds, laps, blisters and internal pores were similar in terms of chemistry and physical disposition, these defects could all be categorised as folds of one type or another. Examples of fold-type defects on a polished section and on the fracture surface of an aluminium casting are illustrated in Figures 2.23 and 2.24. On the polished section a fold is recognisable as a thin black line separating two areas of the matrix and when the casting is fractured, a smooth shiny surface is revealed.

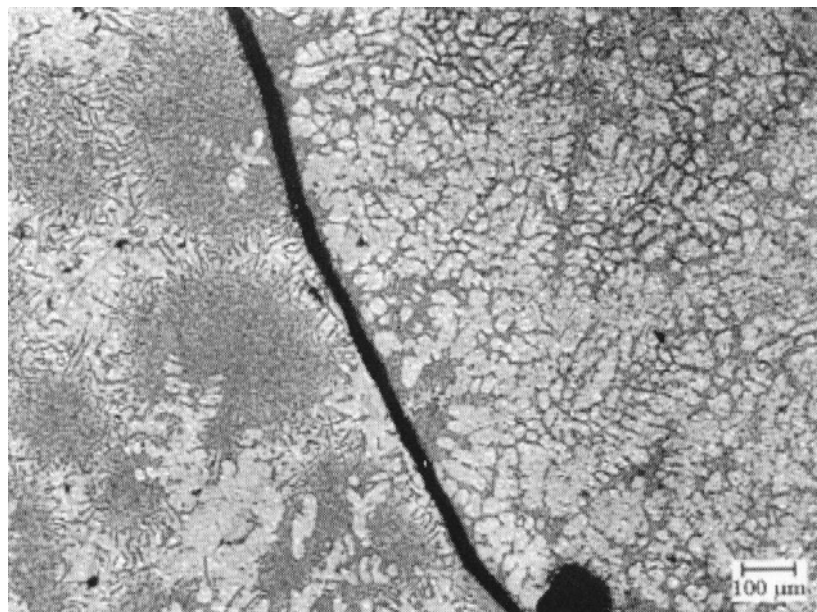


Figure 2.23: Photomicrograph of a fold defect observed in an aluminium flange casting [40].

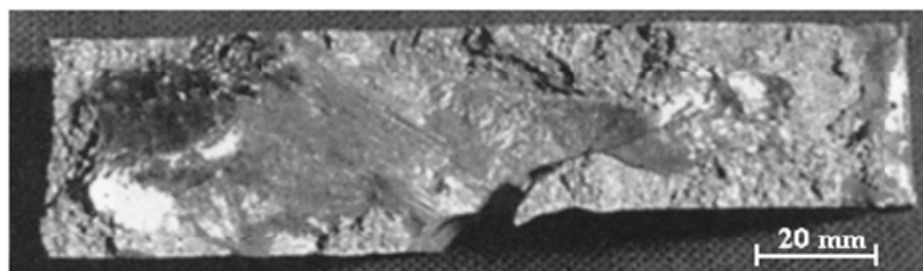


Figure 2.24: A fold defect in an aluminium flange where two metal streams met [40].

Zhao et al. [15] examined a number of process-specific defects that they collected from production and research environments in order to characterise and understand fold defect formation. Visual inspection, both real time and post cast, as well as surface analysis indicated that all the defects observed had similar surface structures and shared the same root cause in defect formation. It was only the formation path of a specific fold defect that led to the complexity in defect appearance. Based on their analyses they concluded that all folds originated from the initial formation of a gas bubble in the liquid metal and proposed nucleation kinetics for such a bubble as illustrated in Figure 2.25.

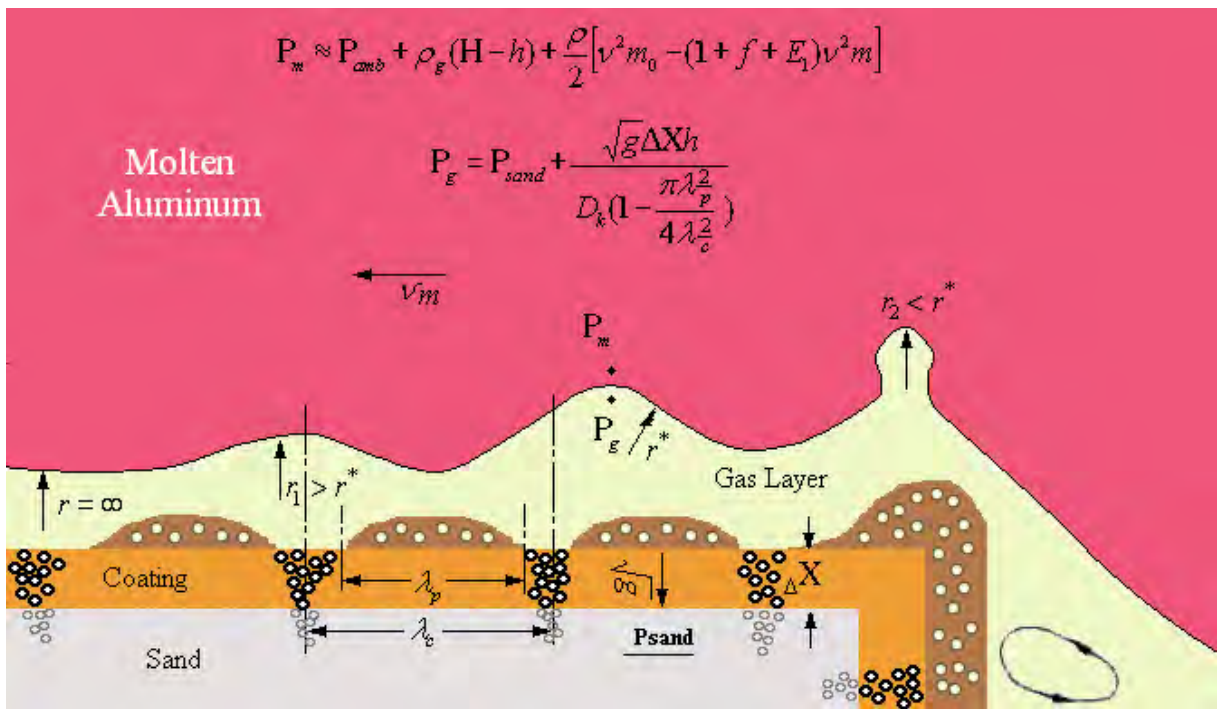


Figure 2.25: Illustration of fold nucleation whilst casting aluminium by means of the Lost Foam process.

They postulated that the size of the equilibrium, spherical, gas bubbles that would be nucleated at the interface,  $r^*$ , could be represented by the following equation:

$$r^* = \frac{2\sigma}{p_g - p_m} \quad \text{Equation 2.5}$$

where  $p_g$  is the local gas pressure,  $p_m$  is metallostatic pressure and  $\sigma$  is the surface tension of the liquid metal.

By application of Darcy's Law [51] and Bernoulli's engineering equation [82] and discounting any pressure drops that might occur in the sand mould itself (i.e.  $p_{\text{sand}} \approx p_{\text{amb}}$ ), they expanded equation 2.5 as follows:

$$r^* = \frac{2\sigma}{\frac{v_g \eta \Delta X}{D_k \left(1 - \frac{\pi \lambda(t)^2}{4 \lambda_{p0}^2}\right)} - \rho g (H - h) - \frac{\rho g}{2} [v_{m0}^2 - (1 + f + K)v_m^2]} \quad \text{Equation 2.6}$$

where  $v_g$  is the gas flux through the coating,  $\eta$  is the gas viscosity,  $\Delta X$  is the coating thickness,  $\lambda_{p0}$  is the initial, average linear spacing between plastic globs,  $\lambda_p(t)$  is the diameter of remaining plastic globs at time  $t$  after the metal front has passed,  $H$  is the total metal head,  $h$  is the local metal height,  $\rho$  is the metal density,  $v_{m0}$  is the initial metal pour velocity,  $v_m$  is the local metal velocity,  $f$  is the friction factor, and  $K$  is the overall velocity head loss factor due to sudden changes in a mould filling path.

As illustrated in Figure 2.25, any perturbation on the liquid metal surface that has a radius smaller than  $r^*$  would nucleate into a bubble in the liquid metal. The authors suggested that bubbles generated in this fashion would form folds in one of a number of ways. The type of fold would be determined by the susceptibility for liquid residue to accumulate behind the metal front at the metal-coating interface, the local gas transfer rate into the surrounding sand, the ratio of local casting thickness to  $r^*$ , the local metal temperature and associated cooling rate, and the degree of melt surface contamination. For example, blisters were categorised as bubbles that managed to rise to within a short distance of the upper surface of the mould cavity and pores found within the casting were given the name of internal pores. Finally, cold laps were reported to form between converging metal streams, usually in thin sections. The slow filling rates associated with these thin sections resulted in metal fronts being exposed to the carbon rich gases of polystyrene decomposition which had the effect of hindering their fusion. A number of papers have since been published [83-85], that empirically explored the effect of various parameters on minimising fold defects, which supported the theories put forward by Zhao et al. [15].

### **2.2.3 Surface Roughness and Staining**

Positive surface roughness on a Lost Foam casting is caused by liquid metal breaking through the mould coating and penetrating into the surrounding sand. The coating itself has little mechanical strength and, if not supported by well-compacted moulding sand, can rupture when subjected to the thermal and dynamic loads applied to it by the liquid metal. The resultant fissure provides a route for the liquid metal to exit the mould cavity and force its way between the sand grains. Poor coating control and rough cluster handling can result in localised coating thicknesses falling below a level required to prevent metal penetration.

Negative surface roughness is caused primarily by the liquid metal front advancing through the mould at a faster rate than the liquid and gaseous degradation products can exit into the surrounding moulding sand. The liquid polystyrene collects at the metal coating interface where a small amount is wicked into the coating [54] and the remainder degrades further into the gaseous form before it can permeate into the sand. The phase change from liquid to gas is associated with a pressure increase, especially if the coating is of low permeability and this pressure change causes rippling on the surface of the metal. Hill et al. [40] observed rough surfaces on a number of castings that had been filled at high velocity. It was considered that this defect had been caused by liquid polymer that had been displaced to the upper surface of the mould but had not had time to escape through the coating prior to solidification. Liu et al. [42] also observed rough surfaces in the upper regions of castings. Interestingly, this defect was again reported to be associated with rapid mould filling.

Although not a defect in the mechanical sense of the word, surface staining of aluminium castings has also been reported. Warner et al. [32] observed brown splotches on the surfaces of aluminium bar castings which were attributed to deposits of liquid polystyrene remaining on the casting surface after the metal had solidified. Not only can this staining result in the reject of a casting for aesthetic reasons but can also indicate that conditions in the mould are approaching those conducive to the formation of the more serious “orange peel” defect.

## 2.2.4 Effect on Mechanical Properties

Mechanical failure of a casting is usually caused by the initiation of a propagating crack from the most serious defect in the structure [86]. The significance of any one defect in the structure of a casting depends not only on its size and shape but also on its location relative to the applied stress.

The most widely reported type of defect found in Lost Foam castings is the fold. Although this type of defect can manifest itself in a number of forms, for example bubble trails, cold laps and blisters, it is always associated with an oxide film. Campbell [87] suggested that many of these films were entrained into the bulk liquid by surface turbulence and their dry surfaces folded together. As the opposing faces constituted a ceramic to ceramic interface they could not bond and created a crack in the liquid. The doubled over nature of these films led to them being named “bifilms” and the variable strength that they imparted to castings was dependent upon the level of mechanical interlocking of their opposing faces as well as their alignment to any tensile force applied [88]. A planar “bifilm” oriented in the same direction as this force would cause no significant reduction in tensile strength whereas one lying across the axis of the force would have almost no strength at all.

Green and Campbell [89] illustrated these effects by varying the surface turbulence in the region of the metal front whilst casting Al-7Si-0.4Mg alloy into chemically bonded sand moulds. The castings produced in this experiment were subjected to tensile testing and the resultant values analysed using Weibull statistics [90]. The reliability of the castings was found to vary in accordance with the amount of surface turbulence present during mould filling and hence the content of “bifilms” present in the finished castings. The reliability results obtained by each method of manufacture are illustrated in Figure 2.26. Nyahumwa et al. [91] showed that “bifilms” also influenced the fatigue life of aluminium castings. Liquid Al-7Si-0.4Mg alloy was encouraged to enter test bar moulds in a manner that either encouraged or suppressed surface turbulence. After a T6 heat treatment the bars were subject to a high cycle fatigue life test where they were cycled in alternating tension-tension with stress ratio  $R = +0.1$ . They found that oxide films initiated 98% of the fatigue cracks observed

and the other 2%, which were created by slip planes, exhibited up to 100 times greater fatigue lives as shown in Figure 2.27.

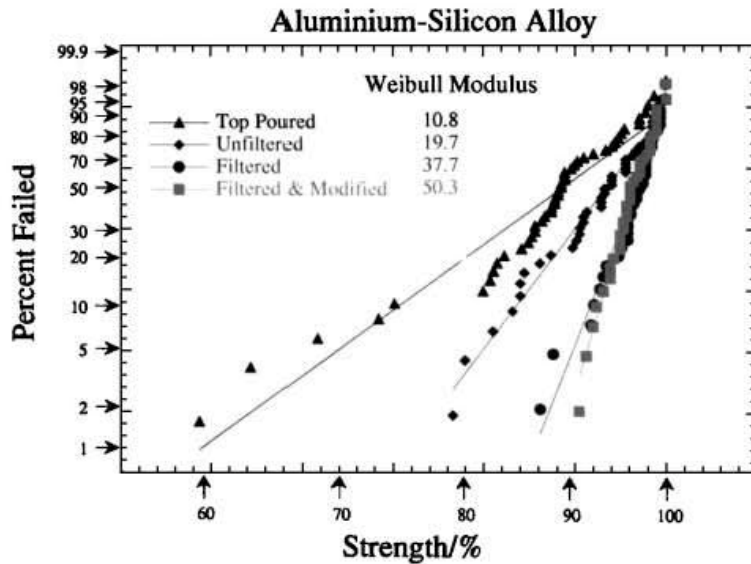


Figure 2.26: Relative reliability of Al-7Si-0.4Mg alloy cast by different methods, assessed by Weibull Plot and showing the scatter of tensile strengths [89].

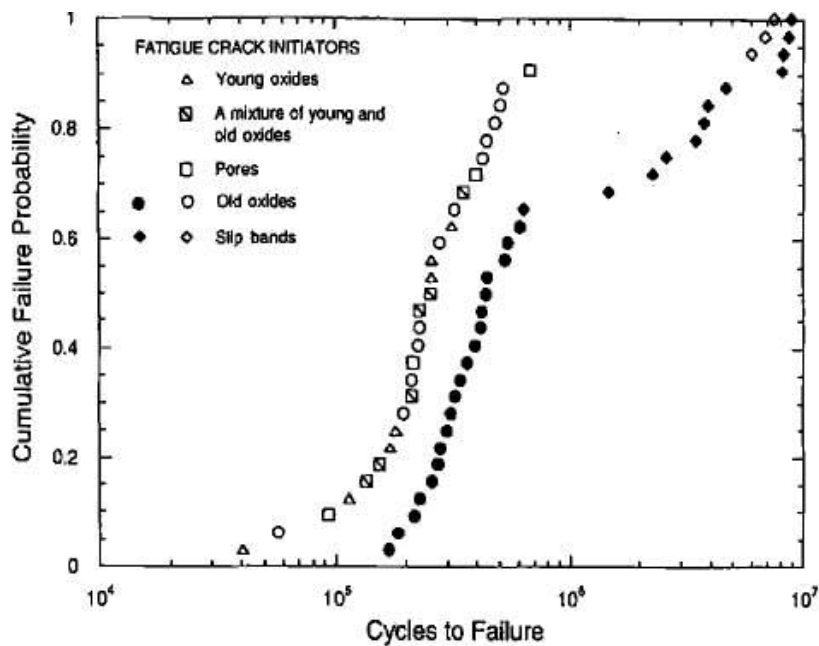


Figure 2.27: Effect of Bifilms on the fatigue life of unfiltered (open symbols) and filtered (solid symbols) castings where surface turbulence was reduced by filtration [91].

In addition to oxide films, internal pores also have a detrimental effect on the mechanical strength of a casting. Ammar et al. [92] studied the effects of porosity on the fatigue life of test bars made by low-pressure die-casting and Lost Foam moulding. The authors found that

96% of the die-cast specimens and 89% of those made using the Lost Foam technique failed as a result of a surface defect that acted as the initiator for the propagation of a fatigue crack. Additionally, they reported that an increase in pore area had a deleterious effect on the fatigue strength irrespective of the method of manufacture. However, for a similar pore area, for example  $100\,000\ \mu\text{m}^2$ , the die-cast samples exhibited a five-fold increase in fatigue life. The authors reasoned that propagation of a crack by a small pore took longer because it was constrained by the solid matrix between the individual pores. A large pore on the other hand, commonly found in the castings made by the Lost Foam method, failed much earlier because of the high stress levels associated with it.

Recently, pressurisation has been applied to Lost Foam moulds immediately after casting in an attempt to minimise the deleterious effects of shrinkage and gas porosity [71,93]. This was achieved by placing a mould in an open pressure vessel and, immediately after casting it, sealing the vessel with the mould still inside. The vessel was then pressurised with either air or a mixture of nitrogen and air to various levels ranging between 0.5 MPa and 1.47 MPa. Porosity levels fell rapidly from around 4% when solidified under normal atmospheric conditions to 1% or less when a pressure of 0.5 MPa was applied during solidification. Although tensile strength increased slightly it was elongation that was most affected. This rose by up to 130% compared to castings solidified under atmospheric pressure. The severe effect that porosity had on elongation was supported by earlier work that determined the effect of second phase particles, including pores, on the ductility of copper [94]. The results are illustrated graphically in Figure 2.28.

It is interesting to note that some researchers report that pores are more important in initiating mechanical failures than “bifilms” [95,96] whilst others suggest the opposite [87,88]. This may be somewhat irrelevant if both are considered as entrainment defects with the pore being treated only as a more open form of “bifilm”.

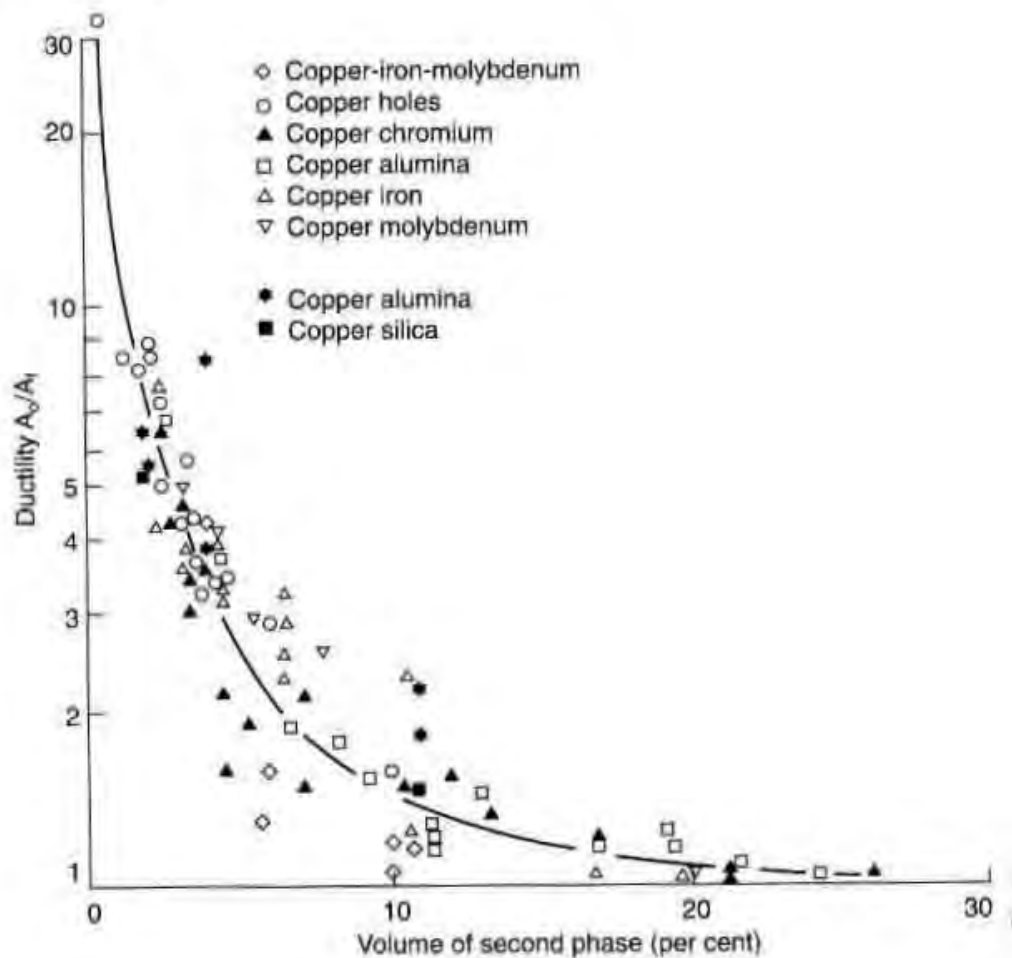


Figure 2.28: Ductility of copper containing a dispersion of second phases (including pores) [94].

### 2.3 COUNTER-GRAVITY FILLING OF LOST FOAM CASTINGS

The velocity of the liquid metal front entering and travelling through the mould during the filling operation has a significant effect on the severity of defects found in Lost Foam castings. Conventional gravity filling, however well regulated by application of automated filling systems and control of process characteristics such as polystyrene foam pattern density and coating permeability, is inherently prone to the creation of defects because of the influence of gravity. If the casting is top-gated, the complete filling cycle is carried out in the direction of the gravity vector. In this case, not only does the metallostatic head increase throughout the filling process but also degradation products (of lower density than the liquid metal), move counter to the direction of metal flow. These two phenomena promote formation of defects through entrainment and entrapment. The situation is improved somewhat if the

casting is bottom-gated because the gaseous pattern degradation products flow in the same direction as the incoming metal, and therefore away from the metal front. However, in this case, metallostatic pressure and metal front velocity decrease throughout the fill process whether this is required or not.

A radical change to the system of metal transfer can be achieved by upward displacement of metal into a mould. Filling the mould in the opposite direction to the gravity vector allows precise control over the metal front velocity throughout the filling cycle whilst promoting optimum removal of degradation products. A number of counter-gravity casting systems have been developed in the last few decades. The most common method is low pressure casting in which air or an inert gas is used to pressurise an enclosed furnace [97]. This forces the melt up a riser tube and into the mould. Other systems use partial vacuum, or various forms of pump or electromagnetic action [87,98] to draw up the metal.

The first mention of counter-gravity casting being applied to Lost Foam moulds was in 1997 when Bast [99] brought together Lost Foam moulding and low-pressure casting. A mould, with its inlet located centrally in the base of the flask, was placed on top of a sealed pressure chamber that contained a crucible of liquid metal. A riser tube was placed in the liquid metal so that the other end was flush with the upper face of the chamber. The mould flask was positioned in such a way that the riser tube and the mould inlet were aligned. All joints were sealed and the chamber was filled with air at a pressure of up to 10 kPa (0.1 bar) which caused the metal to flow up the riser tube and into the mould. This early paper described the operation of the equipment, including the effects of pressure variation on filling rate, but did not provide any information on resultant casting quality.

Since that time, a number of other authors have applied counter-gravity casting to the Lost Foam process. Bakhtiyarov et al. [72] used a ductile iron treatment ladle as a moulding flask. The base of the ladle was modified to accommodate a vertically arranged riser tube, the upper opening of which was inside the ladle just above the base and the lower part protruded through the base into a reservoir of liquid metal. A foam cluster was located in the upper opening of the riser tube with thermocouples and pressure sensors attached, so that temperature, vacuum levels and metal front position could be monitored during filling. The

ladle was filled with dry, unbonded olivine sand and then a double skinned lid, fitted with a series of 25.4 mm diameter vents, was fixed to its upper face. This lid was connected to a variable vacuum source of between 76.2 and 84.8 kPa (0.75 – 0.85 bar) which, when applied, caused ductile iron at about 1 400 °C to travel up the riser tube and into the mould. The vacuum was only released when the ingate between the riser tube and the casting had solidified and this caused any remaining metal in the riser tube to fall back into the crucible.

Bakhtiyarov et al. [100] cast a number of plates, but in some cases the flasks were inverted a few seconds after mould filling was complete. This procedure was named “a modified vacuum assisted counter-gravity casting method”. The idea of the inversion was to provide hot liquid feed metal to the solidifying casting. The metal density of the samples produced by the standard counter-gravity casting method ranged from 7.17 g/cm<sup>3</sup> to 7.25 g/cm<sup>3</sup> whereas those cast using the technique involving inversion had densities of between 7.28 g/cm<sup>3</sup> and 7.45 g/cm<sup>3</sup>. Inverting the flask within a few seconds of filling reduced the difference in the temperatures recorded throughout the casting and resulted in a slower overall solidification time. The authors suggested that these two effects encouraged the escape of gaseous products into the moulding sand and therefore reduced casting porosity.

Finally, Penumadu et al. [74] has used an electromagnetic pump to fill Lost Foam moulds in a counter-gravity fashion. By varying the power to the pump, metal flow rate and pressure was varied during the filling of a number of plate castings in A356 aluminium alloy.

Although interest in the application of counter-gravity filling to the Lost Foam process has grown in the past few years, the flow controls have been very primitive. These include using a gas pressure profile to encourage the liquid metal to fill the mould in the desired manner and direct pressure measurement in the launder system of the electromagnetic pump to approximate metal flow. The main drawback with these methods was that neither used a real-time, closed-loop feedback system. Although thermocouples, inserted at various positions within the patterns, gave some insight into the position of the metal front at certain points throughout the fill process, these are only snapshots of the complete filling cycle. Another aspect lacking from the published literature was quantitative data concerning the number and deleterious nature of defects associated with counter-gravity filling. This is not surprising

because, without knowing exactly how liquid metal filled the mould, it was not possible to determine whether the filling technique or the level of process control exerted the most influence on casting quality results.

## **2.4 FOAM-METAL INTERFACE PHENOMENA**

Three distinct zones are present during the filling of a Lost Foam mould. These are, (i) the volume occupied by the liquid metal, (ii) the volume occupied by the polystyrene pattern and (iii) a region in between these two in which the pattern material is in one or more stages of decomposition. As filling proceeds the liquid metal volume increases at the expense of that of the polystyrene pattern. The dynamics of the foam-metal interface region not only influence the rate at which the metal advances but also the mechanism that allows this to occur.

Published literature puts forward a number of filling mechanisms some of which are stable, for example the contact mode [17] and some which are unstable, like the collapse mode [19]. However, all authors concur that the foam-metal interface region contains varying levels of liquid and gaseous degradation products depending upon the properties of certain elements of the system being used. These characteristics include the casting alloy, pouring temperature, pattern composition, coating permeability and coating conductivity.

Hirt [101] observed the filling of a number of Lost Foam moulds by means of real-time X-ray radiography in order to verify modelling predictions made by FLOW 3-D. He remarked that there appeared to be a gravity influence on the motion and an asymmetrical appearance to the metal front that was unrelated to the hydrostatic pressure and proposed that this phenomenon might have occurred as a result of a Rayleigh-Taylor instability being present at the foam-metal interface during filling.

### **2.4.1 Hydrodynamic Instabilities**

A hydrodynamic instability is essentially the unstable flow of a fluid whilst in motion. Any unstable flow can evolve into a chaotic state of motion called turbulence. A flow is unstable if small disturbances in the initial flow do not die out but instead grow into larger disorders that influence a significant part of the system.

Although Hirt [101] is the only author to have hitherto postulated the occurrence of a hydrodynamic instability at the foam-metal interface, the significant density and viscosity differences between the liquid metal and the liquid polystyrene [102-104] could encourage the existence of one of a class of instabilities to which the Rayleigh-Taylor type belongs.

#### ***2.4.1.1 The Rayleigh-Taylor Instability***

In 1880, as part of an effort to better understand the formation of cirrus clouds, Lord Rayleigh first investigated the interfacial motion that occurs when a heavy fluid is supported by a lighter one [105]. He considered the idealised case of two incompressible immiscible fluids in a constant gravitational field. Some seventy years later Taylor [106] recognized that Rayleigh's interfacial instability also occurs for accelerations other than gravity. Although the classical case involves constant acceleration, a Rayleigh-Taylor instability can also occur for time-dependent accelerations whenever the acceleration is directed from the light to the denser fluid.

A simple but explicit example of a Rayleigh-Taylor instability is when a glass of water is held inverted. This causes the water to fall out at the sides of the glass whilst a column of air rises along the centre in its place. Although the atmospheric pressure of the air column is sufficient to support the weight of water, the instability is caused by tiny perturbations at the interface. It is not difficult to make the comparison between this example and that of Lost Foam casting, with the glass substituted for a mould, the water for liquid metal, and the air for liquid or gaseous polystyrene.

The interfacial perturbations may be of a single wavelength,  $\lambda$ , or comprise a superimposition of many waves, known as a spectrum. Structures of the light fluid penetrating the heavy fluid are called bubbles whilst the corresponding fingers of the heavy fluid are called spikes. An illustrative example of a Rayleigh-Taylor instability is shown in Figure 2.29. A single wavelength grows exponentially in time before saturating to a constant terminal velocity, but when a spectrum of modes is present the interactions between the modes result in turbulent flow characterised by high levels of mixing between the fluids.

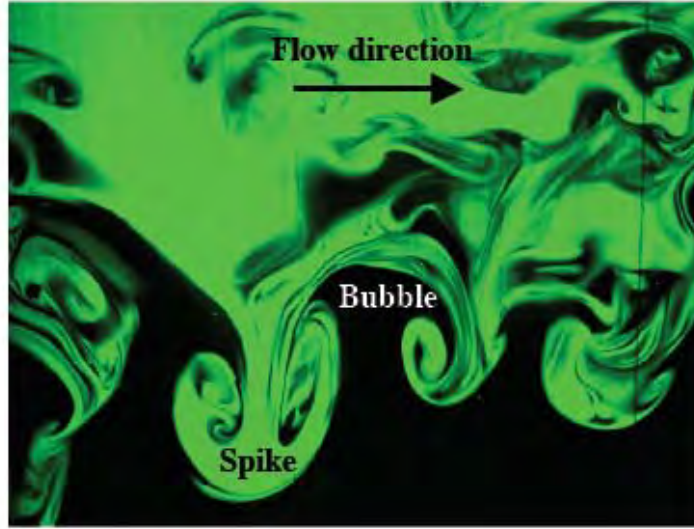


Figure 2.29: Example of a Rayleigh-Taylor instability set up by co-flowing streams (heavy above light) of different densities.

A Rayleigh-Taylor instability that propagates at the interface between two miscible fluids obeys the following equations of motion [107]:

$$\frac{\partial \rho Y_i}{\partial t} + \nabla \cdot (\rho Y_i \vec{u} + \vec{J}_i) = 0; \quad (i = 1, 2) \quad \text{Equation 2.7}$$

$$\frac{\partial \rho \vec{u}}{\partial t} + \nabla \cdot [\rho \vec{u} \vec{u} + p \vec{\delta} - \vec{\tau}] = \rho \vec{g} \quad \text{Equation 2.8}$$

$$\frac{\partial E}{\partial t} + \nabla \cdot [(E + p) \vec{u} - \vec{\tau} \cdot \vec{u} + \vec{q}_c + \vec{q}_d] = \rho \vec{g} \cdot \vec{u} \quad \text{Equation 2.9}$$

where  $\rho$  is density,  $Y_i$  is the mass fraction of the species  $i$ ,  $\vec{u}$  is velocity,  $\vec{J}_i$  is a diffusional mass flux,  $p$  is pressure,  $\vec{\delta}$  is the unit tensor,  $\vec{\tau}$  is the viscous stress tensor,  $\vec{g}$  is gravity (or frame acceleration),  $E = \rho(e + \vec{u} \cdot \vec{u}/2)$  and is the total energy (with  $e$  being internal energy),  $\vec{q}_c$  is the conductive heat flux and  $\vec{q}_d$  is enthalpy diffusion.

For incompressible fluids, Equation 2.7 reduces to

$$\frac{\partial \rho}{\partial t} + \vec{u} \cdot \nabla \rho = \rho \nabla \cdot \left( \frac{D}{\rho} \nabla \rho \right) \quad \text{Equation 2.10}$$

where  $D$  is diffusivity [108] and the pressure field satisfies a Poisson equation [109].

For two incompressible immiscible fluids with an interfacial perturbation of wave number  $k$  and amplitude  $\eta$ , such that  $\eta \ll \lambda$  (where  $\lambda = 2\pi/k$  is the wavelength), inviscid linear stability theory [105] predicts that  $\eta$  will satisfy the following ordinary differential equation:

$$\frac{d\eta}{dt} = (Agk)^{1/2}\eta \quad \text{Equation 2.11}$$

where  $g$  is a constant acceleration and  $A$  is the Atwood number:

$$A \equiv \frac{\rho_2 - \rho_1}{\rho_2 + \rho_1} \quad \text{Equation 2.12}$$

with  $\rho_1$  and  $\rho_2$  being the densities of the light and heavy fluids respectively [110]. Thus, the initial growth rate is exponential as in Equation 2.13.

$$\eta(t) = \eta_0 \exp[(Agk)^{1/2}t] \quad \text{Equation 2.13}$$

where  $\eta_0 = \eta(0)$

Viscosity and diffusivity inhibit high wave number growth and diffusion stabilizes the flow above a critical wave number. Including viscous and diffusive effects, the growth rate derived from a linear stability analysis is:

$$\eta(t) = \eta_0 \exp\left\{[(Agk/\psi + v^2k^4)^{1/2} - (v + D)k^2]t\right\} \quad \text{Equation 2.14}$$

where  $v$  is kinematic viscosity and  $\psi$  is a function of  $A$ ,  $k$  and the initial diffusion thickness of the interface [111].

#### **2.4.1.2 The Saffman-Taylor Instability**

In 1956 Sir Geoffrey Taylor visited a small oil company and became interested in the specific problem associated with recovery of oil from porous rock. Initially, oil could be extracted by the intrinsically high pressure in the reservoir, but once this had been exhausted another fluid

such as water was injected to allow further extraction to take place. During this “water-flooding” operation a hydrodynamic instability developed at the interface between the oil and the water. The instability arose because the less viscous water was used to push the more viscous crude oil in a porous or relatively confined space. As a result ‘fingers’ of the less viscous fluid grew into the viscous one. These became narrower as the flow proceeded through the reservoir and reached the entrance to the well prior to the displacement of all the oil.

In a paper written jointly with P.G. Saffman, they considered an idealised version of the problem in which they studied the interfacial instability of a flow between two fluids of differing densities and viscosities within a Hele-Shaw cell [112]. A Hele-Shaw cell comprises two parallel glass plates separated by a small gap  $b$ , and was used because representative transparent porous media were not available. In the original experiment only one stable finger was observed to propagate steadily. The width of the finger resulted from the competition between the capillary forces that tended to maximise the radius of the curvature at the tip of the finger and therefore widen it, and the viscous forces that sought the smallest resistance for finger propagation and hence encouraged it to narrow.

The Saffman-Taylor instability is essentially the over-damped analogue of the Rayleigh-Taylor instability and can be envisaged in terms of Lost Foam casting where the pattern has a relatively thin cross section, for example a plate, and is filled from the bottom so that the heavier, more fluid liquid metal is being forced into the mould below the lighter, more viscous polystyrene residue, and tries to displace it. Two examples of the Saffman Taylor instability, taken from the same set of experiments, are illustrated in Figure 2.30.

In both cases, a horizontally arranged Hele-Shaw cell was used in which the gap between the plates was set at approximately 0.2 mm [113]. The cell was filled initially with pancake syrup at a viscosity of 3 200 cP (3.2 Pa.s), and then isopropyl alcohol was forced through it by means of a syringe. The isopropyl alcohol had a viscosity of only 2.43 cP (0.0024 Pa.s) and the resultant displacement of the pancake syrup produced the image depicted as Figure 2.30 (a). The experiment was repeated with the pancake syrup being substituted by corn syrup with

a viscosity of 24 000 cP (24.0 Pa.s), and the pattern of fingering was thicker, as shown in Figure 2.30 (b).

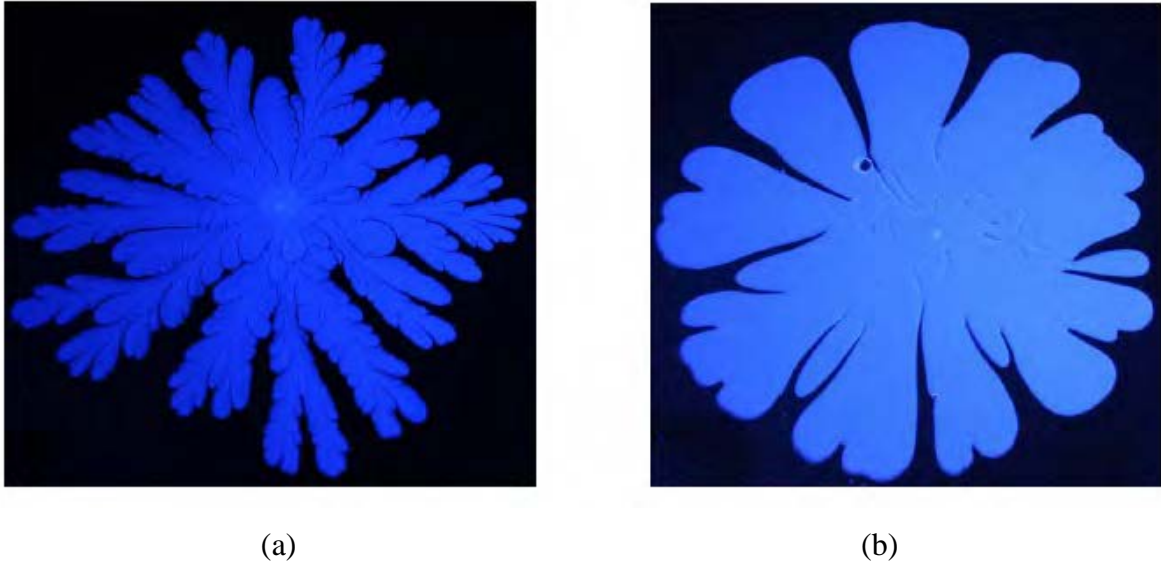


Figure 2.30: Illustration of the Saffman-Taylor instability where the viscosity of the displaced fluid is significantly smaller in (a) than in (b).

Ladtkow [113] reasoned that the difference in the two patterns was caused by viscosity differences between the two displaced fluids and suggested that in the first experiment, where there was a smaller viscosity difference between the two interacting fluids, a lower pressure gradient was present during displacement. This permitted the isopropyl alcohol to flow at a higher velocity and form longer, thinner fingers that, in some cases, broke up into sub-fingers.

When flow through a porous medium is considered in terms of a co-ordinate system where  $x$  is directed vertically upwards in the direction of the base state fluid flow at velocity  $V$ , and  $y$  and  $z$  lie in a horizontal plane, flow over distances greater than the pores themselves can be considered in terms of Darcy's law [51]:

$$\nabla \cdot \mathbf{u} = 0 \quad \mathbf{u} = -\frac{k}{\mu} \nabla(p + \rho g x) = \nabla \phi \quad \text{Equation 2.15}$$

where  $\mathbf{u}$  is velocity of the penetrating liquid,  $k$  is permeability of the porous medium,  $\mu$  is dynamic viscosity of the penetrating liquid,  $p$  is pressure,  $\rho$  is density of the penetrating liquid,  $g$  is the gravitational constant and  $\phi$  is the velocity potential.

Saffman and Taylor [112] solved Laplace's equation for pressure in both fluids, subject to continuity of velocity and a prescribed pressure difference across the complete interface. Although Saffman and Taylor acknowledged that there could have been a transient zone between the two fluids, in which both intermingled, the authors suggested that this zone would have been so thin that its width was small compared to the length scale of motion. Therefore, for the purpose of mathematical analysis, they assumed that a sharp interface was present, across which the normal component of velocity was continuous and, neglecting surface tension effects, the pressure difference was zero.

To examine stability, the interface in the base state was taken to be  $x = 0$ , as depicted in a coordinate frame moving upwards at velocity  $V$ , and a small time-dependent perturbation,  $ae^{iny+\sigma t}$ , was added, where  $a$  was an arbitrarily small constant,  $n$  was an arbitrary integer and the sign of  $\sigma$  denoted stability (if negative) or instability (if positive).

The authors reasoned that, from the continuity of normal velocity, that the velocity potential gradients on  $x = 0$  equalled the velocity of the interface and could be given by:

$$\frac{\partial \phi_1}{\partial x} = \frac{\partial \phi_2}{\partial x} = V + a\sigma e^{iny+\sigma t} \quad \text{Equation 2.16}$$

The velocity potential functions are harmonic functions subject to the above boundary condition at the interface and such that the effects of the interface perturbation decay as the distance from it increases.

$$\phi_1 = Vx - \frac{a\sigma}{n} e^{iny-nx+\sigma t}, \quad \phi_2 = Vx - \frac{a\sigma}{n} e^{iny+nx+\sigma t} \quad \text{Equation 2.17}$$

Neglecting surface tension effects, Saffman and Taylor [112] found the solutions  $p_1, p_2$  ( $p_i = -\mu_i/k_i \phi_i - \rho_i g x$ ,  $i = 1, 2$ ) equating the pressures on the interface showed that the stability condition is as follows: when fluid 2 is forced upwards towards fluid 1 such that the undisturbed interface at  $x = 0$  is travelling at velocity  $V$ , the interface is stable if

$$\left(\frac{\mu_2}{k_2} - \frac{\mu_1}{k_1}\right)V + (\rho_2 - \rho_1)g > 0 \quad \text{Equation 2.18}$$

and unstable if the reverse inequality holds (for all wavelengths  $n$ ). Therefore, the authors showed that the effect of the more viscous fluid lying above the less viscous fluid, when the lower fluid was forced upwards, was destabilizing. Similarly, the effect of the more dense fluid lying above the less dense fluid, as in the Rayleigh-Taylor instability, was destabilizing.

By using a Hele-Shaw cell in their experimental work, Saffman and Taylor [112] were able to study fluid motion in essentially two dimensions and make use of the result that the motion of a viscous fluid, when the plates of the cell were vertically arranged, was such that the components of mean velocity across the interface could be written:

$$u = \frac{b^2}{12\mu} \left( \frac{\partial p}{\partial x} + \rho g \right), \quad v = -\frac{b^2}{12\mu} \frac{\partial p}{\partial y} \quad \text{Equation 2.19}$$

where  $b$  was the distance between the plates, the  $x$  axis was vertically upwards, the  $y$  axis parallel to the plates and the  $z$  axis perpendicular to the plates.  $u$  and  $v$  were then the components of mean velocity in the  $x$  and  $y$  directions respectively.

The components of velocity in Equation 2.19 were for flow in a porous media with a permeability of  $b^2/12$  and because there is direct analogy between flow in a porous media and that between parallel plates,  $k_1$  and  $k_2$  in Equation 2.18 can be replaced by  $b^2/12$ . Therefore, the critical velocity for the onset of the instability can therefore be determined from:

$$V = \frac{-g(\rho_2 - \rho_1)}{\frac{\mu_2}{b^2/12} - \frac{\mu_1}{b^2/12}} \quad \text{Equation 2.20}$$

where  $\mu$  = dynamic viscosity,  $b^2/12$  = permeability,  $V$  = velocity and  $\rho$  = density. Subscripts 1 and 2 refer to the upper and lower fluids respectively, for a case where fluid 1 is less viscous than fluid 2, and fluid 1 is driven upwards into fluid 2.

The authors also observed that when a finger developed in the channel, the ratio  $\lambda$  of the width of the finger to the width of the channel was approximately one-half, except when the flow speed was slow. Additionally, they determined the shape of the interface for one finger in a channel analytically. They found an infinite family of solutions dependent on the value of the

parameter  $\lambda$  which was undetermined analytically. Taking  $\lambda = 1/2$  in accordance with experimental observations of systems in which the flow is not slow, yielded a solution which was in good agreement with observations made experimentally. When the flow was slow, however, the experimental observations and the analytical results differed significantly. Saffman and Taylor were unable to explain this discrepancy.

### ***2.4.1.3 Kelvin-Helmholtz Instability***

Since Lord Kelvin [114] and Helmholtz [115] first pointed out that the relative motion of two media caused an unstable wave at the boundary between them, many theoretical and experimental efforts have been devoted to understand its properties. Today, the growing wave at such an interface is known as a Kelvin-Helmholtz instability after the names of the first two contributors. An example of such a wave is shown in Figure 2.31.

When a light fluid is located on top of a heavy fluid and shear is induced, for example, by moving the heavy fluid one way and the lighter fluid the other way, an unstable condition is created between the two. A slight wave forms at the interface between the fluids and grows and develops "rolls" which mix the light fluid into the heavy fluid e.g., waves on the sea. However, in many cases, one or both fluids are continuously stratified with density decreasing smoothly with height, for example the atmosphere above the sea. Nonetheless, a strong, smooth, shear (wind) can induce a similar instability and produce layers of turbulence. Whether or not the small disturbance triggers instability depends on the value of the Richardson number. This is a dimensionless parameter that measures the ratio of stratification, (*i.e.* how fast the density changes with height), to shearing.

$$R_i = \frac{gh}{u^2} \qquad \text{Equation 2.21}$$

where  $g$  is the acceleration due to gravity,  $h$  a representative vertical length scale, and  $u$  a representative speed. For a flow with a sufficiently small Richardson number, the noise will produce "rolls", as in the conventional Kelvin-Helmholtz problem, that lead to turbulent mixing.

If surface tension can be ignored, and for some short wavelengths, two fluids in parallel motion with different velocities and densities will yield an interface that is unstable for all speeds. However, the existence of surface tension stabilises the short wavelength instability until a velocity threshold is reached. The theory with surface tension included broadly predicts the onset of wave-formation in the case of wind-over-water.

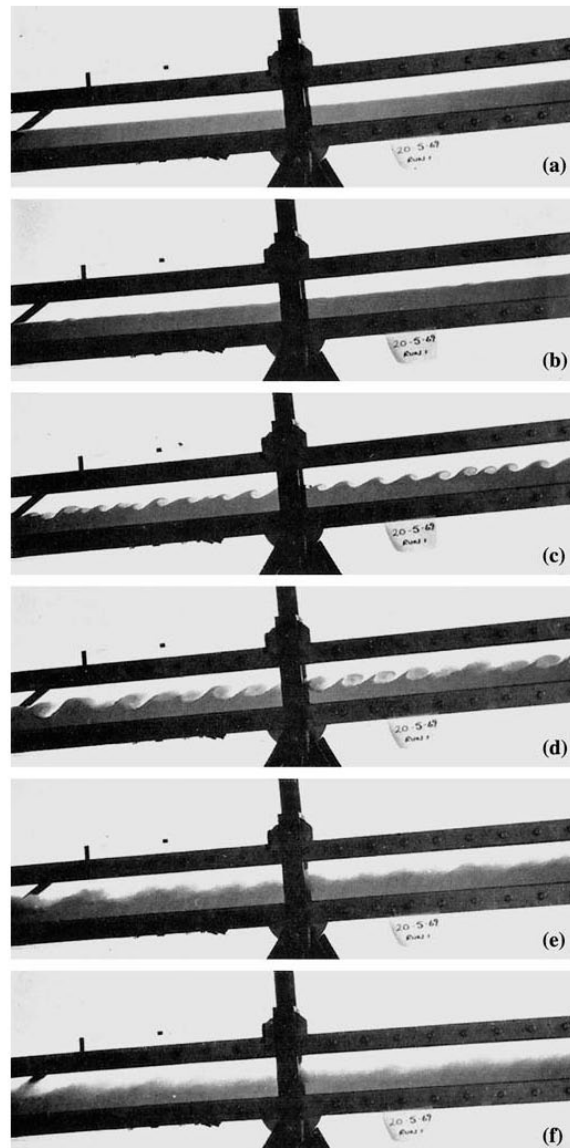


Figure 2.31: Laboratory demonstration of a Kelvin-Helmholtz instability. A long tank, filled with two resting fluids of different densities was tipped slightly. As the denser fluid sank towards the bottom and the lighter fluid rose, a counter flow was generated and the interface between the two fluids became unstable [116].

The prototypical case is that with one layer of lighter fluid overlying another of denser fluid, with the two moving horizontally in the same direction but with different velocities. The theory then states that a sinusoidal perturbation of wave number  $k$  on the discontinuous velocity and density interface is unstable if it meets the following inequality:

$$(\rho_2^2 - \rho_1^2)g < \rho_1\rho_2k(U_1 - U_2)^2 \quad \text{Equation 2.22}$$

where  $\rho_1$  and  $\rho_2$  are the upper and lower densities, respectively,  $g$  the gravitational acceleration and  $U_1$  and  $U_2$  the upper and lower velocities, respectively [117].

Figure 2.32 illustrates the growth of the instability and it can be seen that the initial perturbation grows into an oscillation because the pressure in a concavity is greater than that associated with a convex region of the interface. This encourages the wave peaks to be carried by the upper, faster flowing fluid and the velocity of the trough regions to be influenced by the slower moving, lower fluid. This results in a “rolling up” of the interface, in this case, in the direction of the vorticity direction of the mixing layer. The situation is the same where the upper and lower fluids move in opposite directions but in this case the velocity of one of the fluids, usually the lower, is represented as a negative value.

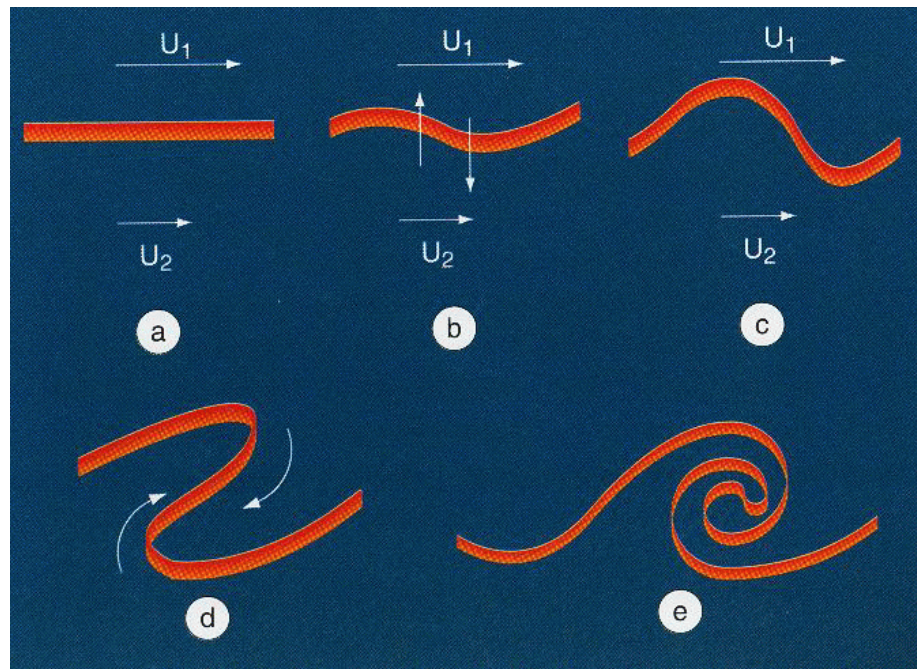


Figure 2.32: Illustration of the formation of a Kelvin-Helmholtz instability which subsequently grows into a roll [118].

## 2.4.2 Viscosity of Liquid Polystyrene

Fluid density and viscosity are important in promoting or suppressing instabilities. When a fluid is subjected to shear stress, it flows and resists the shear through molecular momentum transfer. The macroscopic effect of this molecular action, for most common fluids, is the physical property called viscosity. Since shear stresses cause motion in a fluid and result in differences in normal stresses at a point, it follows that a fluid at rest must have zero shear and uniform pressure at a point. This is the hydrostatic condition. In general, in any flow, layers move at different velocities and the fluid's "thickness" arises from the shear stress between the layers that ultimately oppose any applied force.

In Figure 2.33 two plates, each of area  $A$ , are kept apart by a distance  $H$ , by an intermediate fluid. If the two plates are then moved relative to each other at velocity  $V$  by a force  $F$ , Newton's law [119] states that the shear stress, the force divided by the area parallel to the force,  $F/A$ , is proportional to the shear strain rate,  $V/H$ . The proportionality constant is known as the dynamic viscosity,  $\eta$ . The effect of shear strain is quantified by the displacement per unit height,  $D/H$ , and the rate of this effect, i.e., the strain rate, is the velocity per unit height,  $V/H$ . Therefore, the viscosity  $\eta$  can be defined by:

$$\eta = \frac{\textit{Shear Stress}}{\textit{Strain Rate}} \quad (\textit{Pa.s}) \quad \text{Equation 2.23}$$

Thus, as the viscosity of a fluid increases, it requires a larger force to move the top plate at a given velocity. For simple, Newtonian fluids, the viscosity is a constant dependent only on temperature, but in the case of polymers such as liquid polystyrene, the shear strain rate also has an effect [120]. Figure 2.34 represents the effect that strain rate has on a liquid polystyrene melt at constant temperature, known as shear thinning.

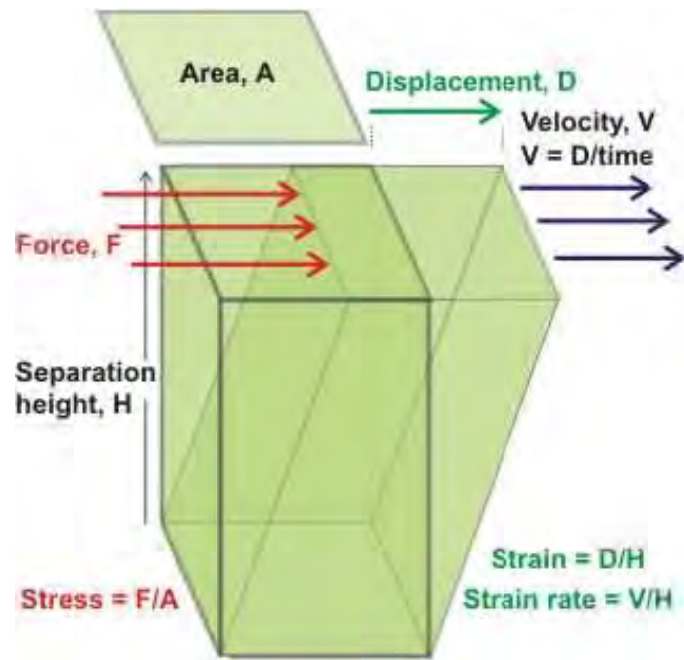


Figure 2.33: Steady shear flow of a fluid between a fixed and a parallel plate.

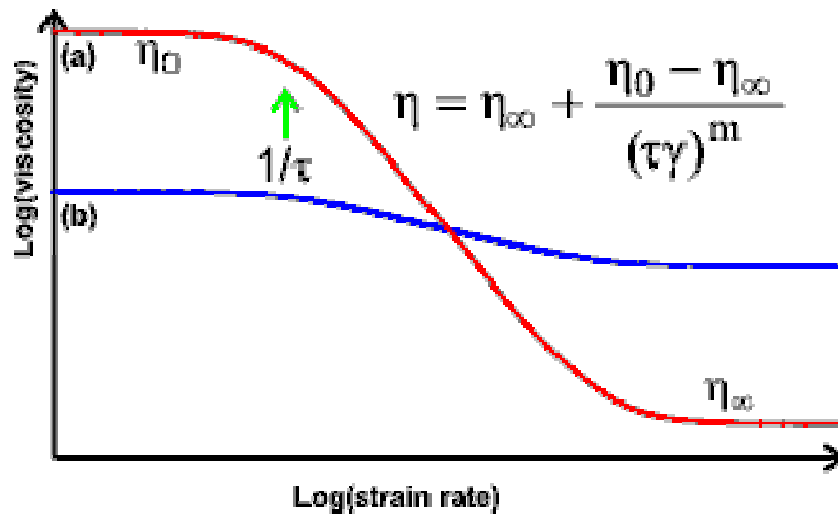


Figure 2.34: The effect of strain rate on the viscosity of (a) a strongly and (b) a mildly shear-thinning fluid [120].

The viscosity at any point on either of the two curves in Figure 2.39 is represented by:

$$\eta = \eta_\infty + \frac{\eta_0 - \eta_\infty}{(\tau\gamma)^m}$$

Equation 2.24

where  $\eta_0$  and  $\eta_\infty$  are the viscosities at zero and infinite shear strain rate respectively,  $\tau$  is a shear-dependant time constant that represents the reciprocal of the shear strain rate required to halve the viscosity,  $\dot{\gamma}$  is the shear strain rate and the exponent ( $m$ ) gives the degree of thinning (0 = no thinning, i.e., Newtonian behaviour and 1 = maximum thinning)

The viscosity of shear thinning fluids such as liquid polystyrene depends on the cross-sectional area in the direction of flow. At low flow rates, the long, thin molecules have large effective cross-sections due to them moving in random orientation to one another. However, as the shear strain rate increases they align with the flow and thereby reduce their effective cross-sections [121]. This results in a significant reduction in viscosity.

Published literature contains a number of references to the viscosity of liquid polystyrene melts measured over a range of shear strain rates at temperatures between 170 °C and 230 °C [120,122,123]. Although there was some difference in the actual values reported, probably due to slight chemical and molecular weight differences of the melts, the order of magnitude of each set of results was similar. Williams et al. [124] put forward an expression for the temperature dependence of viscosity for glass-forming systems, as shown in Equation 2.25.

$$\log a_T = \frac{-8.86(T - T_g)}{101.6 + T - T_g} \quad T_g < T < (T_g + 100) \quad \text{Equation 2.25}$$

where the parameter  $a_T$  is the Ferry temperature shift factor, which is approximately equal to the ratio of the zero shear viscosity at temperature  $T$  to that at the reference temperature  $T_g$ . In their paper the authors specify  $T_g = 135$  °C as the reference temperature for polystyrenes.

Figure 2.35, from work published by Osswald [122], approximates  $\eta_0$  for a melt of Polystyrol 144 CH at three different temperatures, and quantifies the effects of shear strain rate and temperature on this value.

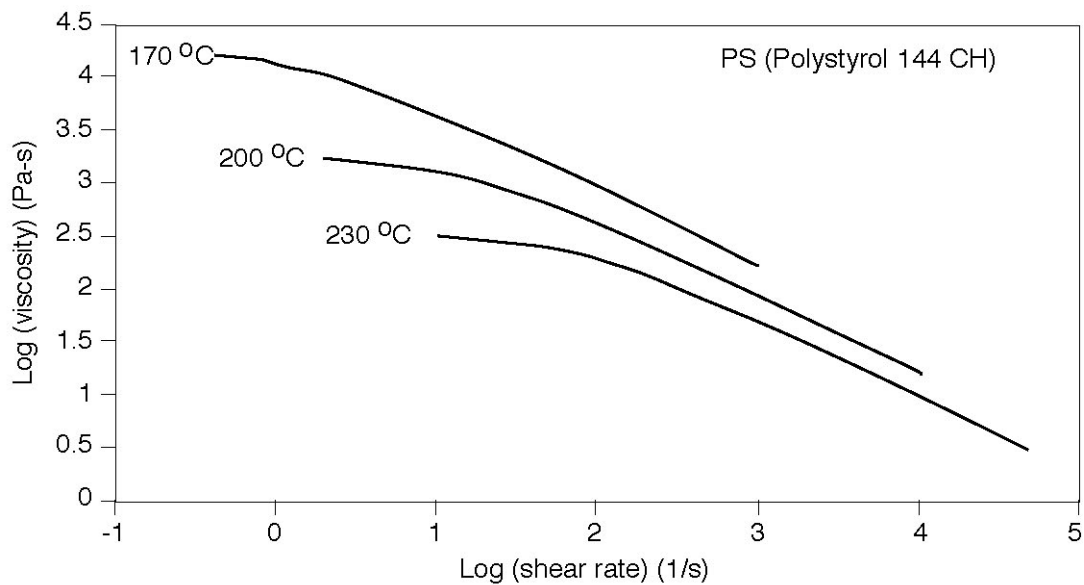


Figure 2.35: Influence of shear rate and temperature on the viscosity of a polystyrene melt [122].

Although polystyrene remains in the liquid phase at temperatures well over 300 °C [54], the bulk of published literature only considers melt viscosity up to 230 °C. This is probably because most of the research conducted relates to plastic injection moulding where the melt temperature is kept intentionally low to minimise any material degradation [125]. However, Merz and Colwell [126] showed empirically that it was also applicable to a melt at 450 °C. Additionally, Lomellini [127] studied the rheology of polystyrene with the aim of determining whether the Williams-Landel-Ferry equation was valid at temperatures in excess of  $T_g + 100$  °C,  $T_g$  being the glass transition temperature which has been reported at 95 °C for polystyrene [128]. He concluded that this approach was valid for polystyrene up to at least  $T_g + 185$  °C, the upper limit of his experiment, but did not comment on its accuracy at higher temperatures.

Apart from shear rate and temperature, a number of studies have suggested that the molecular weight of a polystyrene melt has a significant effect on viscosity. For linear polymers in which the monomeric units were linked together in linear fashion with little or no long chain branching, i.e., low-density polyethylene and high-density polyethylene,  $\eta_0$  increased linearly with molecular weight [129,130]. However, Fox and Flory [131] showed that when the molecular weight of a polystyrene melt,  $M_c$ , exceeded 38 000,  $\eta_0$  became proportional to  $M^{3.4}$ ,

(see Equation 2.26). They reasoned that individual chains became entangled with one another and this caused a sharp increase in zero shear viscosity above  $M_c$ .

$$\log\eta_0 = 3.4\log M + K \quad M > 38\,000 \quad \text{Equation 2.26}$$

where  $K$  is a constant at a particular temperature, and has the value of  $-13.40$  for polystyrene at a temperature of  $217\text{ }^\circ\text{C}$ .

Equations 2.25 and 2.26 only considered the effect of a single variable on the viscosity of a polystyrene melt. By combining them, Cox and Ballman [39] generated an expression that described both molecular weight and temperature dependence simultaneously. This is shown in Equation 2.27 below.

$$\log\eta_0 = 3.4\log M + [900.2/(T - 306.4)] - 18.38 \quad \text{Equation 2.27}$$

A comparison of calculated values for  $\eta_0$  with those obtained experimentally led to the conclusion that there was a “satisfactory agreement”. Equation 2.27 appears to be even more robust in terms of molecular weight variation. Fox and Flory [131] showed that the viscosity of a number of discrete polystyrene melts, each held at a temperature of  $217\text{ }^\circ\text{C}$ , but ranging in molecular weight from  $38\,000$  to  $316\,000$ , corresponded accurately with the prediction made by the equation that they put forward.

A polystyrene melt can also be characterised by the molecular weight distribution of the chains within its total mass. This is known as the level of polydispersity and is measured by means of the polydispersity index,  $I$ , which is the ratio between the weight average molecular weight,  $\overline{M}_w$ , and number average molecular weight,  $\overline{M}_n$ , of the melt such that  $I = \overline{M}_w/\overline{M}_n$  [102]. A melt where  $I < 1.1$  is monodisperse whereas above that value it is considered to have some level of polydispersity. The accuracy of the viscosity exponent of the Fox and Flory equation, i.e.,  $3.4$ , has been questioned by a number of researchers when applied to polydisperse melts [132,133]. However, Bernard and Noolandi [134] examined these claims using model molecular weight distributions and found them to be completely unjustified.

## 2.5 ALTERNATIVE PATTERN MATERIALS

### 2.5.1 Polymethyl Methacrylate

Expanded polystyrene is the most commonly used material for manufacturing patterns in the Lost Foam process. However, decomposition of this material at elevated casting temperatures produces carbonaceous substances that have been reported to be responsible for carbon pick-up in low carbon steel castings and surface imperfections across the complete range of ferrous alloys [135]. To overcome this limitation Moll and Johnson [136] developed polymethyl methacrylate (PMMA).

The principal advantage associated with PMMA is its ability to decompose with minimal carbon residue. This results from both the chemical composition of the material and the mechanism by which the material decomposes. Figure 2.36 illustrates the differences in chemical structure between polystyrene and PMMA. It can be seen that whilst the polystyrene monomer is made up of eight carbon atoms, that of PMMA consists of only five. Hence the potential to form carbon residues is reduced by over a third.

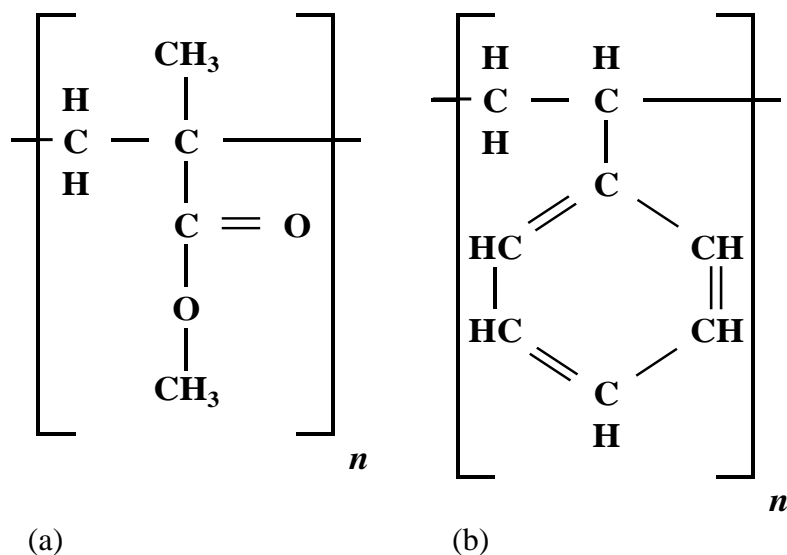


Figure 2.36: Chemical structure of (a) polymethyl methacrylate (PMMA) and (b) polystyrene

The PMMA molecule also contains two oxygen atoms and it is thought that these contribute to a decrease in carbon residue by reacting with and carrying away some of the carbon from the mould cavity. Madorsky [13] studied the degradation of this material in vacuum at elevated

temperatures and found that at 500 °C the products of volatilisation consisted almost entirely of monomer. However, at 1200 °C this had dropped to around 10% and the gaseous products were made up of lighter hydrocarbons and large amounts of carbon monoxide and carbon dioxide. PMMA is also devoid of a benzene ring in its structure and therefore another source of carbon is eliminated. In aluminium casting, where polystyrene patterns are used widely, the benzene ring does not pose a quality problem because casting temperatures are not high enough to decompose it into elemental carbon.

Mehta and Shivkumar [137] used thermogravimetric analysis (TGA) and differential scanning calorimetry (DSC) to evaluate the physicochemical phenomena that occurred during the thermal degradation of PMMA between 50 °C and 600 °C. They found that, although PMMA started to collapse and melt at a higher temperature than polystyrene, it began to volatilise some 25 °C to 50 °C earlier. In addition, the end temperature at which it had fully volatilised was approximately 50 °C lower than that of polystyrene.

The researchers also noted that, during the degradation process, PMMA produced a larger quantity of gas than a corresponding amount of polystyrene and suggested that this was because the mechanism of degradation was by “unzipping” rather than by the random scission mechanism associated with polystyrene. Their graph comparing the gas production from both materials is contained in Figure 2.37.

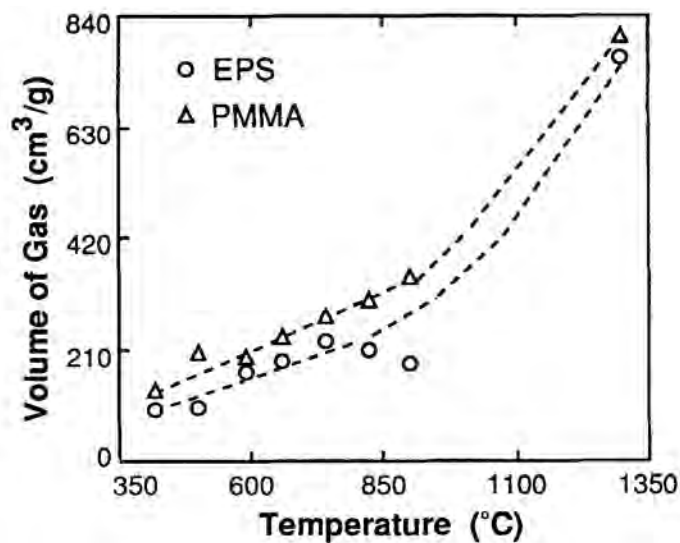


Figure 2.37: Volume of gases (standard temperature and pressure) produced upon the degradation of a unit mass of PMMA and polystyrene as a function of temperature [137].

Since foamed PMMA is relatively expensive to produce, a number of copolymers of polystyrene and PMMA have been developed as pattern materials for ferrous use. Typically, these consist of 70 wt.% polystyrene – 30 wt.% PMMA and 30 wt.% polystyrene – 70 wt.% PMMA.

## 2.5.2 Bromine-based Additives

Brominated additives, such as hexabromocyclododecane, have been used as flame retardants in structural polystyrene components since the 1970's [138] and experiments have shown that bromine in the polystyrene matrix promotes cleavage of the polymer chain into smaller units which increases the rate at which depolymerisation takes place [139]. In the last few years, a variety of bromine bearing materials have been added to polystyrene pattern material used in the Lost Foam process with the primary goal of eliminating fold defects. The chemical structures of three of these additives are shown in Figure 2.38 [140].

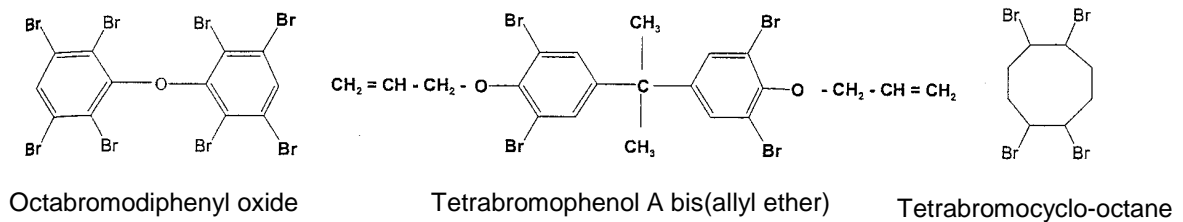


Figure: 2.38: Chemical structure of some organic brominated additives used in the Lost Foam process [140].

Both Bertini [139] and Molibog et al. [141] showed that a polystyrene that had been treated with a bromine-based additive decomposed more quickly than a standard one and this resulted in a reduction of the amount of partially decomposed polymer in the mould which could form defects in the casting. Molibog et al. [141] simulated foam decomposition by pushing treated and untreated foam bars against a strip heater, during which the liquid foam decomposition products were collected and subsequently analysed using gel permeation chromatography. The residue from the treated foam bars was found to have a lower molecular weight than that of the untreated bars, and this was thought to have resulted in the residue having a lower viscosity. Sonnenberg et al. [142] determined that this molecular weight reduction was due to

the liberation of free radicals from the additives during the heating cycle and these attacked the polystyrene matrix and reduced its molecular weight.

Hess et al. [143] examined the effect of three foam characteristics (bead type, bead fusion and nominal pattern density) on metal velocity and defect formation in aluminium casting. Two chemistries of expanded polystyrene beads were examined, including untreated beads and those treated with a bromine-based additive. Both beads had a molecular weight of 280,000 and an average size of 350 microns. The bromine additive reduced the incidence of pyrolysis-related defects with the measured defect area being approximately 12% of that obtained when untreated foam was used. However, the reduction in defect area was not as noticeable in thick pattern sections where the area-to-perimeter ratio was large, probably because, even though the foam was decomposing more quickly, the liquid residue had to be transported to the mould walls a longer distance, before removal through the pattern coating.

The lower activation energy in brominated foam makes its filling speed less sensitive to metal temperature. However, this dependence is weak even in non-brominated foam, and the filling speed remains essentially unaffected [17].

## **2.6 TECHNIQUES FOR MONITORING FILLING BEHAVIOUR**

The earliest and probably simplest way to visualise the filling sequence in Lost Foam casting was to build a transparent window into the side of the mould. This method was used by Butler and Pope [3] in 1964 to study the filling of lost foam moulds in detail. In their experiment they placed uncoated blocks of polystyrene on a mica window that acted as one vertical side of a sand mould. The patterns were filled from the bottom and the flow of molten aluminium recorded on film. Other researchers [8,29,45,145] have since used this method to study the influences of the pattern material, coating thickness and sand fineness on the filling of simple patterns with molten aluminium. Figure 2.39 contains a single frame from a video that captured the displacement of a vertically oriented polystyrene pattern by liquid aluminium as viewed through a transparent window.

However, mica windows are not permeable and therefore, in all of these experiments, the pattern decomposition products were not able to escape from the region adjacent to the window in the same manner as they would have in a conventional Lost Foam mould. Therefore, this technique, although easy to use, was not suitable for making quantitative measurements of mould filling behaviour.

Detection devices embedded in the foam pattern have also been used to monitor the position of the liquid metal as it flowed through the mould cavity. Yao and Shivkumar [145] used the thermometric technique to study filling behaviour in rectangular plate patterns when pouring different molten liquids, such as wax, tin, aluminium and copper. Figure 2.40 shows the typical thermocouple response times for each of these liquids and it can be seen that the temperature rose sharply as soon as contact was made.



Figure 2.39: Single frame of a video used to record the filling of a Lost Foam mould through a transparent window (*courtesy of Lovink B.V., The Netherlands*)

Detection devices embedded in the foam pattern have also been used to monitor the position of the liquid metal as it flowed through the mould cavity. Yao and Shivkumar [145] used the thermometric technique to study filling behaviour in rectangular plate patterns when pouring different molten liquids, such as wax, tin, aluminium and copper. Figure 2.40 shows the

typical thermocouple response times for each of these liquids and it can be seen that the temperature rose sharply as soon as contact was made.

By using an array of thermocouples, Yao and Shivkumar [145] were able to plot contour maps showing the position of the liquids during the filling cycle. They were also used to assess any variations in the speed of the fronts as they travelled through the moulds. This was done by approximating the front velocity from the time recorded for it to travel between two thermocouples of a known distance apart.

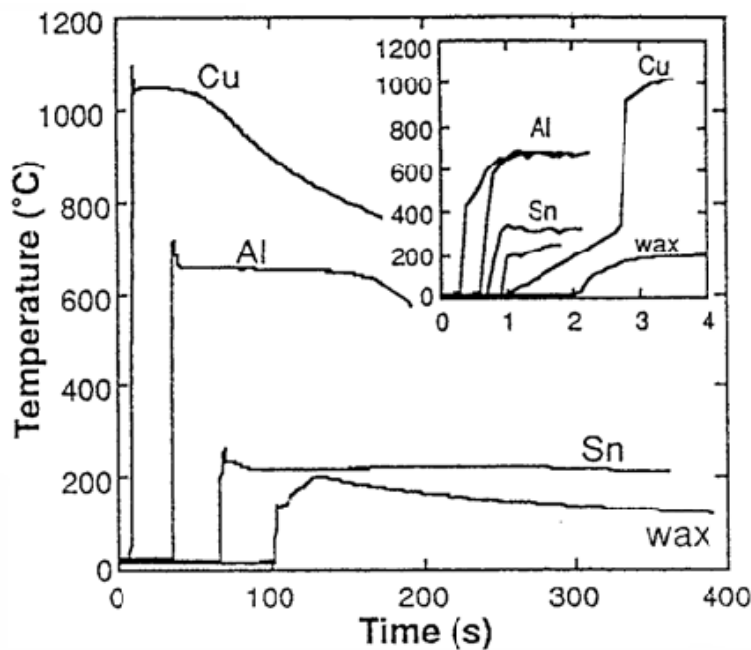


Figure 2.40: Typical response times of closed thermocouples located in polystyrene plates and displaced by different liquids [145].

This technique has the benefits of utilising conventional Lost Foam moulds and generating quantitative data, but it cannot determine in detail how the metal front moves between any two detectors, making any set of results open to multiple interpretations.

Although the first attempts at using real-time X-ray to observe metal filling behaviour were over 60 years ago [146] its application for this task only became more widespread in the mid 1990's. In 2002 Sun et al. [21] observed the effects of bead fusion and coating permeability on the filling of vertically oriented polystyrene plates with liquid aluminium. The X-ray system that was used included a 320 kV metal ceramic tube with a spot size of 0.8 mm x 0.8 mm and

a 228 mm tri-field image intensifier linked to a video camera. The complete system was housed in a lead lined room with remote control of the X-ray and data acquisition systems.

Subsequently real-time X-ray has been used to study many other aspects of the process, such as the formation of lustrous carbon and the effect of glue joints [63,148]. For example, Sun et al. [147] also made a number of iron castings from vertically oriented plate patterns that had either a low or normal level of bead fusion. Figure 2.41 contains two real-time X-ray images of the filling of a normally fused pattern together with the resultant casting, and Figure 2.42 shows a similar set of images but relating to a poorly fused pattern.

From resultant videos the authors determined metal velocity changes and the profile of the metal front during filling as well as the total filling time. Additionally, they were able to superimpose a map of the advancing metal front on the casting and relate it to the location and morphology of any lustrous carbon defects.

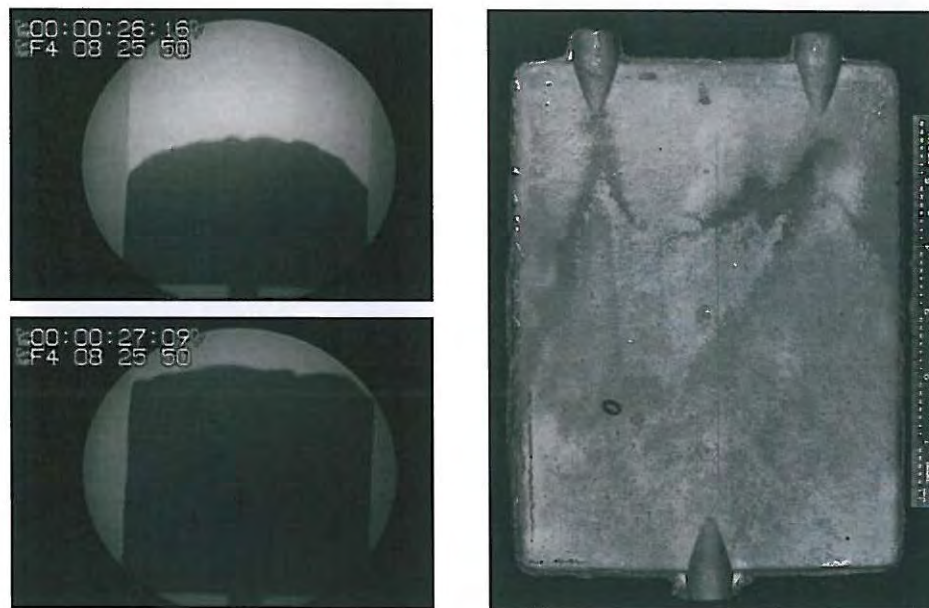


Figure 2.41: Real-time X-ray images of the filling behaviour with a polystyrene pattern whose beads had undergone the correct amount of fusion and a photograph of the resultant casting [147].

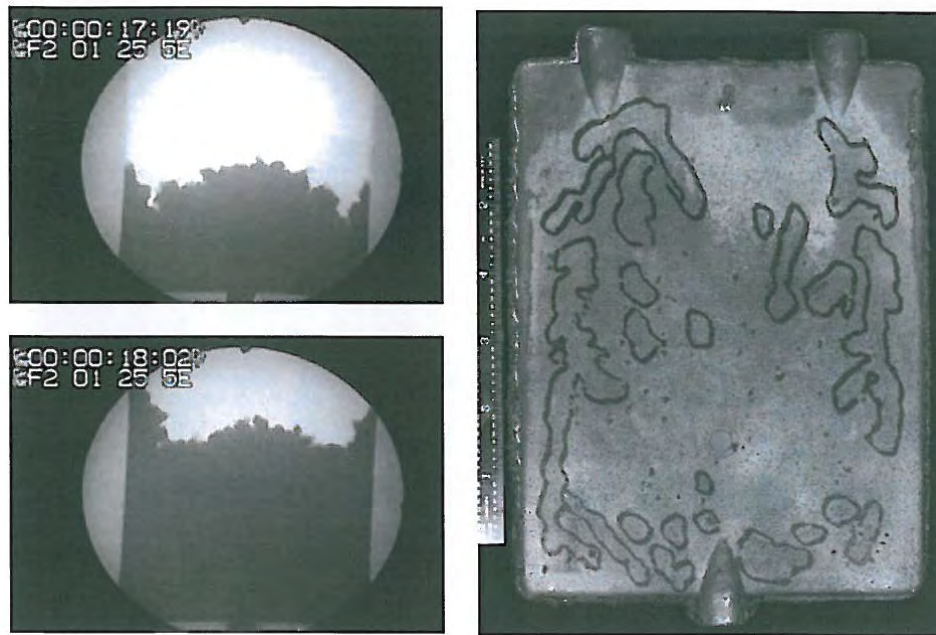


Figure 2.42: Real-time X-ray images of the filling behaviour with a poorly fused foam pattern together with a photograph of the resultant casting [147]. The black lines on the surface of the casting denote the location of lustrous carbon defects.

The main limitations to this technique are that as the pattern thickness, mould thickness or the density of the cast alloy increases, the X-ray source intensity also needs to increase in order to be detected by the receiving unit. Also, three-dimensional patterns with hollow sections are difficult to interpret because the flow of liquid metal up one face of a pattern may mask filling of a section of the pattern behind it. Therefore, this technique has been limited to observing the filling of simple 2-dimensional shapes.

## 2.7 STATISTICAL ANALYSIS OF THE PROPERTIES OF CASTINGS

When a set of specimens from a single casting or a batch of castings made under seemingly identical conditions are subject to mechanical testing, the measured strengths are normally scattered about a median value. The extent of this scatter provides an indication of the reliability of the material in respect of the mechanical properties being assessed. A number of statistical techniques, such as normal distribution, Weibull distribution and the type I extreme value distribution, have been used to describe the scatter of data.

Green and Campbell [148] evaluated these three distributions, to determine which most accurately described the scatter of tensile test data, and determined that the Weibull distribution was most accurate. The Weibull distribution function linearises most engineering data distributions and therefore makes it possible to estimate the behaviour of a population of infinite size from a small amount of data. Unlike the normal distribution, a Weibull distribution is skewed such that it has a long tail of low strengths and a sharp fall off in the high strength region.

The Weibull distribution can be used as a tool for casting quality analysis because it enables a single figure quantification (modulus,  $\lambda$ ) to be used to describe the strength distribution. This is a more accurate description than a standard deviation, which assumes a symmetrical distribution of strength about a mean value [89,149]. Generally, a minimum of 20 to 30 samples is required for a good characterisation of the strength of a brittle material [149]. The Weibull distribution can be expressed in the cumulative, three-parameter form as [90]:

$$F_w = 1 - \exp \left\{ - \left( \frac{x - \mu}{\sigma - \mu} \right)^\lambda \right\} \quad \text{Equation 2.28}$$

where  $F_w$  = the cumulative fraction of failures in the mechanical property,  $x$  = variable being measured, e.g. tensile strength,  $\sigma$  = characteristic stress at which 1/e of specimens survived,  $\mu$  = boundary value below which no failure can occur and  $\lambda$  = a width parameter, often referred to as the Weibull modulus.

As the value of  $\lambda$  increases, the spread of  $x$  narrows. When characterising fracture distributions, the Weibull distribution is often used in two-parameter form with  $\mu$  set to zero:

$$F_w = 1 - \exp \left\{ - \left( \frac{x}{\sigma} \right)^\lambda \right\} \quad \text{Equation 2.29}$$

The value of modulus,  $\lambda$ , can be calculated by taking the logarithm of Equation 2.29 twice to give a linear equation:

$$\ln \left\{ \ln \left( \frac{1}{1 - F_w} \right) \right\} = \lambda \ln(x) - \lambda \ln(\sigma) \quad \text{Equation 2.30}$$

By plotting  $\ln\{1/(1-F_w)\}$  versus  $\ln(x)$  a straight line graph is obtained with slope  $\lambda$  and intercept  $-\lambda \ln(\sigma)$ , often referred to as a Weibull plot. Linear regression analysis is widely used to evaluate  $\lambda$ . The x values (e.g. UTS or elongation) are arranged in order of increment and a probability of failure, a number between 0 and 1, is assigned to each corresponding  $F_w$ . Since the sample tested is considered representative of a large population, the true value of  $F_{w,j}$  (the probability of failure of the  $j^{\text{th}}$  specimen) is not known and has to be estimated. This estimator equation should be chosen such that, on average, the errors arising each time due to this estimation compensate each other, and several estimators have been reported [149]. For the  $j^{\text{th}}$  specimen failure from a total of N results, four of the most common estimators are as follows:

$$F_j = \frac{j - 0.5}{N} \quad \text{Equation 2.31}$$

$$F_j = \frac{j}{N + 1} \quad \text{Equation 2.32}$$

$$F_j = \frac{j - 0.3}{N + 0.4} \quad \text{Equation 2.33}$$

$$F_j = \frac{j - 0.5}{N + 0.25} \quad \text{Equation 2.34}$$

Examples of skewed distributions and associated  $\ln\{\ln\{1/(1-F_w)\}\}$  versus  $\ln(\text{UTS})$  plots of three sets of data that were used to evaluate the effect of ingate design in open channel casting of aluminium are shown in Figure 2.43 [150]. It can be seen that the cumulative distributions are characterised by skews to the right with tails of weak specimens extending into the low-strength regions.

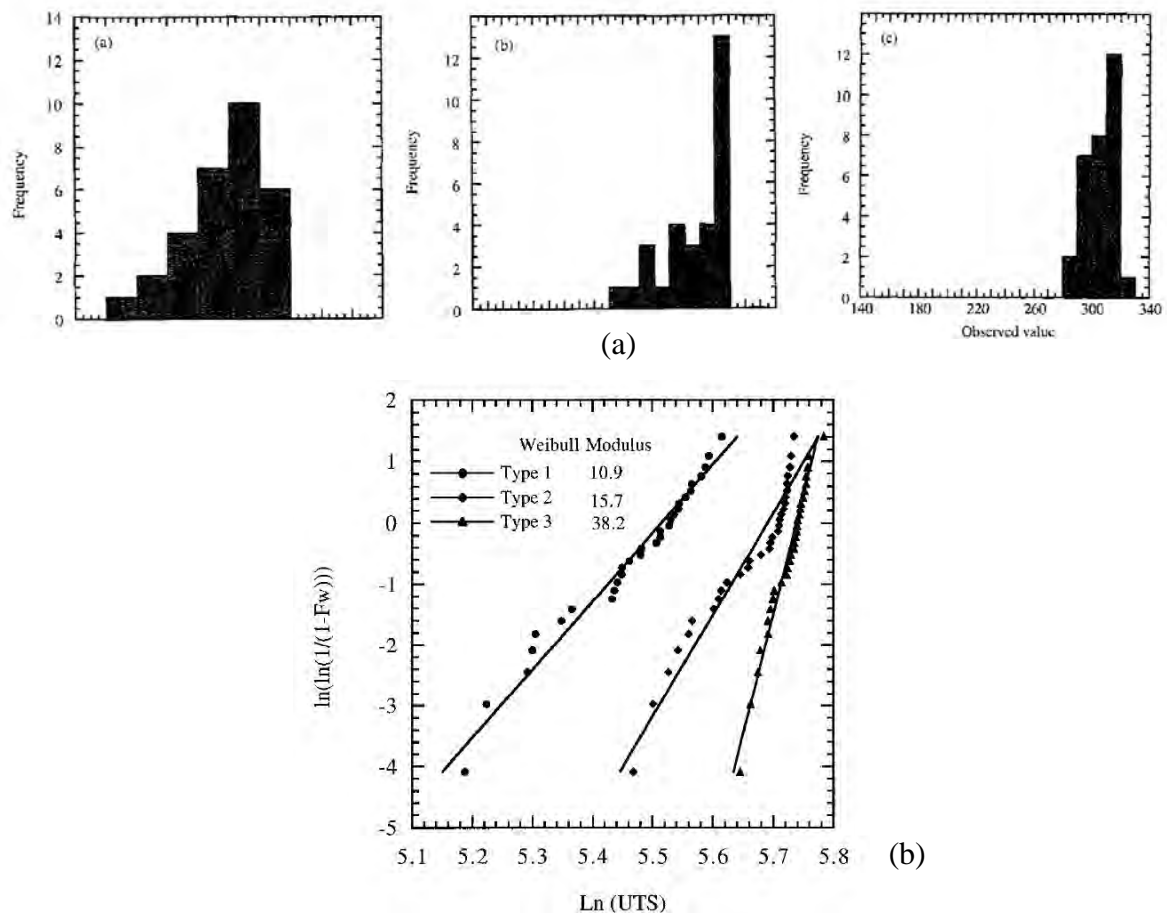


Figure 2.43: (a) Frequency and (b)  $\ln\{\ln\{1/(1-F_w)\}\}$  versus  $\ln(UTS)$  plots of aluminium castings made with three different designs of ingate [150].

## 2.8 SUMMARY

In contrast to all other casting processes, the filling of a Lost Foam mould with liquid metal is heavily influenced by the presence of the pattern, made from polystyrene, PMMA or a copolymer. This pattern must decompose and exit through the coating into the surrounding sand mould at such a rate that the metal front neither freezes prematurely nor hinders the transport of liquid and gaseous degradation products to the pattern walls and through the coating into the sand mass. To encourage this condition a large number of variables are controlled so that they either directly or indirectly affect the filling speed.

The running system has little or no influence on the velocity of the liquid metal as it travels through the mould and, up until recently, the main focus of attention in controlling this parameter has been the properties of the pattern coating. A highly permeable coating allows

the metal to move at a faster rate through the mould because the degradation products can escape more easily. Although this situation reduces misrun defects, it can disrupt the transport of liquid and gaseous phases of the pattern material to the mould walls and promote an unstable metal front that may result in entrapment of degrading pattern material. The application of a low permeability coating has essentially the opposite effect.

A significant amount of viscous, liquid polymer is generated when polystyrene patterns are used in conjunction with aluminium alloys. The liquid aluminium has a relatively low viscosity and this contrast between the two liquids may influence the stability of the interface as front velocity increases. To reduce the amount of liquid residue formed, bromine additives have been introduced into the polystyrene pattern material.

With such a critical parameter as velocity being controlled indirectly, it is not surprising that the Lost Foam process has been fraught with casting production and process reliability problems. However, over the past twenty-five years, systems have been developed for filling open channel moulds with direct and, in some cases, closed loop control of the metal velocity. For aluminium alloys it has been shown that controlled filling from the bottom of the mould eliminates surface turbulence and improves the reliability of the process.

The main purpose of this research has been to determine whether aluminium castings made by the Lost Foam process benefit from the application of controlled counter-gravity filling techniques. This involved a thorough study of the nature of the interaction between the advancing metal front and the receding Lost Foam pattern in order to understand its effect on casting quality. The initial part of this research applied conventional gravity-filling techniques in order to expose their level of inadequacy and this was followed by use of a directly controlled, counter-gravity filling technique so that velocity control could be maintained throughout the filling cycle.

## **3 EXPERIMENTAL PROCEDURE**

### **3.1 GRAVITY FILLING OF LOST FOAM CASTINGS**

A series of simple plate castings was made to determine the differences in the filling behaviour of Lost Foam moulds when patterns were gated either from the top or the bottom. In addition, a set of more complex frame castings was produced with identical running systems. This casting design encouraged the formation and subsequent recombining of multiple metal fronts during the mould filling process. Samples taken from these castings were subjected to tensile testing and the results compared with the observations made during mould filling.

#### **3.1.1 Mould Filling Observations**

##### ***3.1.1.1 Datalogger Method***

Plate and frame patterns were produced from pre-expanded, T-grade polystyrene beads with an average diameter of 1 mm, made on the same industrial pattern moulding machine from one set of horizontally parted, aluminium tooling. Both pattern types had overall dimensions of 363 mm long, 197 mm wide and 15 mm thick and, whereas the plate was essentially solid, the frame had seven large rectangular holes moulded in. The arrangement of these holes was such that the frame had a simple, 15 mm square section that consisted of two long bars with a further eight small ones arranged perpendicularly. Figure 3.1 shows the dedicated drag tools used to make both pattern designs. The tool on the left was for making frames and illustrates the arrangement of the bars.

After aging for 24 hours, one pattern of each design was sectioned into 15 mm cubes and density profiles obtained by measuring the mass and volume of each specimen. The patterns were then attached to dedicated running systems to form clusters as shown in Figure 3.2. Each running system consisted of a set of common elements as follows,

- (i) A pre-formed, proprietary brand, ceramic pouring basin.
- (ii) A 40 mm diameter, expanded polystyrene downsprue (but with a 10mm diameter hollow centre to minimise the temperature loss of the cast metal).

- (iii) A solid, expanded polystyrene runner bar (6.0 cm<sup>2</sup> cross section).
- (iv) A solid, expanded polystyrene ingate (10.4 cm<sup>2</sup> cross section), to which was attached the plate or frame pattern.

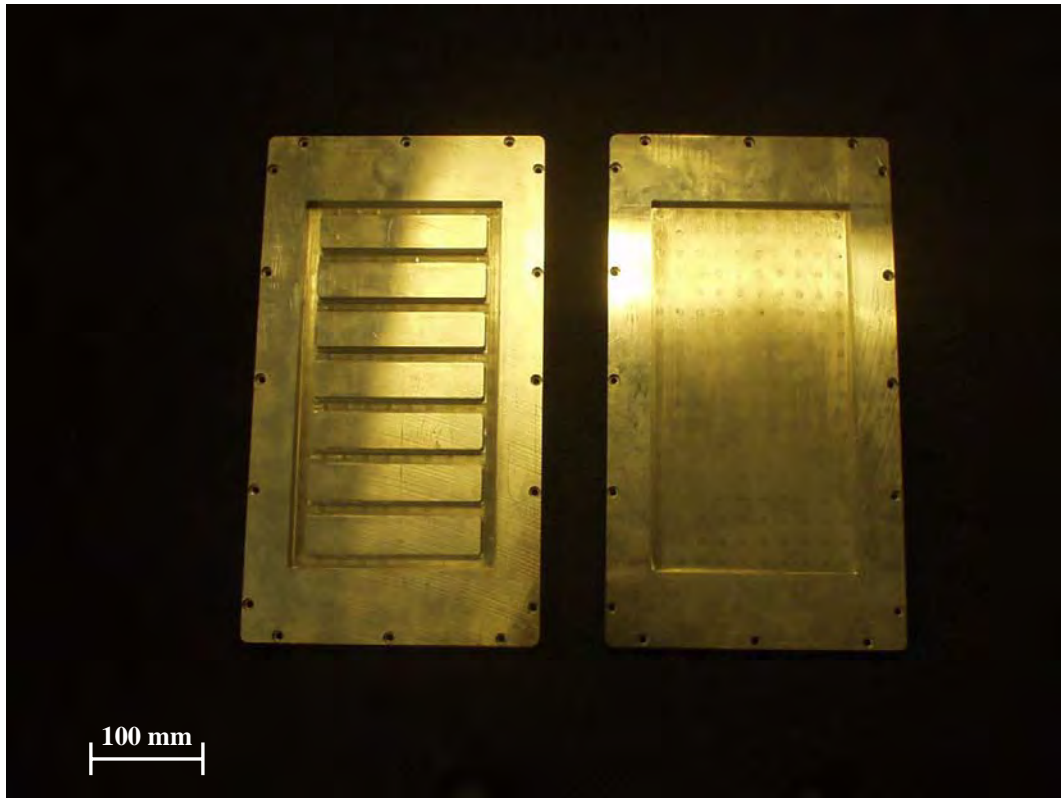


Figure 3.1: Photograph of drag tooling for making frames (left) and plate (right) patterns.

The pattern and running system components were manually assembled using a hot-melt ethylene vinyl acetate adhesive with a melting point of approximately 110 °C. Four clusters were made with the runner bar and ingate located above the pattern plate and a further four with the runner bar and ingate located underneath. Each cluster incorporated a single pattern, either a plate or a frame, so that two frame-type and two plate-type clusters of each running system configuration were available for casting. Figure 3.2(a) shows the cluster design of a top-gated plate and Figure 3.2(b) illustrates the same pattern design, assembled into a cluster, where the ingate is placed at the bottom. A metallostatic head height of 200 mm between the top face of the pattern and the lower face of the pouring basin was maintained in each design.

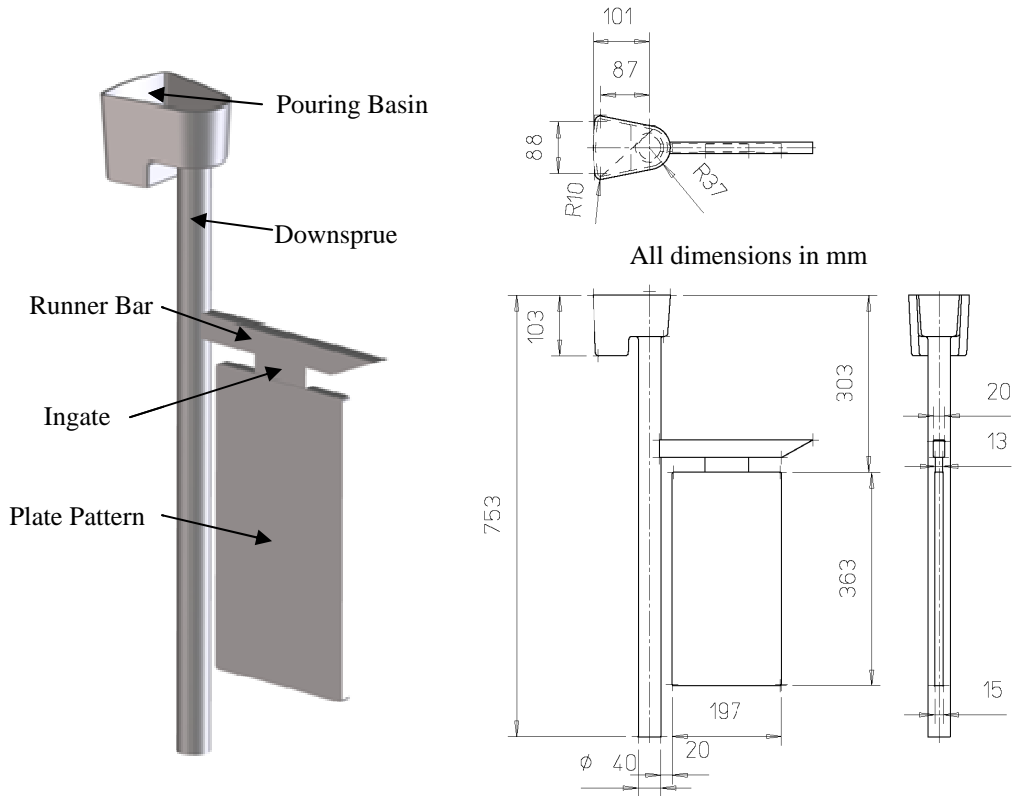


Figure 3.2(a): General arrangement and main dimensions of a top-gated plate cluster.

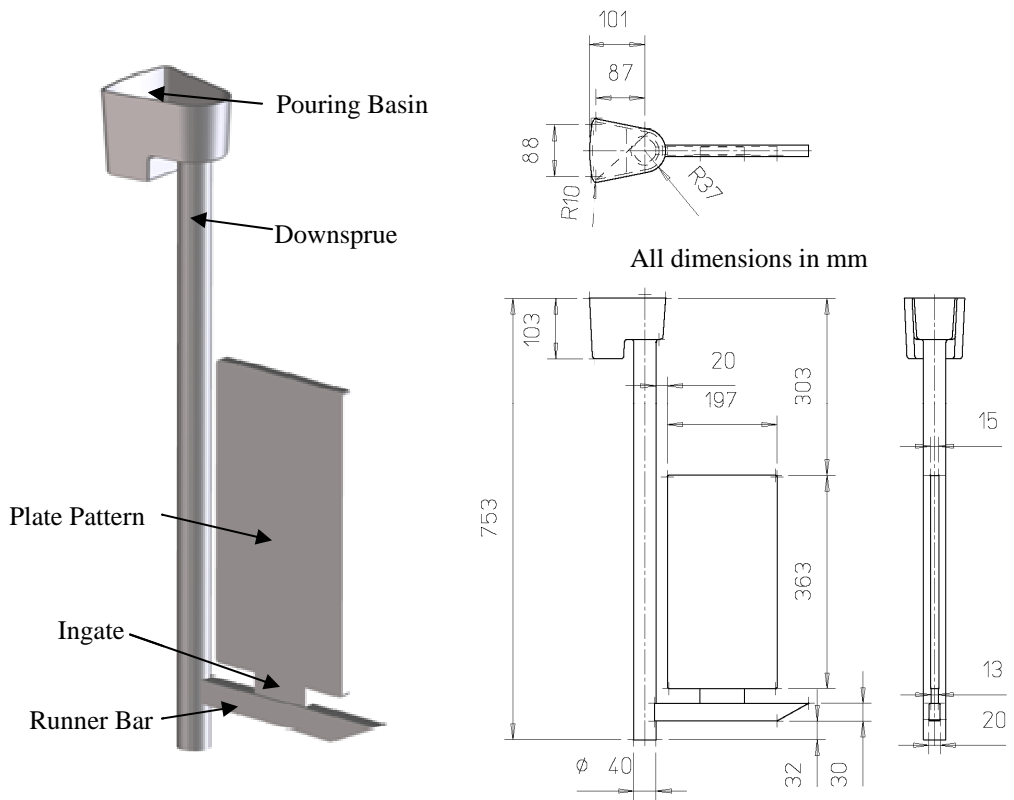


Figure 3.2(b): General arrangement and main dimensions of a bottom-gated plate cluster.

A water based alumino-silicate refractory (Semco Perm C2) was applied by manually dipping each cluster into a tank of this material until all but the pouring basin was submerged. The capacity of the coating to adhere to the polystyrene surfaces was measured by immersing a stainless steel plate (100 mm x 100 mm x 2 mm thick) into the bath and then determining the weight of wet coating adhering to the plate. The wet weight tolerance of the coating was maintained within the supplier recommended limits of  $4.5 \text{ g} \pm 0.5 \text{ g}$  by adding coating or distilled water to the tank and mixing by means of an electrically driven paddle. Coating samples were collected by dipping 100 x 100 stainless steel wire mesh discs which had a diameter of 65 mm into the mixed material. These samples were dried, together with the coated clusters, for 4 hours in a gas fired, circulating air oven at  $55 \text{ }^\circ\text{C}$ . After this they were used to determine coating permeability in accordance with the procedure described by Kocan [47] as described in section 2.1.4.

Loose, dry, recycled silica sand with an average grain size of  $370 \text{ }\mu\text{m}$  was used as the moulding media and was contained in fabricated, steel flasks that had internal dimensions of  $0.9 \text{ m} \times 0.9 \text{ m} \times 0.9 \text{ m}$ . Each flask was filled with a “bedding layer” of sand approximately 150 mm deep. Two clusters were placed on the sand base and centrally located in the flask by means of a jig as shown in Figure 3.3.

The flask was then filled with sand and subjected to horizontal and vertical vibration with an acceleration of 0.8 G to bring about compaction. Maximum sand grain compaction was considered to have been achieved when there was no longer any reduction in bulk density of the sand in the flask, generally achieved within 10 s. of completion of filling of the moulding box.

Ingots of Al-10wt.%Si alloy that had been pre-modified with strontium were melted in a gas-fired crucible furnace of 500 kg capacity. The metal was superheated to approximately  $830 \text{ }^\circ\text{C}$  before it was tipped directly into a preheated crucible furnace that used electrical resistance heating to maintain metal temperature. A permanently immersed chromel-alumel thermocouple measured and controlled the temperature of the metal in conjunction with a proportional integral derivative (PID) controller. When the temperature had stabilised to  $784 \text{ }^\circ\text{C}$  each plate cluster was cast one at a time. After casting a single cluster, any metal

remaining in the ladle was discarded and it was refilled from the holding furnace. The frame clusters were cast in the same manner but at the higher temperature of 909 °C. This was because the modulus of the frame casting, i.e., the ratio between the volume and the surface area of all cooling faces, was significantly lower than that of the plate (0.38 cm against 0.67 cm) and the higher temperature was needed to counteract premature freezing.

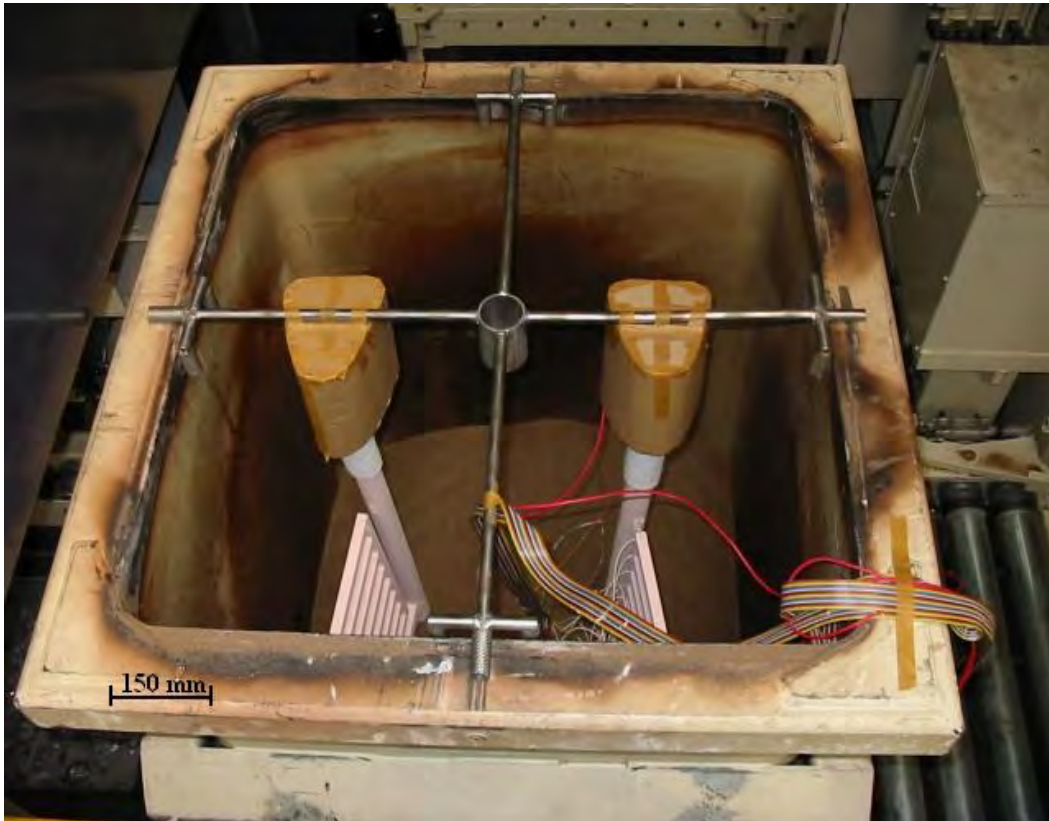


Figure 3.3: Arrangement of two bottom-gated clusters resting on the “bedding layer” of sand and located at the top of the flask by means of a steel jig.

Castings were left to cool in the mould for one hour before being separated from the moulding sand on a vibratory grid. Any coating still adhering to the castings was removed using compressed air and a wire brush.

Mould filling of one top-gated and one bottom-gated cluster of each pattern design was monitored by means of a datalogger unit that was connected to a disposable, 25 strand copper wire. A schematic representation of this unit is illustrated in Figure 3.4.

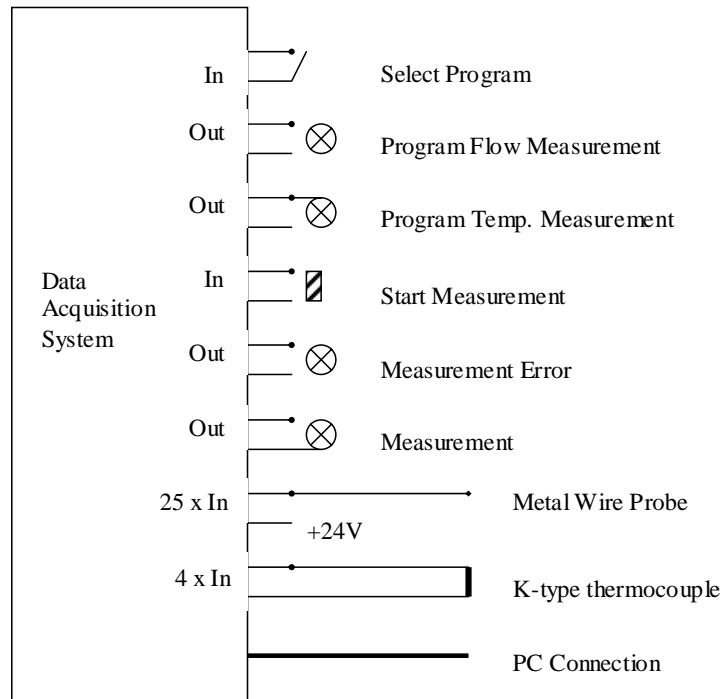


Figure 3.4: Schematic representation of the datalogger unit that was used to measure mould filling characteristics.

Each strand was attached at a pre-chosen point to the pattern cluster by inserting its open end into the polystyrene substrate and fixing its outer sheath to the pattern coating with hot melt glue. One strand, which acted as a trigger to start the datalogger recording, was located alongside the common earth wire in the pouring basin. At the start of mould filling the trigger and common earth strands were shorted through contact with the liquid metal. This action caused the datalogger to start a series of internal timers, each related directly to a specific strand in the cable. As the metal continued its passage through the mould it made contact with the other strands of the cable and shorted them out, causing the timer associated with the shorted out wire to stop counting. A map could then be constructed of the time taken for liquid metal to reach various points throughout the mould.

### 3.1.1.2 Real Time X-ray Method

Determination of the progress of mould filling by means of a datalogger was limited in the scope of information that could be collected. Firstly, data could only be measured at a small number of points throughout the casting and, secondly, it focused only on one variable, in this case the time taken for the metal front to reach each of the pre-determined monitoring

positions. By means of a real time X-ray device a section of the complete mould cavity could be viewed throughout the filling cycle and the image recorded for subsequent playback.

For this experiment plate and frame clusters were produced in the same way. To ensure that a good image resolution was achieved from the real time X-ray unit, a modified moulding flask was used, that had a steel frame construction, but had 10 mm thick plywood sheets to form the two large opposing faces of the flask. Internal dimensions measured 0.45 m long by 0.11 m wide by 0.83 m deep. Loose, dry silica sand was again used to support the clusters in the mould. A bedding layer of 150 mm was placed in the bottom of the flask and a single cluster centralised on top of it. The remaining space in the flask was manually filled with sand whilst being subject to vertical vibration of approximately 0.8 G to bring about sand compaction. Filling of each flask took approximately 30 s. and maximum sand grain compaction was achieved within 10 s. after the flask was full. Although the moulding flask was of a different configuration to that used in the previous experiments and the moulding sand was compacted without the use of a horizontal vibration component, sand packing density was considered to have been similar because the patterns were very simple in design (no cavities and limited undercuts) and were always positioned in a vertical orientation in the flask.

Each completed mould was placed, one at a time, in a lead lined, real time X-ray facility that was used to monitor and record the filling of the mould in a pre-selected area. This unit was equipped with a 160 kV X-ray tube, an image intensifier and a high-speed camera linked to an S-VHS video recorder. The X-ray source was located on one side of the mould and the image intensifier on the other as illustrated in Figure 3.5. This arrangement produced an image of the mould being filled of about 150 mm diameter.

Approximately 8 kg of the pre-modified Al-10wt.%Si alloy was melted using a high frequency induction furnace, and then superheated to about 50 °C above the desired pouring temperature so that sufficient time was available for transfer of the crucible from the furnace to the pouring device of the real time X-ray facility without the temperature of the metal dropping below the desired pouring temperature. Metal temperature was measured continuously by means of a chromel-alumel thermocouple connected to a digital thermometer.

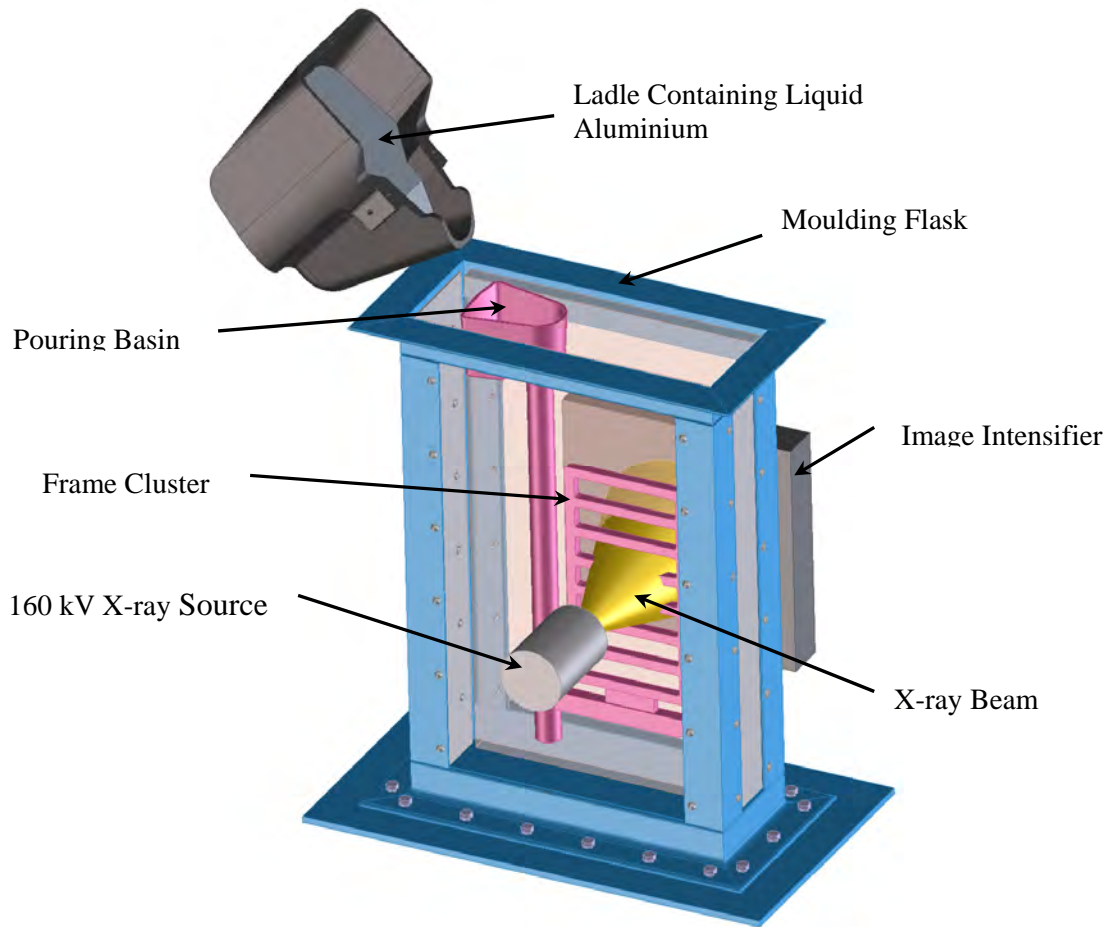


Figure 3.5: Real time X-ray observation of the mould filling of a gravity cast, bottom-gated frame pattern.

When the desired temperature was reached, the pouring device was driven up to the mould in the X-ray unit and the liquid aluminium discharged into the pouring basin by motor driven tilting about an axis through the lip of the crucible. A pouring temperature of 784 °C was used to cast all the plate clusters and the first frame cluster. However, it was raised to 909 °C for casting of the remaining three frames because real time X-ray imaging had revealed that the metal front had frozen prematurely whilst filling the frame at 874 °C. Once the filling cycle was complete the casting was allowed to cool in the mould for 1 hour before being removed.

### 3.1.2 Tensile Strength Testing

Top and bottom-gated castings of both pattern designs were selected for the determination of their as-cast tensile strength. Eight test bars, with a length of 115 mm and a 15 mm by 15 mm square section, were extracted from each of the chosen castings and machined to produce

tensile test bars with a gauge length of 60 mm and diameter of 10 mm. The source, identification and dimensions of each of the eight test bars relative to the cluster type from which they were taken are illustrated in Figures 3.6 and 3.7.

Tensile testing was performed on a Losenheim Universal Testing Machine S/N 3617 in accordance with British Standard EN 10 002-1:2001 [151], with a strain rate of  $1\text{mm}\cdot\text{min}^{-1}$ .

### 3.1.3 Examination of Fracture Surfaces

One fracture surface of each of the test bars from the experiments was observed using a JEOL 6060 scanning electron microscope. Defect types were characterised by means of their morphology and a small region of the surface of each defect was subject to electron microprobe analysis (EMPA).

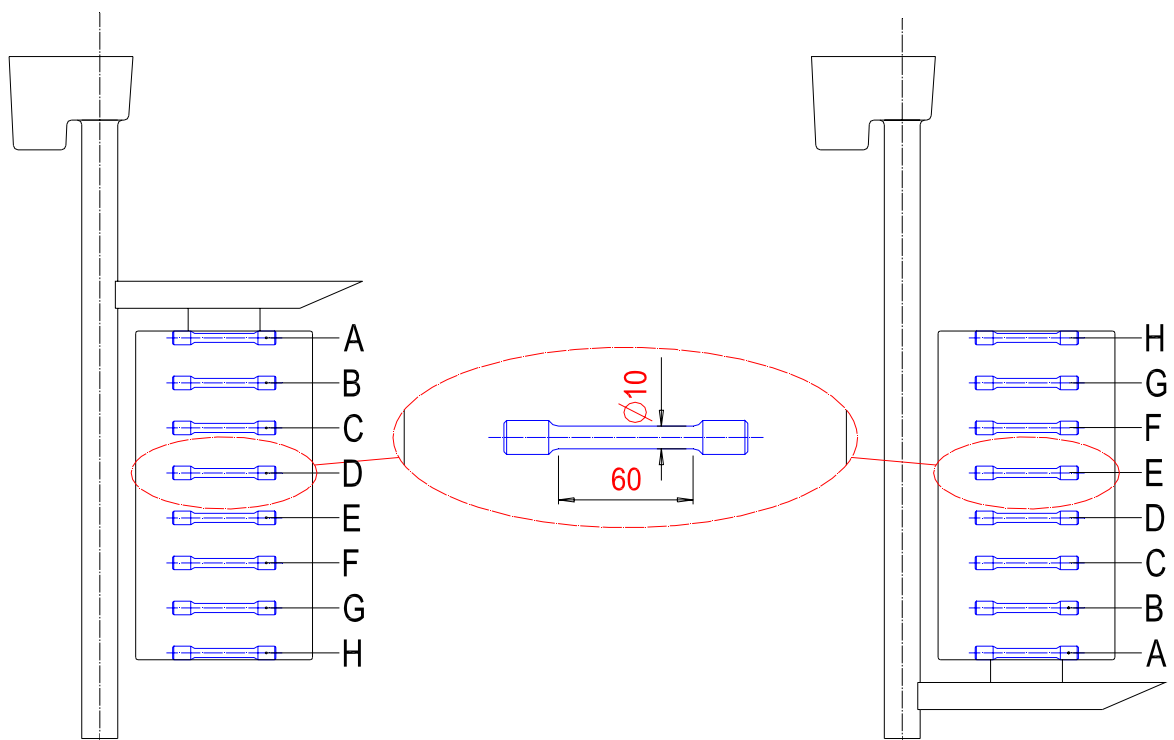


Figure 3.6: Tensile test piece sampling and labelling system for top and bottom-gated plate castings.

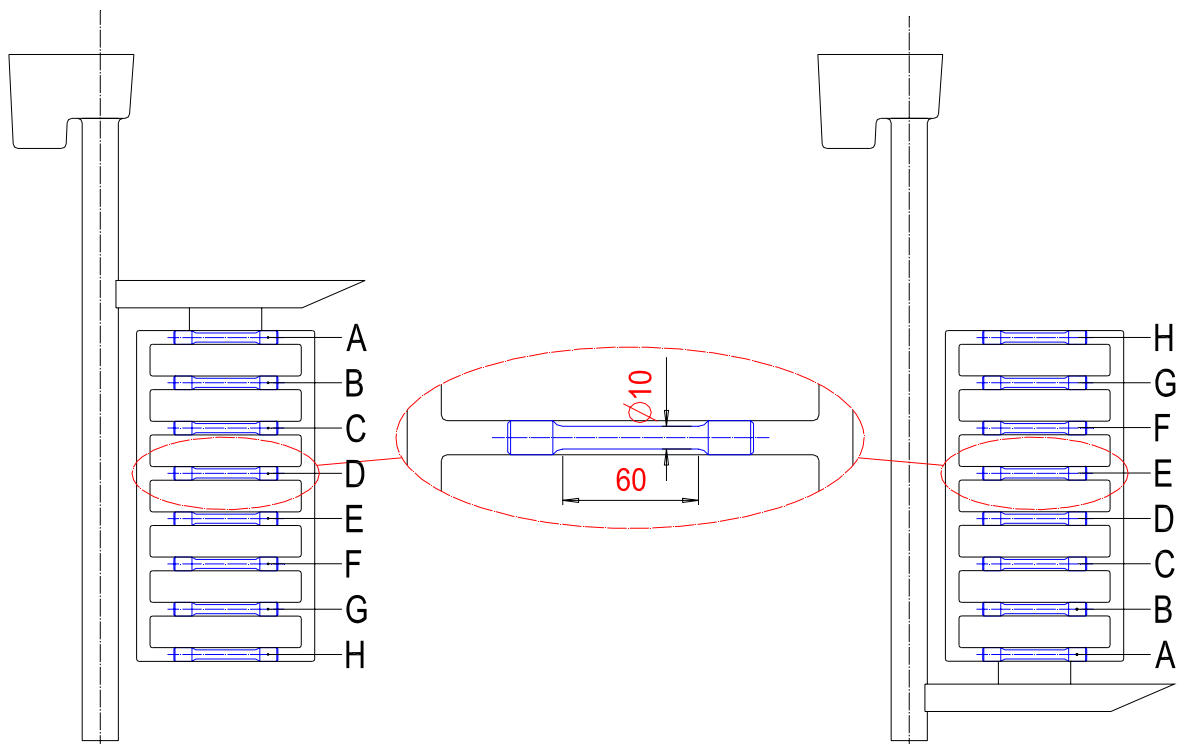


Figure 3.7: Tensile test piece sampling and labelling system for top and bottom-gated frame castings.

### 3.2 COUNTER-GRAVITY FILLING OF LOST FOAM CASTINGS

The control over metal flow during gravity casting is limited because, for at least some portion of the filling cycle, the metal travels in the direction of the gravity vector. When the metal travels against the gravity vector, as is the case with bottom-gated castings, the flow rate is also affected by the constantly changing head differential between metal in the pouring basin and the metal front in the mould cavity. In the uncontrolled condition, fingers of metal can precede the general front and then later recombine entraining degraded polystyrene. Introducing the metal into the mould from below and filling vertically upwards throughout the complete cycle can remove this limitation. Such a system requires the ladle of metal to be located under the mould and the liquid metal to be transferred into the mould by a pump that is equipped with suitable controls.

### 3.2.1 Mould Filling Observations

This set of experiments made use of the original plate pattern and also a number of patterns supplied by Foseco Morval Ltd. of Tamworth, UK. These patterns were also of a plate design but with a length of 440 mm, a width of 180 mm and a thickness of 10 mm and some contained a proprietary organic brominated substance. This material had been added to the expanded polystyrene beads prior to the moulding process, and was added in order to reduce the amount of liquid degradation products produced during casting.

In order to cast these plates in a counter-gravity fashion the previously applied bottom gating system was substantially modified. Firstly, the pouring basin, downsprue and runner bar were discarded altogether and these items were replaced with a single pre-expanded polystyrene upsprue. This upsprue had a diameter of 40 mm (with a 10 mm diameter hollow centre) and a length of 95 mm. The upsprue and pattern plate were attached to an ingate of the original design by means of hot-melt glue and the complete cluster was coated and dried in the same manner as described previously.

The moulding flask used in conjunction with the real time X-ray facility was also modified by drilling a centrally located, 70 mm diameter hole through its base. This hole was fitted with a compressible ceramic sleeve that was 40 mm in height and had an internal diameter also of 40 mm. The sleeve was inserted so that one face was flush with the bottom of the flask while the other end protruded into the flask. The pattern cluster was positioned by locating its upsprue into the sleeve so that its face was also flush with the base of the flask. By locating the pattern in this way the hole in the base of flask was sealed and this permitted the mould to be filled in the same manner as described previously.

To cast each mould approximately 8 kg of a pre-modified LM25 alloy (Al-7wt.%Si0.3%Mg) was melted in a clay graphite crucible that was located in a small, high frequency induction furnace. The metal was superheated to approximately 100 °C above the desired casting temperature and then the crucible was transferred to the counter-gravity casting machine which is illustrated in Figure 3.8.

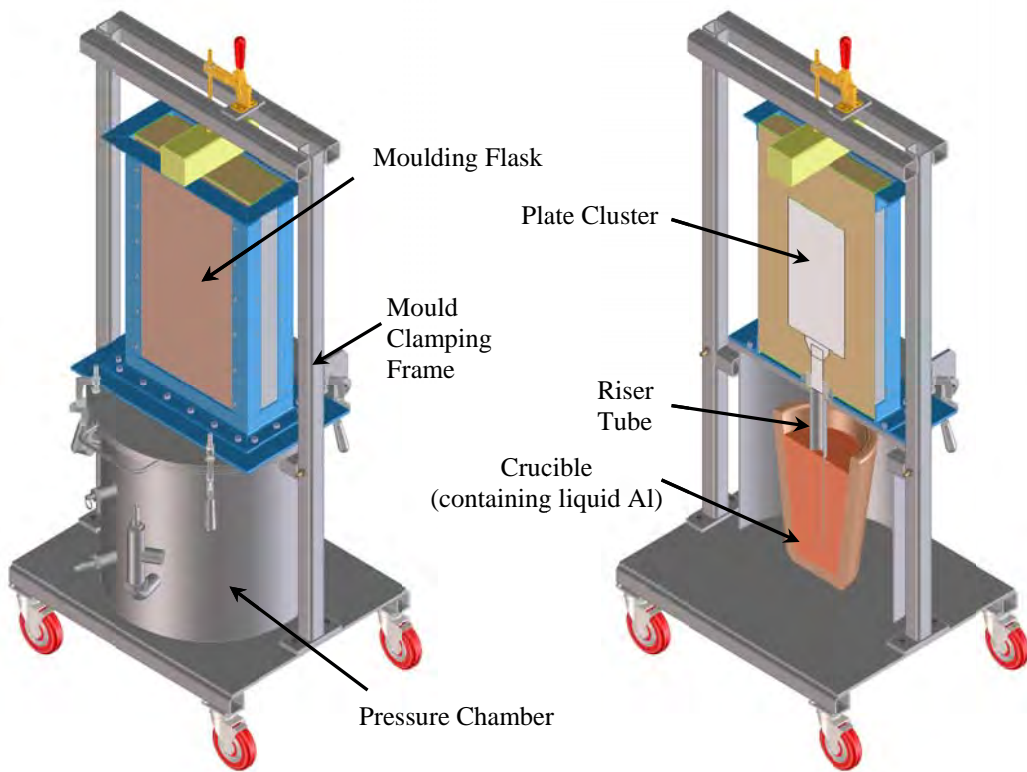


Figure 3.8(a): 3-D surface and section views of the counter-gravity casting machine.

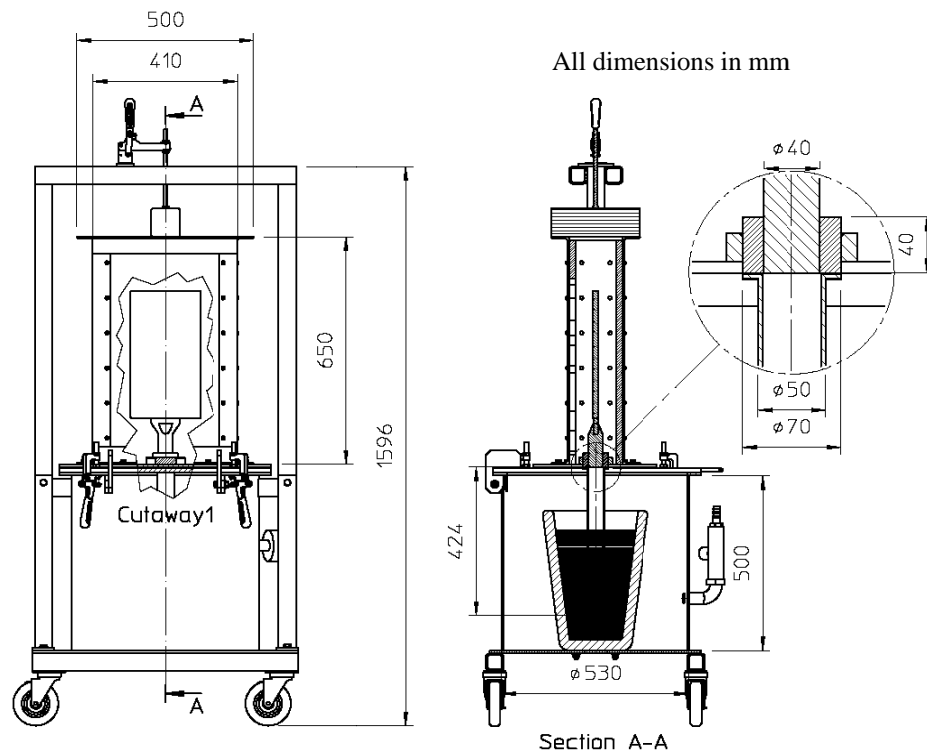


Figure 3.8(b): 2-D section views of the counter-gravity casting machine including main dimensions and a detailed view of the interface between the mould and the pressure vessel.

This device consisted of a cylindrical steel pressure vessel mounted on a square base plate with wheels attached. The vessel was fitted with a pressure gauge, a pressure relief valve and a chromel-alumel thermocouple that could measure the temperature of the liquid metal at all times. The inside of the vessel was accessed by means of a hinged lid which was fitted with an O-ring seal. When in the closed and clamped position, this seal mated with the upper flange of the vessel and formed an air-tight joint. The lid had a 50 mm diameter hole located in its centre and this was used to locate a steel “riser” tube.

The crucible of liquid aluminium was placed on a refractory brick in the pressure vessel, the thermocouple placed in the liquid metal and the lid closed and clamped. A ring gasket made from compressed refractory fibre blanket was placed in the recess in the lid and the steel “riser” tube, previously coated with a refractory wash, was lowered through the hole in the lid. The upper end of the tube was fitted with a flange that located it in a recess in the lid which left it flush so that the opposite end was submerged in the liquid metal centrally and to a suitable depth.

A second gasket of the same material was placed on the upper flange of the “riser” tube and then the completed mould was placed on the lid of the pressure vessel so that the hole in the bottom of the flask aligned with the riser tube. The gasket provided a seal between the edge of the tube and that of the flask inlet hole. The mould was clamped to the pressure vessel by means of an A-frame arrangement across the upper face of the flask.

The complete assembly was wheeled in to the real time X-ray facility and connected to a compressed air supply that was pressure regulated. A manual shut-off valve was built into the pipeline between the regulator and pressure vessel to prevent premature pressurisation. When a metal temperature of 785 °C was recorded by the thermocouple in the melt, the shut-off valve was moved to the open position. This caused the vessel to pressurise and the liquid metal to be forced up the “riser” tube and into the mould. Moulds were cast at different upwards velocities by varying the overpressure in the vessel within the range of 24.1 to 68.9 kPa (3.5 to 10 psi). The metal front velocity averaged 22 mm.s<sup>-1</sup> at the highest overpressure applied and only 5 mm.s<sup>-1</sup> at the lowest setting.

Filling was recorded by means of the X-ray source, image intensifier, camera and recording equipment used previously. Once the mould was fully filled or the metal front had stopped advancing for more than 10 s. the shut-off valve was closed manually. Pressure in the vessel was maintained for 30 s., after which time it was released to atmosphere. After one hour the metallic cluster was removed from the flask together with the sand and cleaned in the conventional manner.

### 3.2.2 Tensile Testing

Test pieces were cut from the counter-gravity cast plates for tensile testing in the same manner as was used for the gravity filled castings. Sampling locations and the specimen labelling system for the castings made from 15 mm thick, conventional polystyrene patterns are illustrated in Figure 3.9.

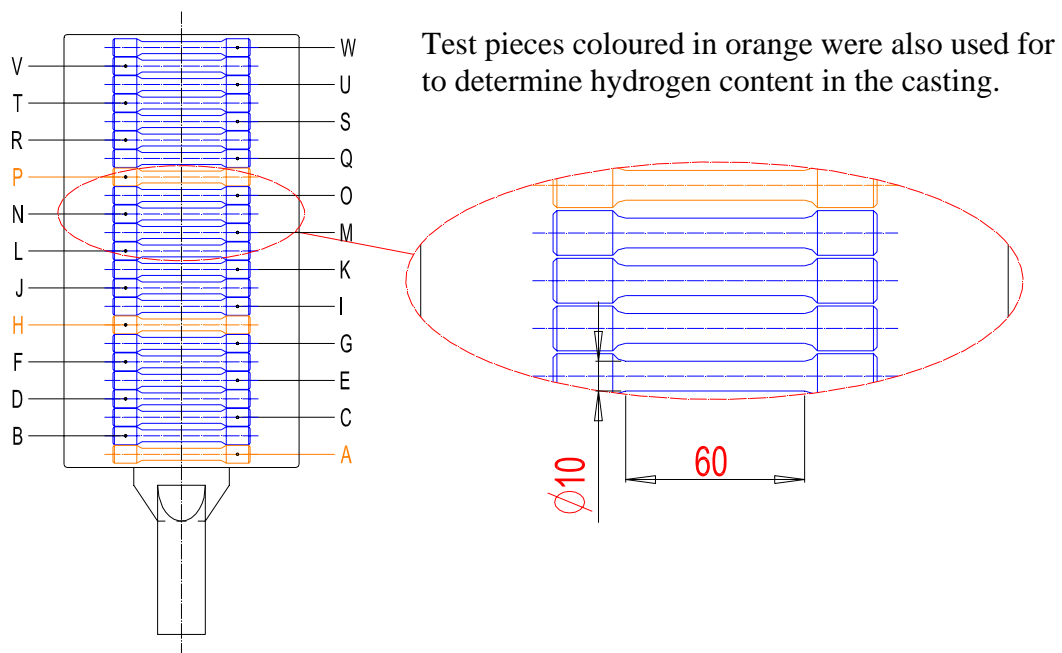


Figure 3.9: Tensile test piece sampling and labelling system for counter-gravity filled castings made from 15 mm thick, conventional polystyrene pattern plates.

The number of test pieces taken from castings in this experiment was increased from 8 to 23, the maximum number that could be obtained from a single plate casting whilst maintaining original specimen size and horizontal positioning. In some cases test pieces were extracted from the thinner, narrower and longer plates that had been supplied by Foseco Morval Ltd.

and these had a smaller machined gauge diameter of 6.7 mm as a result of the reduction in plate thickness. However, as is shown in Figure 3.10, the sampling and labelling system remained the same as used in conjunction with the 15 mm plates so that as direct a comparison as possible could be made between the various sets of results obtained.

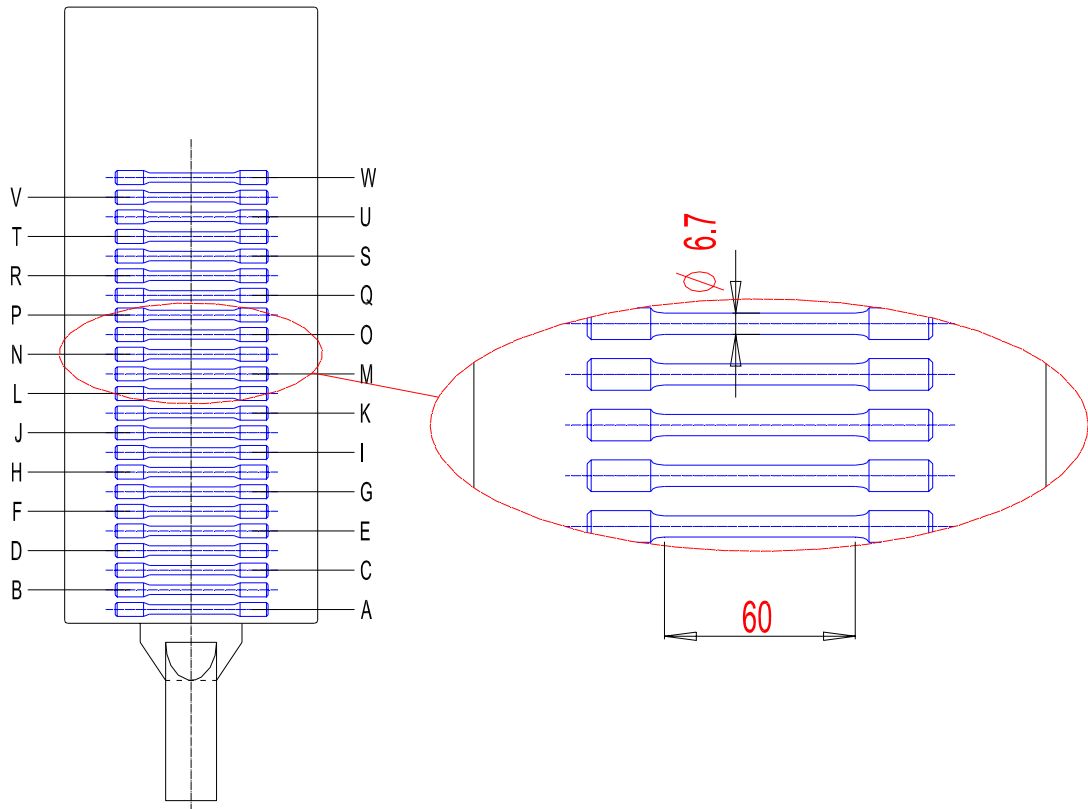


Figure 3.10: Tensile test piece sampling and labelling system for counter-gravity filled castings made from 10 mm thick polystyrene pattern plates (with and without bromine additions).

### 3.2.3 Determination of Hydrogen Pick-up

In order to determine if hydrogen pick-up occurred during the counter-gravity casting experiments, due to the much slower filling velocities, a sample from three separate melts was poured into a steel mould to form “keel” block samples before casting. The remainder of each melt was then used immediately to produce the plate castings by the counter-gravity method described. Three fractured test bars, previously used for tensile testing as described in Section 3.2.2, were also selected from the lower, middle and upper regions of each plate, and used for hydrogen determination. The location in the plate from which each bar originated is highlighted in Figure 3.9.

The hydrogen contents of the “keel” block and samples from the plates were determined by Sci-Lab Analytical Ltd., Chester, UK, using the Inert Gas Fusion technique. In this method a known sample weight was induction melted in a graphite crucible and any hydrogen present removed by nitrogen. The gas was then processed and cleaned by a number of filters after which it flowed into a thermal conductivity cell. The cell consisted of two pairs of matched filaments that made up four legs of a Wheatstone bridge. The “reference” filaments were maintained in a constant flow of nitrogen gas, at a constant temperature, whilst the gas composition around the “measuring” filament was allowed to vary. The temperature in the oven where the filaments were housed was set at  $45\text{ }^{\circ}\text{C} \pm 0.2\text{ }^{\circ}\text{C}$  in order to eliminate any effects of normal room temperature variation, while the filament temperature was maintained at a significantly higher level.

As hydrogen was introduced into the measuring chamber, the measuring filament increased in temperature relative to the reference filament that was surrounded by a nitrogen atmosphere, due to hydrogen having a higher thermal conductivity than nitrogen. The resultant imbalance in the bridge produced a positive current output which was related to the quantity of hydrogen present, measured in parts per million (ppm).

### **3.3 ACCELERATED LIQUID-LIQUID INTERFACE EXPERIMENTS**

Metal fronts, observed during the filling of Lost Foam moulds, were seen to adopt one of a number of profiles depending upon the casting conditions used. Slow moving and stationary fronts were planar in appearance but those with a higher velocity had an irregular or unstable profile. A number of authors have suggested that, at aluminium casting temperatures, the region immediately ahead of the advancing metal front consists predominantly of viscous liquid polystyrene [12,141,152]. Therefore, a physical model was constructed to simulate the interaction of molten aluminium and liquid polystyrene during mould filling and, if possible, examine the mechanism by which the metal front became unstable.

The model, illustrated in Figure 3.11, consisted of a vertically oriented, thin glass cell containing a layer of glucose syrup above a layer of liquid mercury, attached to the discharge end of a horizontally positioned air cylinder that was fixed to a steel profile base. The distance

between the two opposing internal faces of the cell was 15 mm, in order to replicate the thickness of the polystyrene pattern plates used in previous experiments, and the upper face of the mould was left open to atmosphere so that fluids could be added and displaced easily from the model. Glass was used as the material for the cell walls so that observations could be recorded using a high-speed video camera.

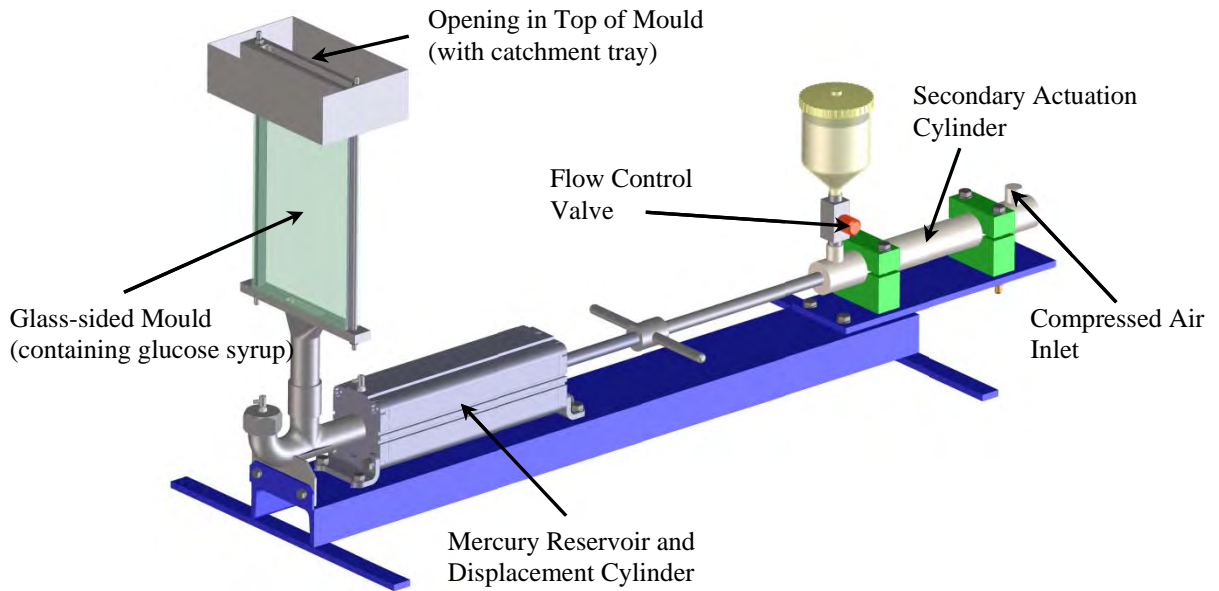


Figure 3.11(a): 3-D view of the physical model used to observe fluid interface morphologies at various glucose displacement velocities and viscosity levels.

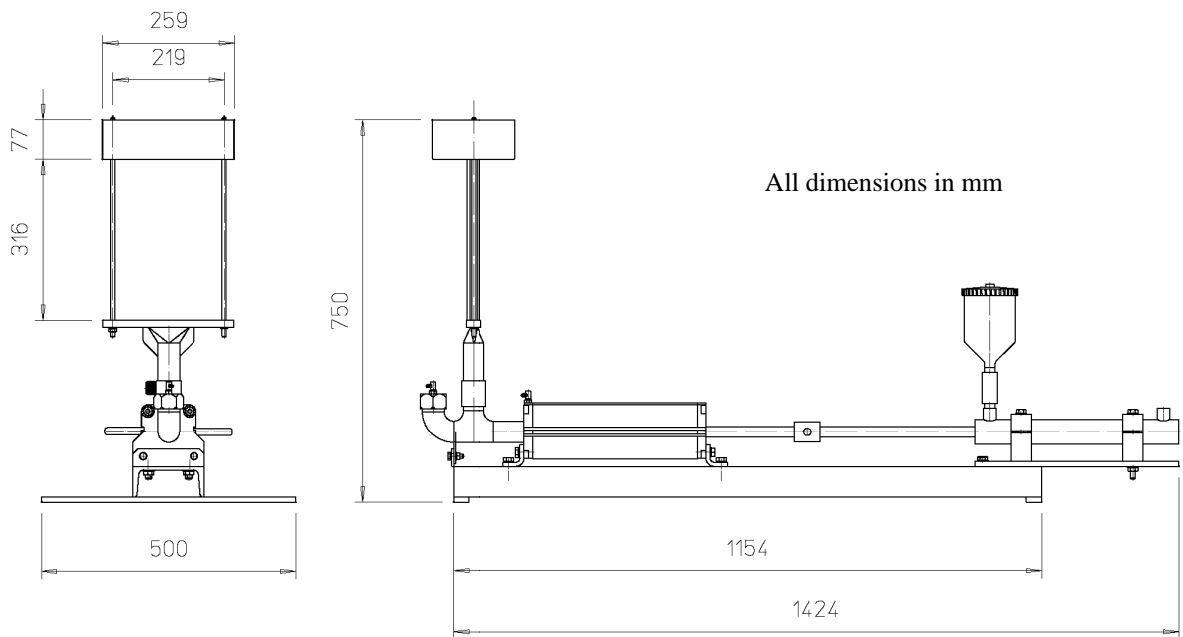


Figure 3.11(b): 2-D views of the physical model used to observe fluid interface morphologies and including main dimensions.

Clear glucose syrup was chosen to represent liquid polystyrene because it had a similar density,  $1\,050\text{ kg.m}^{-3}$ , for concentrated glucose syrup at  $20\text{ }^{\circ}\text{C}$  [153] compared with  $1\,040\text{ kg.m}^{-3}$  for a virgin grade polystyrene melt at  $200\text{ }^{\circ}\text{C}$  [120]. Its initial viscosity could easily be reduced by dilution with water. Also, the long molecular chains associated with this material were thought to mimic those of liquid polystyrene.

Although mercury has a very high density,  $13\,545\text{ kg.m}^{-3}$  at  $20\text{ }^{\circ}\text{C}$  [154] compared to only  $2\,364\text{ kg.m}^{-3}$  at  $702\text{ }^{\circ}\text{C}$  [155] for liquid aluminium, it was selected for use in the model because it remained a liquid metal at room temperature and had a similar viscosity to liquid aluminium. The viscosity of mercury is  $1.55\text{ mPa.s}$  at  $20\text{ }^{\circ}\text{C}$  [156] while liquid aluminium at  $702\text{ }^{\circ}\text{C}$  is only slightly lower at  $1.24\text{ mPa.s}$  [155].

Three samples of glucose syrup were prepared with differing levels of water dilution. The first was undiluted and as-received from the supplier. The other two samples were diluted slightly by adding  $2.5\text{ wt.}\%$  and  $5.0\text{ wt.}\%$  water, respectively. The dynamic or absolute viscosity of each sample was measured on a TA Instruments AR500 rheometer using parallel plate geometry. A sample of the glucose syrup was placed on a horizontally positioned plate within the machine, pre-heated to  $25\text{ }^{\circ}\text{C}$ . A stainless steel disc with a diameter of  $40\text{ mm}$  was placed on top of the sample and the gap between the plate and disc set to  $200\text{ }\mu\text{m}$ . At the upper side of the disc was a vertical shaft through which a torque was applied. This resulted in the sample being subjected to a shear stress that was initially increased (ramped up) and then gradually decreased (ramped down). Any angular displacement of the disc was measured by an optical encoder and related to the strain of the sample and hence its viscosity. In undiluted form the glucose syrup had a viscosity of  $93\text{ Pa.s}$  which fell to  $35\text{ Pa.s}$  when diluted with  $2.5\text{ wt.}\%$  water. The addition of a further  $2.5\text{ wt.}\%$  of water produced a solution with a viscosity of  $16\text{ Pa.s}$ . The ratio of density for the glucose-Hg system was therefore about  $1 : 13$ , while the ratio of viscosity was about  $10^4 : 1$ .

After filling the model with Hg and the glucose solution with a viscosity of  $16\text{ Pa.s}$ , the piston in the air cylinder was actuated by means of an oil-over-air cylinder that was coupled in-line with it by a shaft-to-shaft connection. The secondary drive cylinder was connected to the mains air supply (at  $8\text{ bar}$  pressure) and its piston speed, and therefore speed of mercury

displacement into the mould, were controlled via a flow regulator situated on the oil outlet side of the unit. During displacement, the appearance of the interface of the fluids was recorded using a high-speed video camera. The experiment was repeated initially with the glucose solution of 35 Pa.s viscosity and subsequently with the undiluted glucose syrup at 93 Pa.s.

### **3.4 APPROXIMATION OF THE VISCOSITY OF LIQUID POLYSTYRENE**

As reported by Saffman and Taylor [112], a large variation in the viscosity of two interacting fluids within a narrow channel can have an influence on the stability of the interface between them. Although published literature reports viscosity data of polystyrene melts, viscosity in polymers is known to vary widely because the material is shear-thinning, viscoelastic and has flow properties that are temperature dependant [122] (see Section 2.4.2). Additionally, bromine-based additives have the effect of reducing the viscosity by decomposing at relatively low temperatures and forming bromine radicals. These radicals accelerate the degradation of the polystyrene ahead of the advancing metal front [15]. Therefore an experiment was designed to capture and measure the molecular weight of suitably degraded samples of conventional and brominated pattern material from which their viscosity might be inferred.

A series of small, cylindrical vessels was manufactured from copper tubing, with a length of 120 mm, wall thickness of 1 mm, and an inside diameter of 21 mm. A copper end plug was welded to the bottom of each tube and the other end was fitted with a brass cap with a screw fitting. Each cap had a 1 mm hole drilled through its centre to allow the insertion of a sheathed thermocouple that remained in position for the duration of the experiment.

Expanded polystyrene samples were cut manually from sections of previously manufactured plate patterns. The diameter of the samples matched the internal diameter of the copper tube and the thickness was equivalent to that of the pattern section. A single sample of brominated or unbrominated polystyrene was inserted as far into each tube as possible so that one flat face of the sample came into contact with the internal face of the copper end cap and the cylindrical face of the sample remained in contact with the internal walls of the tube. The brass cap was secured to the other end of the tube and a K-type thermocouple, contained

within an Inconel 600 sheath of outside diameter 0.5 mm, was fed through the hole in the cap until its tip penetrated into and through the polystyrene sample and made contact with the internal base of the tube. The other end of the thermocouple was attached to a datalogger device that recorded the measured temperature every 0.05 s. Figure 3.12 shows a sketch of the experiment.

Liquid aluminium was melted and held at approximately 780 °C in a small electric induction furnace. A retort stand was placed next to the furnace and the associated grips positioned immediately over the centre of the crucible. For each experiment, a fully assembled tube was placed within the grips of the retort stand, as shown in Figure 3.12, in such a position that the tube became immersed to a depth of 70 mm within the liquid aluminium in the furnace.

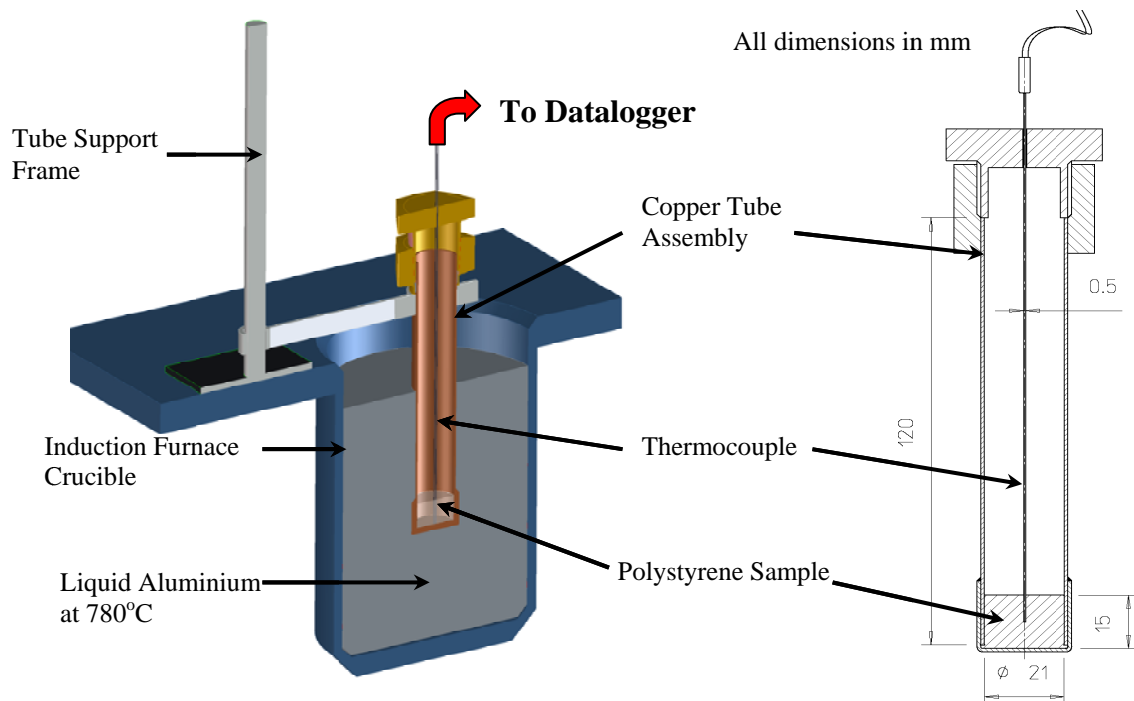


Figure 3.12: Test rig used to capture solidified samples of degraded liquid polystyrene (including detailed view of copper tube assembly and thermocouple location with main dimensions).

The temperature increase within the polystyrene sample was recorded by the datalogger until a set temperature was reached, and at that point the tube was removed from the liquid aluminium and plunged into cold water. This rapid quench had the effect of minimising any

further degradation of the polymer, thereby preserving the characteristics of the degraded polymer at the temperature of removal from the liquid aluminium.

Gel Permeation Chromatography, undertaken by RAPRA Technology Ltd., was used to determine the average molecular weight of each of the samples. This analysis technique separated polymer molecules in solution by their size as they passed through a column containing tightly packed, highly porous particles. Small, low molecular weight molecules were trapped by the porous particles whereas the higher molecular weight particles passed through the column more freely. Molecules exited the column at different rates depending on their size and this effect was quantified by means of a refractive index detector.

A single solution of each sample was made up by the addition of 10 ml of tetrahydrofuran to approximately 20 mg of each polystyrene sample. All specimens were held for at least 4 hours to allow total dissolution to take place. After thorough mixing, the solutions were filtered through a 0.2 micron polyamide membrane and transferred to sample vials, and placed in an autosampler.

The Gel Permeation Chromatography system used for the work was calibrated with a sample of unbrominated polystyrene. Data capture and subsequent data handling was carried out by means of Viscotek 'Trisec 2000' and 'Trisec 3.0' software. The weight average molecular weights obtained in this experiment were inserted in Equation 3.1 [39] to estimate the apparent viscosity (or dynamic viscosity at zero shear) of each of the liquid polystyrene samples obtained.

$$\log\eta_0 = 3.4\log M + [900.2/(T - 306.4)] - 18.38 \quad \text{Equation 3.1}$$

where  $\eta_0$  = zero shear viscosity  
 $M$  = molecular weight  
 $T$  = the temperature of the melt (in degrees Kelvin)

Equation 3.1 was put forward by Cox and Ballman [39] as a combination of the Williams-Landel-Ferry equation (see Equation 2.25) and the Fox and Flory equation (see Equation 2.26) in order to overcome the limitations of the former in terms of molecular weight and the latter with respect to temperature. Whilst calculation of the viscosity of liquid polystyrene at zero

shear ignores the effect of this force on the polystyrene inside a Lost Foam mould during its displacement by the advancing metal front, the low filling speeds observed in this process will exert low levels of stress such that  $\eta \rightarrow \eta_0$ .

## 4 RESULTS

### 4.1 CLUSTER CHARACTERISTICS

Pattern density and coating thickness have been reported to be very influential in determining the filling speed in Lost Foam casting [4,33]. Pattern making and cluster coating techniques were adopted which minimised variation in these parameters from one pattern to the next. However, a certain amount of variation was likely to exist across any one pattern and this was measured and recorded in case it had an influence on observations made during mould filling experiments.

#### 4.1.1 Pattern Density Variations

Figure 4.1 shows a typical density profile of a 15 mm thick, expanded polystyrene pattern plate. Each column represents a cube of material of a side length of 15 mm and the reference given to each cube denotes the position from within the plate that it was taken.

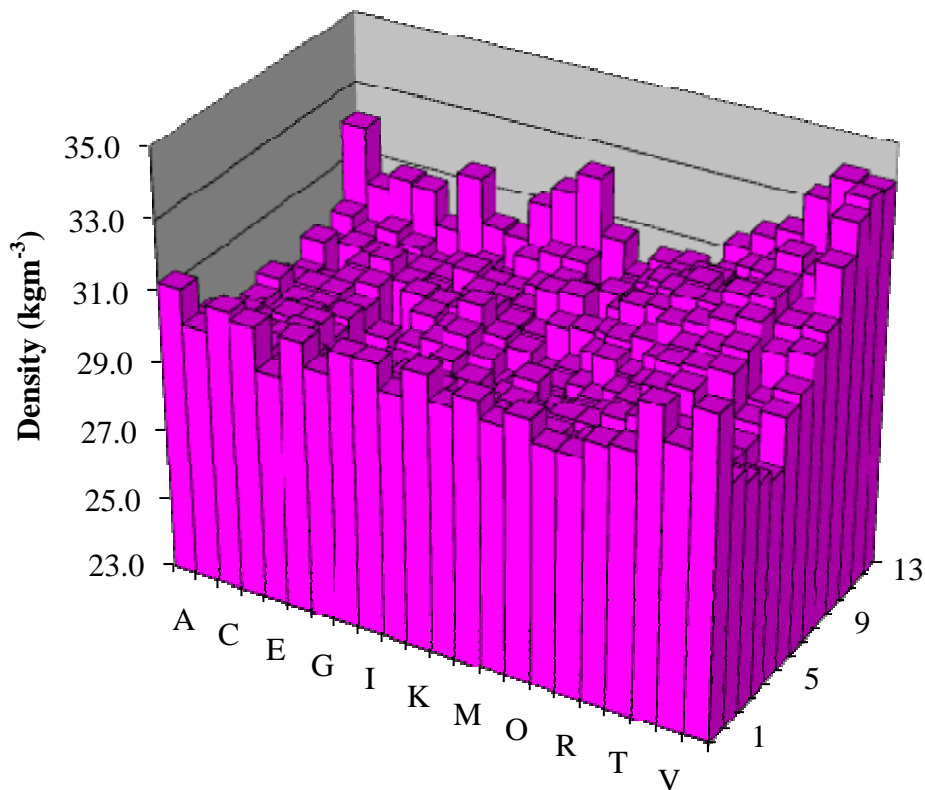


Figure 4.1: Density profile of a 15 mm thick polystyrene pattern plate.

The density varied across the plate with the highest values being found around three sides of the perimeter and the lowest values towards the centre of the plate. The highest value recorded was  $34.1 \text{ kg.m}^{-3}$  and the lowest was  $27.3 \text{ kg.m}^{-3}$ . The spread of results between these two values resulted in an average density of  $29.9 \text{ kg.m}^{-3}$ .

The maximum density of a cube taken from the 15 mm thick polystyrene frame pattern was  $34.5 \text{ kg.m}^{-3}$ . Although this was similar to the maximum value obtained from the plate, the minimum density of  $24.3 \text{ kg.m}^{-3}$  was lower. Figure 4.2 illustrates the variation found throughout the frame and follows the same general trend as observed in the plate, i.e. higher densities on the perimeter of the pattern and lower densities within the inner bars.

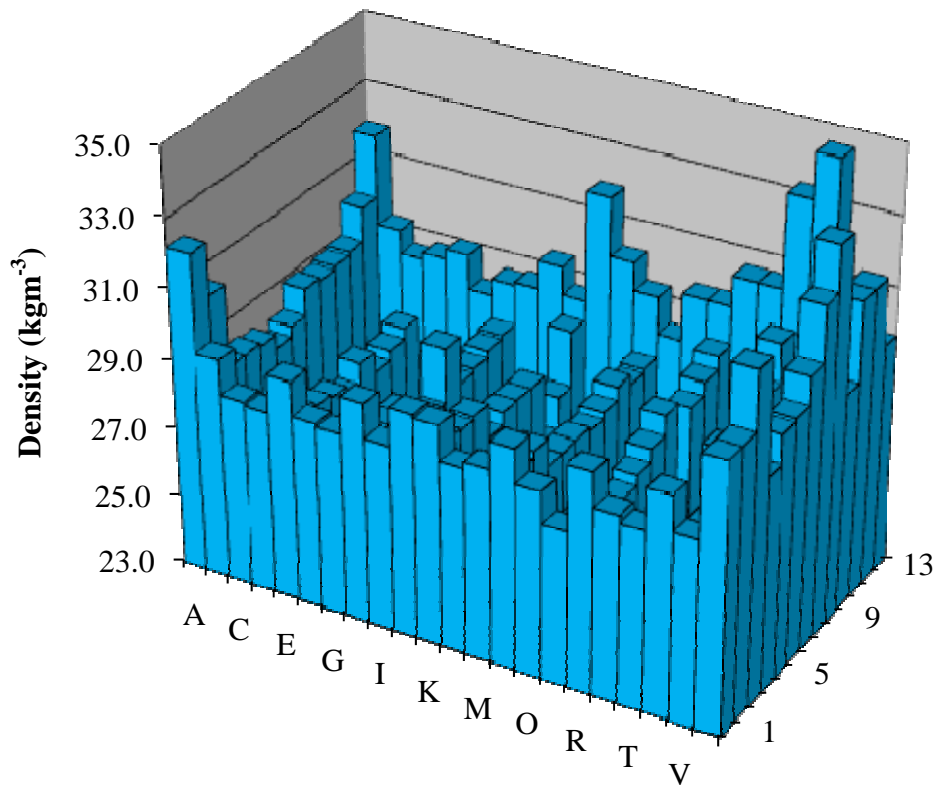


Figure 4.2: Density profile of a 15 mm thick polystyrene frame.

A number of casting experiments were carried out that examined the effects of a proprietary brominated additive contained within the pattern material. These experiments made use of plates that were 10 mm thick. Some of the 10 mm thick plates contained the additive and others, used as comparators, were untreated. The density profiles of these two types of plate

are shown in Figures 4.3 and Figure 4.4 respectively. Each column in these figures represents a 20 mm x 20 mm x 10 mm section of the plate.

The density variation throughout these plates was less than those measured in the thicker patterns. The lowest value obtained in an untreated plate was  $25.1 \text{ kg.m}^{-3}$  and the highest  $28.8 \text{ kg.m}^{-3}$ . The spread of results between these two values produced an average density of  $27.2 \text{ kg.m}^{-3}$ .

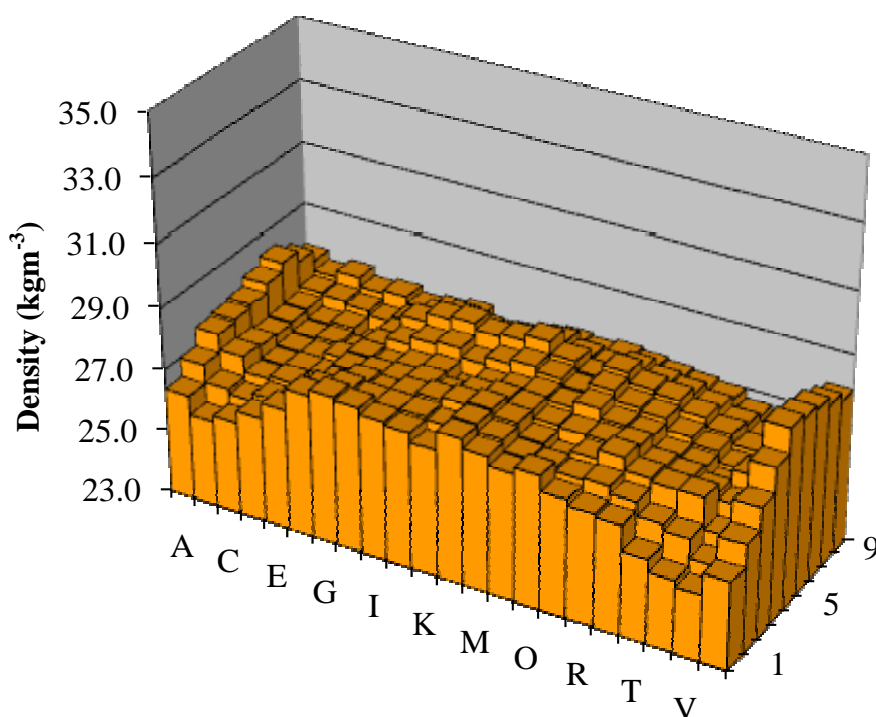


Figure 4.3: Density profile of a 10 mm thick, untreated polystyrene plate.

The highest, lowest and average density values of the plate that had been treated with a bromine compound were similar to those recorded in the plate without additive and were  $28.1 \text{ kg.m}^{-3}$ ,  $23.5 \text{ kg.m}^{-3}$  and  $26.6 \text{ kg.m}^{-3}$  respectively. Although these values were similar to the equivalent figures recorded in the untreated plate, their density profiles were significantly different. The highest densities in the untreated plate were at both ends and across its middle region whereas the plate containing the brominated additive was least dense across its central area. Both plates, however, exhibited similar densities at their ends.

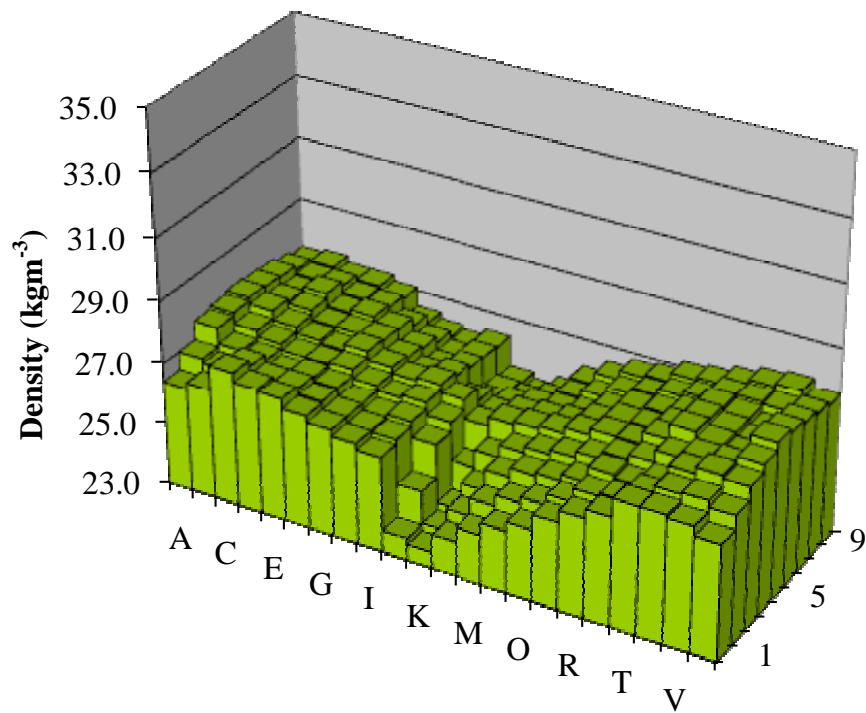


Figure 4.4: Density profile of a 10 mm thick plate containing a proprietary brominated additive.

#### 4.1.2 Coating Permeability and Coating Thickness

All patterns were coated with a single batch of alumino-silicate material that was pre-mixed prior to application in order to produce a uniform suspension. The thickness of the coating was determined by sectioning two frame patterns at 8 points along each side and measuring the cross section of the coating at a magnification of  $\times 20$  by means of a graticule with  $100 \mu\text{m}$  divisions. The results, shown in Figure 4.5, were very similar to each other and did not exhibit any particular trend. The average coating thickness was  $200 \mu\text{m}$  on both patterns with a range of  $150 \mu\text{m}$  between the highest and lowest measurement.

At the same time as the frame patterns were coated, two samples of the material were taken from the coating tank to determine its permeability. Based on the Kocan method [47] of measurement as described in Chapter 3, where the volume of air (in  $\text{cm}^3$ ) that can pass through a specimen of  $1 \text{cm}^2$  cross-sectional area and  $1 \text{cm}$  in height, at a pressure difference of  $1 \text{g/cm}^2$  in one minute is reported as a unitless value known as the Permeability Number, the values obtained were 15 and 17 respectively.

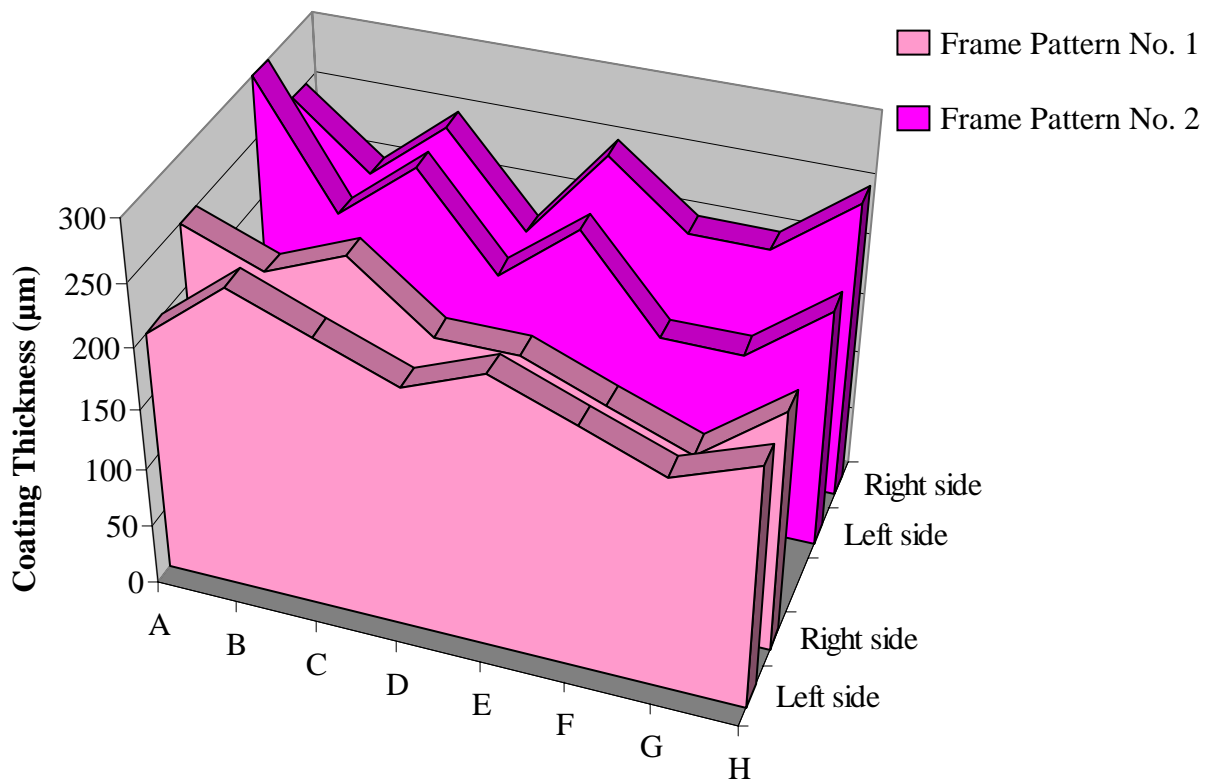


Figure 4.5: Coating thickness variation along either side of two frame patterns.

## 4.2 GRAVITY FILLING

Filling of a mould cavity from the top, so that the liquid metal flows throughout the filling cycle in the direction of the gravity vector, is simple and promotes good conditions for directional solidification. However, it has been shown that filling open channel moulds vertically upwards by means of a well-designed running system has resulted in a higher quality casting by reducing the number of entrainment defects [87]. By observing and comparing the filling conditions prevalent during the casting of top- and bottom-gated polystyrene patterns, it was possible to assess the effectiveness of conventional methoding techniques to the Lost Foam casting process.

### 4.2.1 Metal Flow Characteristics Through Plate Patterns

Vertically oriented, 15 mm thick, expanded polystyrene plates were cast at 784 °C using a gravity-fed method through a single ingate mounted either on the top or the bottom face of the pattern. All castings were made from a single melt of Al-10wt.%Si alloy and the filling

characteristics observed by two means, short-circuited electrodes connected to a datalogger, and imaging using a real-time X-ray unit.

The filling observations from the datalogger have been displayed graphically in Figures 4.6 and 4.7 and show at what point in the filling cycle the liquid metal front made contact with each of 24 separate electrodes that were arranged throughout each cluster. The top-gated plate took 49 s. to fill completely but surprisingly, the other plate with a bottom mounted ingate filled 8 s. quicker.

The average metal velocity, calculated over the complete mould filling time, was  $12.2 \text{ mm.s}^{-1}$  in the case of a top-gated plate and  $12.67 \text{ mm.s}^{-1}$  when bottom gating was used. Although these two values were similar, a single recording at the very end of the pour of the top-gated plate heavily influenced the result obtained. This can be seen in Figure 4.6 where a value of 44.76 s. was recorded in the bottom right hand corner of the plate and where there was a corresponding reduction in the gradient of the line that depicted the time taken for the liquid metal to travel the 87 mm between the lowermost electrodes in that region. This delay was probably caused by a local increase in density in the corner region of the pattern as illustrated in region V11 to V13 of Figure 4.1. By discounting that particular result the average filling speed of the top-gated plate increased to  $15.3 \text{ mm.s}^{-1}$ .

Real time X-ray observations of the filling of top- and bottom-gated plates were made in the ingate and upper region of each cluster configuration. Because the X-ray beam was not wide enough to cover both areas simultaneously, two moulds of each cluster type were cast with the field of view in each case being adjusted to focus on one particular region. Figure 4.8 and Figure 4.9 illustrate the size and position of the field of view for each of the moulds cast and relates to a specific set of 6 frames that have been extracted from a video of a particular mould filling sequence. The uppermost row of white numbering in the top left hand corner of each frame represents the time (in seconds) from the beginning of the fill and row directly underneath it is a number given to that particular filling sequence.

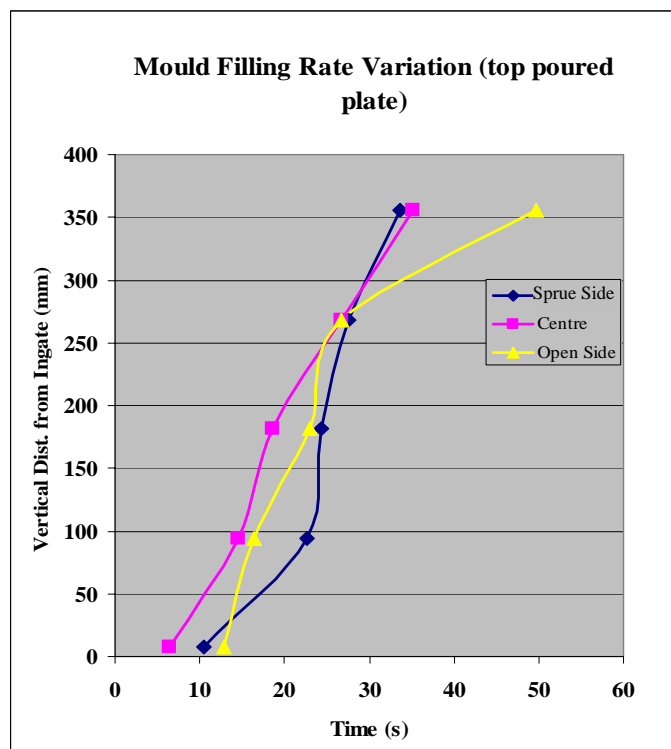
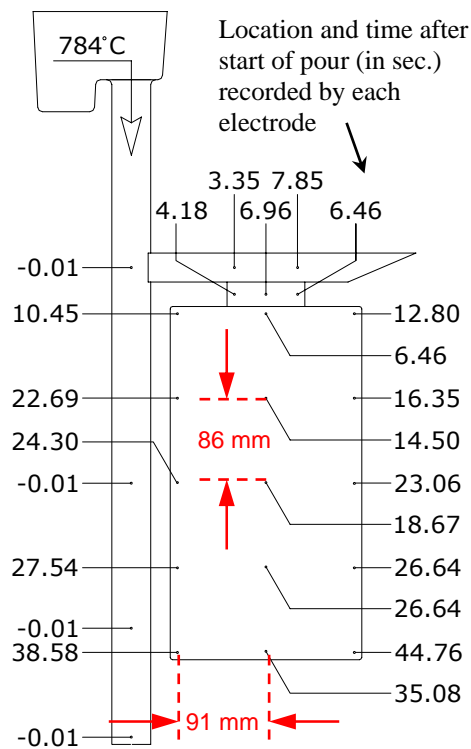


Figure 4.6: Datalogger recordings during the gravity filling of a top-gated plate

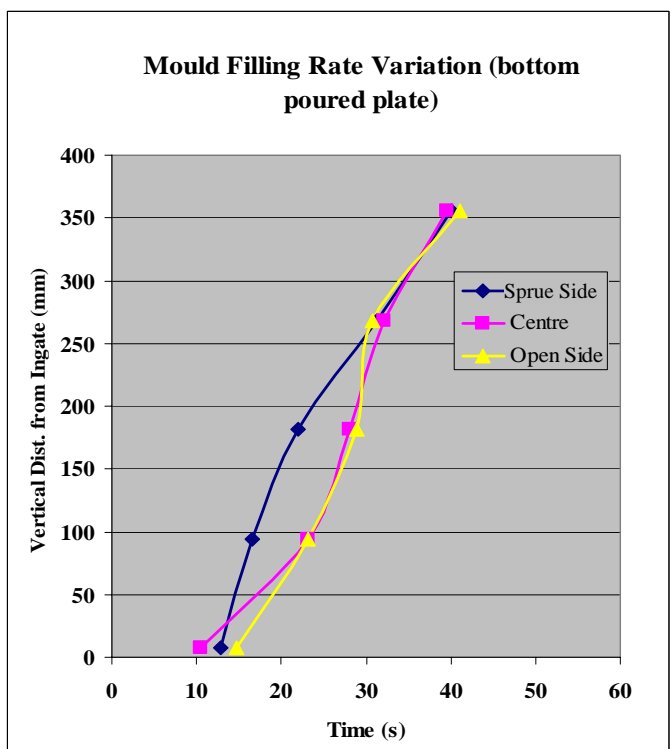
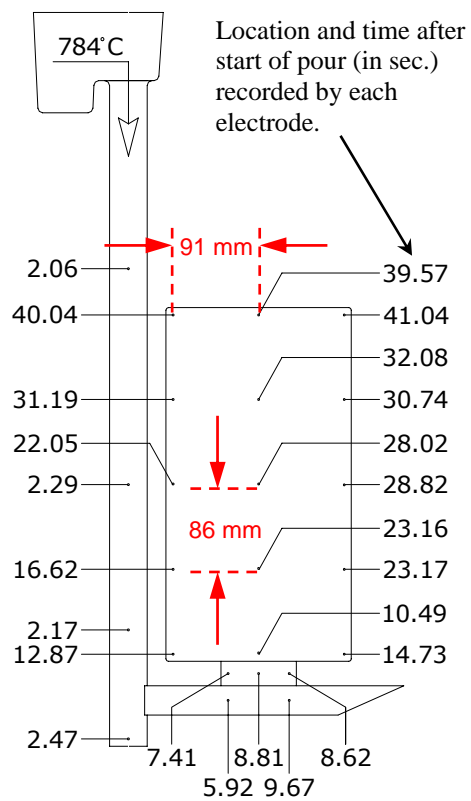


Figure 4.7: Datalogger recordings during the gravity filling of a bottom-gated plate

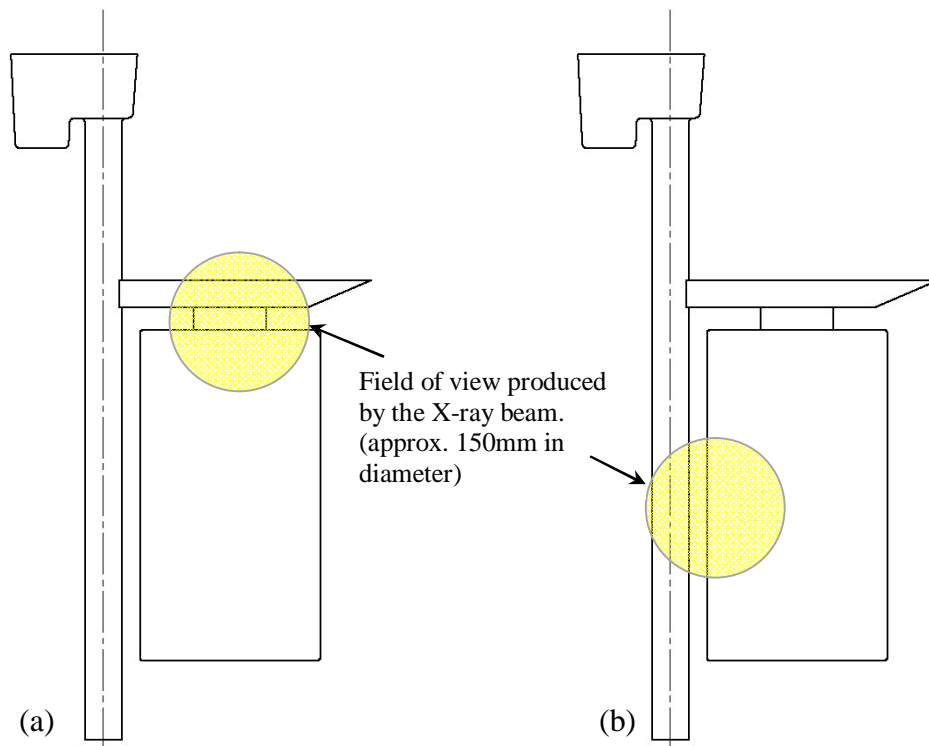


Figure 4.8: Fields of view during the filling of top-gated plates (a) in the ingate region and (b) in the central region of the plate adjacent to the ingate. (see Figures 4.10 and 4.11).

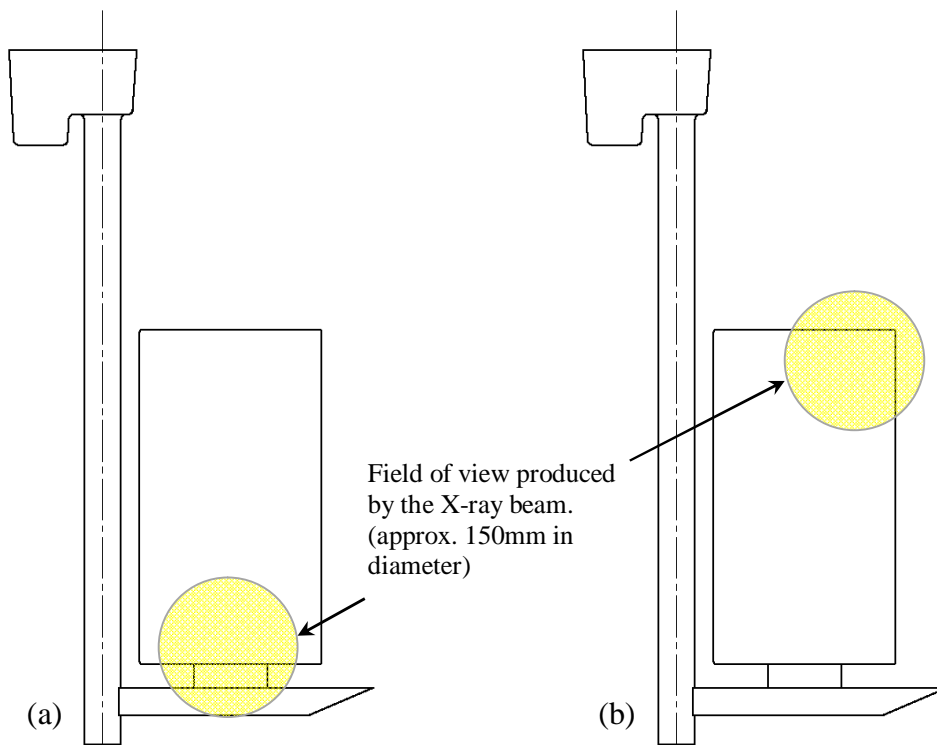


Figure 4.9: Fields of view during the filling of bottom-gated plates (a) in the ingate region and (b) in the upper region of the plate. (see Figures 4.12 and 4.13).

Figure 4.10 illustrates observations made in the ingate region of a top poured plate. The liquid metal front was observed to occupy the complete cross section of the runner bar and flow along it with a convex profile. As soon as the ingate was reached the heat from the metal front began degrading the glue joint connecting it to the runner bar. At the same time the metal front continued to degrade the foam material of the runner bar and flow along the runner bar horizontally. The glue took longer to degrade than the polystyrene and when the glue line was finally breached, flow into the ingate proceeded at a faster rate and in a direction vertically downward through the ingate. The same mechanism occurred at a second glue joint between the ingate and the pattern and this can be seen in Frame 1 of Figure 4.10 as distinct steps in the metal front at each of these joints.

Filling continued in a diagonal fashion across the plate with the upper corner nearest the downsprue filling first. This general flow of metal through the mould was supported by the timing measurements as shown in Figure 4.6. However, there was significant difference at the ingate region where the timing probes detected metal in the pattern in under 7 s. and the real time X-ray suggested that this did not happen until a further 10 s. had elapsed. As the liquid metal advanced through the mould it exhibited some irregularities or perturbations at its front. These can be seen in Frame 3 of Figure 4.10 and had a wavelength of approximately 12 mm and a height of about 4 mm.

Towards the central region of the plate the metal front was observed to have developed into three “stubby” fingers or streams with a wavelength of around 30 mm and a height of 12.5 mm (see Figure 4.11), each showing the same type of surface irregularity or perturbation that was mentioned previously. The average velocity of these fingers was estimated at approximately  $10 \text{ mm.s}^{-1}$  and distinct gaps were observed between them, as shown in Frames 2 and 3 of Figure 4.11, where foam material was being trapped. As they all flowed towards the vertical, left side wall of the plate, they converged together so that any gap between them was eliminated or became too narrow to be detected by the real time X-ray unit. As illustrated in Frames 5 and 6 of Figure 4.11, this convergence into a single front also diminished the number of surface perturbations until they disappeared altogether. This resulted in the front becoming convex in nature.

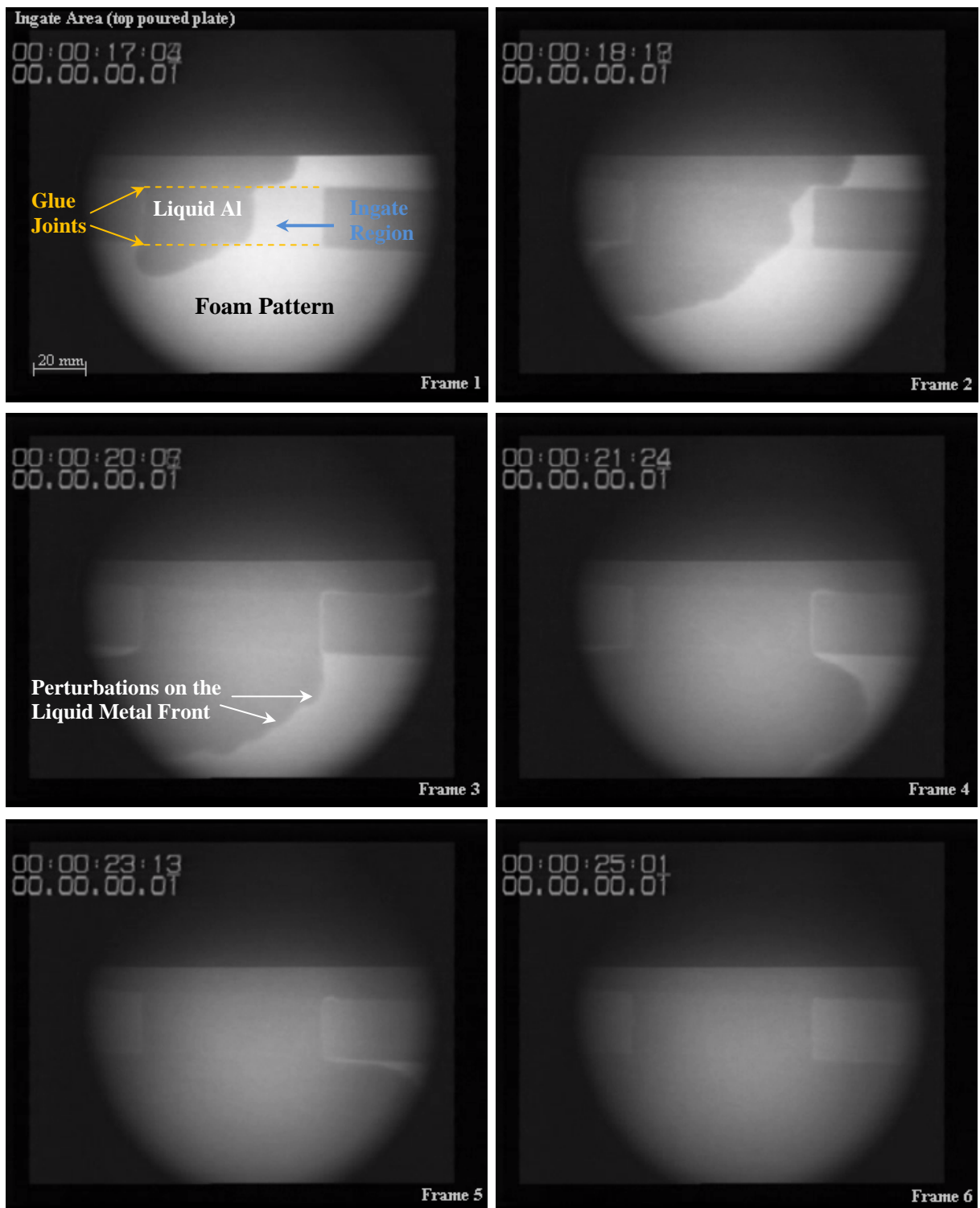


Figure 4.10: Filling behaviour in the ingate region of a top-gated plate.

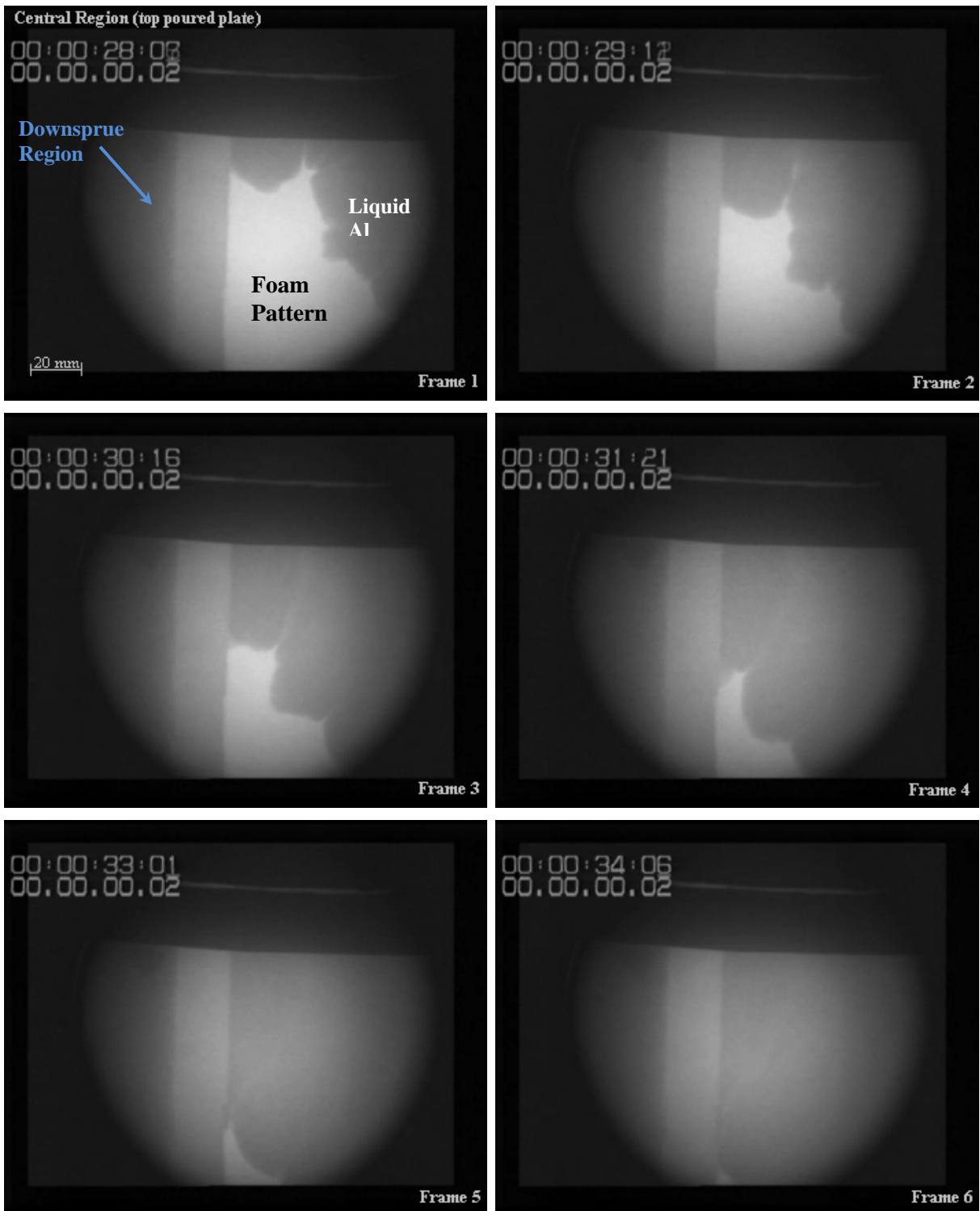


Figure 4.11: Filling behaviour in the central region of a top-gated plate.

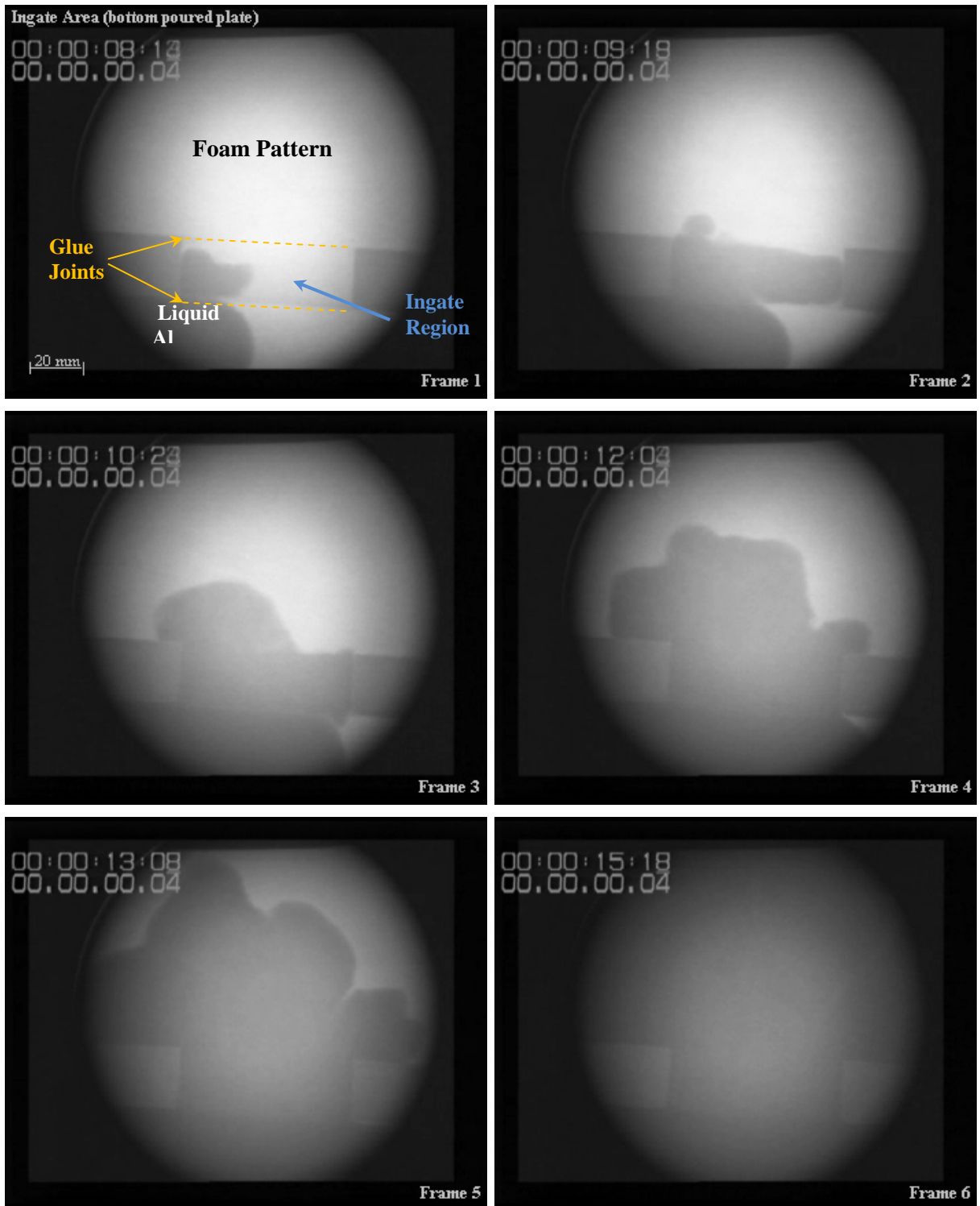


Figure 4.12: Filling behaviour in the ingate region of a bottom-gated plate

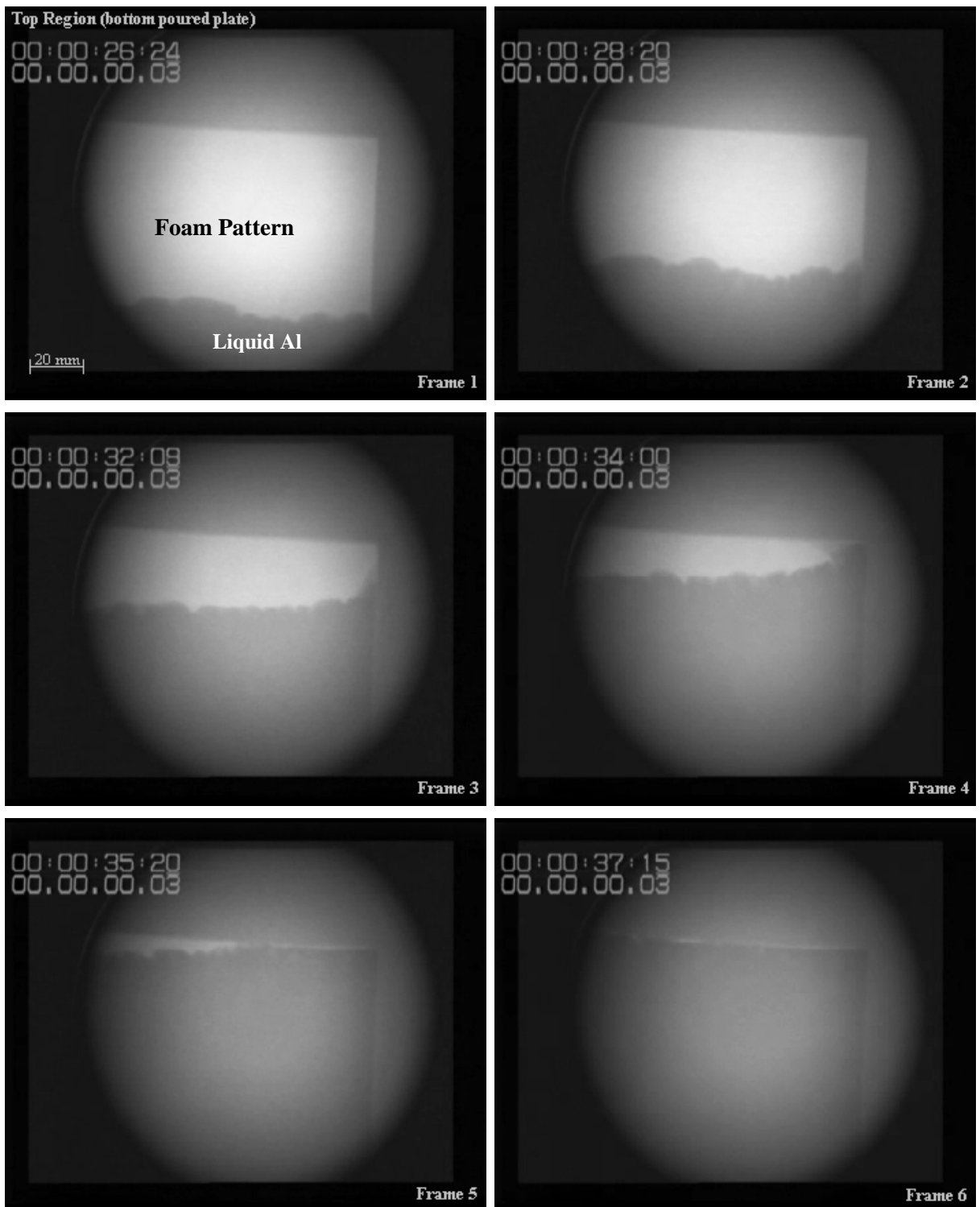


Figure 4.13: Filling behaviour in the upper region of a bottom-gated plate

The initial filling of a bottom-gated plate proceeded in essentially the same manner as that observed during top filling with the glue joints between runner bar, ingate and pattern plate hindering metal flow through that region. Although a step was observed in the metal front as it passed through the ingate, the glue joint between runner bar and ingate was breached much sooner and the ingate filled before the metal in the runner bar had proceeded past the ingate. Approximately 10 s. after start of pouring the metal front entered the pattern by means of a localised break through the glue joint and mushroomed up from the ingate with a convex profile, as shown in Frame 3 of Figure 4.12. However, in less than 2 s. the metal flow had transformed into four stubby fingers that are easily distinguishable in Frames 4 and 5 of the same figure. The thickness of these fingers varied from 22 mm to 42 mm and in height from 12 mm to 19 mm. This similarity between metal flow into top- and bottom-gated plates was unexpected, bearing in mind the results of research into the filling of open cavity moulds where a significant difference is observed.

By the time that the liquid metal had reached the top region of the plate, as depicted in Figure 4.13, the fingers had merged together into a single, almost horizontal front. However, the advancing liquid metal front exhibited similar perturbations as were observed during the filling of the central region of a top-gated plate (see Figure 4.11). The perturbations shown in Frame 1 of Figure 4.13 had a wavelength of around 9 mm and a height of 2 mm, where the average speed of the metal front was about  $6.5 \text{ mm.s}^{-1}$ . The timing electrodes, on the other hand, registered an average vertical velocity in this region of about  $9.5 \text{ mm.s}^{-1}$ . However, this value was estimated over a vertical height of 87 mm and did not include the upper 10 mm of the plate as was the case for the real time X-ray velocity measurements.

Photographs of the castings produced during the real time X-ray experiments have been shown in Figures 4.14 and 4.15. Each casting was fully filled and exhibited a pattern of staining across its surface. The staining was essentially the same on both castings and consisted of a series of brownish grey streaks fanning out from the ingate area in a principally vertical direction. Independent of the location of the ingate the staining was noticeably more pronounced towards the top of the casting and was thought to be caused by the viscous liquid pattern degradation products that were unable to pass through the coating and became trapped at the metal-coating interface.



Figure 4.14: Top-gated plate casting (*made as part of the real time X-ray mould filling analysis. Reference Figures 4.10 and 4.11*)



Figure 4.15: Bottom-gated plate casting (*made as part of the real time X-ray mould filling analysis. Reference Figures 4.12 and 4.13*)

## 4.2.2 Metal Flow Characteristics Through Frame Patterns

The techniques used to make and pour moulds containing frame clusters were effectively the same as used in the previous plate casting experiments. The use of timing electrodes and real time X-ray imaging to monitor the metal front during mould filling were also both used. Although none of the frame castings was fully filled, even at a pouring temperature of 909 °C, which was 125 °C higher than that used to cast the plates, sufficient data were collected to provide meaningful results.

The filling observations collected by means of the timing electrodes are displayed graphically in Figures 4.16 and 4.17. Although the overall filling time for the top-gated frame was approximately 3.5 s. longer than when bottom-gated, the resultant casting exhibited a higher degree of misrun. Bottom gating of the frames was associated with markedly higher average filling velocities and filling distances than when top pouring the same pattern. The flow of liquid aluminium through the bottom poured frame exhibited an average filling velocity of 13.1 mm.s<sup>-1</sup> and a maximum vertical fill height of over 250 mm compared with 8.81 mm.s<sup>-1</sup> and about 160 mm respectively for the top-filled equivalent.

The flow of metal through the top-gated frame was much less uniform than when filled from the bottom. The metal front that travelled through the vertical leg of the frame nearest the downsprue reached the entrance to the third horizontal bar from the ingate more than 12 s. earlier than the front that flowed down the other side of the casting. Although this faster moving front managed to travel further, it reduced in speed dramatically and stopped altogether approximately 50 mm in front of, and 6 s. earlier than, the other one.

Irrespective of the position of the ingate, filling speed reduced as pouring progressed. However, this was most pronounced when a top-gated frame was cast because the metallostatic pressure driving the liquid aluminium through the ingate and into the pattern was lower than when bottom gating was used. Interestingly, plates and frames were made with identical running systems but only the plates were fully formed, even though an additional 125 °C of superheat was used in the casting of frames. This was due to the marked difference in modulus between the two pattern types (i.e. 0.67 cm for a plate and only 0.38 cm for a frame).

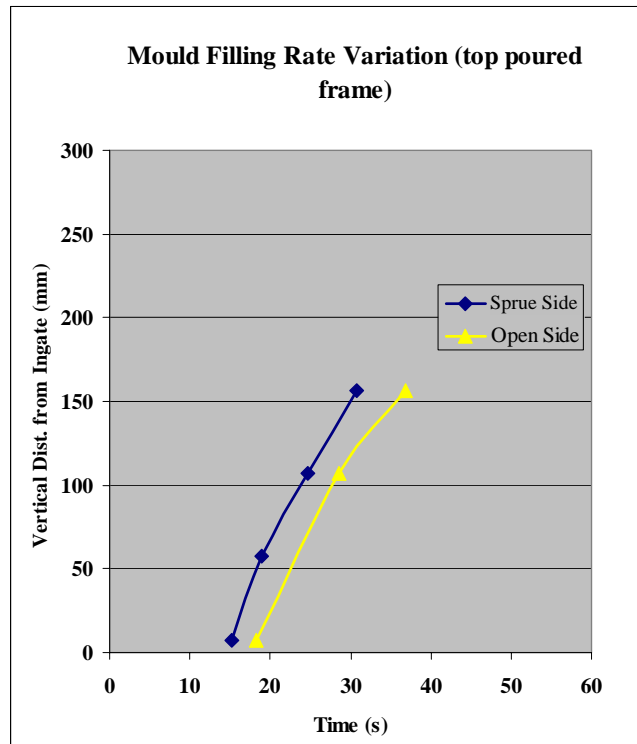
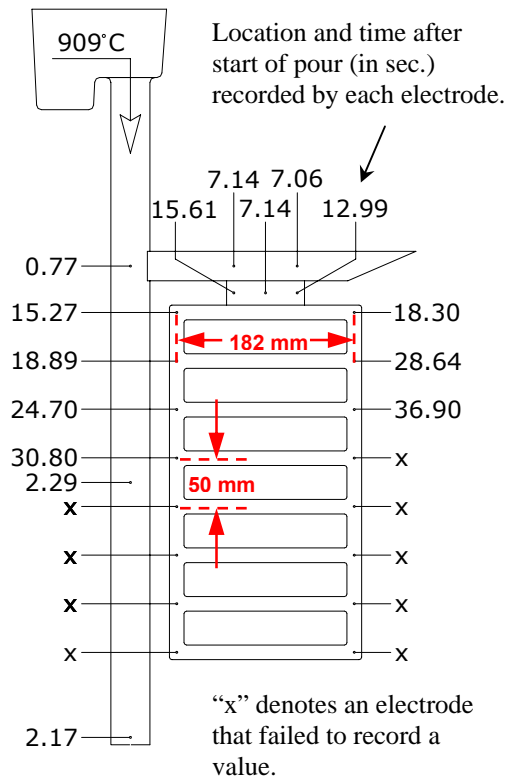


Figure 4.16: Datalogger recordings during the gravity filling of a top-gated frame.

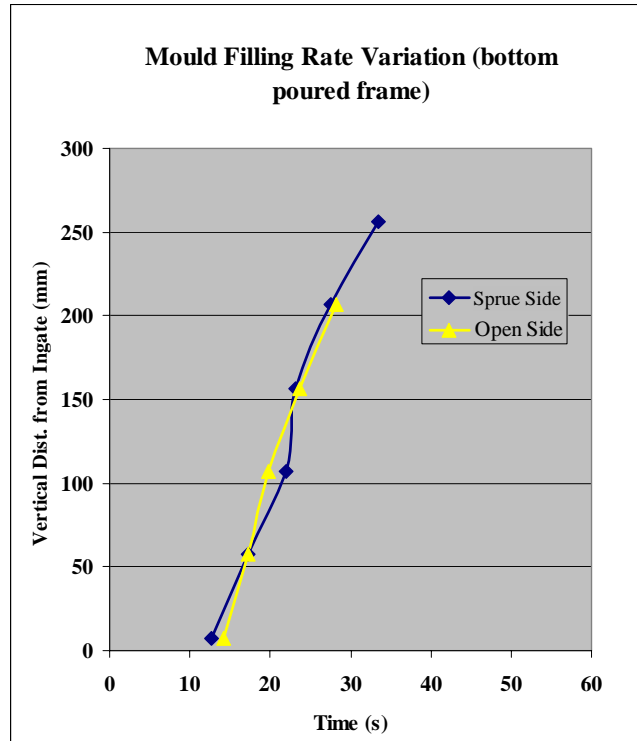
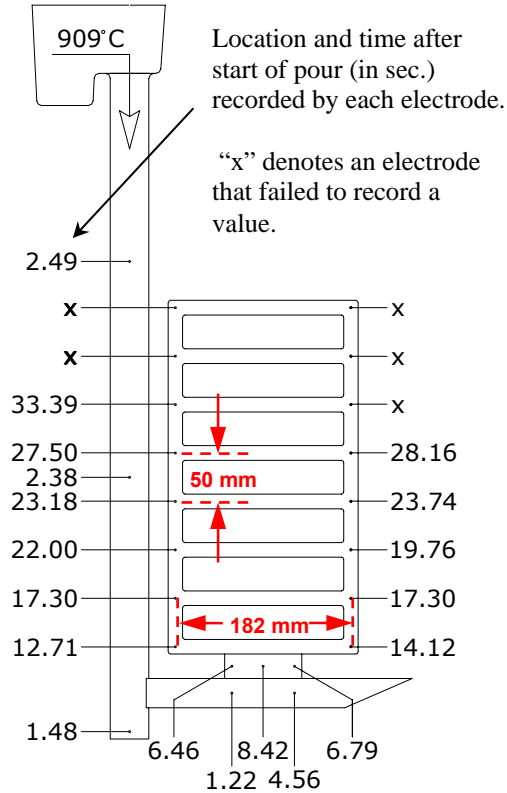


Figure 4.17: Datalogger recordings during the gravity filling of a bottom-gated frame.

Real time X-ray observations of the filling of top- and bottom-gated frames are shown in Figures 4.20 to 4.23 and Figure 4.18 and 4.19 illustrate the region in each mould where filling was observed. As the metal entered a frame it split into two streams that flowed horizontally, in opposite directions, towards the corners of the pattern. At these corners the metal was forced to change direction by  $90^\circ$  and began to fill the vertical sections of the frame. When a junction with another horizontal bar was reached, each stream of metal split into two distinct fronts. One front began to fill this bar from the end whilst the other front continued up along the vertical section of the frame. The splitting of the front in this manner can just be seen in Frame 2 of Figure 4.20, Frame 1 of Figure 4.21 and more clearly in all frames of Figure 4.22. This meant that each horizontal bar was filled by two opposing liquid metal fronts which met towards the middle. This general pattern of filling continued until the fronts froze prematurely, before the casting was fully formed.

Initially the horizontally travelling metal fronts occupied the complete cross section of the bar and exhibited a somewhat convex shape. As they approached one another their profiles became more elongated in the horizontal plane so that they occupied more of the lower region of the bar. As their tips met the faster flowing metal immediately behind caught up and caused the junction to grow vertically in height. This is well illustrated in Frames 3 to 6 of Figure 4.21. The last part of the horizontal bar to fill was its uppermost region, just behind the tip of each front, and evidence of pattern degradation product entrapment was observed in some of these regions as shown in the second of three horizontal bars in Frame 5 of Figure 4.21.

On dividing into two fronts at the junction between two bars, one metal stream was observed to flow faster than the other. Where a top gate had been applied, the front flowing through a horizontal section was the most prominent and where a bottom gate had been used, flow along the vertical section was faster. The average front velocity, estimated during observations of the filling process by real time X-ray, supported those of the timing electrodes. Bottom-gated castings filled with an average front speed of around  $10 \text{ mm.s}^{-1}$  and top-gated castings at approximately half that value. This is consistent with the fact that bottom gating was associated with a significantly higher metallostatic head than when the ingate was placed at the top of the casting and this difference also accounted for the disparity in speed of the horizontal and vertical advancing liquid metal fronts.

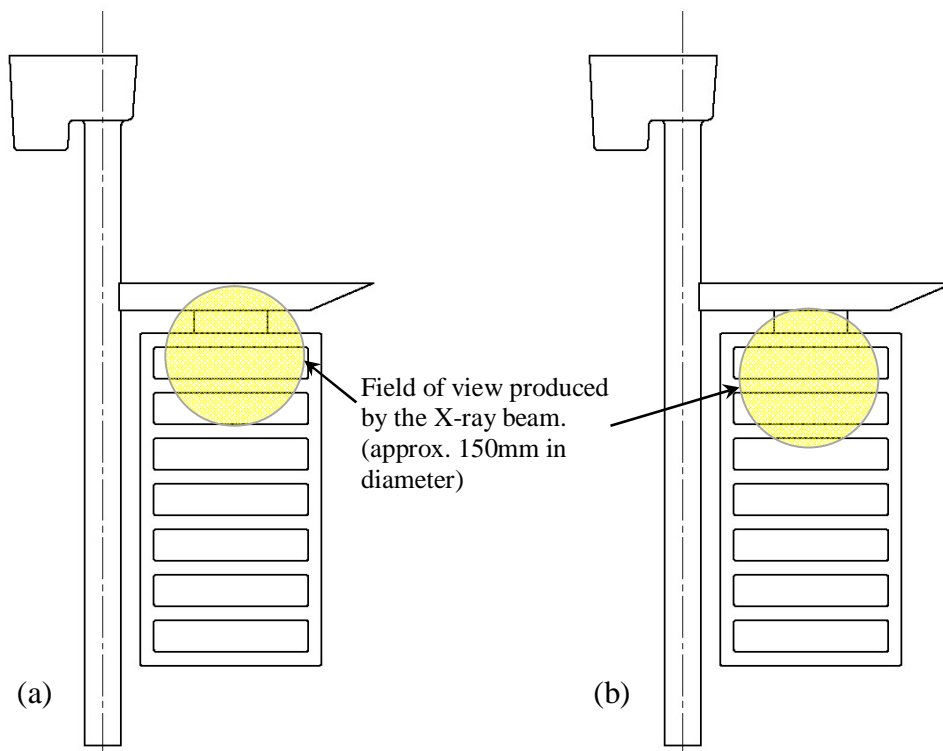


Figure 4.18: Fields of view during the filling of top-gated frames (a) in the ingate region and (b) slightly below the ingate (see Figures 4.20 and 4.21).

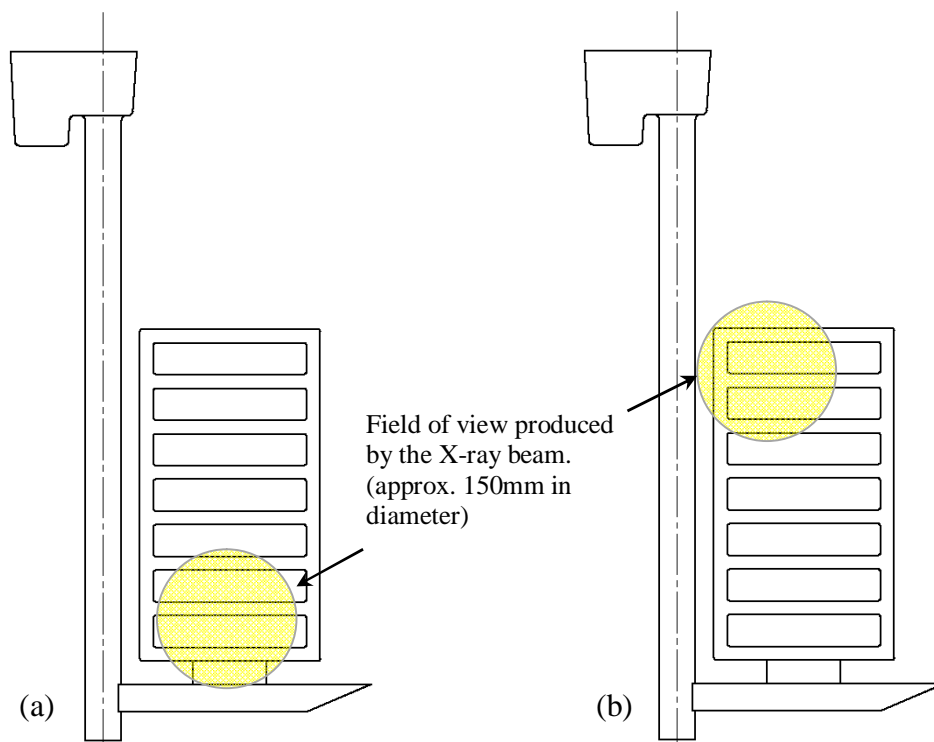


Figure 4.19: Fields of view during the filling of bottom-gated frames (a) in the ingate region and (b) in the top corner nearest the sprue (see Figures 4.22 and 4.23).

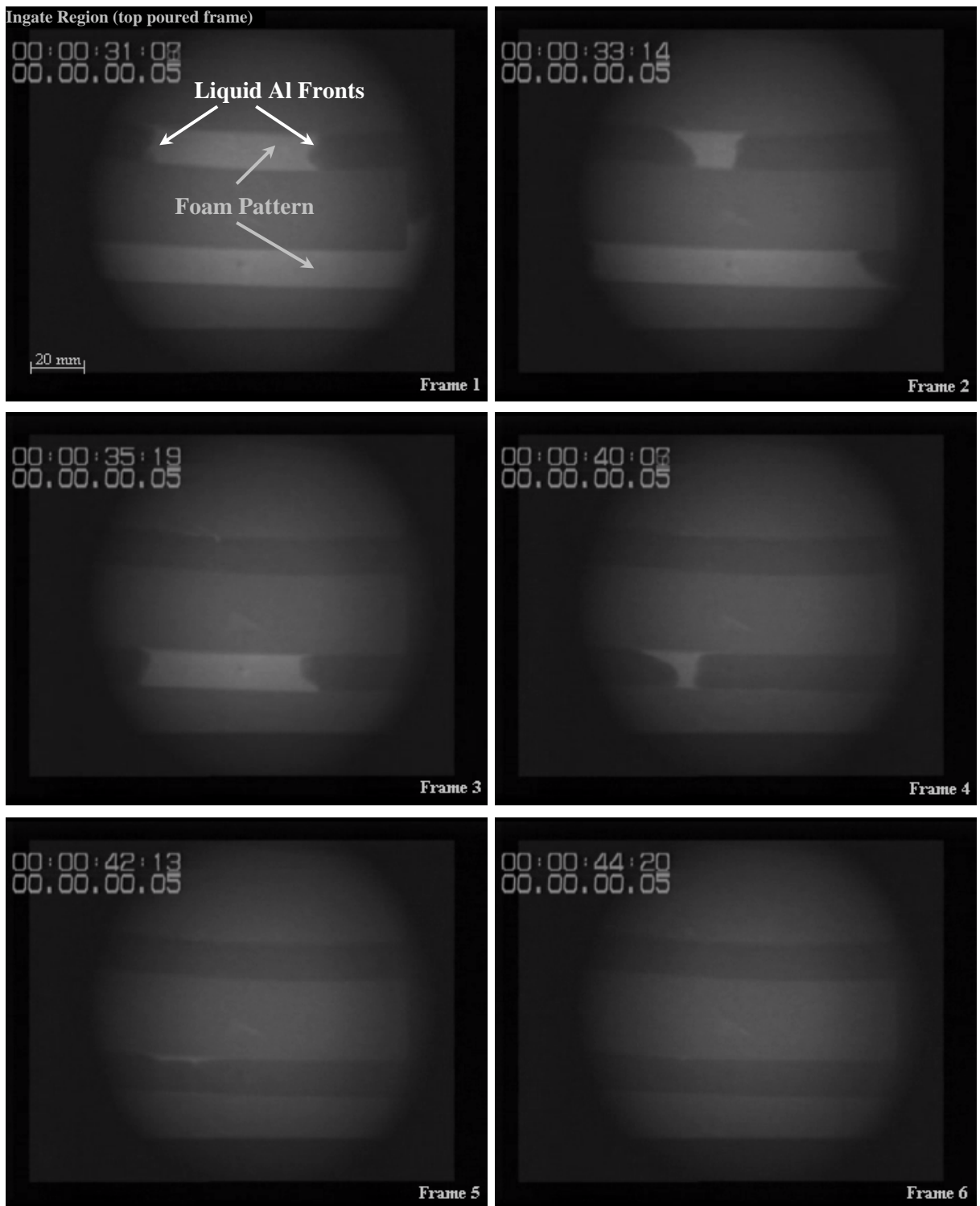


Figure 4.20: Filling behaviour in the ingate region of a top-gated frame

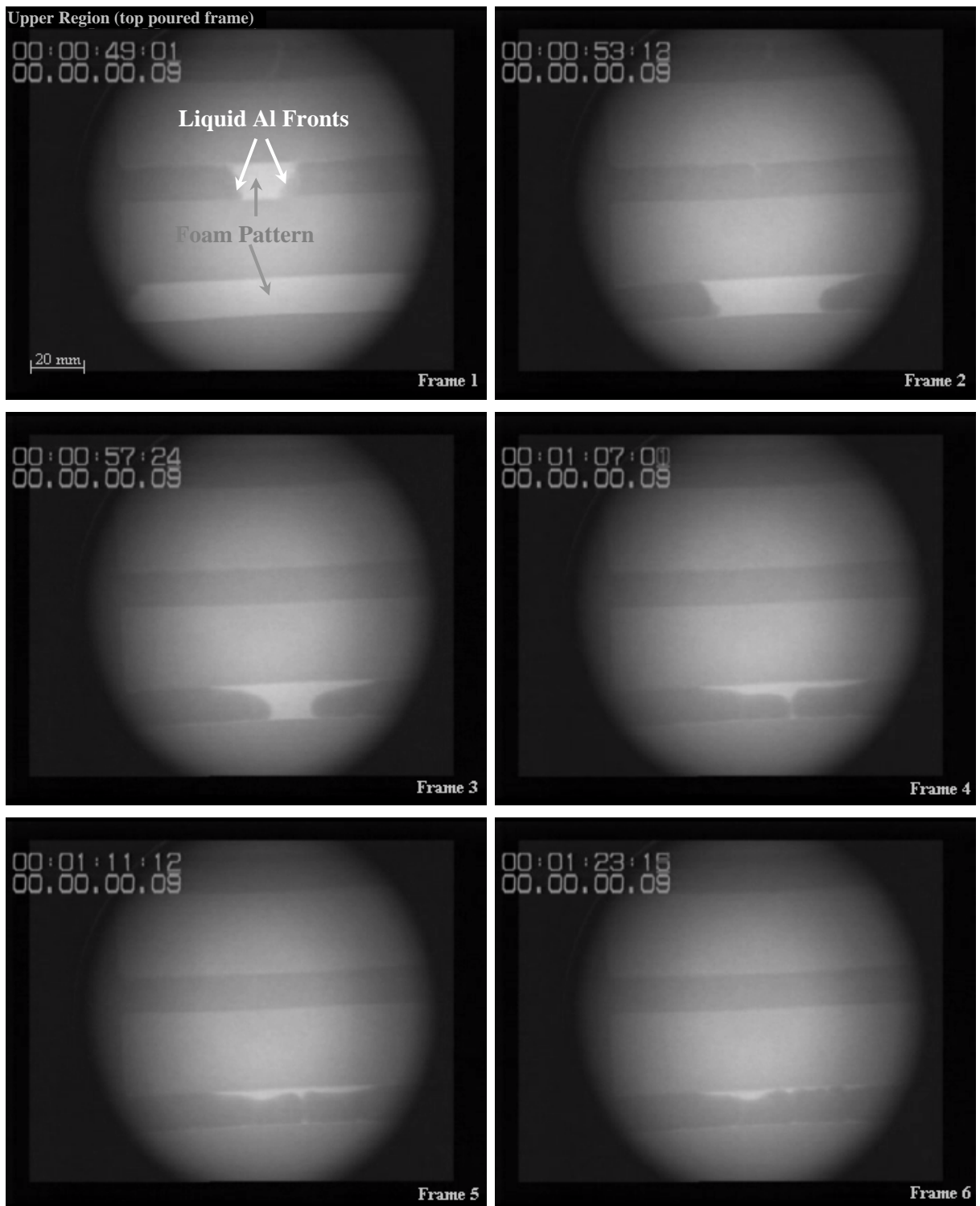


Figure 4.21: Filling behaviour in the upper region of a top-gated frame (just below the ingate)

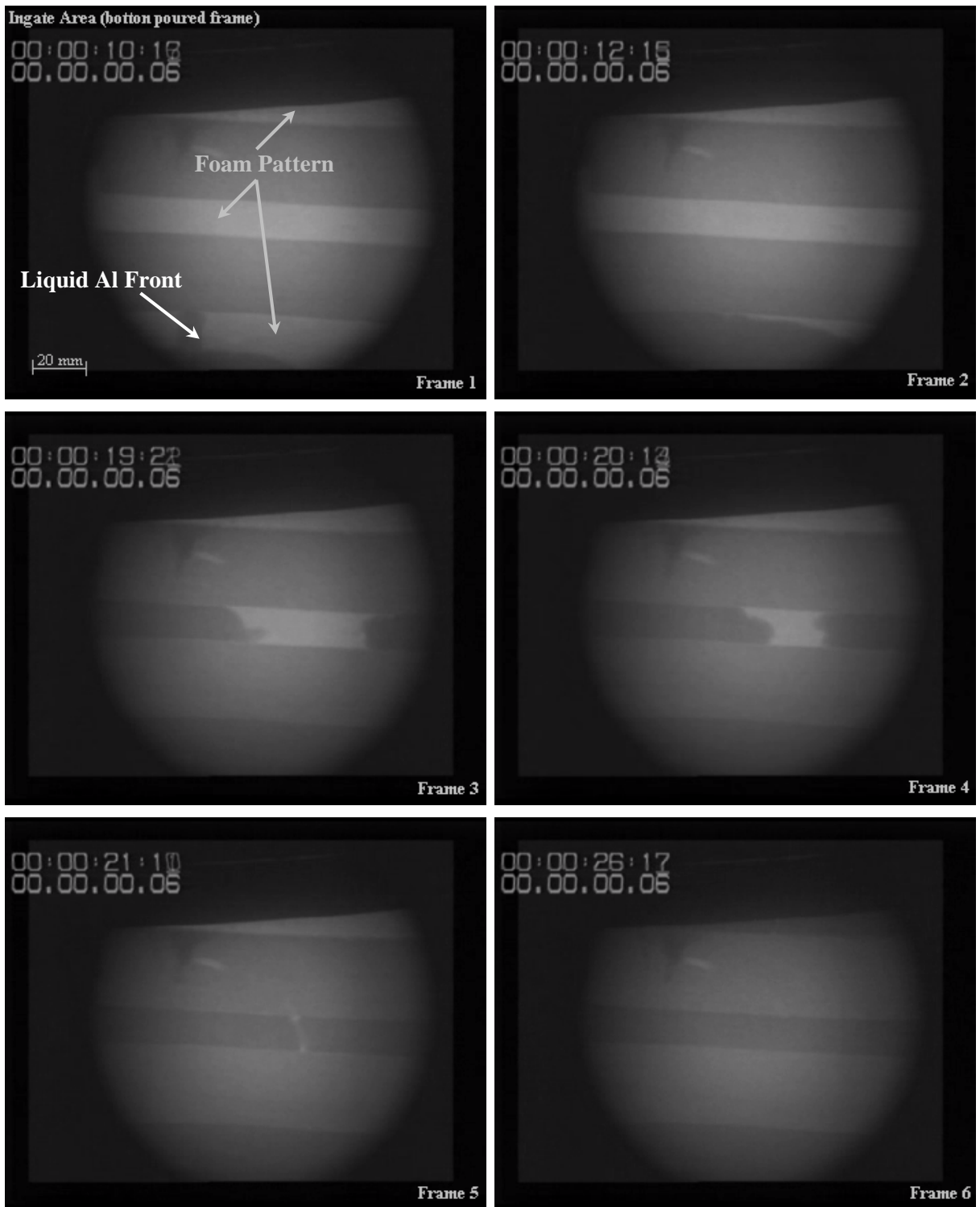


Figure 4.22: Filling behaviour in the ingate region of a bottom-gated frame.

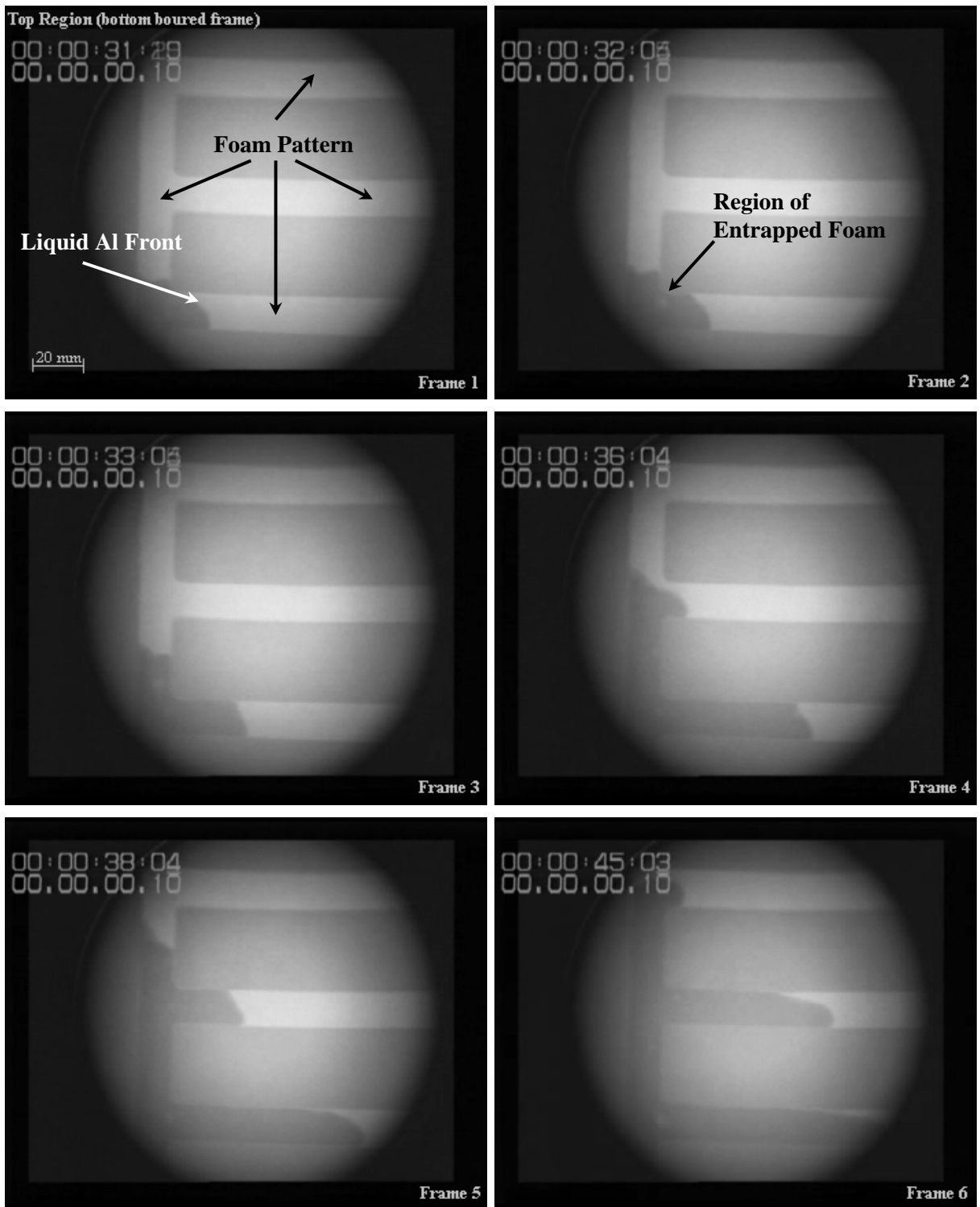


Figure 4.23: Filling behaviour in the upper region of a bottom-gated frame.



Figure 4.24: Top-gated frame casting (*made as part of the real time X-ray mould filling analysis. Reference Figure 4.20 and 4.21*)



Figure 4.25: Bottom-gated frame casting (*made as part of the real time X-ray mould filling analysis. Reference Figure 4.22 and 4.23*)

Misrun was observed on each of the frame castings that were made and is illustrated in Figures 4.24 and 4.25. Although the appearance of the defect was independent of the location of the ingate, the lower metallostatic head available during the filling of top-gated frames resulted in the most poorly formed castings. This can be seen by comparison of the top- and bottom gated frames shown in Figures 4.24 and 4.25 respectively.

### 4.3 PROPERTIES OF GRAVITY FILLED CASTINGS

The ultimate tensile strength (UTS) of a number of samples taken from castings made during the gravity filling experiments was used as a measure of the quality associated with the different filling techniques that had been applied. Fracture surfaces were examined to determine the possible cause of failure and characterise any defects found.

#### 4.3.1 Tensile Strength Variation in the Castings

Table 4.26 contains the UTS results from top and bottom gated plates and Table 4.27 contains the equivalent data for frames.

Ultimate Tensile Strength Results of Plate Samples (MPa)							
Top Gated Castings				Bottom Gated Castings			
Location	Plate 1	Plate 2	Plate 3	Location	Plate 4	Plate 5	Plate 6
A	120	114	89	A	130	130	127
B	73	96	108	B	114	113	101
C	125	108	99	C	104	111	121
D	125	129	103	D	111	116	101
E	129	131	125	E	124	130	123
F	141	130	129	F	136	123	127
G	140	141	131	G	141	135	136
H	136	150	151	H	145	149	155
Range	68	42	62	Range	41	38	54
$\bar{\chi}$	123.63	124.88	116.88	$\bar{\chi}$	125.63	125.88	123.88
$\sigma$	21.82	17.76	20.51	$\sigma$	14.92	12.79	17.69
Group Range		78		Group Range		54	
Group $\bar{\chi}$		121.79		Group $\bar{\chi}$		125.13	
Group $\sigma$		19.54		Group $\sigma$		14.61	

Table 4.26: UTS results of samples taken from top- and bottom-gated plates.

The location in a casting from which each test bar was taken is shown in Figures 3.6 and 3.7. However, sample “A” always represented the one taken from nearest the ingate and “H” the one taken furthest from it.

Ultimate Tensile Strength Results of Frame Samples (MPa)									
Top Gated Castings					Bottom Gated Castings				
Location	Frame 1	Frame 2	Frame 3	Frame 4	Location	Frame 5	Frame 6	Frame 7	Frame 8
A	156	152	147	161	A	156	145	140	153
B	166	65	127	164	B	172	92	55	133
C	171	140	58	67	C	171	47	92	171
D	139	63	89	122	D	132	57	68	160
E	174	97	76	126	E	135	143	145	148
F	163	158	51	-	F	-	-	168	-
G	-	-	129	-	G	-	-	-	-
H	-	-	-	-	H	-	-	-	-
Range	35	95	96	97	Range	40	98	113	38
$\bar{\chi}$	161.50	112.50	96.71	128.00	$\bar{\chi}$	153.20	96.80	111.33	153.00
$\sigma$	12.69	43.21	37.78	39.20	$\sigma$	19.10	46.22	46.02	14.12
Group Range				123	Group Range				125
Group $\bar{\chi}$				123.38	Group $\bar{\chi}$				127.76
Group $\sigma$				41.37	Group $\sigma$				41.37

Table 4.27: UTS results of samples taken from top- and bottom-gated frames.

Bottom poured plates produced slightly better UTS values than those achieved when the same type of casting was filled from the top. The group average was higher at 125 MPa as compared to 122 MPa and the group range and standard deviation values were lower. This contrasted sharply with the results obtained from frames where the group results were similar whether filled from the bottom or the top.

To determine the statistical significance of the variation of individual values recorded within each of the four groups, an analysis of variance (ANOVA) was carried out that applied 95% confidence limits to the mean of each casting. The results are contained in Tables 4.28 to 4.31 where SS is the sum of squares, df is the degrees of freedom, MS is the mean square, F is the F statistic and equals the MS between groups divided by MS within groups, P-value is the probability of the F statistic value occurring under the assumption of the null hypothesis and  $F_{crit.}$  is the value of F at the 95% confidence level based on the degrees of freedom between the groups and the error.

**SUMMARY**

Groups	Count	Sum	Average	Variance
Plate 1	8	989	123.625	475.98214
Plate 2	8	999	124.875	315.55357
Plate 3	8	935	116.875	420.69643

**ANOVA**

Source of Variation	SS	df	MS	F	P-value	F crit
Between Groups	296.33333	2	148.16667	0.3666789	0.6973822	3.4667949
Within Groups	8485.625	21	404.07738			
Total	8781.9583	23				

Table 4.28: ANOVA of UTS values obtained from top-gated plates

**SUMMARY**

Groups	Count	Sum	Average	Variance
Plate 4	8	1005	125.625	222.55357
Plate 5	8	1007	125.875	163.55357
Plate 6	8	991	123.875	312.98214

**ANOVA**

Source of Variation	SS	df	MS	F	P-value	F crit
Between Groups	19	2	9.5	0.0407673	0.9601283	3.4667949
Within Groups	4893.625	21	233.02976			
Total	4912.625	23				

Table 4.29: ANOVA of UTS values obtained from bottom-gated plates

**SUMMARY**

Groups	Count	Sum	Average	Variance
Frame 1	6	969	161.5	161.1
Frame 2	6	675	112.5	1866.7
Frame 3	7	677	96.714286	1427.5714
Frame 4	5	640	128	1536.5

**ANOVA**

Source of Variation	SS	df	MS	F	P-value	F crit
Between Groups	14513.1964	3	4837.7321	3.8934798	0.0242433	3.0983927
Within Groups	24850.4286	20	1242.5214			
Total	39363.625	23				

Table 4.30: ANOVA of UTS values obtained from top-gated frames.

**SUMMARY**

Groups	Count	Sum	Average	Variance
Frame 5	5	766	153.2	364.7
Frame 6	5	484	96.8	2136.2
Frame 7	6	668	111.33333	2118.2667
Frame 8	5	765	153	199.5

**ANOVA**

Source of Variation	SS	df	MS	F	P-value	F crit
Between Groups	12832.876	3	4277.6254	3.3992361	0.0418871	3.1967744
Within Groups	21392.933	17	1258.4078			
Total	34225.81	20				

Table 4.31: ANOVA of UTS values obtained from bottom-gated frames

The critical value for P was 0.05 which was set by the use of 95% confidence limits. Table 4.28 and Table 4.29 determined that the P-value for top-gated and bottom-gated plate castings was much higher than  $P_{crit}$ . This meant that in combination with low F statistic values, any variation in the results was within the boundaries of acceptable statistical error. However, when the same analysis was conducted on the results obtained from the frame castings, as shown in Figures 4.30 and 4.31, both P-values were lower than  $P_{crit}$ , and F statistic values were higher than  $F_{crit}$ . This indicated that the variation in the tensile values was significant and due to something other than statistical error.

In order to test the null hypothesis that the results for plates cast by means of either a top or bottom ingate were independent of its location, tensile strength data from Table 4.26 were subjected to a Fisher exact one-sided analysis on the median. The median value for the combined set of results was 126 MPa and this allowed the construction of Table 4.32.

<b>No. of Plate Casting UTS Results on Each Side of the Median</b>			
<b>Data Description</b>	<b>Top gated</b>	<b>Bottom gated</b>	<b>Combined</b>
No. of scores above combined median	12	12	24
No. of scores below combined median	12	12	24

Figure 4.32: 2 x 2 Contingency table for UTS results obtained from top- and bottom-gated plate castings about the combined median.

The chance probability of obtaining the same or a more extreme array of results is 0.613 and therefore the higher average UTS results obtained from bottom gated plates cannot be attributed statistically to the location of the ingate.

The results of this analysis clearly showed that the location of the ingate had no statistical significance on the UTS values obtained in any of the plates. However, it was not possible to determine if the same was true for top- and bottom-gated frames, or between plates and frames, because a statistically significant difference was found between the UTS values of each of the top-gated frames and also between the UTS values of each of the bottom-gated frames. This was due the influence of one or more uncontrolled variables in the casting process.

Green and Campbell [148] suggested that the Weibull distribution, rather than the normal or the type 1 extreme distributions, most accurately described the scatter of tensile test data derived from cast specimens. The validity of this statement to the UTS results obtained from top- and bottom-gated plates was examined by adopting the same methodology as used by the original authors. Firstly, they determined a linear relationship for each distribution and then measured the ‘goodness of fit’ of each set of data to these relationships by means of the regression coefficient. For normally distributed data, where any scatter was purely the result of random experimental errors, the cumulative distribution of failures,  $F_N$  (as in Equation 4.1), vs. tensile strength resulted in a straight line when plotted on normal probability paper.

$$F_N = \frac{1}{2\pi} \int_{-\infty}^x \exp \left[ -\frac{1}{2} \left( \frac{x - \mu}{\sigma} \right)^2 \right] \frac{dx}{\sigma} \quad \text{Equation 4.1}$$

where  $x$  is the tensile strength of the specimen,  $\mu$  is the sample mean value and  $\sigma$  is the standard deviation.

For a Weibull distribution, the data was described in two-parameter form as in Equation 4.2.

$$F_w = 1 - \exp \left[ - \left( \frac{x}{\sigma} \right)^\lambda \right] \quad \text{Equation 4.2}$$

where  $F_w$  is the fraction of specimens failed at or below a given value of  $x$ , e.g. a measured UTS value,  $\sigma$  is a characteristic value of  $x$  at which 62.8% of the population of specimens have failed and  $\lambda$  is the Weibull modulus. A straight line was obtained by rearranging and plotting  $\ln\{\ln[1/(1-F_w)]\}$  vs.  $\ln(x)$ .

Finally, for the type 1 extreme distribution, the cumulative distribution was expressed in the form

$$F_1 = \exp\left[-\exp\left(\frac{x - \mu}{\sigma}\right)\right] \quad \text{Equation 4.3}$$

where  $x$  is the fracture stress,  $\mu$  is the position parameter and  $\sigma$  is a width parameter. A straight line for this type of distribution was obtained by  $\ln[-\ln(F_1)]$  vs.  $x$ .

The frequency plots of the normalised UTS data for top- and bottom-gated plates are shown in Figure 4.33 and it can be seen that the top-gated data set is more heavily skewed to the right than the bottom-gated set.

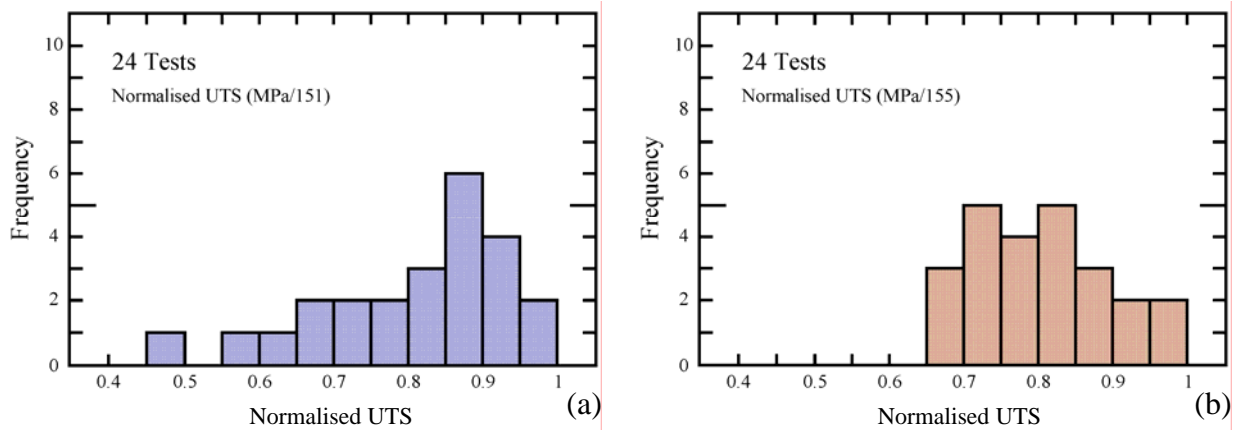


Figure 4.33: Frequency plots of normalised UTS data for (a) top-gated and (b) bottom-gated plate castings.

The corresponding regression coefficients for each type of distribution are listed in Table 4.34 and they indicate that the Weibull distribution was most accurate in describing the spread of results of the top-gated data set whilst the normal distribution best applied to that from the bottom-gated plate. However, the Weibull distribution was, on average, the most accurate overall and therefore used as the comparator between the data sets.

Cluster design	Analysis	Regression coefficient	Best-fit parameters
Top-gated plate	Normal	0.9462	$\mu = 0.8066, \sigma = 0.1294$
	Weibull	0.9689	$\sigma = 0.8637, \lambda = 6.2272$
	Type 1 extreme	0.8345	$\mu = 0.8648, \sigma = 0.1009$
Bottom-gated plate	Normal	0.9840	$\mu = 0.8073, \sigma = 0.0943$
	Weibull	0.9668	$\sigma = 0.8685, \lambda = 9.2487$
	Type 1 extreme	0.9590	$\mu = 0.8497, \sigma = 0.0735$

Table 4.34: ‘Goodness of fit’ of normal, Weibull and type 1 maximum extreme value distributions to the UTS data from top- and bottom gated plate castings.

Figure 4.35 contains Weibull plots of the UTS results from both top-gated and bottom-gated plates and showed that bottom gating produced the more consistent result over the three separate castings that were evaluated.

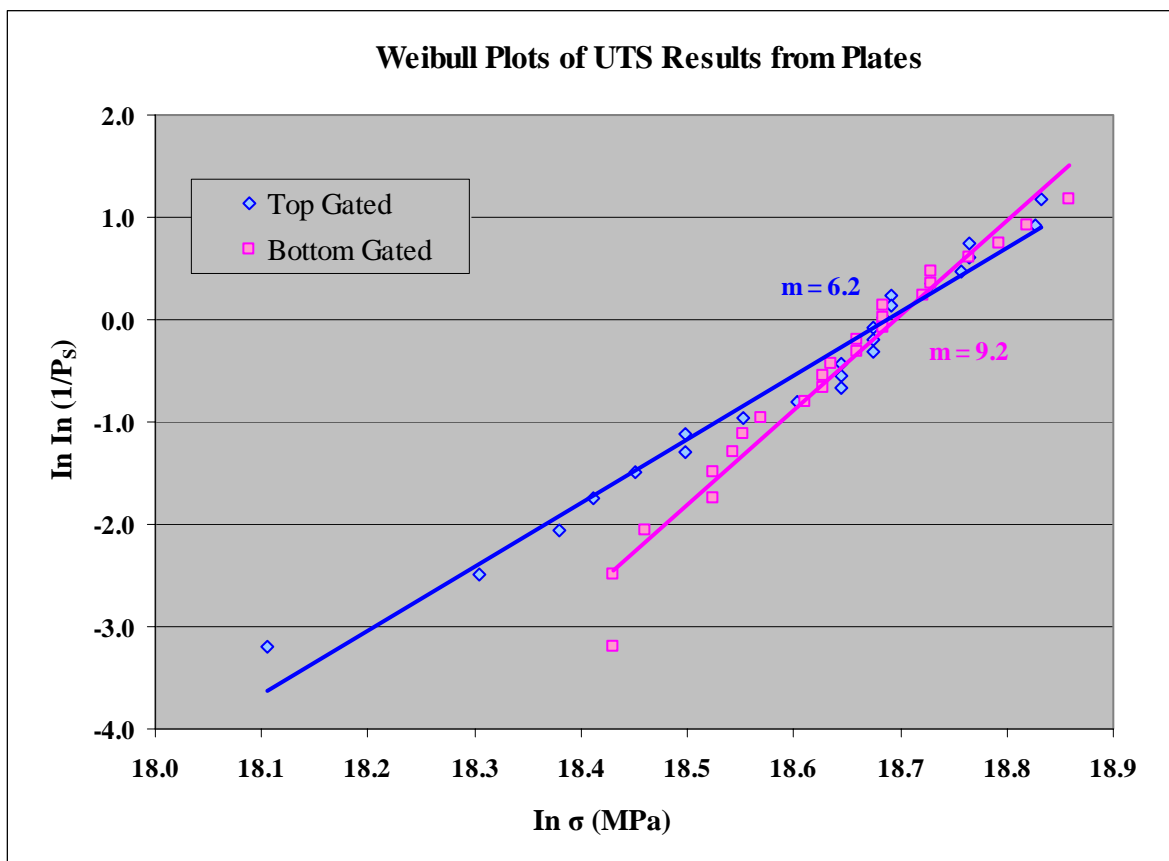


Figure 4.35: Weibull plots of UTS results from top- and bottom-gated plates.

There was much less difference in the Weibull plots related to top- and bottom-gated frames, which are shown in Figure 4.36. The Weibull modulus related to bottom-gated frame results was only 2.5 and that for top gating was only 0.2 higher at 2.7.

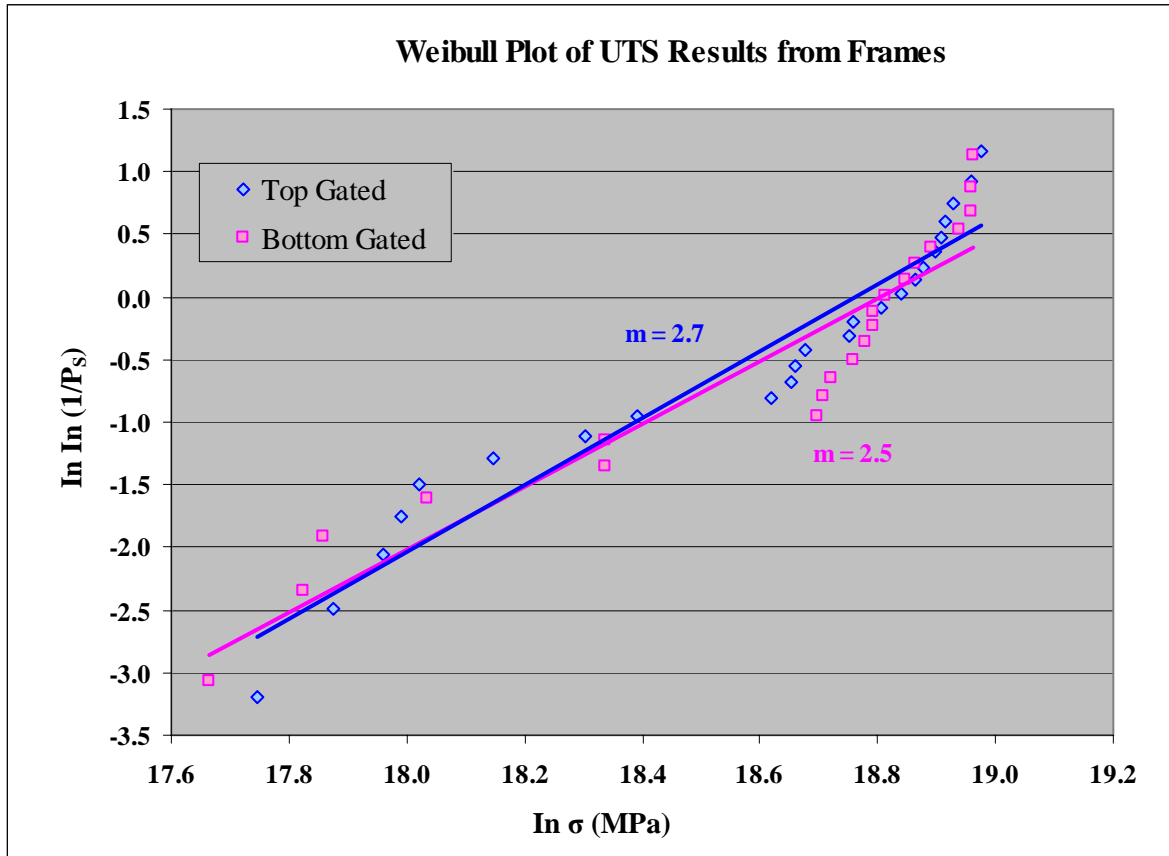


Figure 4.36: Weibull plots of UTS results from top- and bottom-gated frames.

The Weibull plots shown in Figure 4.36 indicated that, for each set of data, at least two distinct subgroups might exist, each represented by its own straight line. However, the sample sizes of these subgroups were well below 20 and considered by Holland et al. [157] to be too small to provide an estimate of a high probability of survival. Also, no correlation could be found between samples with low tensile strength and the locations from which they had been taken from the castings (see Table 4.27). Therefore, although the regression coefficients for the complete top-gated and bottom-gated data sets were only 0.9279 and 0.8915 respectively, it was not considered that any analytical benefit would be achieved by dividing the data sets into subgroups.

Irrespective of pattern type or ingate location, the Weibull moduli were extremely low in comparison with values reported for castings made by open cavity methods. For example, Green and Campbell [89] cast a number of test bars in Al-7Si-0.4Mg aluminium alloy using the open cavity method and reported a Weibull modulus of 10.8 when the ingate was at the top of the casting and 19.7 when it was located at the bottom. The highest value of 50.3 was obtained when the researchers modified and filtered the alloy before it entered the mould cavity through bottom ingates. Frame casting results even compared poorly with those obtained from ceramic materials where a Weibull modulus of 5 has been commonly regarded as describing the least reliable of this class of materials [158].

### **4.3.2 Fracture Surface Defects**

Scanning electron microscopy was used to examine the fracture surfaces of test bars taken from the four, gravity-filled cluster configurations. Interdendritic porosity, as shown in the photomicrograph of Figure 4.37a, was observed on each fracture surface. This defect varied in diameter from 300  $\mu\text{m}$  to about 1500  $\mu\text{m}$  and was randomly dispersed over the whole fracture surface. A localised region, as depicted by the white square on the photomicrograph of Figure 4.37a, was subject to microprobe analysis. The results are depicted as a Spectrum A in Figure 4.38 and indicated the presence of about 18 wt.% of carbon and about 4% by weight of oxygen in that region. The high concentration of carbon was caused through degradation of the polystyrene pattern material whereas the oxygen may have been associated with an oxide film.

In addition to pores, film-type defects were also detected but only on the fracture surfaces of frame castings. An example of this defect is shown in Figure 4.37b and is characterised by a relatively smooth appearance of the surface in the upper two thirds of the photomicrograph. It was much less prevalent than the porosity defect but was generally much larger, extending up to 3 mm in length in one case. Spectrum B in Figure 4.38 was produced by microprobe analysis of the area bordered by the white square in Figure 4.37b. This indicated that the surface of the film type defect had a carbon content of approximately 8 wt.%, and an oxygen content of about 4 wt.%, which was similar to that of the pore in Figure 4.37a.

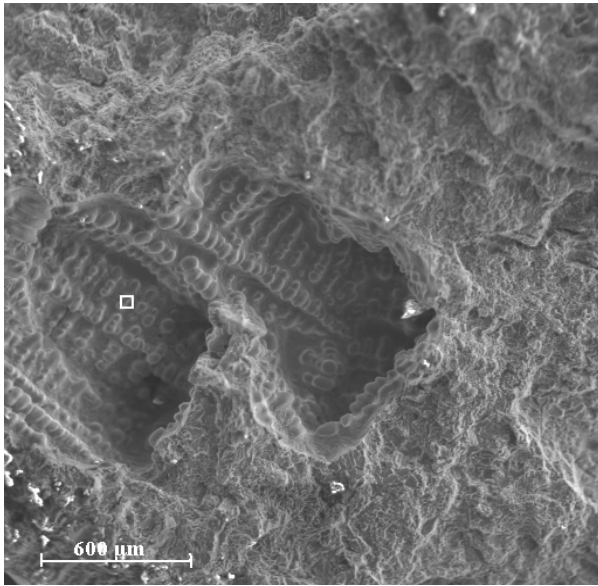


Figure 4.37a: Interdendritic porosity on the fracture surface of a top-gated frame.

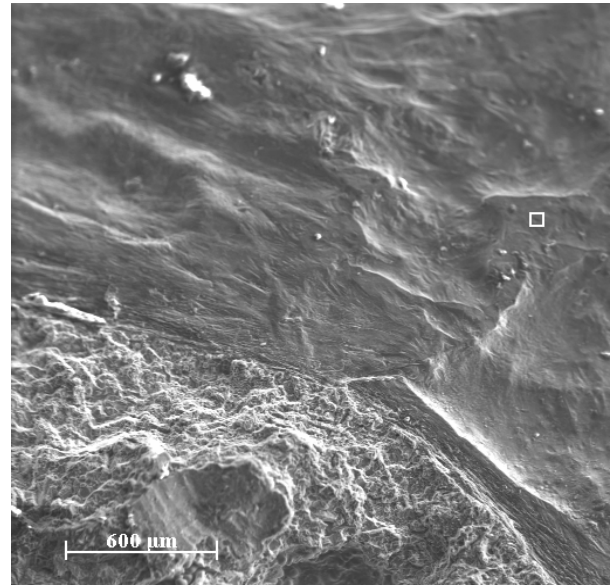


Figure 4.37b: Film defect on the fracture surface of a bottom-gated frame.

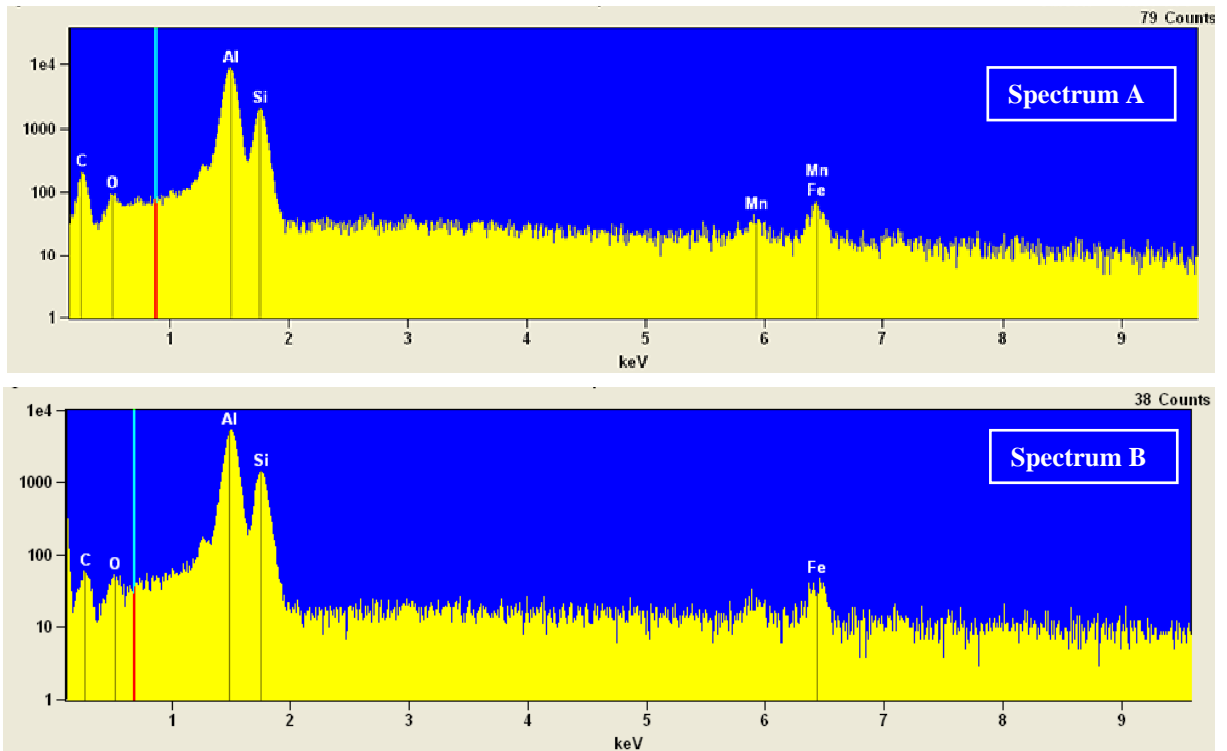


Figure 4.38: EDX spectra obtained from (A) the surface of a pore defect and (B) the surface of a film defect (see Figure 4.37)

#### 4.4 COUNTER-GRAVITY FILLING

Having shown that top- or bottom-filling, under the action of gravity, produced essentially the same, low results in terms of casting quality, it was decided to apply a counter-gravity casting technique to the filling of Lost Foam moulds. In the past, counter-gravity filling has been used successfully to fill open cavity moulds in order to overcome the problems associated with high metal velocity that are prevalent in conventional gravity casting. Application of this technique to the Lost Foam process would produce results that allow direct comparison with those from the gravity filling experiments and provide quantitative as well as qualitative evidence of any improvement.

A number of clusters, each incorporating a vertically oriented, 15 mm thick, expanded polystyrene plate, were cast in a counter-gravity fashion. Frames were not cast in this case, owing to the difficulty in filling. A single ingate of the same size and in the same location as that used to bottom-fill the gravity-cast plates was used. The crucible used in casting was only large enough to hold sufficient metal for filling of one mould and therefore a new melt was prepared for each casting. However, each melt originated from a single batch of ingots. Filling characteristics were observed by means of the same two systems used in the gravity filling experiments, i.e., a set of timing electrodes and real-time X-ray radiography.

Figure 4.39 contains the results that the timing electrodes recorded during counter gravity filling of a plate cluster at a vessel pressure of 68.9 kPa (10 psi). The metal flowed up through the central region of the plate at a faster rate than up either side, and reached the top of the plate about 26 s. after filling began and achieved an average speed of about  $22 \text{ mm}\cdot\text{s}^{-1}$ .

The metal that flowed up the right hand side of the plate lagged only slightly behind the front in the central region and had an average velocity of  $16 \text{ mm}\cdot\text{s}^{-1}$ . The left hand side of the plate was the last to fill and this can be seen in Figure 4.39 by the position of the blue line being to the right, relative to the other two. Interestingly, this offset was brought about almost entirely during the filling through a region between 50 mm and 100 mm above the ingate of the plate. Here the speed of the front to the left side of the casting only advanced vertically at an average

rate of about  $5 \text{ mm.s}^{-1}$  compared with about  $9 \text{ mm.s}^{-1}$  on the right side and  $18 \text{ mm.s}^{-1}$  in the centre.

Location and time after start of pour (in sec.) recorded by each electrode.

**Space between electrodes:**

**Horizontal = 91 mm**

**Vertical = 50 mm**

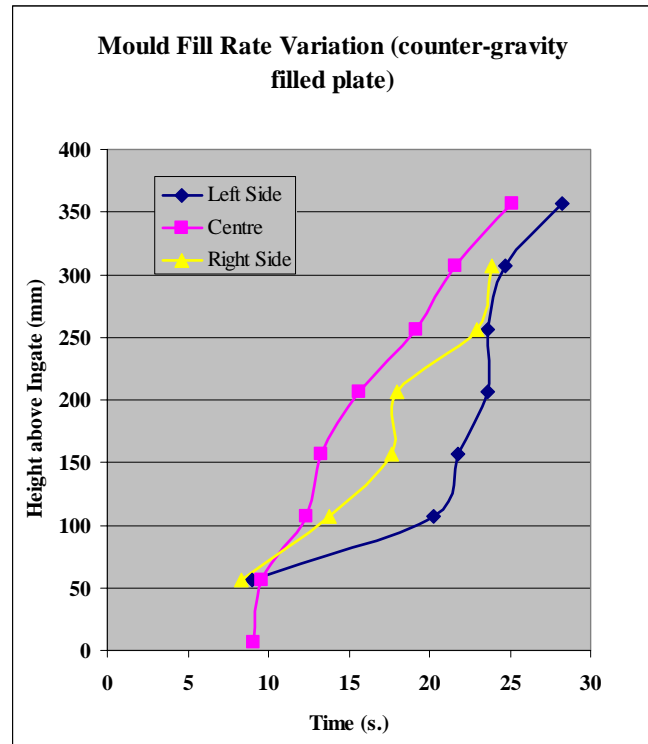
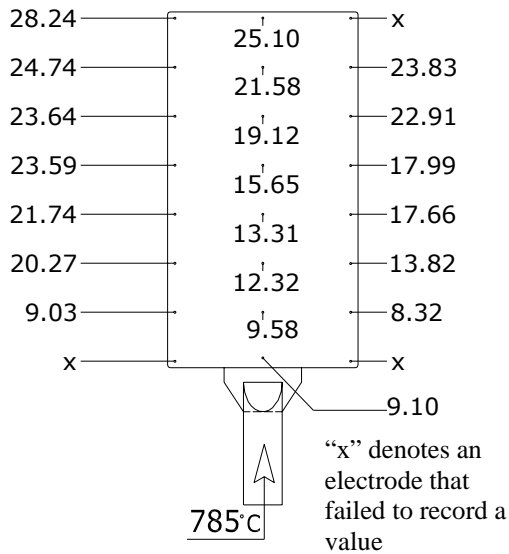


Figure 4.39: Datalogger recordings during the counter-gravity filling of a bottom-gated plate

Real time X-ray observations of the flow of the liquid metal through a plate and filled in the same fashion and at the same vessel pressure of 68.9 kPa (10 psi) are shown in Figure 4.41. The field of observation was located at the top left corner of the plate (see Figure 4.40a) so that the right hand edge of each frame corresponded approximately with the centreline of the plate. The leading edge of the front was generally located to the far right of each frame which indicated that filling was fastest in the central region of the plate. As the metal approached the top of the mould it began to travel in a diagonal fashion across the field of view so that the last region to fill was the upper left corner. The front profile resembled a series of fingers as with the gravity-filled moulds, with a length of about 20 mm and approximately 30 mm between them. As the front approached the top of the plate the length of the fingers decreased and their width increased. Frames 2 and 3 of Figure 4.38 show that, although the distance between the fingers remained approximately the same, the change in their aspect ratios had the effect of creating narrow regions of partially degraded polystyrene between them.

As filling reached the upper region of the plate some metal flowed across from one finger to another in the direction of the metal flow arrow shown in Frames 4 and 5. This merging of two individual fingers entrapped pattern degradation products behind the metal front in the bulk liquid. Frame 6 was captured just as the plate was filled and highlights the entrapped degradation products that were observed as lighter regions in the upper left hand corner of the plate. The average vertical speed of the metal front across the field of view was estimated at approximately  $16 \text{ mm.s}^{-1}$ .

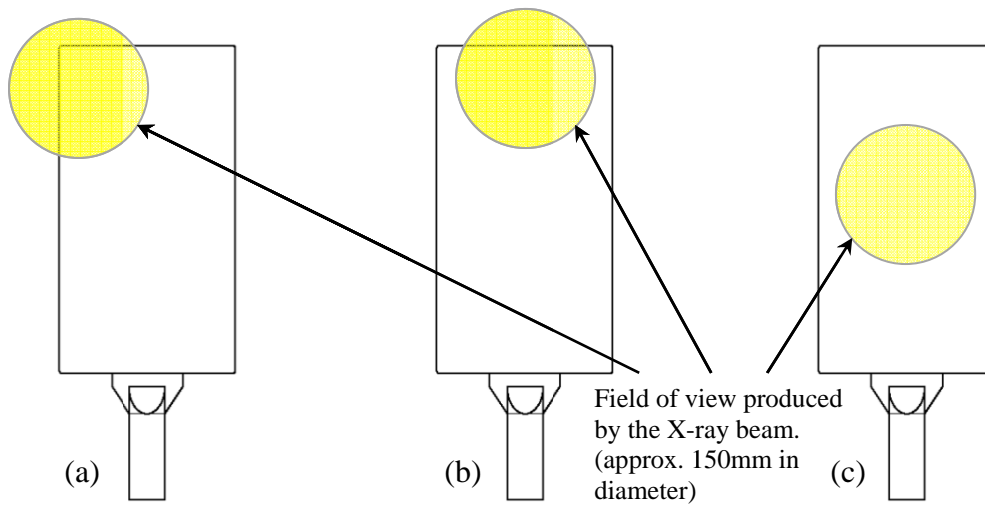


Figure 4.40: Fields of view during the filling of counter-gravity filled plates (a) in the upper left hand corner of the plate (see Figure 4.41), (b) in the top, central region of the plate (see Figures 4.42, 4.43 and 4.45) and (c) in the central region of the plate (see Figure 4.44).

Real time X-ray radiography was also used to observe the characteristics of metal fronts as they filled plate patterns with reduced vessel pressures of 34.5 kPa (5 psi), 27.6 kPa (4 psi) and 24.1 kPa (3.5 psi) which resulted in a reduction in filling velocity. Figures 4.42, 4.43 and 4.44 show the three sets of observations made under these conditions.

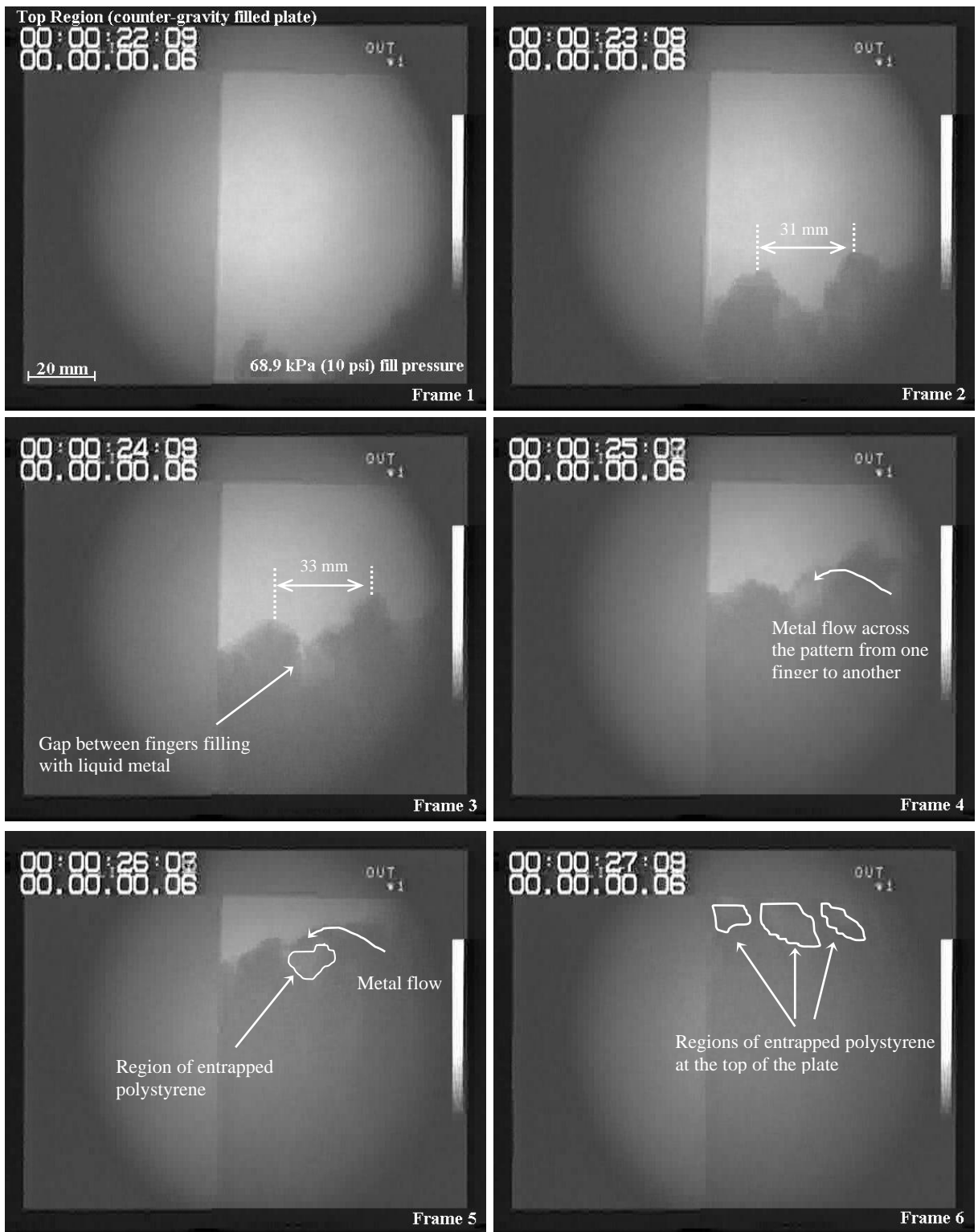


Figure 4.41: Filling behaviour in the upper region of a counter-gravity filled plate (68.9 kPa vessel pressure).

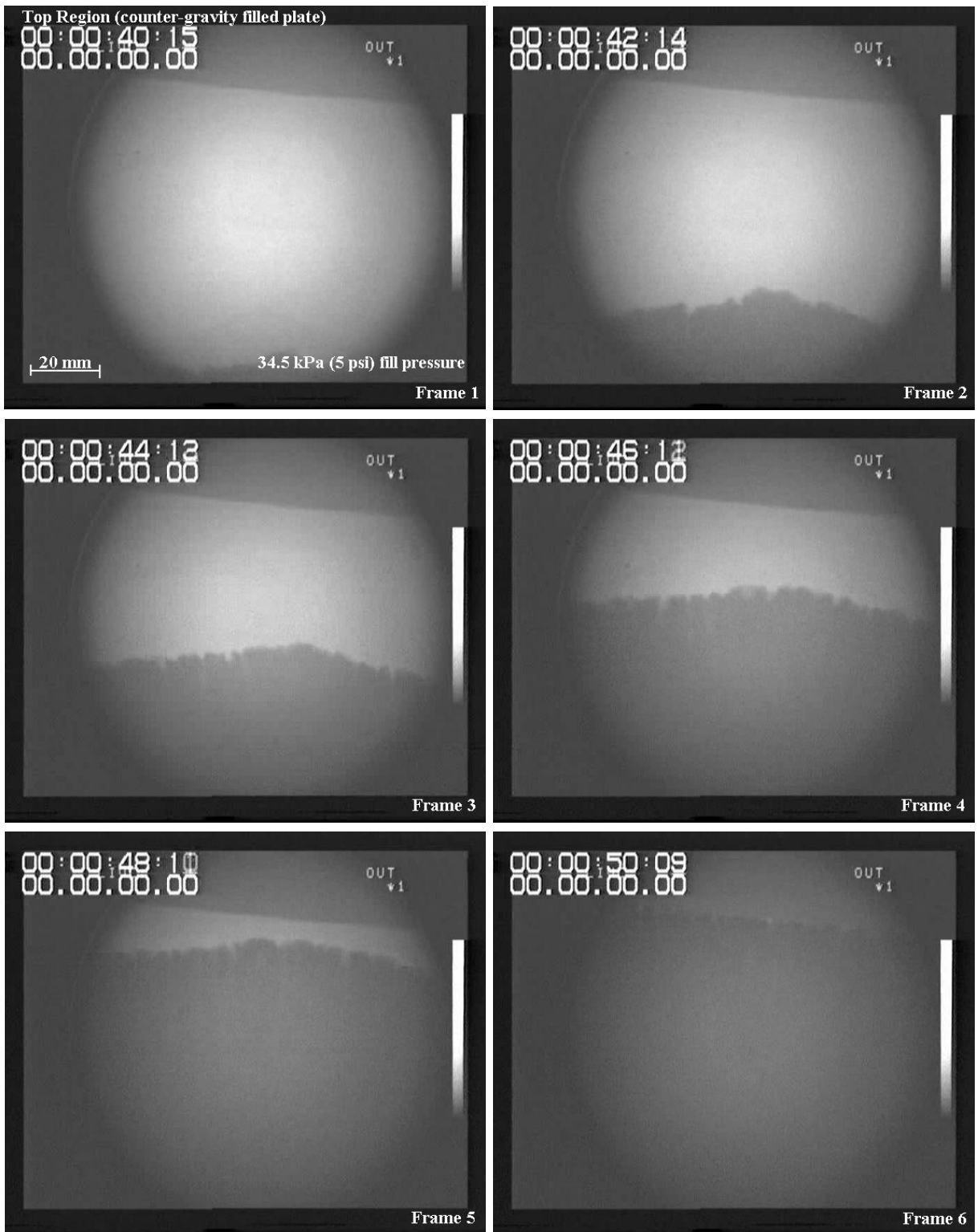


Figure 4.42: Filling behaviour in the upper region of a counter-gravity filled plate (34.5 kPa vessel pressure).

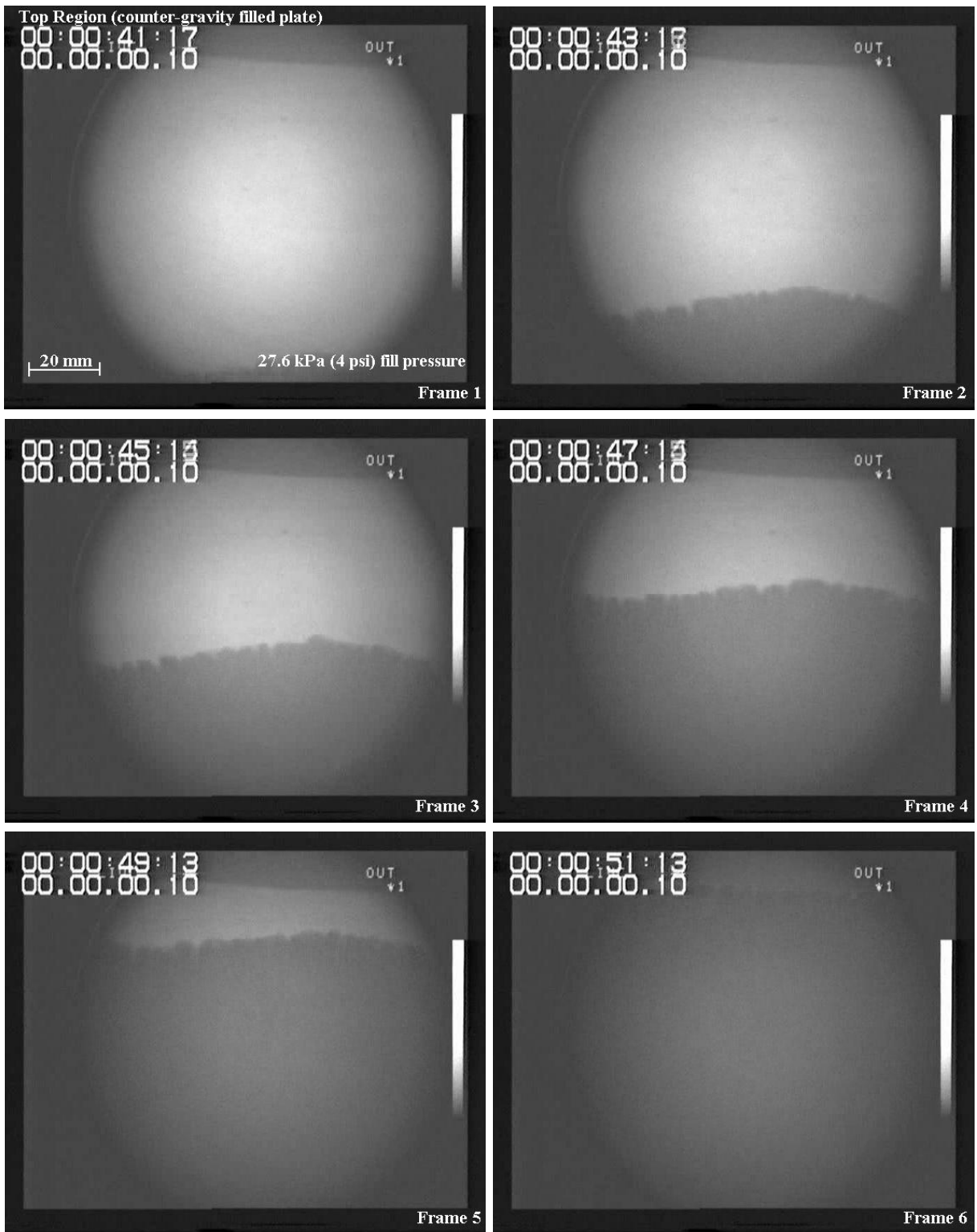


Figure 4.43: Filling behaviour in the upper region of a counter-gravity filled plate (27.6 kPa vessel pressure).

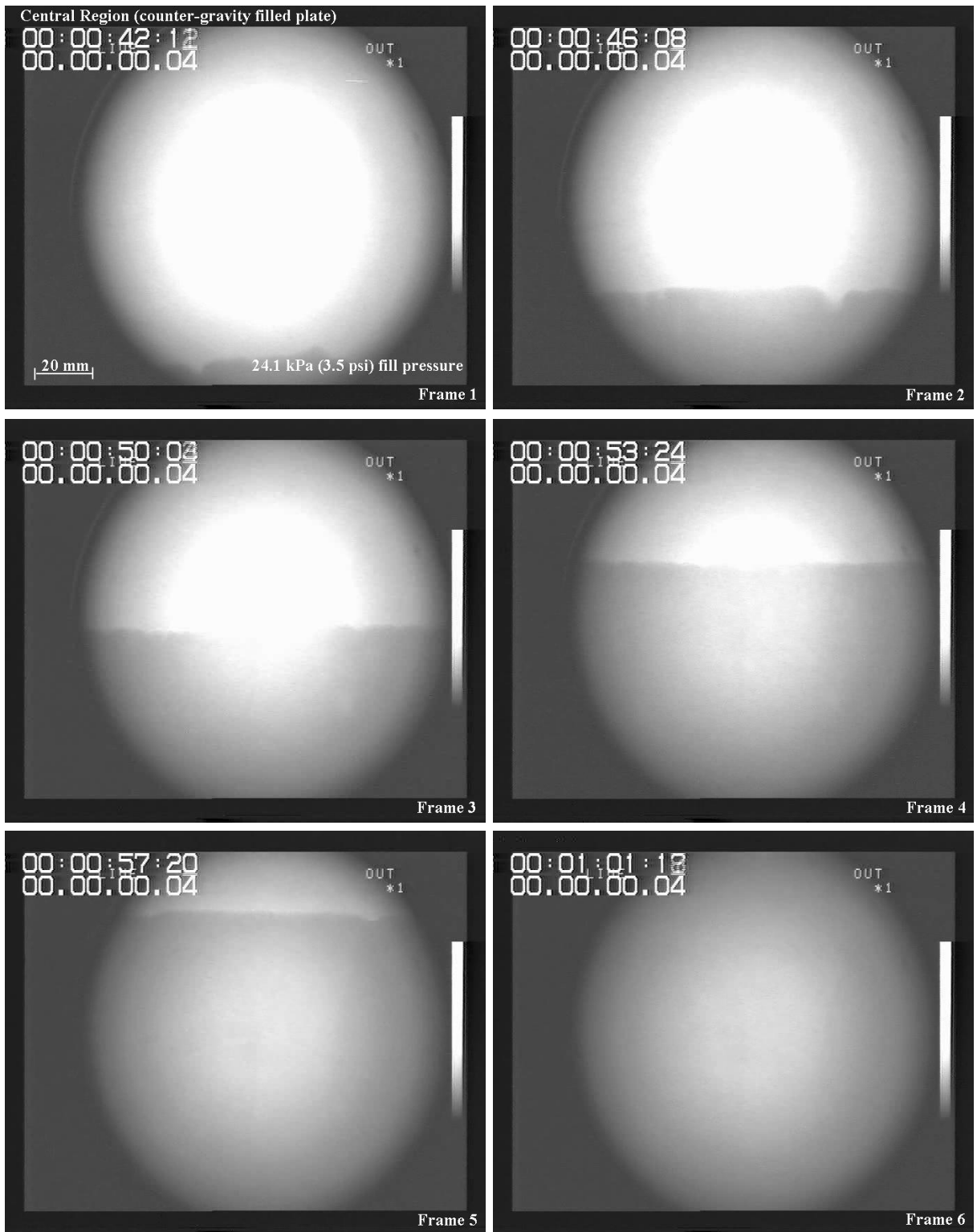


Figure 4.44: Filling behaviour in the central region of a counter-gravity filled plate (24.1 kPa vessel pressure).

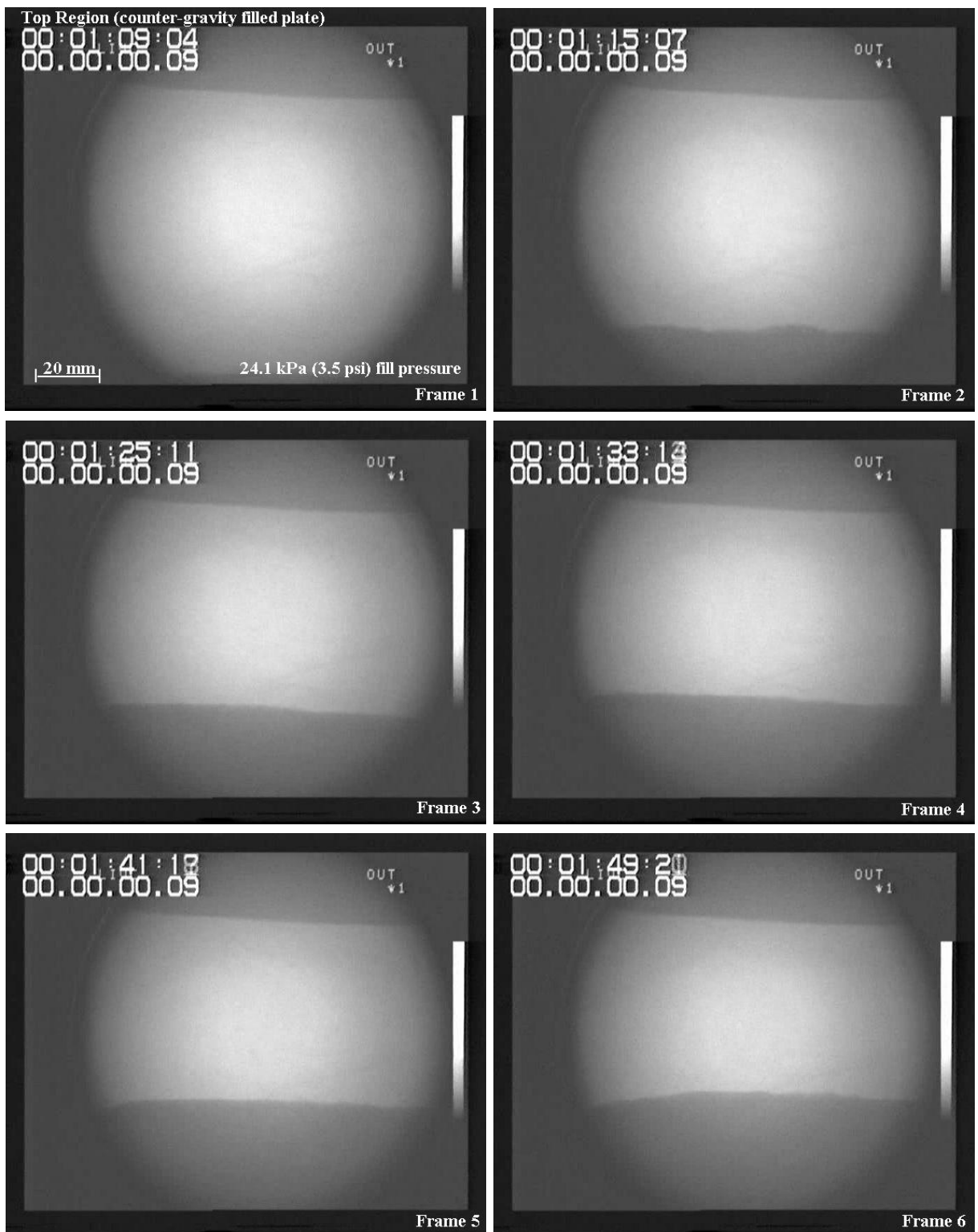


Figure 4.45: Filling behaviour in the upper region of a counter-gravity filled plate (24.1 kPa vessel pressure).

A reduction in the pressure from 68.9 kPa to 34.5 kPa resulted in the metal front adopting a well-defined convex shape that was made up of a number of smaller, closely packed fingers. This can clearly be seen in Frames 2 – 5 of Figure 4.42 and particularly well in Frame 4. With the vessel pressure set at 34.5 kPa, the metal front advanced vertically upwards at about  $8 \text{ mm.s}^{-1}$  and the length of the perturbations on the metal front was between 4 mm and 7 mm, with the distance between them being in the region of 5 mm. As the front reached the top of the plate the fingers closed up so that no discernible gap could be seen between them.

At a vessel pressure of 27.6 kPa (see Figure 4.40) the metal front profile and vertical velocity of the metal front were very similar to those observed at 34.5 kPa. The front was estimated to have been travelling at about  $8 \text{ mm.s}^{-1}$  and, as Figure 4.43 illustrates, had small fingers of around 4 mm in length along the entire length of its slightly convex profile.

Figure 4.44 illustrates the metal flow and metal front conditions in the central region of the plate when counter-gravity filled at a vessel pressure of only 24.1 kPa. The metal front took on a much smoother, horizontal profile that was devoid of any noticeable fingers and travelled through the central region of the plate at approximately  $5 \text{ mm.s}^{-1}$ . The only deviation from this condition was captured in Frame 2, where a small concavity formed temporarily in the front in the right side of the field of view. The diameter of this concavity was estimated to be approximately 8 mm, which was exactly the same size as the vents that had been used as part of the tooling for making the patterns (see Figure 3.1). The way that the metal front split into two in order to flow around this 8 mm diameter region before recombining and engulfing it suggested that the polystyrene had been denser in that area than in the rest of the pattern and the similarity in size between the affected region and a tooling vent supports this argument. Frame 3 of Figure 4.44 clearly indicates that by the time the front had advanced a further 20 mm its profile had reverted back to the planar state.



Figure 4.46: Counter-gravity filled plate casting made at a vessel pressure of 24.1 kPa. (made as part of the real time X-ray mould filling analysis. Reference Figure 4.44 and 4.45).

As the metal rose into the upper region of the plate its velocity decreased to an average of less than  $2 \text{ mm.s}^{-1}$ . This resulted in premature solidification of the metal, resulting in the formation of a misrun defect, approximately 70 mm short of the top of the plate. The frames of Figure 4.45 illustrate the very slow front velocity recorded in this region and Frame 6 the point at which the filling process came to a halt. A photograph of the casting made is shown in Figure 4.46. A smooth, almost horizontal front was clearly visible at the top of the plate and staining of the surface, similar to that observed on gravity cast plates, was also observed.

#### **4.5 PROPERTIES OF COUNTER-GRAVITY FILLED CASTINGS**

The ultimate tensile strength (UTS) of counter-gravity cast samples was compared with that obtained previously from gravity-filled castings. This provided quantitative data on the difference between gravity and counter-gravity filling in terms of casting quality. Fracture surfaces of some of the test bars were also examined so that the cause of failure, defect type and defect severity could also be compared against the defects found in gravity cast samples.

### 4.5.1 Tensile Strength Variation in the Castings

Tensile test bars were taken from a plate that had been cast at a vessel pressure of 27.6 kPa where the velocity of the metal front was  $8 \text{ mm.s}^{-1}$  and a further set extracted from one where the velocity of the front had been reduced to  $5 \text{ mm.s}^{-1}$  by reducing the pressure to 24.1 kPa. The origin and machined dimensions of each specimen are shown in Figure 3.9 and the UTS values are recorded in Table 4.47. Although a full set of 23 results was obtained from the plate cast at the higher pressure, the misrun defect at the top of the plate that was filled slowly meant that only 20 samples, and an equivalent number of UTS results, were available from this casting.

A “goodness of fit” analysis was carried out to determine which distribution (i.e. the normal, the Weibull or the type 1 extreme) most accurately described the spread of each set of data and, although the UTS values from the plate that had been cast at  $5 \text{ mm.s}^{-1}$  had the highest regression coefficient when normally distributed (see Table 4.48), the Weibull distribution was the most accurate at describing both sets of results. Therefore, this type of distribution was adopted for all subsequent statistical analysis and comparison of UTS data.

Figure 4.49 contains the resultant Weibull plots and, for comparative purposes, that of the bottom-gated, gravity filled plate previously shown in Figure 4.35. The Weibull modulus of the bottom-gated, gravity cast plate was 9.2 and this compared very closely to 10.7 obtained in the case of a plate produced in a counter-gravity fashion at a vessel pressure of 27.6 kPa. The metal fronts observed in both cases were similar in speed and appearance. Although gravity filling resulted in an average front speed of  $12.76 \text{ mm.s}^{-1}$ , which was about  $4 \text{ mm.s}^{-1}$  faster than the average value for counter-gravity filling, it fell to less than  $10 \text{ mm.s}^{-1}$  in the upper region of the casting. This was comparable with the  $8 \text{ mm.s}^{-1}$  front speed observed throughout the counter-gravity filling sequence of a plate pattern. In each case the front exhibited small perturbations, as illustrated in Figures 4.13 and 4.43.

Ultimate Tensile Strength Results of Plate Samples (MPa)		
Location	Metal Front Velocity & Pressure in Vessel During Filling	
	v = 8 mm/s (27.6 kPa)	v = 5 mm/s (24.1 kPa)
A	106	227
B	133	196
C	126	205
D	126	197
E	109	203
F	108	212
G	117	199
H	119	198
I	126	206
J	121	209
K	123	205
L	135	207
M	130	215
N	140	222
O	128	211
P	94	190
Q	128	212
R	134	217
S	131	220
T	137	202
U	140	no sample
V	144	no sample
W	124	no sample

Table 4.47: Ultimate tensile strength results of samples taken from counter-gravity cast plates.

Cluster design	Analysis	Regression coefficient	Best-fit parameters
Counter-gravity filled plate (v = 8 mm/s)	Normal	0.9191	$\mu = 0.8692, \sigma = 0.0847$
	Weibull	0.9753	$\sigma = 0.9020, \lambda = 10.6791$
	Type 1 extreme	0.8383	$\mu = 0.9074, \sigma = 0.0660$
Counter-gravity filled plate (v = 5 mm/s)	Normal	0.9865	$\mu = 0.9148, \sigma = 0.0420$
	Weibull	0.9521	$\sigma = 0.9282, \lambda = 23.2266$
	Type 1 extreme	0.9735	$\mu = 0.9337, \sigma = 0.0327$

Table 4.48: ‘Goodness of fit’ of normal, Weibull and type 1 maximum extreme value distributions to the UTS data from counter-gravity cast plates.

The counter-gravity cast plate that had been made at a vessel pressure of only 24.1 kPa pressure yielded a greatly improved Weibull modulus of 23.2. This was associated with a

planar metal front that had flowed at  $5 \text{ mm.s}^{-1}$  through the central region of the plate and only  $2 \text{ mm.s}^{-1}$  in the upper region.

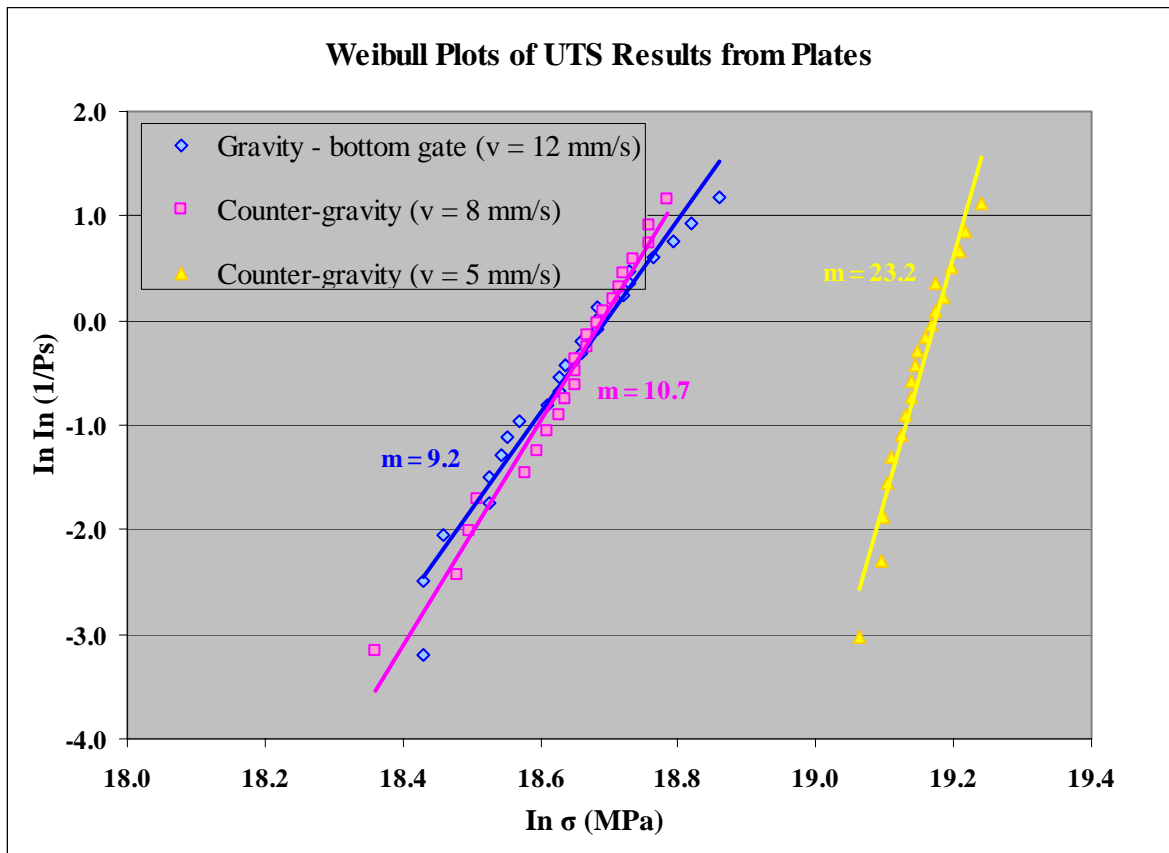


Figure 4.49: Weibull plots of UTS results from two plates that were filled at two different vessel pressures in a counter-gravity fashion and the combined results from three bottom-gated plates that were filled by means of gravity.

Since filling by means of a planar metal front had produced substantially better results than any other, it was decided to try and replicate this condition of filling in the production of three more plate castings and evaluate the results, once again, using Weibull statistics to determine process repeatability.

In each case, the casting temperature was  $785 \text{ }^\circ\text{C}$  but the speed at which the metal front travelled through the mould varied slightly from casting to casting. Whilst filling of the first plate (labelled Plate 1 in Table 4.50) the front was observed to travel at about  $3 - 4 \text{ mm.s}^{-1}$ .

<b>Ultimate Tensile Strength Results of Plate Samples (MPa)</b>			
<b>Location</b>	<b>Plate No. 1</b> ( $P_{\text{vessel}} = 24.1 \text{ kPa}$ ) ( $v = 3 - 4 \text{ mms}^{-1}$ )	<b>Plate No. 2</b> ( $P_{\text{vessel}} = 25.5 \text{ kPa}$ ) ( $v = 6 \text{ mms}^{-1}$ )	<b>Plate No. 3</b> ( $P_{\text{vessel}} = 26.2 \text{ kPa}$ ) ( $v = 7 \text{ mms}^{-1}$ )
A	204	233	172
B	195	202	158
C	228	214	153
D	200	233	138
E	195	204	130
F	200	204	144
G	204	215	161
H	195	214	174
I	213	204	183
J	206	214	198
K	208	215	190
L	216	215	215
M	217	216	218
N	214	201	231
O	207	153	231
P	204	224	234
Q	223	170	239
R	204	214	238
S	no sample	223	240
T	no sample	234	241
U	no sample	229	245
V	no sample	233	244
W	no sample	no sample	242

Table 4.50: UTS results of samples taken from three, separately cast plates made using the counter-gravity filling technique.

Although the metal front observed during filling was planar in nature, the casting solidified prematurely which meant that only 18 specimens could be obtained from it for tensile testing. In order to counter this problem, the vessel pressure was increased slightly to about 25.5 kPa (3.7 psi) during the filling of the second plate. The front velocity rose to approximately  $6 \text{ mm.s}^{-1}$  and the severity of the misrun defect was reduced to such an extent that 22 out of a maximum of 23 test bars were extracted from it. Also, a few small perturbations were observed along its profile as it passed through the real time X-ray's field of view. They were randomly spaced between 10 mm and 50 mm apart from each other, had a wavelength of about 4 mm and a lifecycle, from creation to collapse, of about 2 s., or 12 mm of front movement. As the front reached the upper part of the plate the perturbations subsided altogether and the front assumed a completely planar appearance.

Filling of the third plate was carried out at a vessel pressure of 26.2 kPa (3.8 psi) and this resulted in a front velocity of about 7 mm.s<sup>-1</sup>. The front profile had the same number, size and distribution of perturbations as seen during the casting of Plate No. 2 and their lifecycle was also measured at about 2 s.

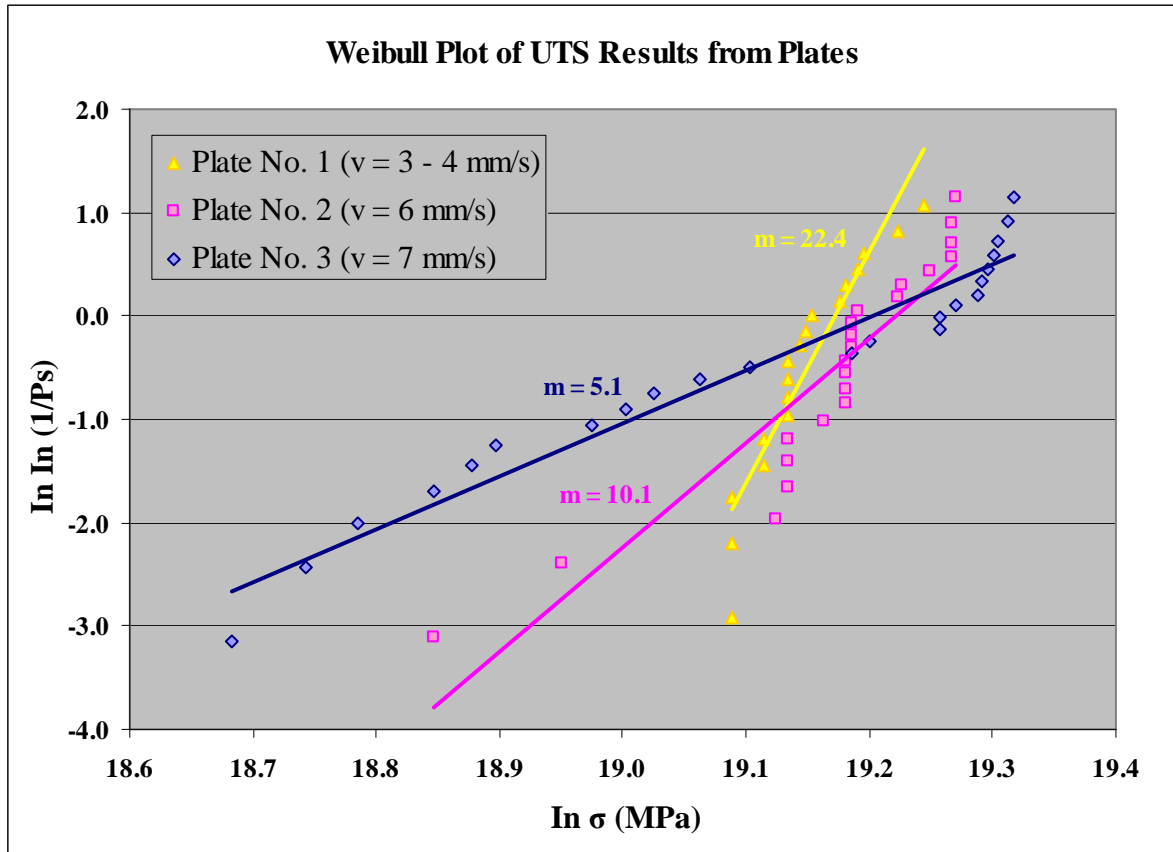


Figure 4.51: Weibull plots of UTS results taken from three counter-gravity cast plates where the metal front velocity had been measured at between 3 and 7 mm.s<sup>-1</sup>.

The Weibull plots generated from the UTS test data are shown in Figure 4.51 and they clearly illustrate that a planar front profile, devoid of any perturbations, produced a casting in which the tensile strength was significantly more consistent from one end to the other. They also reveal that this level of repeatability was severely affected by a very small increase in the metal front velocity. Plate No. 3 had a Weibull modulus of only 5.1, while Plate No. 1, cast at half the velocity, and the only plate to have an unperturbed advancing metal front had a Weibull modulus of 22.4, similar to that of the casting shown in Figure 4.49.

## 4.5.2 Hydrogen Pick-up During Mould Filling

The variability of the tensile strength results taken from counter-gravity cast plates suggested that the velocity of the metal front during mould filling had influenced their structural integrity. However, even at a very low filling speed, where a stable planar front had been observed, the Weibull modulus was only 23. This contrasted with a value of 37 that had been reported by Green and Campbell [89] for a set of unmodified Al-7Si-0.4Mg test bars that had been cast in a gravity fashion using a well designed running system.

It was thought that this could have been due to hydrogen in the gas or liquid phase of the decomposing polystyrene pattern diffusing into the liquid aluminium as it travelled through the mould. This would have resulted in the presence of gas pores in the solidified casting which would have had a detrimental effect on tensile strength.

During the first set of counter-gravity casting experiments, as described in Section 4.4, the amount of dissolved hydrogen in melts that were subsequently cast at speeds of  $8 \text{ mm.s}^{-1}$  (vessel pressure of 27.6 kPa) and  $5 \text{ mm.s}^{-1}$  (vessel pressure of 24.1 kPa) were compared with the hydrogen content in various regions in the resultant plate castings. In this way, the extent of any hydrogen pick-up originating from pattern materials was determined. The hydrogen level in each melt was measured from a keel block sample that was cast immediately before each mould was filled and the level in each casting was obtained from fractured test pieces from the ingate, central and upper regions that had been used previously to generate tensile test data (see Figure 3.9). Each sample was measured twice and the two results labelled “Run 1” and “Run 2” to differentiate them from each other.

The first of the two melts was recorded as having a hydrogen content of about 0.36 ppm just before it was used to make the plate, as described in Section 4.4, where the casting temperature had been  $785 \text{ }^\circ\text{C}$  and the metal front velocity had been  $8 \text{ mm.s}^{-1}$ . During the filling procedure, perturbations were observed on the front which were about 4 mm in length and had a wavelength of 5 mm. As the front reached the top of the plate the fingers closed up so that no discernible gap could be seen between them. The average hydrogen level in the ingate region was 1.36 ppm whereas, in the central region of the plate, it was 1.86 ppm. In the

sample taken from the upper region of the plate the hydrogen level was recorded to be 0.585 ppm in two separate measurements. Figure 4.52 contains the complete set of hydrogen results taken from the metal used to cast this plate and clearly shows that there was an increase in the hydrogen level before and after casting. However, the values recorded in the lower and central regions of the plate were much higher than the 0.69 ppm that commercially pure aluminium could retain in the liquid state [159] and because these regions were associated with high levels of macro porosity, the corresponding results were considered to be erroneous, and due to foam pattern degradation residues trapped in pores within the casting.

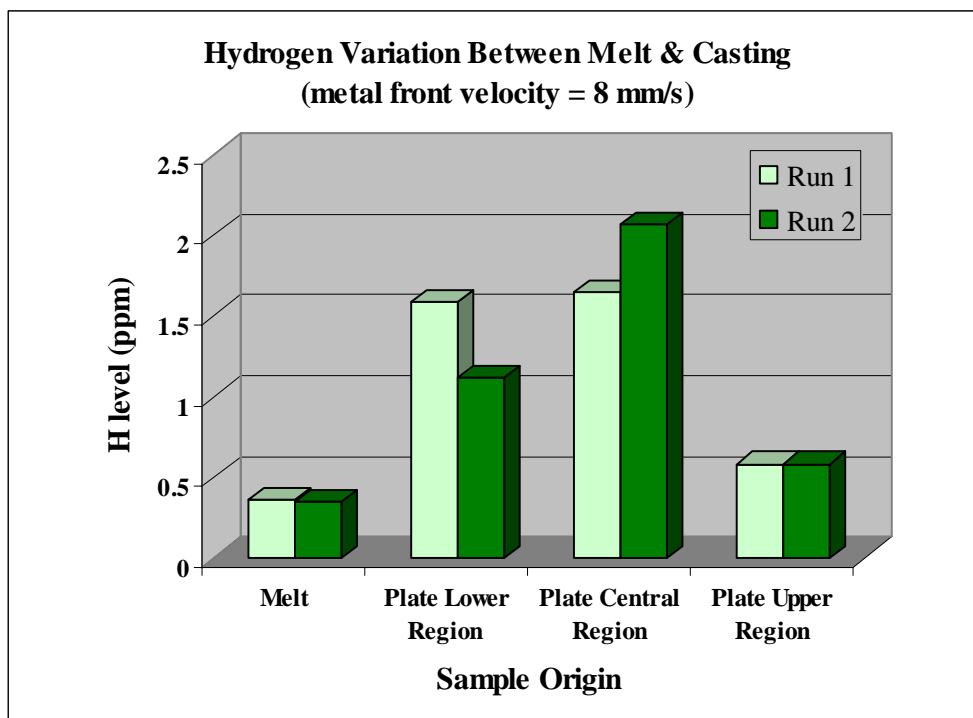


Figure 4.52: Comparison of the dissolved hydrogen in a melt and the casting made from it when filled at a metal velocity of  $8 \text{ mm}\cdot\text{s}^{-1}$ .

It seems likely that a higher front velocity was associated with larger amounts of liquid degradation products because less time was available for heat to be transferred from the metal into the degrading polystyrene and any gaseous layer would have been reduced in thickness or eliminated altogether. The front profile at this velocity was observed to have been unstable and would have entrapped some of the liquid degradation products in the lower and central regions of the plate and would have rendered the hydrogen measurements in these areas invalid. The upper region of the plate was devoid of this type of defect, which was probably the result of a combination of temperature and velocity reduction of the metal front. Under

these circumstances, the 0.585 ppm of hydrogen recorded in the area was considered to be accurate even though it was about 60% higher than in the melt immediately prior to casting. Its source was thought to have been pattern degradation products.

The second plate was also cast at 785 °C and the hydrogen concentration in this melt was measured at 0.403 ppm and 0.423 ppm just before casting. During the mould filling process the metal front took on a smooth, horizontal profile that was devoid of any noticeable fingers and travelled through the central region of the plate at approximately 5 mm.s<sup>-1</sup>. The resultant hydrogen levels inside the casting, as depicted in Figure 4.53, were measured at 0.365 ppm and 0.389 ppm near the ingate, 0.491 ppm and 0.512 ppm in the central region and 0.305 ppm and 0.353 ppm towards the top.

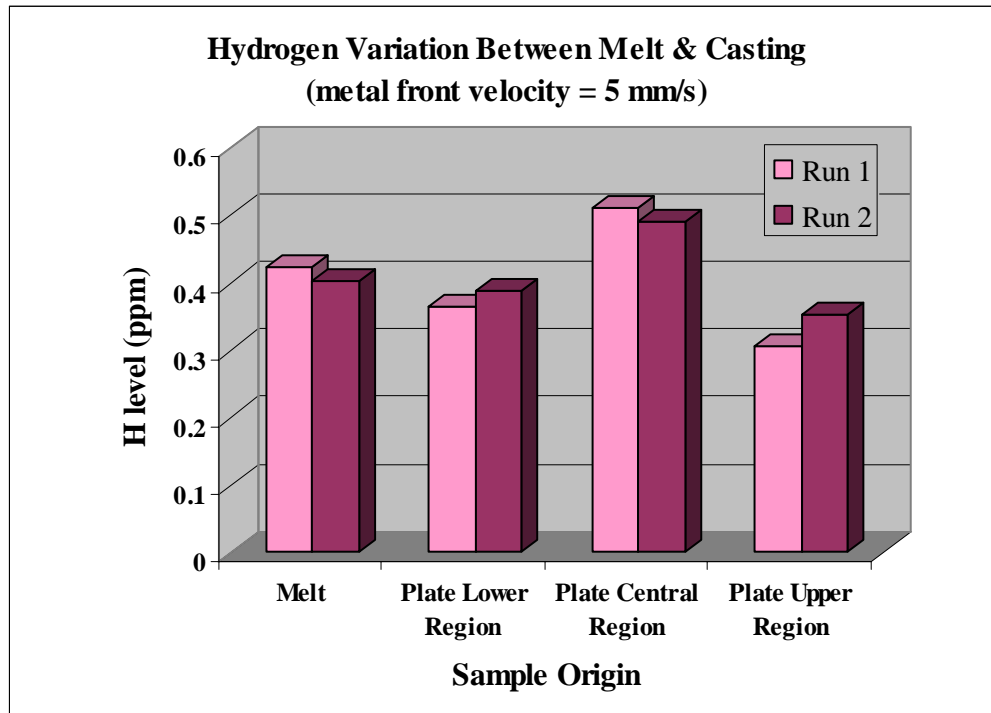


Figure 4.53: Comparison of the dissolved hydrogen in a melt and the casting made from it when filled at a metal velocity of 5 mm.s<sup>-1</sup>.

The plate that had been cast at a metal front velocity of only 5 mm.s<sup>-1</sup> exhibited no macro porosity and the hydrogen level was only found to be higher than the melt in the central region of the casting. In general, the lower filling speed would have resulted in a larger layer of gaseous degradation products between the metal front and the solid pattern and the smooth profile of the metal front would have minimised any entrapment or diffusion of liquid

degradation products in the casting. The elevated hydrogen levels in the central area of this plate, which were approximately 24% higher than in the melt, could have been caused by a localised region of polystyrene that failed to decompose at the same rate as the surrounding material. This phenomenon, illustrated in Frame 2 of Figure 4.44, was observed by means of real time X-ray whilst observing the filling of a plate under similar conditions. A single, localised region of the pattern (thought to be associated with a vent in the tooling and therefore denser) was totally engulfed by a planar metal front prior to decomposing into liquid and gaseous phases.

### **4.5.3 Fracture Surface Defects**

Fracture surfaces produced during tensile testing of counter-gravity filled plate samples were examined using a scanning electron microscope. Every specimen contained pore-type defects that varied in size from approximately 400  $\mu\text{m}$  up to 2500  $\mu\text{m}$ . Those that originated from a plate in which a smooth, planar-type front had been observed travelling through the mould at about 5  $\text{mm}\cdot\text{s}^{-1}$  were relatively spherical in shape and up to about 800  $\mu\text{m}$  in diameter. As the pore size increased above this value, they became more elongated and irregular in its profile.

At x7 magnification, as shown in the left hand photomicrograph of Figure 4.54, large irregular regions of porosity were clearly visible. The right hand photomicrograph of the same figure depicts the area of the fracture surface surrounded by the white square. The magnification in this case was x25 and revealed that porous regions within this area were characterised by numerous dendrite arms with interlocking tips. The pores in the fracture surfaces of the plate where a front speed of 8  $\text{mm}\cdot\text{s}^{-1}$  had been observed were all rounded in nature even at sizes of over 2000  $\mu\text{m}$ . Although the tips of dendrite arms could be seen on the surface of these defects, they were much less well defined as illustrated in Figure 4.55. The size and shape of these defects was much more indicative of entrapped pattern material than those encountered in a casting where the filling velocity had been slower.

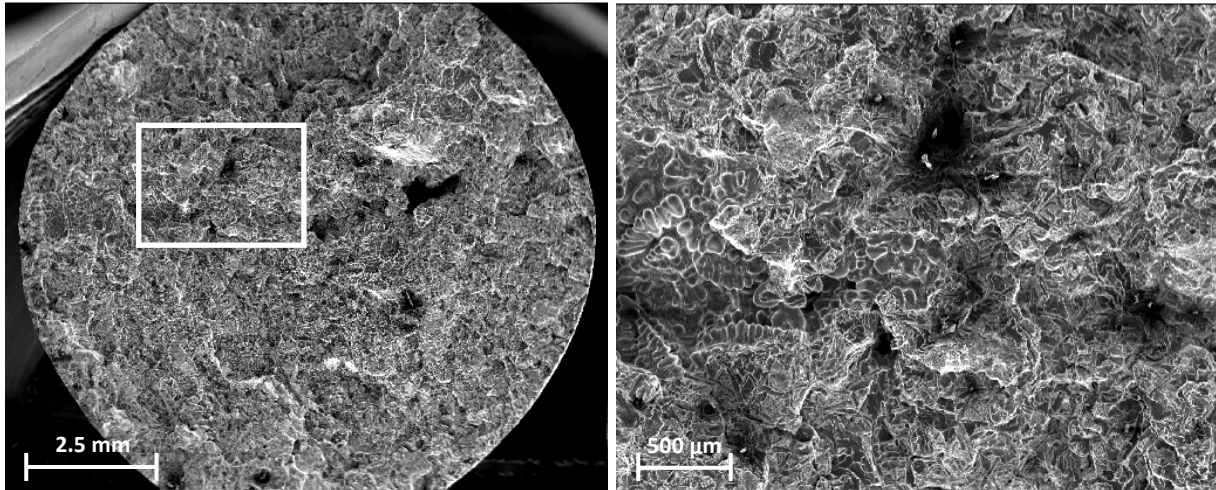


Figure 4.54: Fracture surface of a specimen taken from a plate in which a metal front had been observed travelling through the mould at about  $5 \text{ mm}\cdot\text{s}^{-1}$ . The profile of this front was planar in nature.

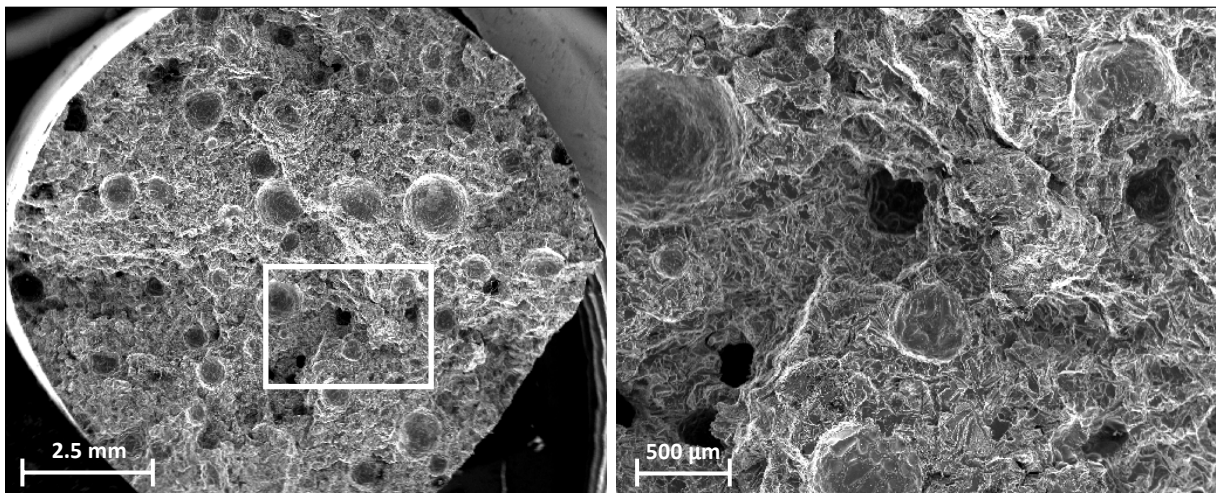


Figure 4.55: Fracture surface of a specimen taken from a plate in which a metal front had been observed travelling through the mould at about  $8 \text{ mm}\cdot\text{s}^{-1}$ . The front profile was associated with small perturbations on its surface.

One pore on each fracture surface was analysed by means of energy-dispersive X-ray (EDX) and the carbon and oxygen results compared with those found from a region of sound material nearby. Figure 4.56 shows an example of an EDX spectrum that was obtained from within a pore on the fracture surface of a sample that had been cast at  $8 \text{ mm}\cdot\text{s}^{-1}$ . The site of the analysis is indicated by a small white square on the associated photomicrograph where the carbon level was determined to be at 15.6 wt.% and the oxygen to be at 2.34 wt.%. The complete set of results for both plates is contained in Table 4.57.

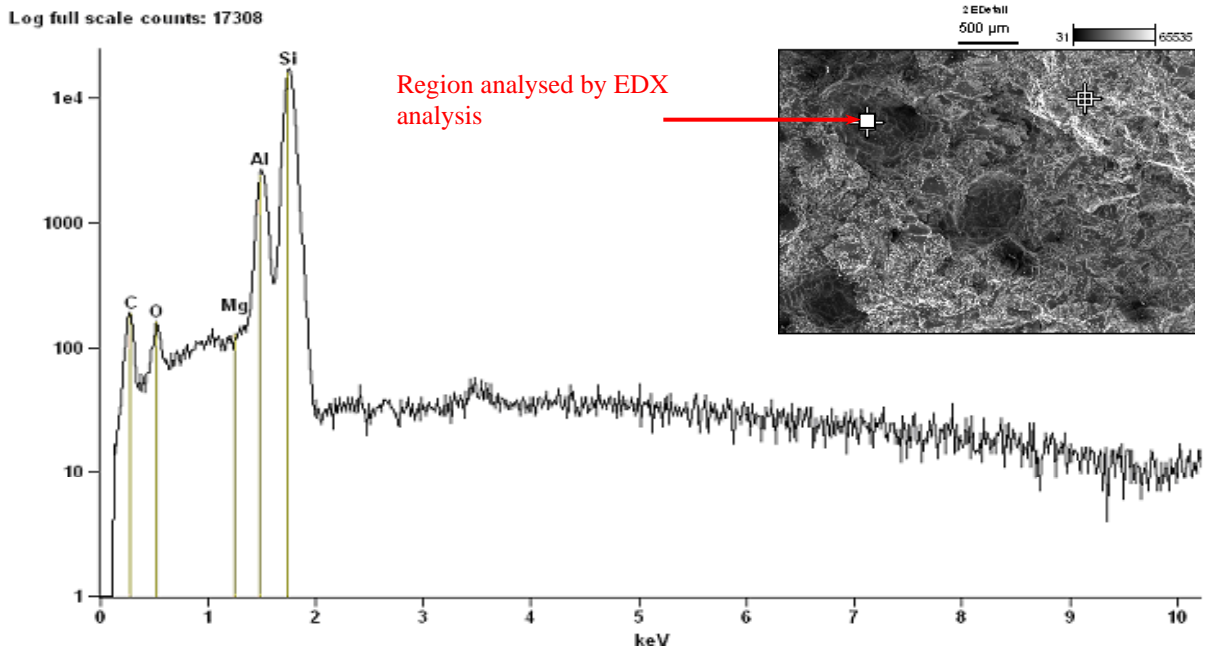


Fig. 4.56: EDX results from a pore defect observed on a fracture surface originating from a plate in which the metal front velocity had been measured at  $8 \text{ mm}\cdot\text{s}^{-1}$ .

EDX Measurements of Carbon & Oxygen								
Location	Plate Filling Speed = 8 mm/s				Plate Filling Speed = 5 mm/s			
	Carbon (by wt)		Oxygen (by wt)		Carbon (by wt)		Oxygen (by wt)	
	Normal	Defective	Normal	Defective	Normal	Defective	Normal	Defective
A	used for H determination				used for H determination			
B	2.88%	3.38%	0.41%	0.88%	1.20%	9.27%	0.31%	3.29%
C	1.61%	3.50%	0.44%	1.13%	2.81%	3.58%	0.66%	0.46%
D	2.93%	3.36%	0.49%	0.70%	1.31%	10.92%	0.29%	1.56%
E	4.82%	15.62%	1.33%	2.34%	1.53%	8.84%	0.18%	1.01%
F	3.32%	4.21%	0.56%	0.75%	3.99%	4.73%	0.46%	0.83%
G	1.22%	3.31%	0.24%	0.47%	1.91%	4.23%	0.35%	1.24%
H	used for H determination				used for H determination			
I	0.66%	2.91%	0.33%	0.30%	1.69%	5.73%	0.64%	1.66%
J	2.62%	2.86%	0.33%	0.61%	1.58%	2.98%	0.42%	0.11%
K	1.68%	6.39%	0.43%	1.28%	2.52%	2.60%	0.63%	0.55%
L	3.91%	22.33%	1.11%	0.31%	3.15%	4.12%	0.68%	1.54%
M	2.91%	2.84%	0.68%	0.93%	2.52%	4.55%	0.06%	0.83%
N	1.17%	1.51%	0.41%	0.42%	1.49%	1.62%	0.34%	0.41%
O	3.41%	3.60%	0.62%	0.85%	1.57%	3.47%	0.44%	0.88%
P	used for H determination				used for H determination			
Q	1.19%	2.95%	0.52%	0.59%	2.79%	4.77%	0.72%	0.75%
R	3.68%	3.80%	1.08%	1.12%	1.26%	3.17%	0.46%	0.46%
S	2.89%	2.58%	0.51%	1.02%	used for H determination			
T	2.44%	5.06%	0.60%	1.00%				
U	0.00%	4.19%	1.05%	0.68%				
V	2.47%	4.25%	0.49%	0.73%				

Table 4.57: Carbon and oxygen levels in pores and sound regions on each fracture surface.

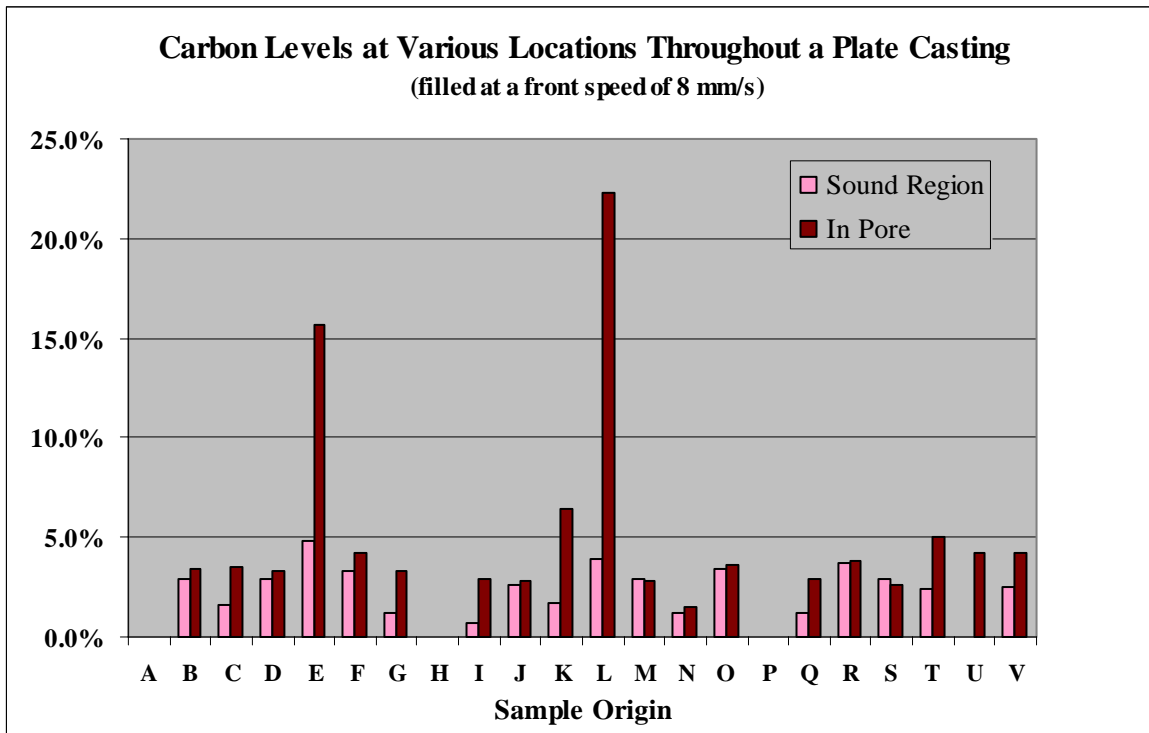


Figure 4.58: Carbon levels detected in pores and on sound regions of the fracture surfaces of a plate casting which had been filled at a metal velocity  $8 \text{ mm}\cdot\text{s}^{-1}$ .

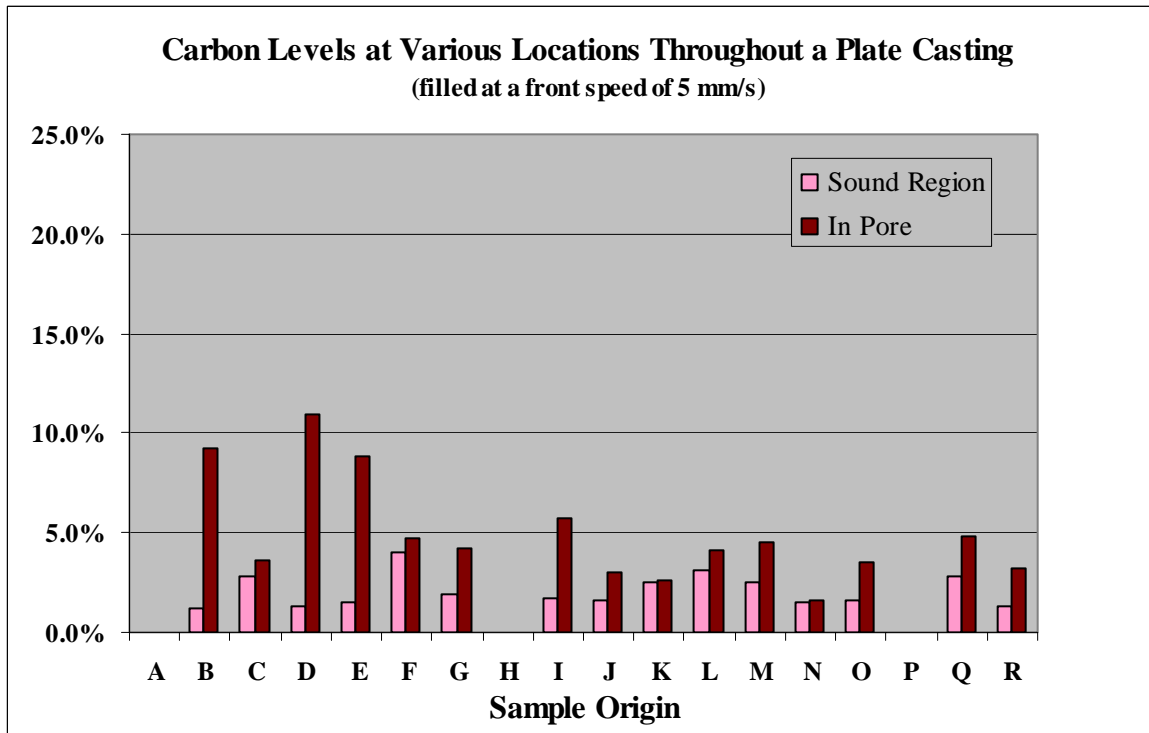


Figure 4.59: Carbon levels detected in pores and on sound regions of the fracture surfaces of a plate casting which had been filled at a metal velocity of  $5 \text{ mm}\cdot\text{s}^{-1}$ .

Figures 4.58 and 4.59, which illustrate the differences in the amount of carbon present in pores and on sound fracture surfaces of castings made at two different fill velocities, clearly show that, in all but two pores the carbon content was higher than on sound regions of the corresponding fracture surfaces. In the two cases where the opposite condition was apparent, the difference in the carbon levels was only 0.07 wt.% and 0.31 wt.% respectively.

The average carbon content found in pores of the plate in which the metal front had travelled at  $8 \text{ mm.s}^{-1}$  and adopted an irregular profile was about 5.2 wt.%. However, the average level detected in the other plate where the front speed had been  $5 \text{ mm.s}^{-1}$  was slightly lower at just under 5 wt.%. Another interesting observation was that the highest individual values in both plates all occurred in the lower and central regions of the castings, not in the upper sections.

Oxygen contents from the same locations are shown in Figures 4.60 and 4.61. Where mould filling had taken place at  $8 \text{ mm.s}^{-1}$  the average oxygen level detected in the pores was 0.9% whereas at the lower filling velocity of  $5 \text{ mm.s}^{-1}$  it was around 1%.

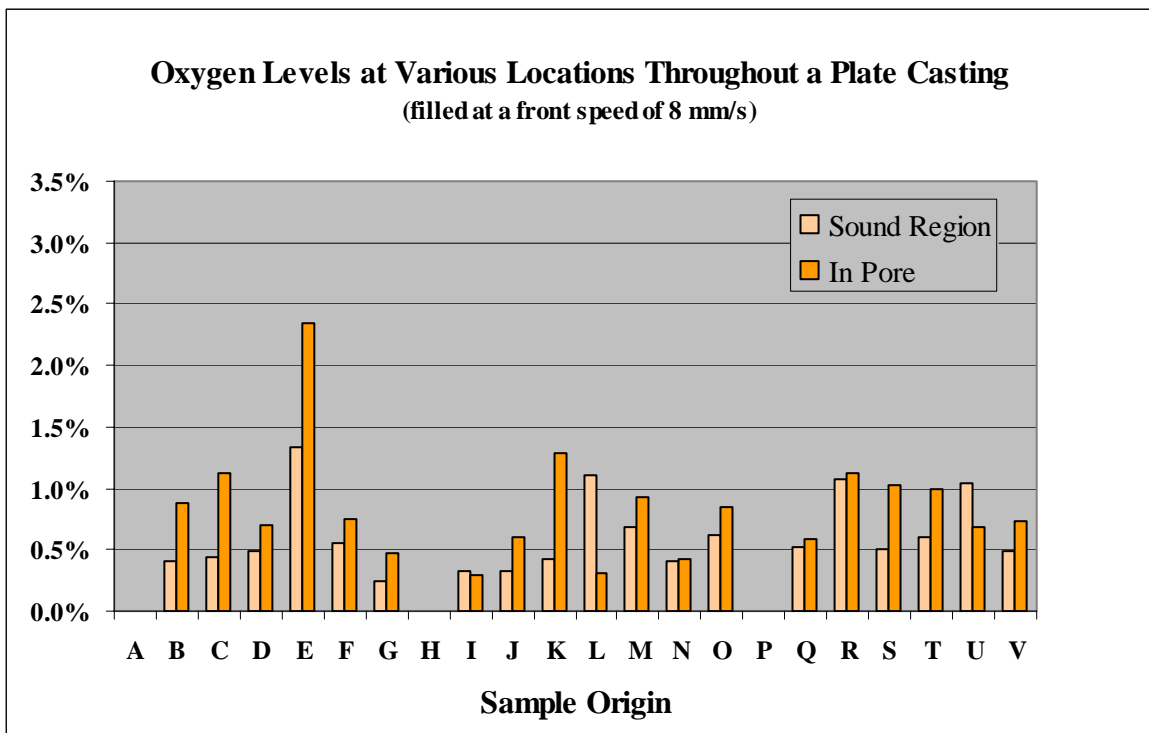


Figure 4.60: Oxygen levels detected in pores and on sound regions of the fracture surfaces of a plate casting which had been filled at a metal velocity of  $8 \text{ mm.s}^{-1}$ .

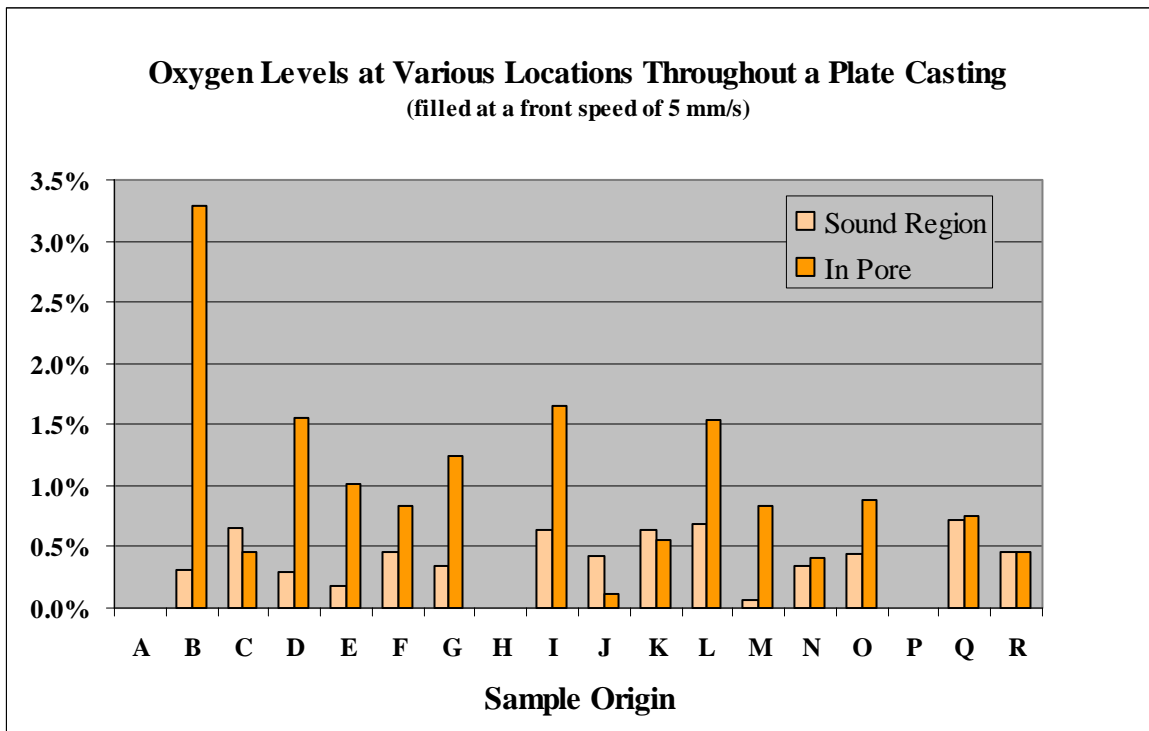


Figure 4.61: Oxygen levels detected in pores and on sound regions of the fracture surfaces of a plate casting which had been filled at a metal velocity of  $5 \text{ mm}\cdot\text{s}^{-1}$ .

The average oxygen levels found in sound regions of each plate were lower than those measured within the pores. The plate made at the higher filling speed of  $8 \text{ mm}\cdot\text{s}^{-1}$  yielded a value of about 0.6 wt.% oxygen whereas the more slowly filled plate only yielded an average of 0.4 wt.%. Additionally, in three separate locations in each plate the sound structure had an oxygen content that was higher than the associated pore. Although no correlation could be found in the locations that these anomalies were detected, the highest oxygen value from each casting was found in a pore in the lower region of the plate.

The hydrogen content in the lower and central regions of the plate that had been cast at a filling velocity of  $8 \text{ mm}\cdot\text{s}^{-1}$  (see Figure 4.52) was much higher than would have been expected to be dissolved in the liquid metal and to have precipitated out during solidification to form a pore. Also, as shown in Table 4.57, carbon was not only detected in every pore that was examined, irrespective of the shape of the metal front during mould filling but in all but two locations was higher in the pore than on the sound fracture surface. This suggests that the porosity encountered on the fracture surface of all specimens was caused by entrapment of the

degradation products of polystyrene and not as a result of excessive levels of dissolved hydrogen in the melt.

At the higher filling velocity of  $8 \text{ mm.s}^{-1}$  the metal front was unstable and this combination of irregular front profile and the rate at which it progressed through the mould was thought to have resulted in entrapment of a large amount of degrading pattern material which manifested itself in the casting as a relatively large area fraction of pores. This is supported by the presence of large, spherically shaped pores which indicated that degradation of entrapped pattern material continued within each pore during solidification. Whilst a reduction in filling velocity resulted in the presence of a planar metal front and a reduced level of porosity in the casting, carbon was still present in each pore that was analyzed. This means that entrapment of pattern degradation products rather than hydrogen precipitation was responsible for pore formation during the filling and solidification of both plate castings.

## **4.6 ACCELERATED LIQUID-LIQUID INTERFACE MODELLING**

A comparison of the appearance of the metal fronts observed during the casting experiments and the tensile properties of the castings suggested that only a completely smooth advancing metal front would give reproducible casting properties. In order to understand the mechanisms that might have controlled the shape of the metal-foam interface and the entrainment of pattern degradation products into the casting, a physical model was constructed that simulated counter-gravity filling of a Lost Foam mould at room temperature. The apparatus, illustrated in Figure 3.11, contained liquid mercury as a replacement for liquid aluminium and glucose syrup as a substitute for the liquid polystyrene that had been reported to be present at the metal-foam interface [6,16,17]. Accelerating the Hg-glucose interface vertically upwards would be an analogue for the counter-gravity Lost Foam process where high density, low viscosity aluminium was being pushed upwards into low density, high viscosity polymer degradation products.

### **4.6.1 Glucose Syrup Viscosity**

Published literature [155] suggests that, over the range of casting temperatures used in the mould filling experiments, i.e. between  $748 \text{ }^{\circ}\text{C}$  and  $909 \text{ }^{\circ}\text{C}$ , the viscosity of the liquid

aluminium would have varied by only 0.3 mPa.s, from 1.2 mPa.s to 0.9 mPa.s. Therefore, the application of liquid Hg in the room temperature analogue closely replicated the viscosity of the metal flowing through the mould. However, the viscosity of any liquid polystyrene degradation products that were present just ahead of the advancing metal front may have varied considerably depending on the rate that heat was transferred from the liquid metal to the degrading foam and also on the speed that the front was advancing through the mould. Figure 2.35, from work published by Osswald [122], shows quite clearly that over a temperature range of only 60 °C (between 170 °C and 230 °C) the viscosity of a polystyrene melt varied dramatically, especially at low shear rates.

During the mould filling experiments, it was not possible to determine accurately the temperature of liquid polystyrene degradation products within the mould but, based on foam pattern collapse, softening and vaporisation experiments carried out by Davies [54] in which the lowest temperature at which liquefaction of any of the samples began was 240 °C, it was predicted that the viscosity of liquid polystyrene just ahead of the metal front would be within the range of 10 Pa.s to 100 Pa.s. depending on the temperature and shear force in that region at that time. Therefore, the glucose syrup that was used as a substitute for liquid polystyrene in the analogue was prepared in three different concentrations by dilution with small amounts of water. The dynamic viscosity of the original syrup was measured at 93 Pa.s and the results are shown in Figure 4.62. When 2.5 wt.% water was added to the original syrup, the dynamic viscosity fell to 35 Pa.s and a further 2.5 wt.% water addition reduced this value to 16 Pa.s. The viscosity measurements taken on both these diluted samples have been presented in Figure 4.63 and Figure 4.64 respectively.

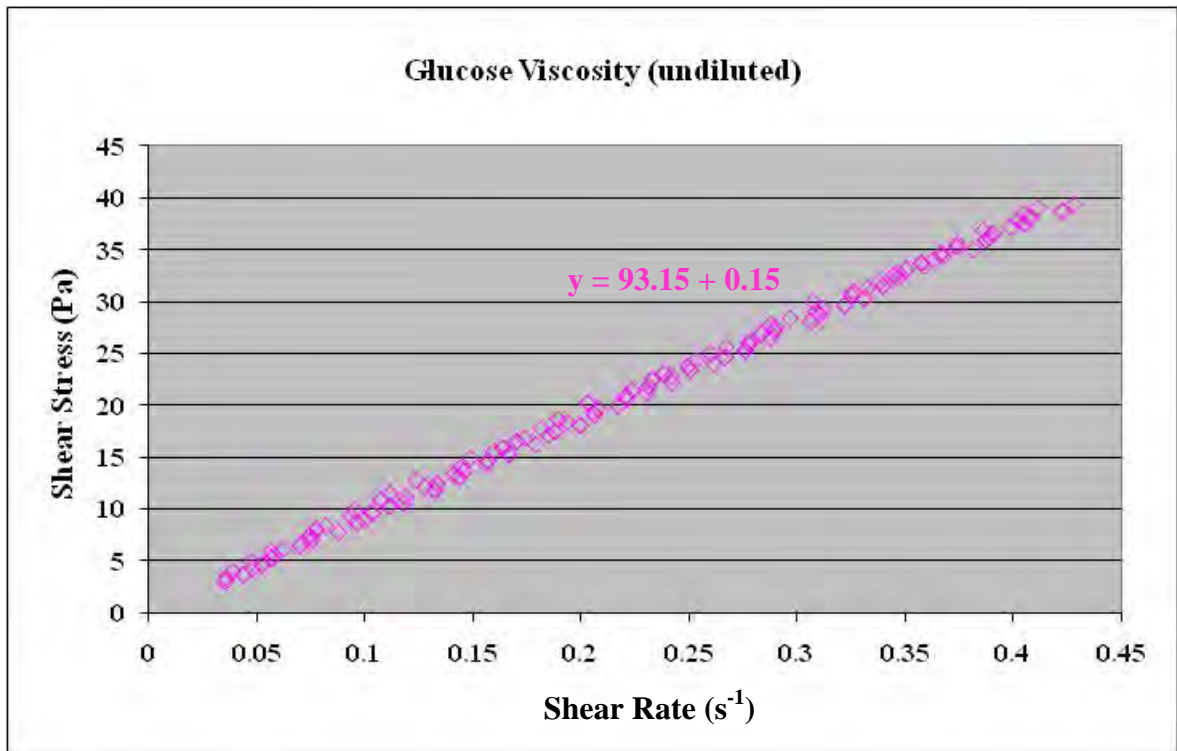


Figure 4.62: Viscosity measurements taken from an undiluted sample of glucose syrup. The dynamic viscosity of this sample was 93 Pa.s.

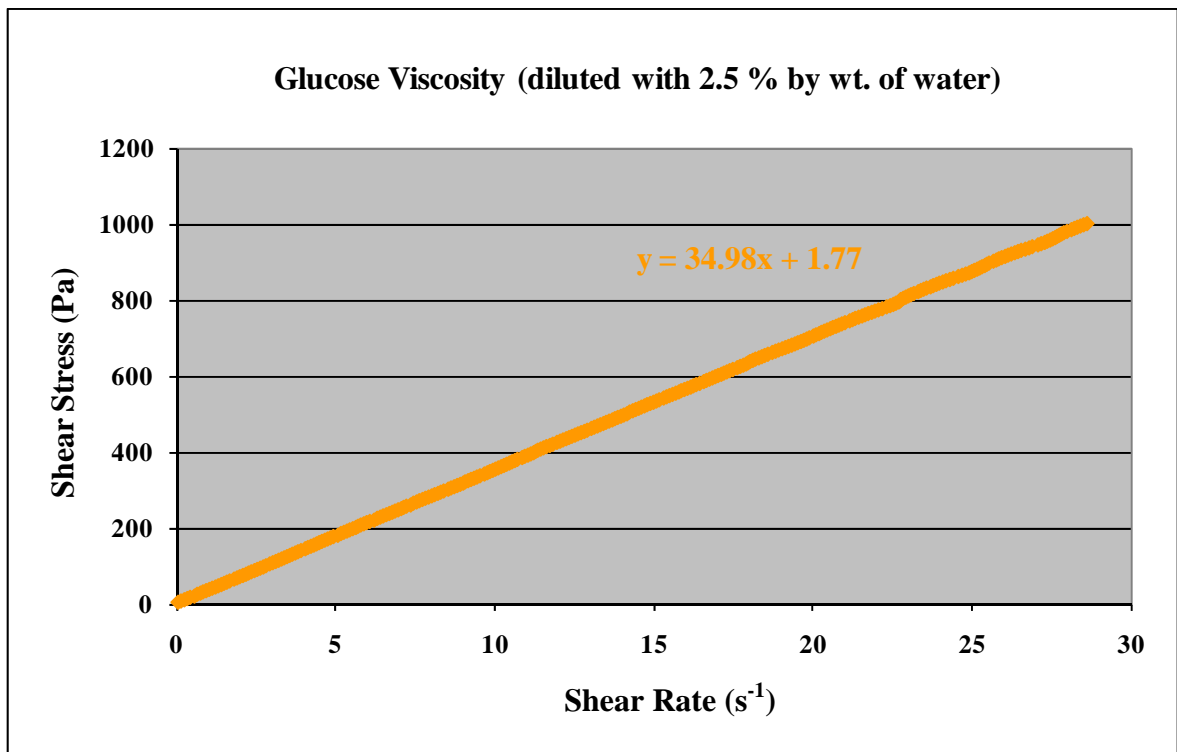


Figure 4.63: Viscosity measurements taken from a sample of glucose syrup diluted with 2.5% by wt. of water. The dynamic viscosity of this sample was 35 Pa.s.

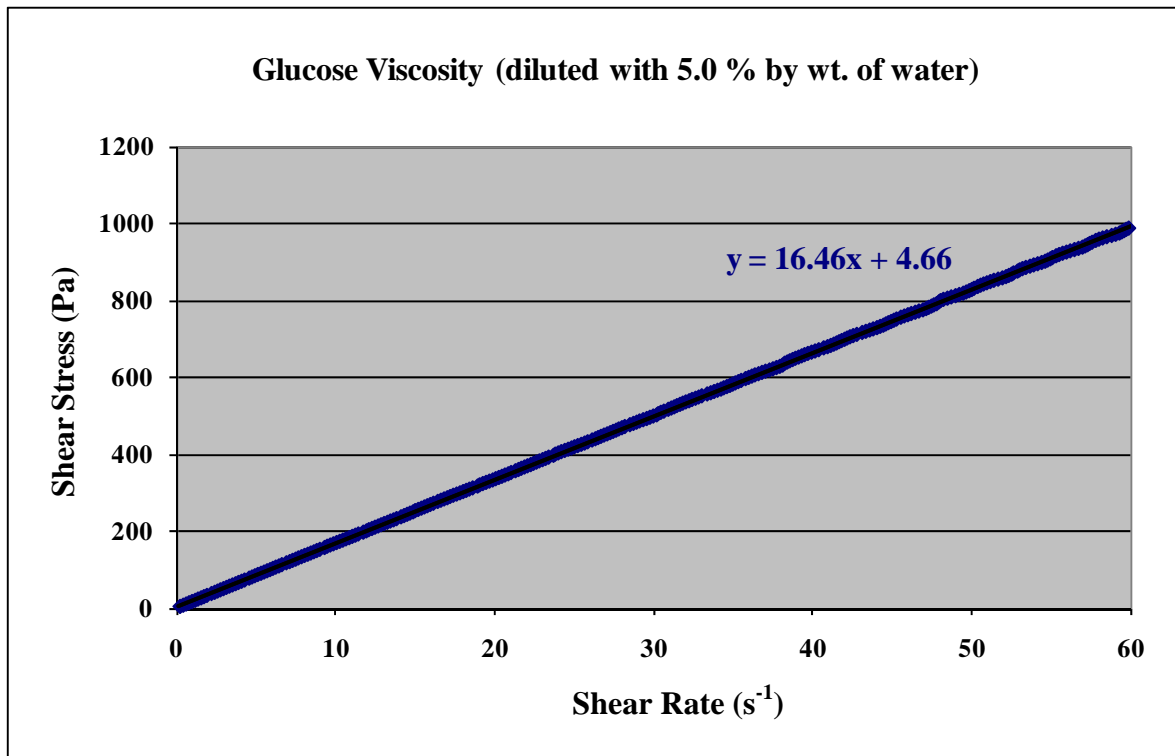


Figure 4.64: Viscosity measurements taken from a sample of glucose syrup diluted with 5.0% by wt. of water. The dynamic viscosity of this sample was 16 Pa.s.

#### 4.6.2 Interfacial Observations During Model Operation

When glucose syrup with a dynamic viscosity of 16 Pa.s was displaced from the region between the two opposing glass plates of the model by the controlled injection of Hg, the interface accelerated upwards in a horizontal, planar fashion until, about 0.5 s. after the displacement began, its speed reached 50 mm.s<sup>-1</sup> as shown in Figure 4.65. However, even at lower speeds the mercury stream was observed to contract away from the faces of the glass plates. This had the effect of reducing the overall cross section of the front and accentuating the curvature of the leading edge.

The interface reached its maximum velocity of around 140 mm.s<sup>-1</sup> about 1 second into the displacement period, and this corresponded to a vertical distance of 70 mm. At that point the Hg began to develop three perturbations that developed into distinct fingers as the front continued to travel vertically upwards to the upper part of the model. Figure 4.65 clearly shows that the largest and most pronounced of these perturbations or fingers was located

between the other two and directly above the region where the mercury had entered the model initially. Although all three fingers became more prominent as displacement continued, the central one grew at a much greater rate, reaching a length of about 80 mm towards the end of the displacement. This caused it to surge ahead and reach the top of the glass cell about 0.75 s. before the other two.

Although shorter and narrower than the central finger, the one observed on the right hand side of the model was well defined. It had a length of approximately 55 mm and the horizontal distance between its tip and the tip of the central finger was about 70 mm. This was in contrast to the left hand finger which was less prominent, having little length development until the latter stages of displacement, by which time it had reached a length of 10 mm. The horizontal distance between its tip and that of the central finger was estimated to be around 60 mm, but it could be seen that, in the latter stages of the displacement, as shown in the last three frames of Figure 4.65, the finger was beginning to divide into two.

When glucose syrup with a dynamic viscosity of 35 Pa.s was used in the model, perturbations at the interface began to appear when the metal front velocity had reached about  $70 \text{ mm.s}^{-1}$ , as shown in the 1.33 s frame of Figure 4.66. This equated to about half the metal front velocity associated with a glucose syrup viscosity of 16 Pa.s. The progression and shape of the interface during the first second of displacement was essentially the same whether a 16 Pa.s or 35 Pa.s viscosity glucose syrup had been used. This was because the model required about one second to accelerate the mercury from standstill up to the desired maximum velocity. The approximate distance between two fingers was about 65 mm and the middle finger, which grew to be the longest, was measured to be about 70 mm from peak to trough. The only noticeable difference was that at the slower displacement speed the division of the left hand finger into two was more pronounced in the latter three frames of Figure 4.66

Increasing the dynamic viscosity of the glucose syrup in the model to 93 Pa.s had the effect of lowering the velocity at which an interfacial disturbance was observed even further. The nine frames contained in Figure 4.67 were taken at intervals of one second. The average speed of the interface was only  $25 \text{ mm.s}^{-1}$ , but even at this slow speed the onset of finger formation was recorded after about 4 s of the displacement cycle had elapsed.

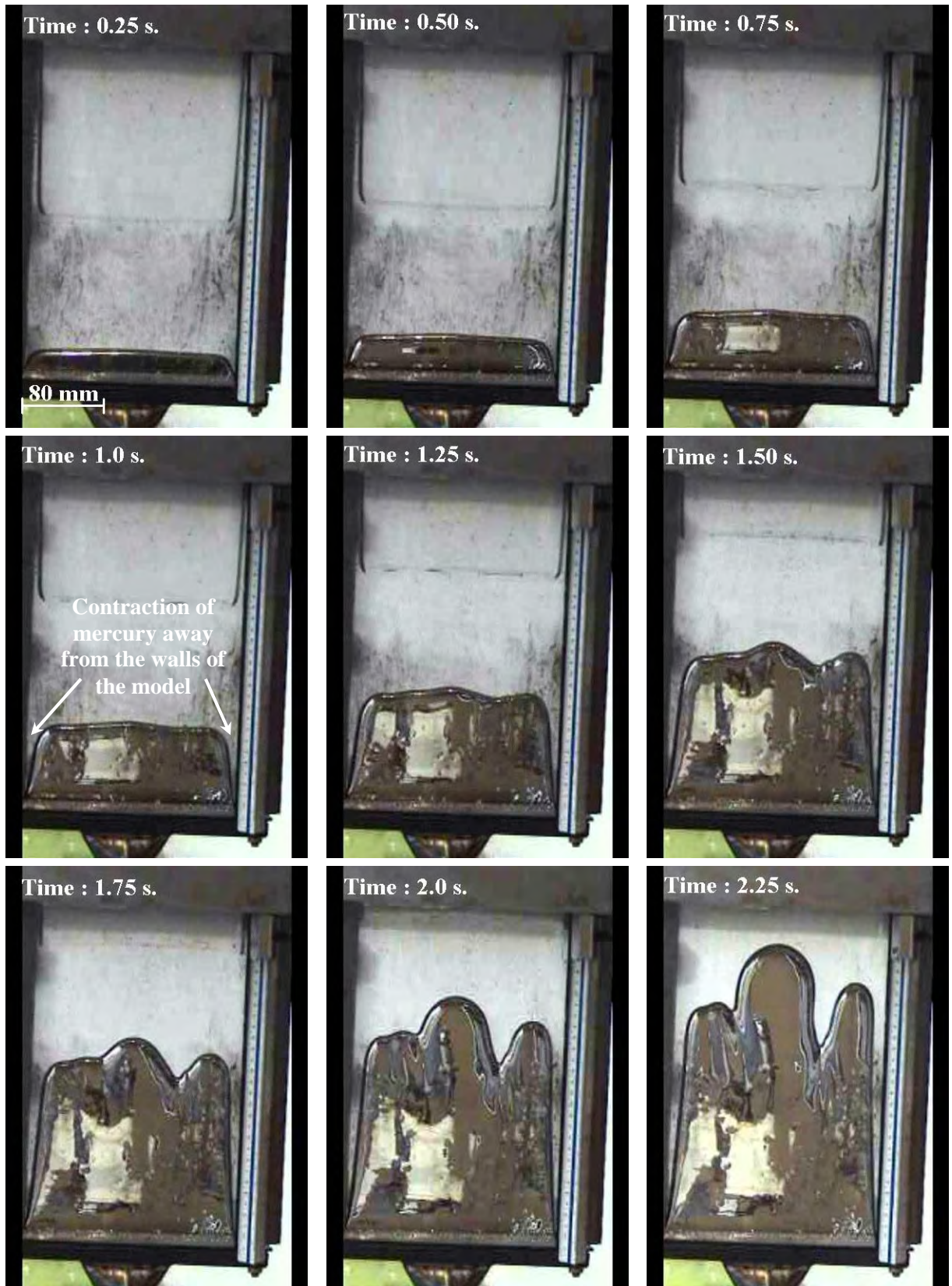


Figure 4.65: Displacement of glucose syrup with a dynamic viscosity of 16 Pa.s and confined between glass plates by liquid mercury travelling at approximately  $140 \text{ mm.s}^{-1}$ .



Figure 4.66: Displacement of glucose syrup with a dynamic viscosity of 35 Pa.s and confined between glass plates by liquid mercury travelling at approximately  $70 \text{ mm.s}^{-1}$ .

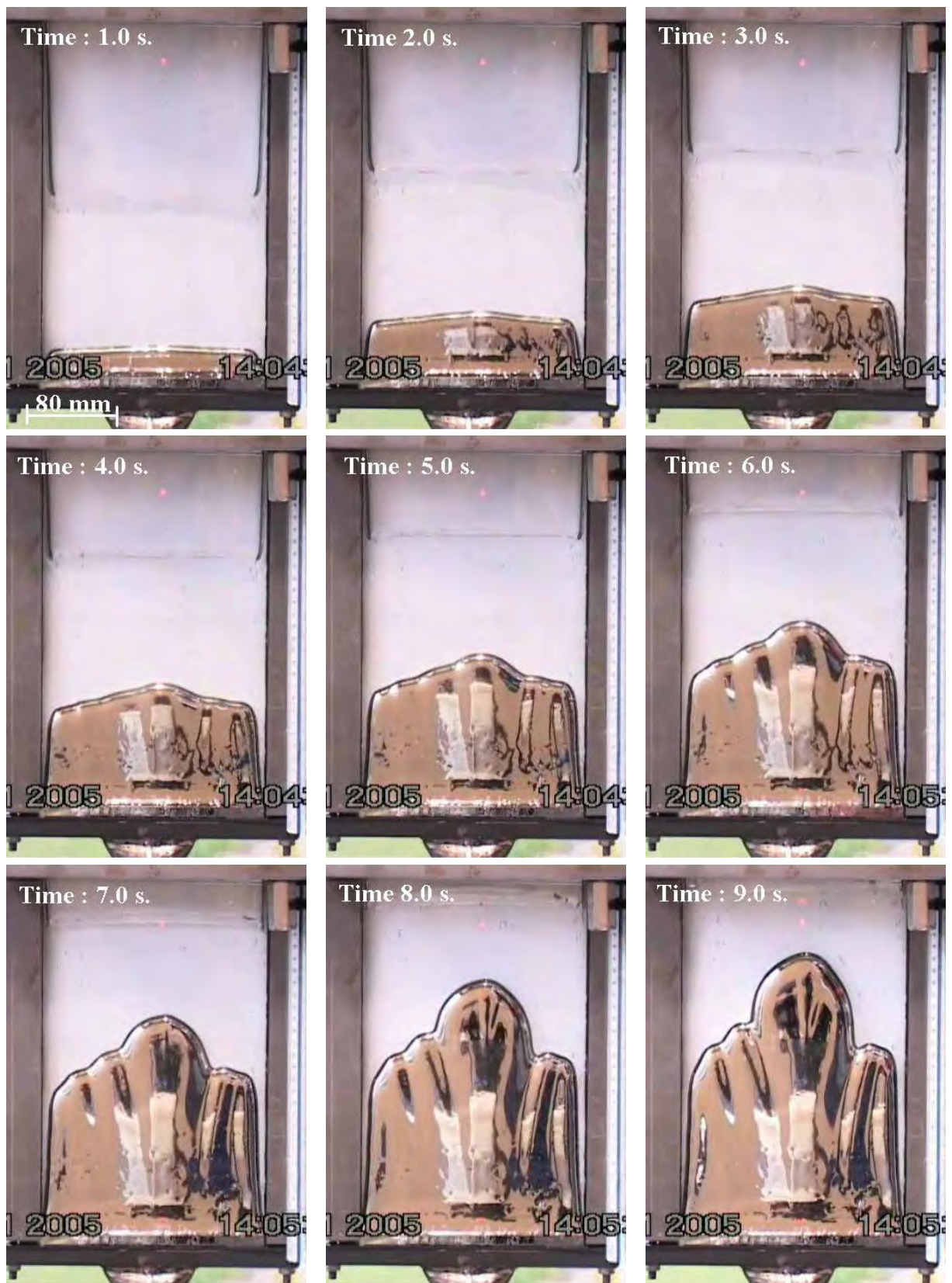


Figure 4.67: Displacement of glucose syrup with a dynamic viscosity of 93 Pa.s and confined between glass plates by liquid mercury travelling at approximately  $25 \text{ mm.s}^{-1}$ .

Although the development of the finger pattern was qualitatively similar to that observed where lower glucose viscosities had been used, i.e. preferential growth of a central finger with a maximum length of 80 mm and a gap between finger tips of about 70 mm, no distinct gap formed between the separate fingers.

In each of the three experiments, the finger spacing varied only slightly from about 65 mm to 70 mm and finger length between 70 mm and 80 mm. When the interface or mercury front speed was increased above the value where a perturbation was observed, no fundamental change occurred in the finger pattern that had initially been created. Instead, the growth of the central finger, in preference to all others, was exaggerated so that it grew vertically upwards at an even greater rate than before and reached the top of the model even sooner than its nearest neighbour. The experiment was repeated on a number of occasions and each successive set of results was found to be almost identical to the previous set. Therefore, it can be concluded that the experiment was highly reproducible.

## **4.7 PROPERTIES OF POLYSTYRENE DEGRADATION PRODUCTS**

A number of authors [8,16,19] have suggested that, during the filling of Lost Foam moulds with aluminium alloys, the majority of the degradation products found at the metal - foam interface were polymer liquids with relatively high viscosities. Although Molibog [16] estimated that these degradation products were about 60% to 80% liquid (depending upon temperature) with the rest being in a gaseous form, none of the authors gave values for the viscosity of this material. The results of the metal - foam interface analogue experiment showed that the speed of the advancing metal front needed to bring about the onset of an interfacial instability fell as the viscosity of the glucose syrup increased. Therefore, it was necessary to approximate the viscosity of the liquid polystyrene present in a Lost Foam mould so that predictions could be made about the influence of a particular filling velocity.

### **4.7.1 The Molecular Weight of Liquid Polystyrene**

It was not possible to measure the viscosity of liquid polystyrene directly, especially when trying to replicate the conditions at the metal – foam interface during Lost Foam casting.

However, Cox and Ballman [39] have determined that the apparent viscosity, or dynamic viscosity at zero shear, of liquid polystyrene could be determined from its molecular weight.

Therefore, samples were collected for molecular weight determination by subjecting conventional polystyrene pattern material (molecular weight of  $413\,000\text{ g}\cdot\text{mol}^{-1}$ ) to degradation at 4 different peak temperatures. Immediately thereafter each sample was quenched to room temperature as quickly as possible in order to capture the degraded material in the solid form. The actual temperature profiles experienced by the polymer have been shown in Figure 4.68 and the figure in brackets next to every sample number in the legend is the temperature at which it was removed from the heat source, (a liquid aluminium melt).

An overshoot was observed in each profile between the temperature at which the sample was removed from the heat source and the maximum temperature reached. This is because a certain amount of time was needed to transfer each sample from the heat source to the cooling medium. The profiles associated with samples U1, U3 and U4 suggested that this manual operation took between 0.5 and 1.5 s, but for sample number 2 took about 3 s. The associated heating curve also indicated that this sample had been subject to much less severe heating and cooling rates than the other three and therefore it was thought that the thermocouple tip had shifted from the surface to the central region of the sample.

Samples of brominated, expanded polystyrene (molecular weight of  $340\,000\text{ g}\cdot\text{mol}^{-1}$ ) were also subject to heating and quenching similar to that applied to the conventional pattern material. Although the experimental procedure was the same, the temperature curves recorded were slightly different. As shown in Figure 4.69, three temperature profiles exhibited an overshoot of approximately  $50\text{ }^{\circ}\text{C}$  compared to the temperature at which they were removed from the heat source. Although this value was similar to those recorded during the degradation of normal polystyrene, a  $150\text{ }^{\circ}\text{C}$  overshoot was observed in respect of sample number B2. This may have been caused by an increase in the time taken to transfer this sample from the heat source to the quenching medium.

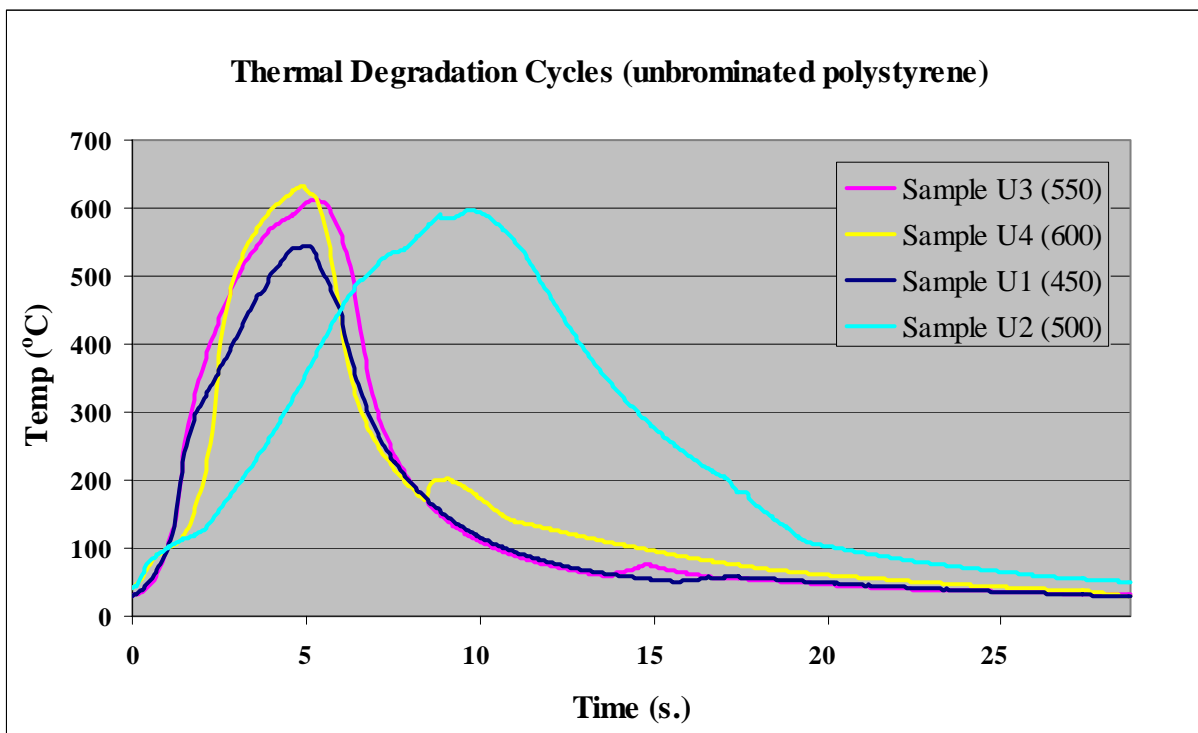


Figure 4.68: Temperature profiles used to capture samples of conventional polystyrene pattern material that had been degraded at various temperatures.

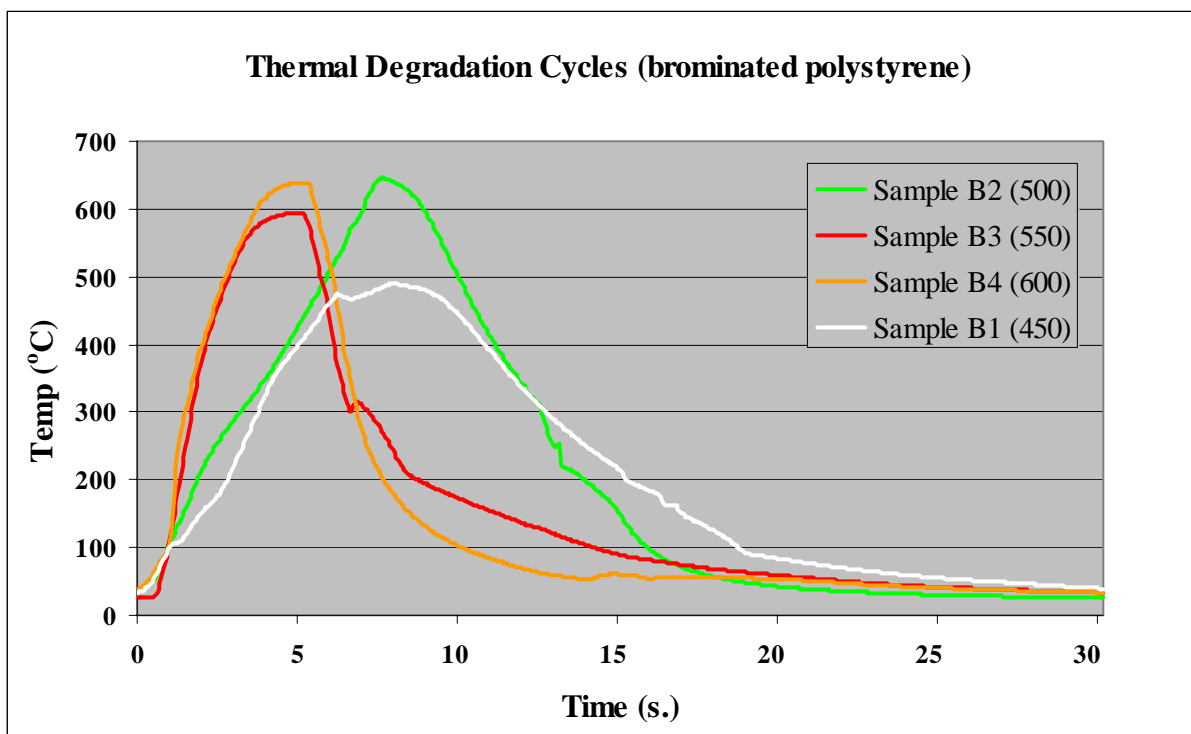


Figure 4.69: Temperature profiles used to capture samples of brominated polystyrene pattern material that had been degraded at various temperatures.

Relationship Between Degradation Energy and Molecular Wt			
Sample Reference	Area Under Degradation Curve ( $^{\circ}\text{C.s}$ )	Molecular Wt ( $\text{g mol}^{-1}$ )	
		Sample No. 1	Sample No. 2
U1	4,037	182,000	184,000
U2	7,252	67,400	67,000
U3	4,459	179,000	176,000
U4	4,674	160,000	155,000
B1	6,215	55,400	54,700
B2	6,247	38,900	41,600
B3	4,898	168,000	164,000
B4	4,555	137,000	136,000

Table 4.70: Molecular weights of conventional and brominated samples of polystyrene pattern material compared with the areas under each of the temperature curves used to degrade them.

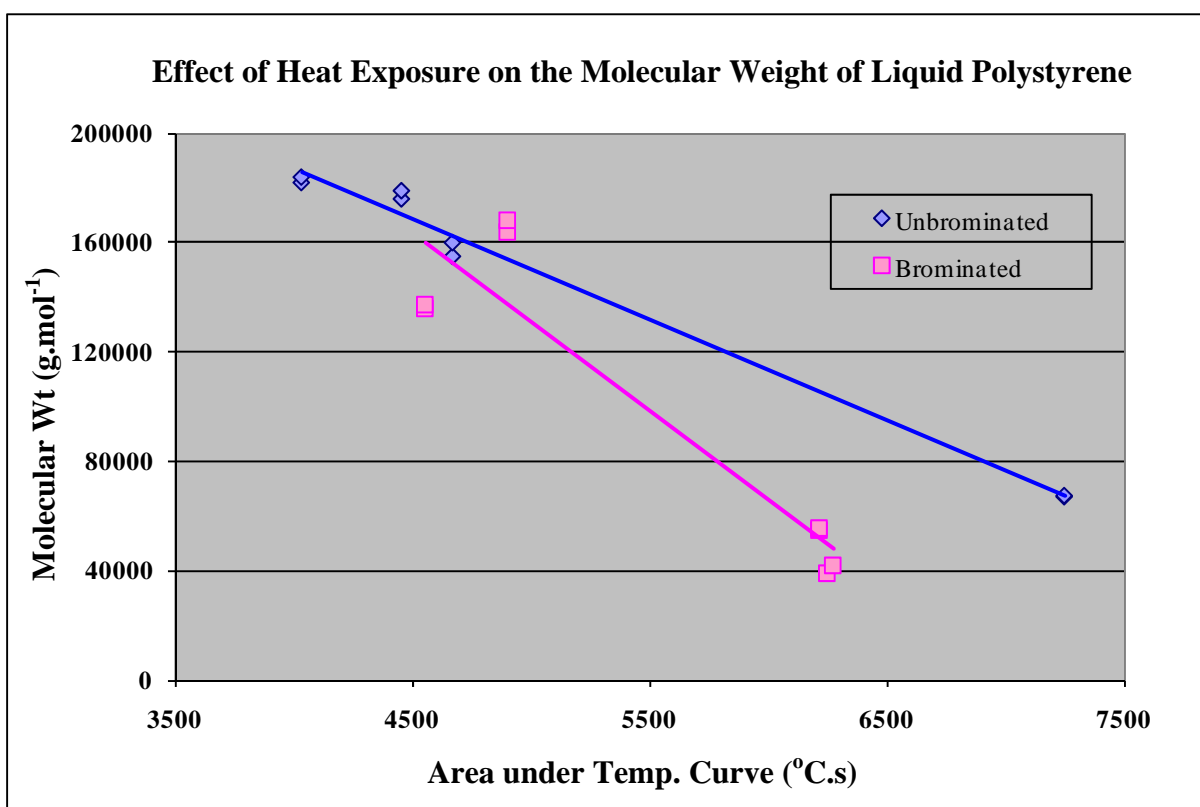


Figure 4.71: Effect of exposure to heat on the molecular weight of samples of polystyrene with and without additions of a bromine compound.

Each degraded sample was analysed in two independent runs by Gel Permeation Chromatography to determine its molecular weight. Table 4.70 lists the molecular weight

results obtained from each sample and the area under each of the temperature curves used to degrade them. This was used as an indication of the degree of exposure to heat that each sample had experienced. Very little difference was found between the two values obtained from any one sample (see Figure 4.71). Also, at heat exposures corresponding to an area under the temperature curve of between 4000 °C.s and 5000 °C.s, the influence of the bromine compound addition was negligible. However, as heat exposure increased above this level, the molecular weights of those samples containing bromine were substantially lower than those where conventional polystyrene had been used. This implied that, above a certain heat exposure level, the presence of bromine compound additions in the polystyrene had the effect of reducing its viscosity in the liquid phase.

#### 4.7.2 The Viscosity of Liquid Polystyrene

With the molecular weights of the polystyrene patterns known, the apparent viscosity (or dynamic viscosity at zero shear) of the liquid degradation products could be estimated according to Cox and Ballman's formula, Equation 4.1 [39].

$$\log \eta_0 = 3.4 \log M + [900.2/(T - 306.4)] - 18.38 \quad \text{Equation. 4.1}$$

where  $\eta_0$  = apparent viscosity at zero shear

$M$  = molecular weight

$T$  = the temperature of the melt (in degrees Kelvin)

Although these researchers had derived this equation for a polystyrene melt with a temperature of between 175 °C to 230 °C, Merz and Colwell [126] showed empirically that it was also applicable to a melt at 450 °C.

According to Equation 4.1 the apparent viscosity of liquid polystyrene is dependant not only upon molecular weight, but also on temperature. The liquid aluminium used to fill the plate castings in this series of experiments was cast at a temperature of about 785 °C as it entered the mould, and would be at a lower temperature at the interface with the pattern. In fact, during Lost Foam casting experiments carried out by Davies [54], the temperature of the metal

front was measured to be at only 605 °C as it advanced through the central region of a 10 mm plate pattern at about 5 mm.s<sup>-1</sup>. This was just below the liquidus temperature of the alloy.

Table 4.72 shows the calculated viscosity at 400 °C, 500 °C and 600 °C, for each of the samples from which a molecular weight value had been obtained. Although it was recognised that, in non-Newtonian fluids such as polystyrene, the viscosity at zero shear would be higher than that encountered during the filling of Lost Foam moulds because of the shearing that occurs in the liquid polymer as it is displaced by the metal front, these values could serve as a guide to approximating the order of magnitude difference in viscosity of the liquid metal and the degraded pattern material.

<b>Calculated Melt Viscosity at Various Temperatures</b>				
<b>Sample Ref.</b>	<b>Mol. Wt. (gmol<sup>-1</sup>)</b>	<b>Apparent Viscosity (Pa.s)</b>		
		<b>400 °C</b>	<b>500 °C</b>	<b>600 °C</b>
U1	183000	92.9	27.6	12.6
U2	67200	3.1	0.9	0.4
U3	177500	83.7	24.9	11.4
U4	157500	55.8	16.6	7.6
B1	55070	1.6	0.5	0.2
B2	40250	0.5	0.2	0.1
B3	166000	66.7	19.8	9.1
B4	136500	34.3	10.2	4.7

Table 4.72: Apparent viscosity of polystyrene melts of known molecular weight at different temperatures (according to Cox and Ballman [39]).

The data are shown in Figure 4.73, where it is clear that the influence of molecular weight on the viscosity of a polystyrene melt was most pronounced at lower temperatures.

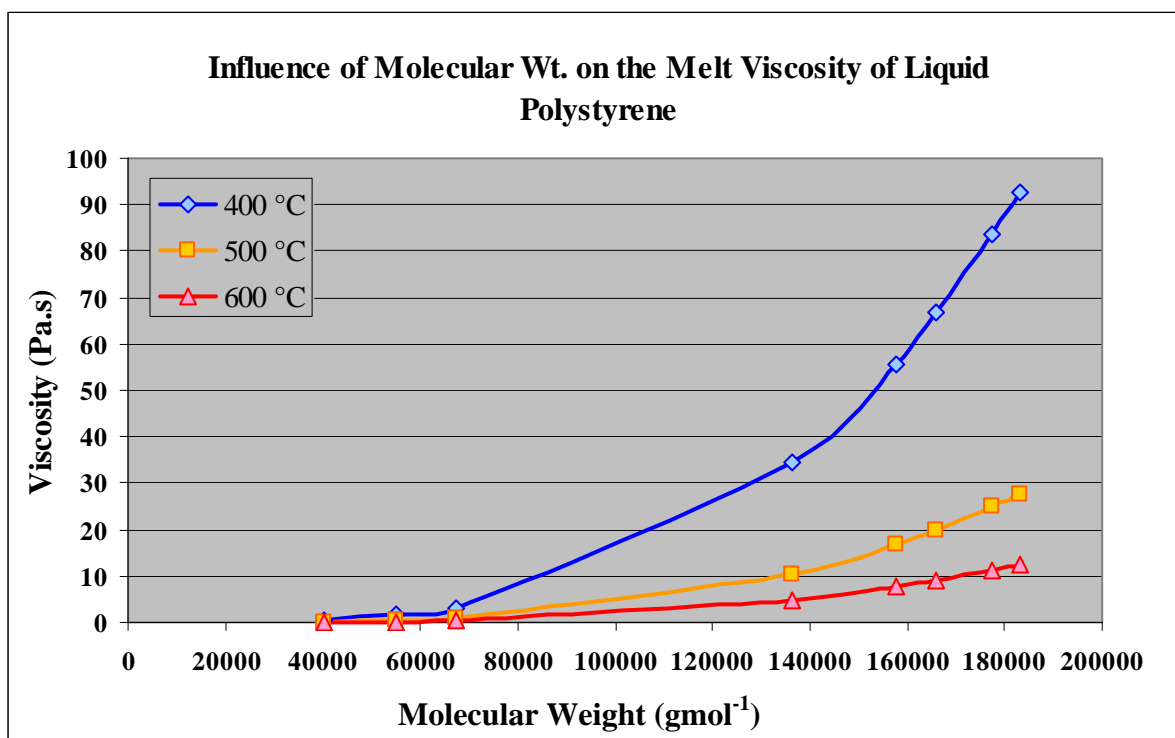


Figure 4.73: Influence of molecular weight on the viscosity of polystyrene melts at different temperatures.

## 4.8 CASTING OF PATTERNS CONTAINING BROMINE COMPOUNDS

It has been shown that by adding bromine to polystyrene pattern material, the molecular weight of the liquid polystyrene residue was reduced and, for a given exposure to heat, the resultant liquid should be less viscous than that of the untreated material. Therefore, it was decided to fill Br-treated and untreated plates in a counter-gravity fashion at two different velocities and compare front behaviour and profile by means of real time X-ray observations and tensile strength variation in the resultant castings by means of a Weibull analysis.

### 4.8.1 Mould Filling Observations

Four separate moulds were cast, each containing a single plate pattern and Figure 4.74 highlights the region in each mould where filling was observed. Figure 4.75 shows real time X-ray images of the aluminium-pattern interface for a 10 mm thick plate made of conventional polystyrene material. This material originated from the same batch that was used to estimate the molecular weights in the previous experiments. As the metal front advanced at

an average velocity of about  $6 \text{ mm.s}^{-1}$ , small perturbations were seen at the interface which had a wavelength of about 6 mm. Although these perturbations are not very pronounced, they can be seen in Frame 3 of Figure 4.75 and in much more clarity on the accompanying video which can be found on the CD that is located in Appendix I of this thesis. Although the ingate was located centrally on the bottom face of the plate, metal entering it favoured the left hand side as viewed from the imaging device. This caused the front to travel at a shallow angle, diagonally upwards across the main field of view.

When the front velocity was increased to about  $10 \text{ mm.s}^{-1}$ , during the filling of a second mould of similar characteristics, it filled in essentially the same manner as the first. However, the angle of diagonal travel of the front was much greater and resulted in an almost horizontal travel from left to right across the field of view as shown in the frames of Figure 4.76. This caused polystyrene degradation products, mainly gases, to rise up across its face in an attempt to escape away from the interface and into the surrounding moulding sand. Such a flow of hot gases carried with it liquid metal which accumulated in a wave at the uppermost corner of the front. This can be seen in Frames 1 and 2 of Figure 4.76 and more clearly on the video from which the individual frames were extracted. This can be found on the CD that is located in Appendix I of this thesis.

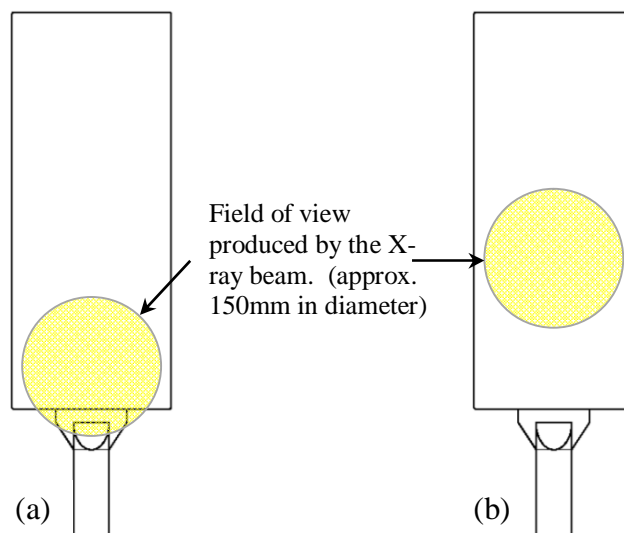


Figure 4.74: Fields of view during the counter-gravity filling of 10 mm thick plates (a) in the ingate region (see Figure 4.75) and (b) in the central region of the plate (see Figures 4.76 to 4.78).

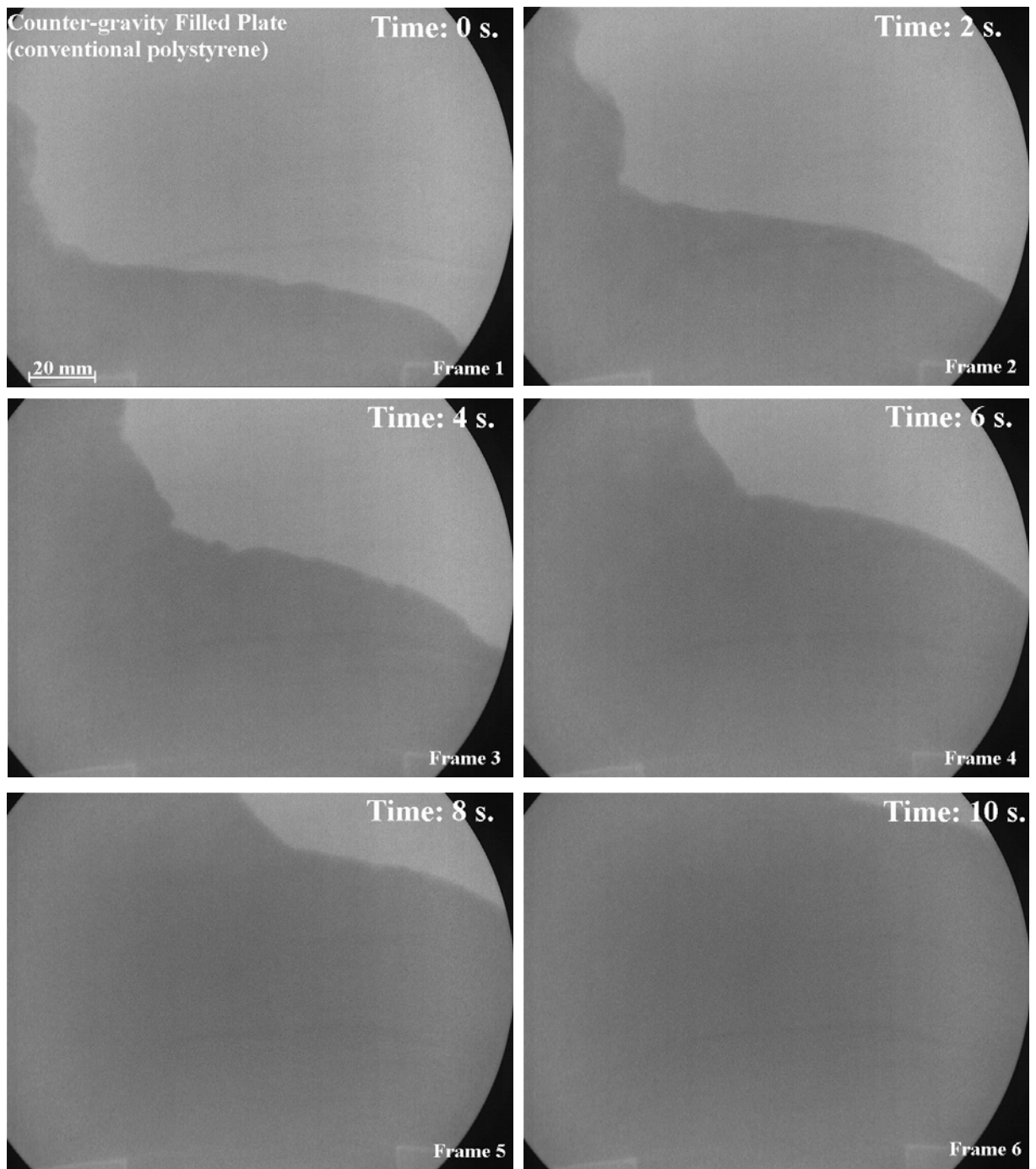


Figure 4.75: Sequence of real-time X-ray frames capturing the behaviour of the interface between molten aluminium and a plate pattern made of conventional polystyrene. (Approximate metal velocity =  $6 \text{ mm}\cdot\text{s}^{-1}$ ).

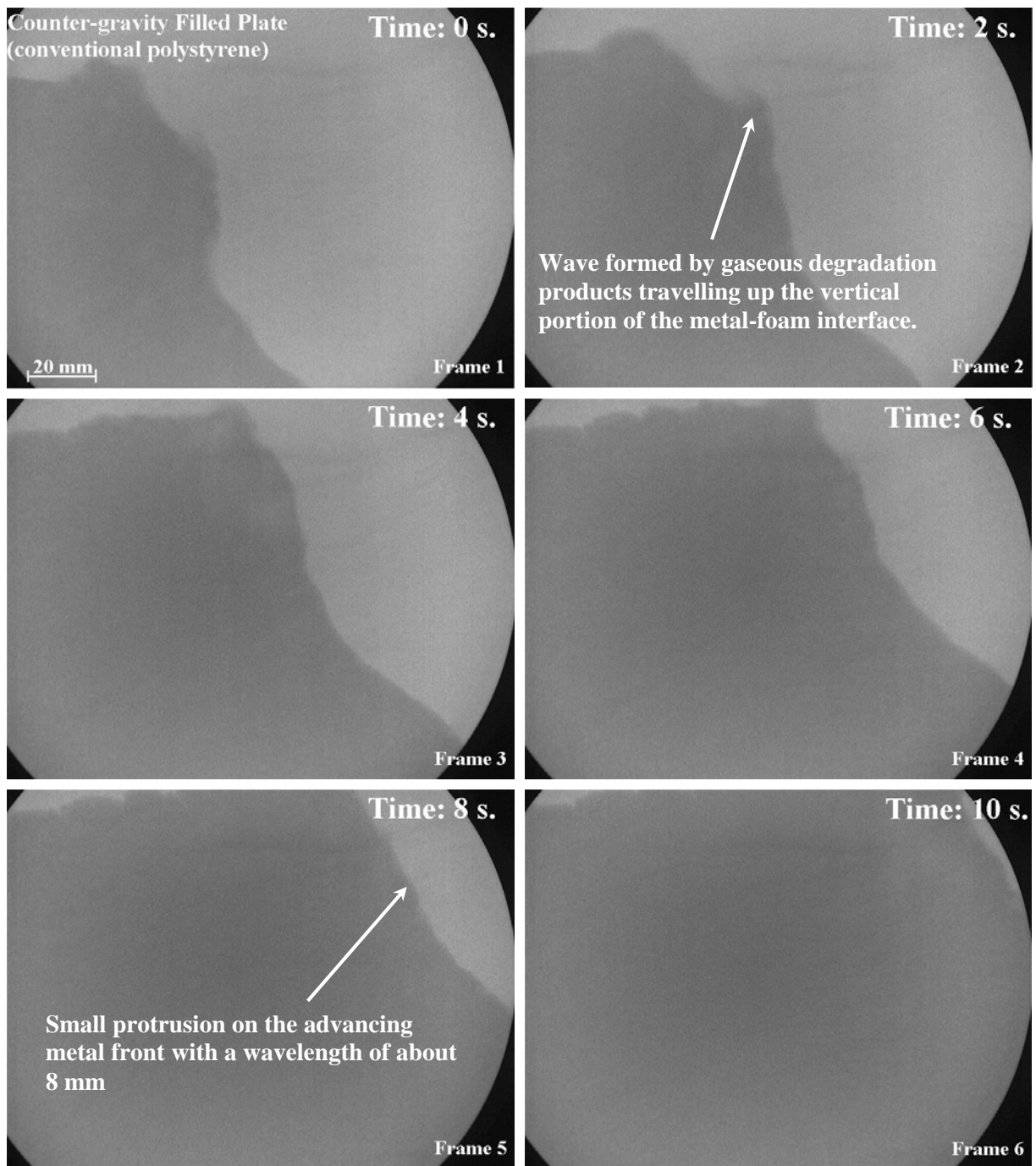


Figure 4.76: Sequence of real-time X-ray frames capturing the behaviour of the interface between molten aluminium and a plate pattern made of conventional polystyrene. (Approximate metal velocity =  $10 \text{ mm}\cdot\text{s}^{-1}$ ).

When the lower region of the metal front reached the right hand vertical sidewall of the mould it started to flow upwards. This had the effect of reducing the length of that part of the front that was flowing in a near horizontal direction and also the amount of gaseous degradation products that were rushing vertically past it. As this flow of gases reduced, their effect on the front profile diminished and, in Frames 4 and 5 of Figure 4.76, perturbations similar to those seen where the front speed had been  $6 \text{ mm.s}^{-1}$  were observed. However, in this case, slightly longer wavelengths of between 6 mm and 8 mm were recorded.

When a mould that contained a 10 mm thick brominated plate pattern was cast such that the metal front velocity averaged  $6 \text{ mm.s}^{-1}$ , the interface between the metal and the foam took on a very different configuration. Figure 4.77 shows that the front adopted a generally smooth, almost horizontal profile and progressed vertically upward throughout the filling sequence. No perturbations were encountered at the interface and the occasional irregularity in the advancing metal front that could be seen had a very large radius.

When the same technique was used to cast a brominated plate at twice the velocity (about  $14 \text{ mm.s}^{-1}$ ), the direction of flow remained essentially in the vertically upward direction. Nevertheless, the front adopted a less uniform profile with the distance between peak and trough reaching a value between two and three times that observed in Figure 4.77. Even then, in the early stages of the filling, as depicted in Frames 1 to Frame 3 of Figure 4.78, no perturbations of a small wavelength were observed.

As filling progressed, a small “mushroom” of metal was seen breaking through the front. This was captured in Frame 4 of Figure 4.78 and can be seen about 60 mm along the front from the far right. Within another 1.5 s. a further two “mushrooms” had broken through the front just to the right of the original one and a few small perturbations, similar to those captured in Figures 4.75 and 4.76, were also observed. The change in height of the front between Frame 4 and Frame 5 suggests that the velocity increased locally to around  $18 \text{ mm.s}^{-1}$  and it was this that brought about the onset of an instability at the interface. The distance between the mushroom peaks ranged from about 10 mm to 15 mm and that between the smaller perturbations that appeared in Frame 5 were about 5 mm.

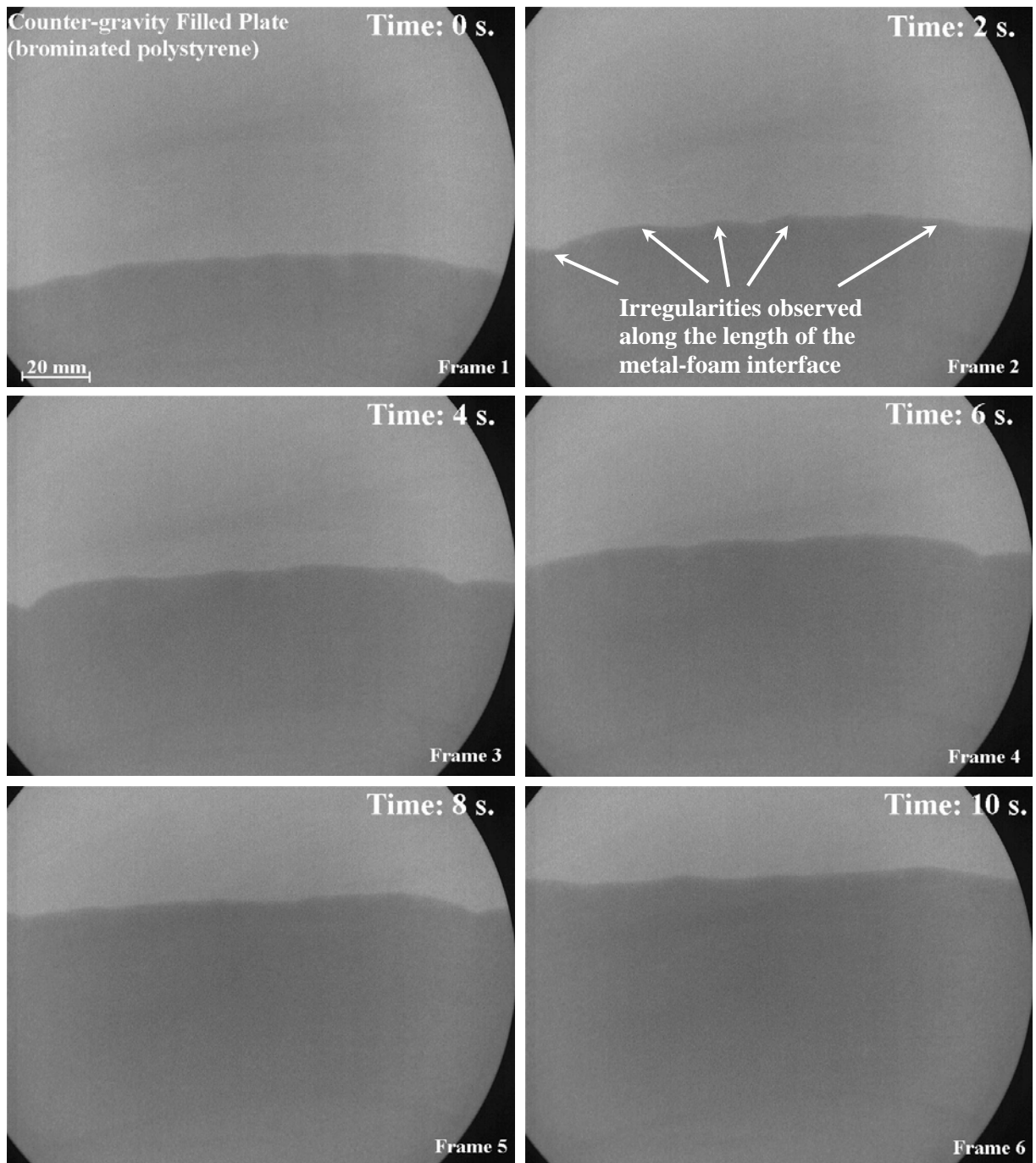


Figure 4.77: Sequence of real-time X-ray frames capturing the behaviour of the interface between molten aluminium and a plate pattern made of brominated polystyrene. (Approximate metal velocity =  $6 \text{ mm}\cdot\text{s}^{-1}$ ).

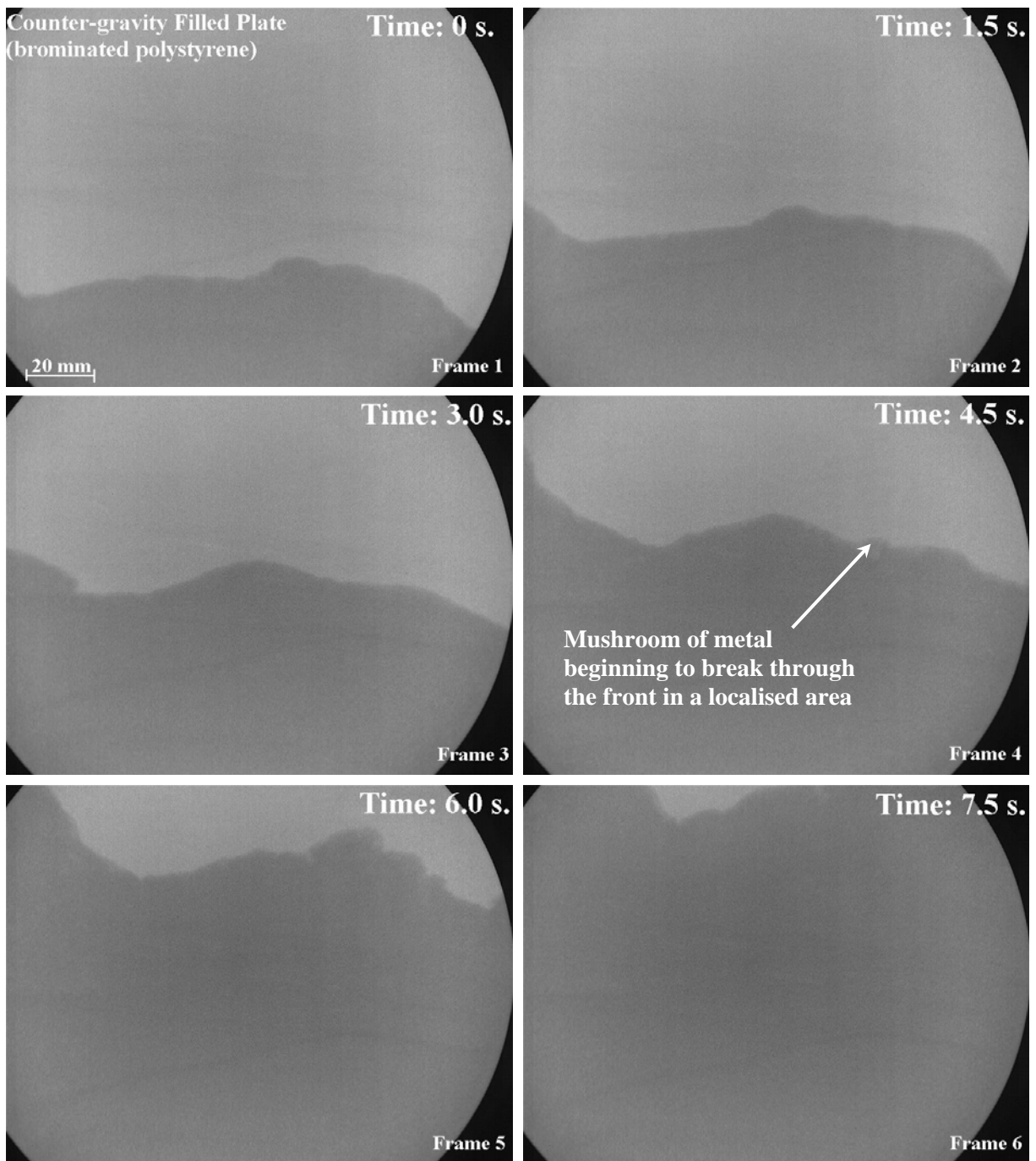


Figure 4.78: Sequence of real-time X-ray frames capturing the behaviour of the interface between molten aluminium and a plate pattern made of brominated polystyrene. (Approximate metal velocity =  $14 \text{ mm}\cdot\text{s}^{-1}$ ).

Although the severity of an instability at the metal – foam interface had been noticeably less when a bromine additive was present in the pattern plate, a completely planar front had not been observed during the filling of any of the four plates, even when the metal front had only been travelling at  $6 \text{ mm.s}^{-1}$ . For example, the metal front that had the most planar characteristics is shown in Figure 4.77 and even during the filling of this plate a number of irregularities were present at the metal-foam interface, particularly during the early stages of the fill as seen in Frame 2. These can be seen much more clearly in the video from which the frames were extracted which is located on a CD in Appendix I to this thesis. Therefore, a further two moulds were cast, one containing a 10 mm thick plate pattern made of conventional polystyrene and the other where the same pattern design had been treated with a bromine compound, such that the metal front speed in each case was observed to travel through the mould at approximately  $5 \text{ mm.s}^{-1}$ . The fields of view revealed by the real time X-ray unit and used to observe the metal as it filled each mould are shown in Figure 4.79.

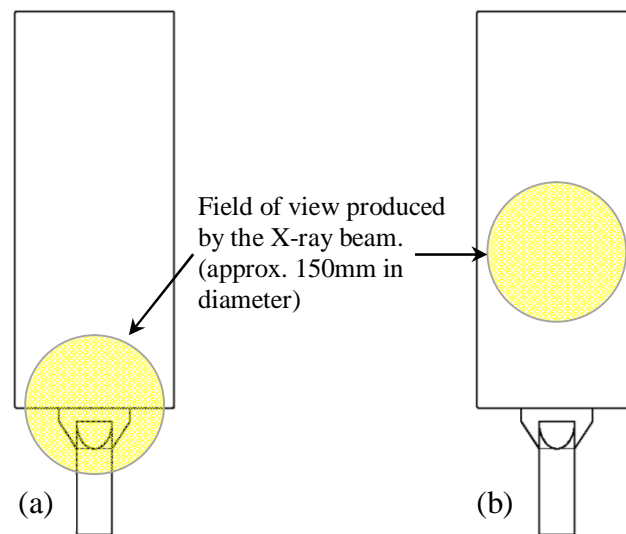


Figure 4.79: Fields of view during the counter-gravity filling of 10 mm thick plates (a) in the ingate region (see Figure 4.80 and Figure 4.82) and (b) in the central region of the plate (see Figures 4.81 and 4.83).

In the case of a conventional polystyrene pattern, the filling of the running system proceeded in the same general fashion as had been observed when the front had been travelling at  $6 \text{ mm.s}^{-1}$ . However, at the interface between the ingate and the pattern plate, the metal broke through the glue joint in a localised region that was slightly to one side of the centre. Frame 1 of Figure 4.80 clearly shows that the initial breach had a cross section of only 8 mm but within

3 s., as illustrated by Frame 4 of the same figure, this had grown to over 30 mm. At that point in the fill, another breach occurred on the opposite side of the ingate and it was only 4 s. after liquid metal began to degrade the pattern plate that the glue joint had disappeared altogether. The liquid metal then began to fill one side of the plate in preference to the other. This mode of filling prevailed until the mould was completely full and, as can be seen in Figure 4.81, resulted in a front profile that moved diagonally across the field of view as observed by the real time X-ray unit. As the metal front reached the central region of the plate a kink was observed in its profile with the lower region being a few degrees offset from the horizontal plane and the upper region being almost vertical in orientation. This was most pronounced in Frames 1 and 2 of Figure 4.81 where it was associated with a wave that travelled up the near vertical part of the front. The wave was caused by gaseous degradation products flowing upwards across the almost vertically oriented metal front in an attempt to escape along the path of least resistance which suggested that it was an interfacial instability of the Kelvin-Helmholtz type. The phenomenon can be seen most clearly on the video from which the frames of Figure 4.81 were extracted which is contained on a CD in Appendix I to this thesis.

As filling progressed, the angle of the lower region of the front increased in relation to the horizontal plane. This caused a relaxation of the kink in the front profile such that, by 14 s. into the fill as shown in Frame 4 of Figure 4.81, the front had become essentially concave and was devoid of any unstable regions. As the metal neared the top of the plate the concave shape of the front became less and less pronounced until, as depicted in Frames 5 and 6, it exhibited an almost planar profile at approximately  $45^\circ$  to the horizontal.

When a brominated plate was cast at the same advancing liquid metal velocity of  $5 \text{ mm.s}^{-1}$ , the filling sequence was observed to be much more controlled and uniform. Figure 4.82 clearly illustrates that the metal entered into the pattern region as a continuous, horizontal front. This meant that the glue joint between pattern plate and ingate degraded uniformly over its entire area and prevented the metal from emerging from the ingate in a number of localised regions. Although the metal front favoured one side of the plate to the other initially, this phenomenon was much less pronounced than during the filling of a conventional polystyrene plate. Moreover, as Figure 4.83 shows, the orientation of the front remained generally horizontal throughout the filling sequence and devoid of any unstable regions or perturbations.

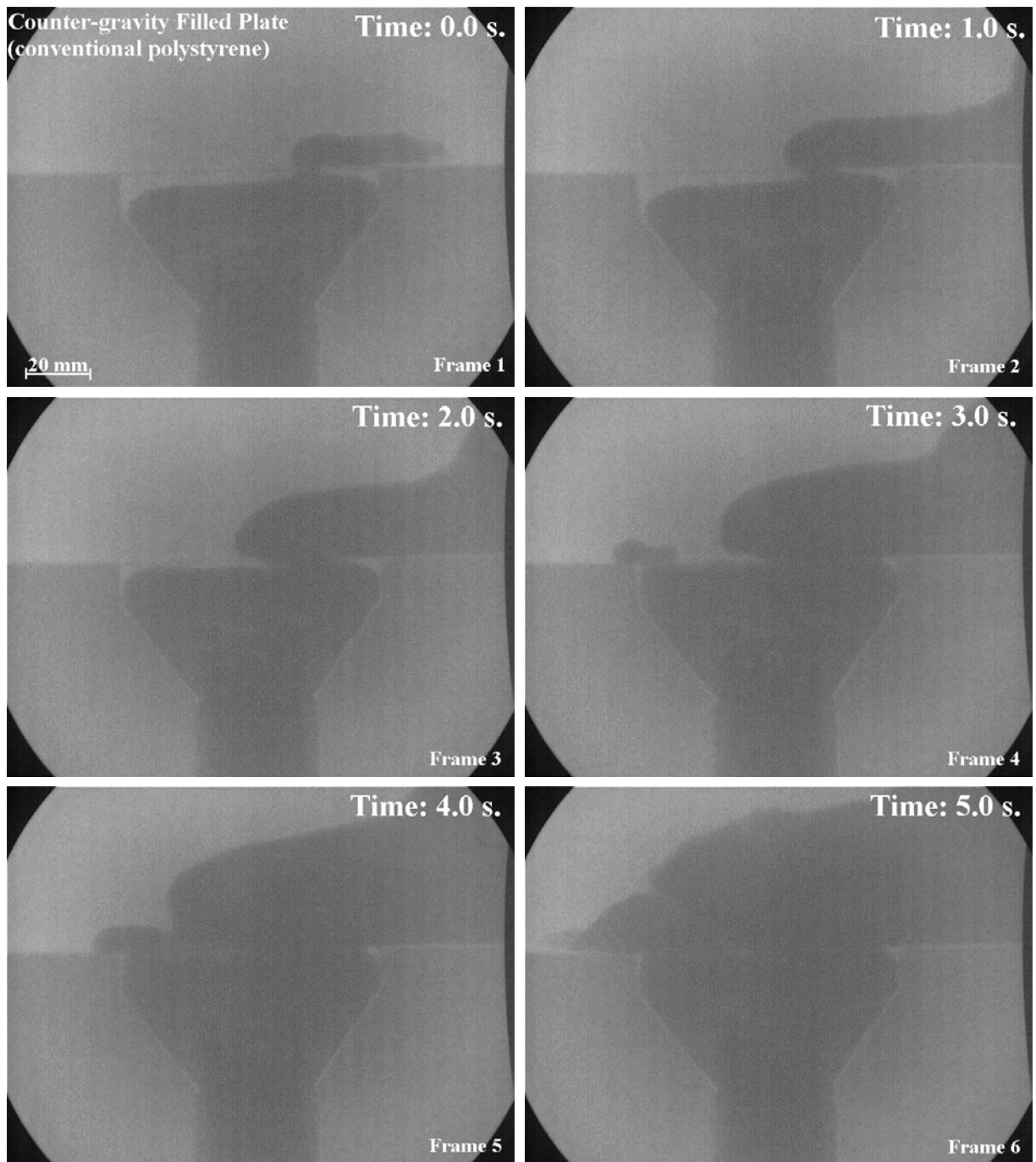


Figure 4.80: Sequence of real-time X-ray frames taken from the ingate region of the mould and depicting the behaviour of the interface between molten aluminium and a plate pattern made of conventional polystyrene. (Approximate metal velocity =  $5 \text{ mm.s}^{-1}$ ).

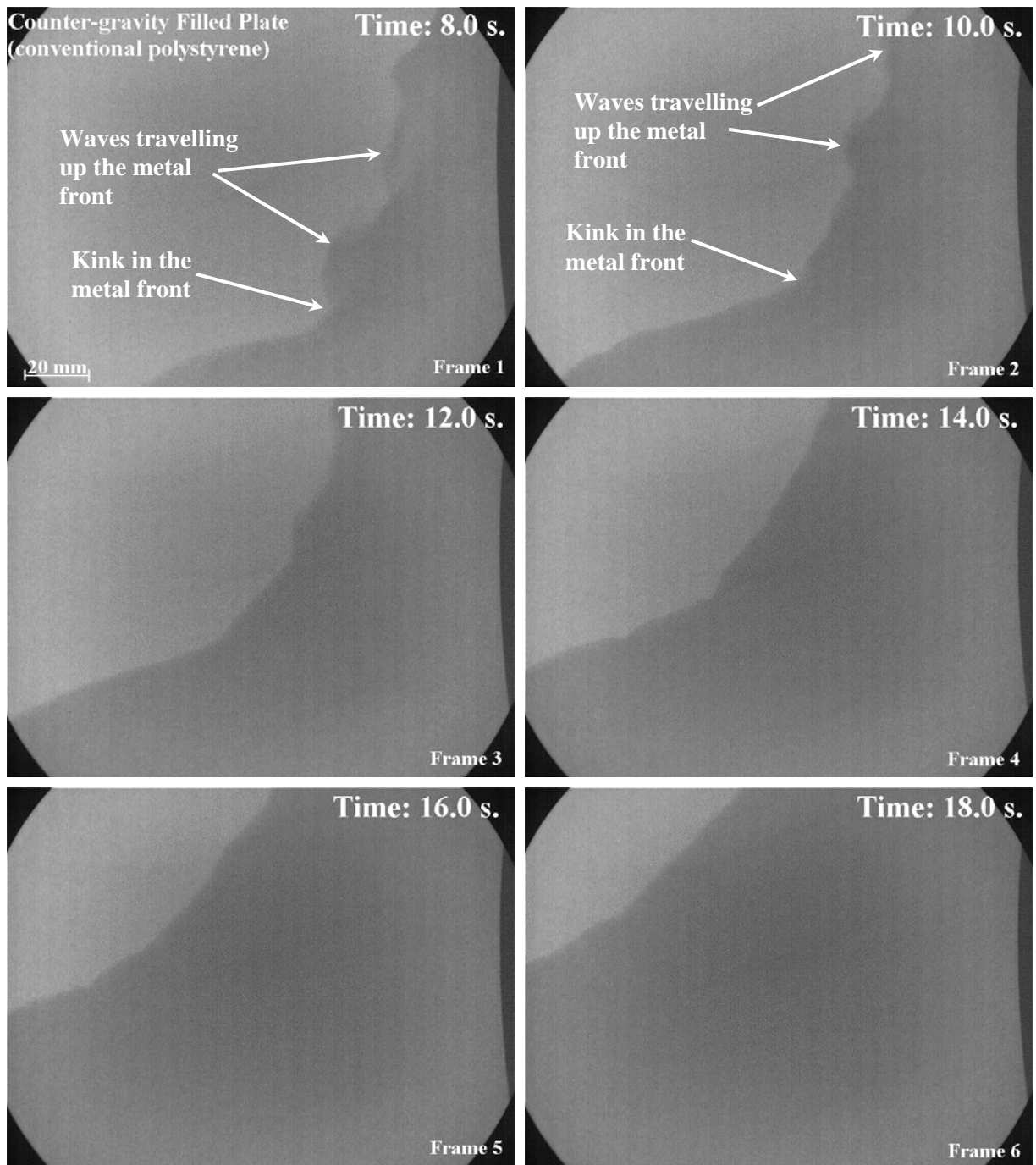


Figure 4.81: Sequence of real-time X-ray frames taken from the central region of the mould and depicting the behaviour of the interface between molten aluminium and a plate pattern made of conventional polystyrene. (Approximate metal velocity =  $5 \text{ mm.s}^{-1}$ ).

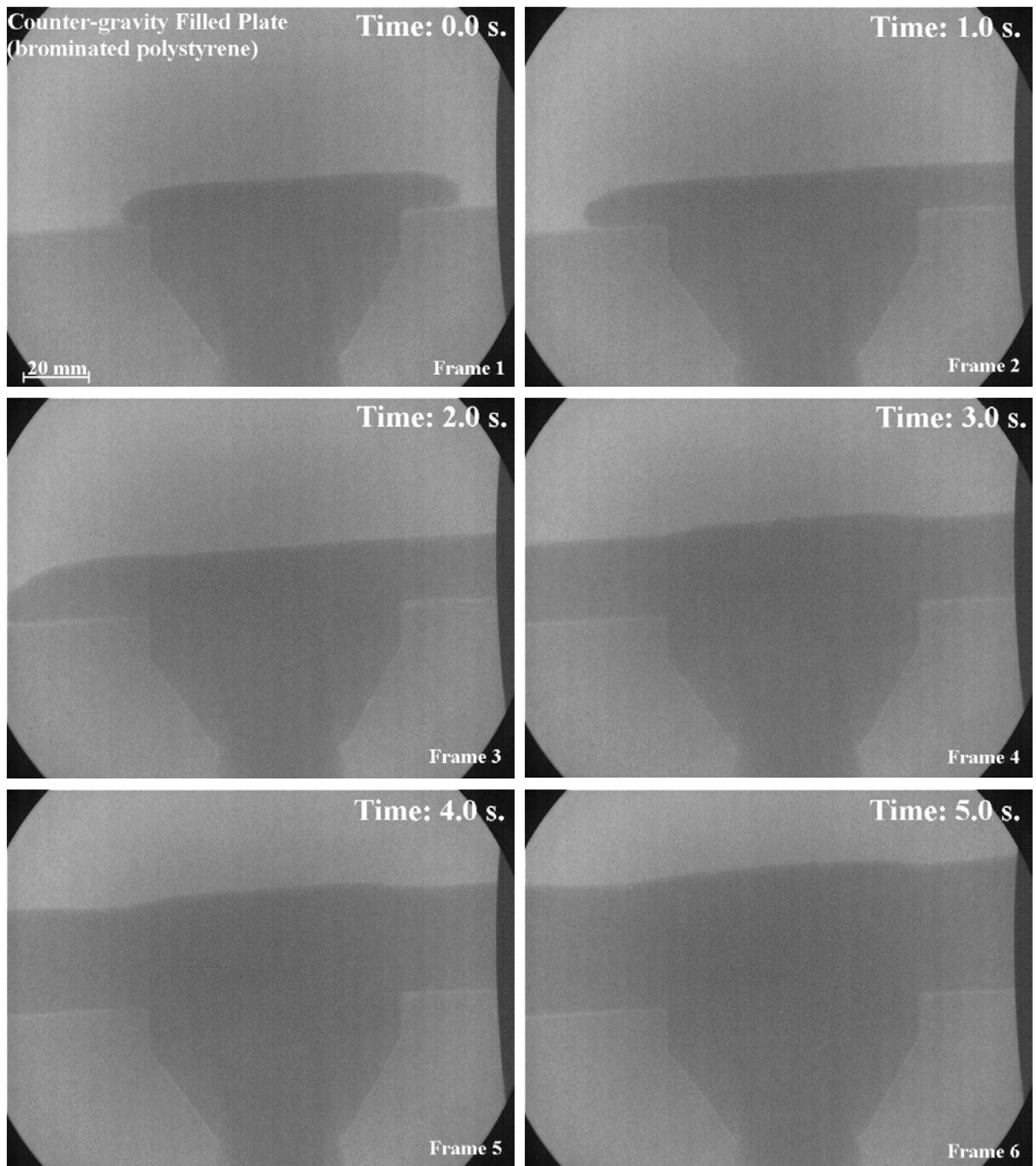


Figure 4.82: Sequence of real-time X-ray frames taken from the ingate region of the mould and depicting the behaviour of the interface between molten aluminium and a plate pattern made of brominated polystyrene. (Approximate metal velocity =  $5 \text{ mm.s}^{-1}$ ).

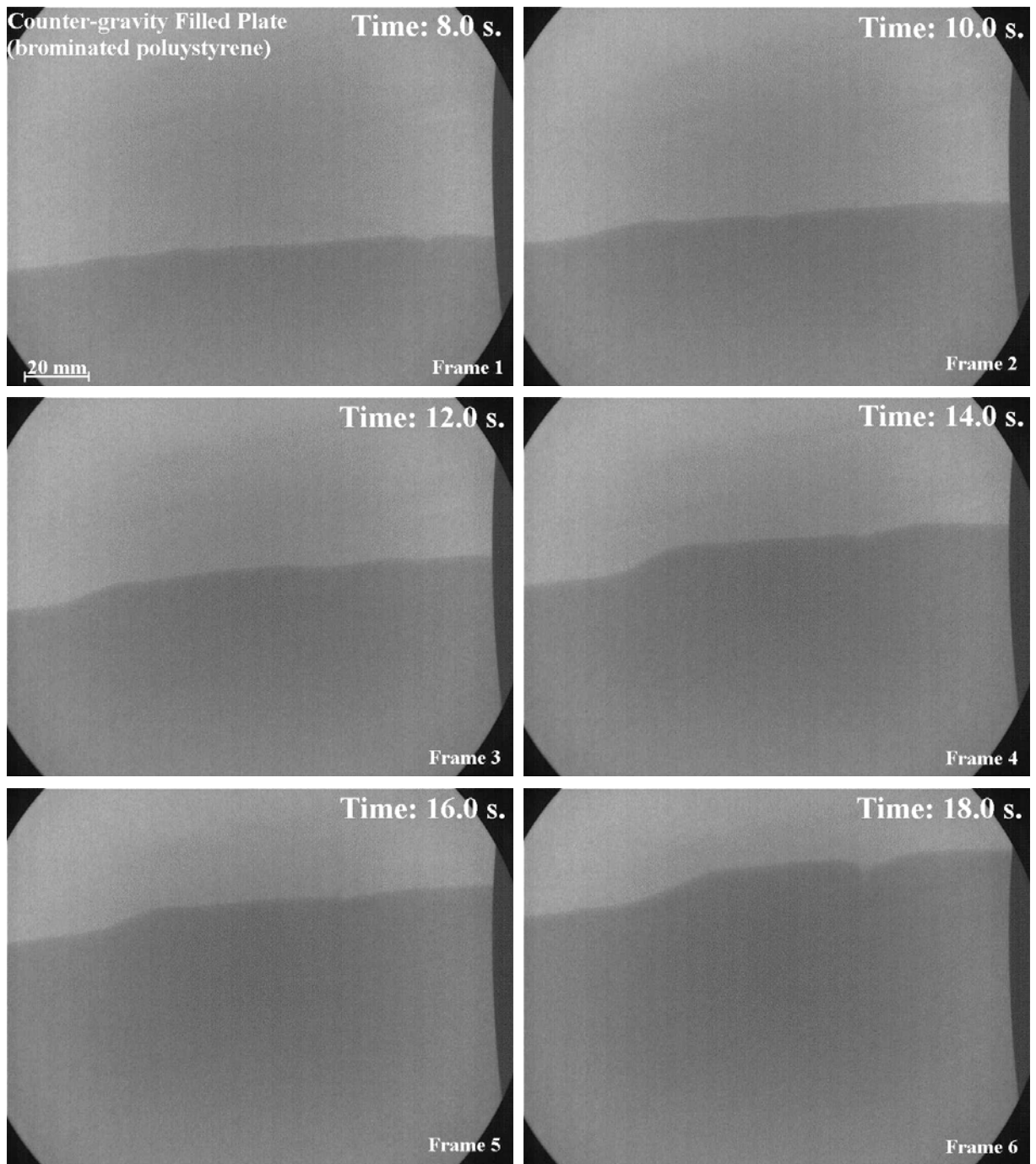


Figure 4.83: Sequence of real-time X-ray frames taken from the central region of the mould and depicting the behaviour of the interface between molten aluminium and a plate pattern made of brominated polystyrene. (Approximate metal velocity =  $5 \text{ mm.s}^{-1}$ ).

### 4.8.2 Tensile Strength Variation in the Castings

Twenty-three tensile test bars were extracted from each of the two plates that had been cast at a filling velocity of  $5 \text{ mm.s}^{-1}$ . The location, label and final machined dimensions of each of these bars are shown in Figure 3.10 and the UTS values obtained from them listed in Table 4.84.

Ultimate Tensile Strength Results of Plate Samples (MPa)		
Location	Conventional Polystyrene $v = 5 \text{ mm/s}$	Brominated Polystyrene $v = 5 \text{ mm/s}$
A	171	211
B	204	221
C	196	212
D	199	217
E	180	227
F	174	214
G	185	214
H	182	222
I	187	224
J	181	217
K	187	223
L	167	210
M	213	230
N	199	227
O	196	227
P	209	229
Q	214	233
R	210	237
S	230	231
T	227	239
U	232	233
V	237	239
W	227	240

Table 4.84: Ultimate tensile strength results of samples taken from a counter-gravity cast pattern plate made of conventional polystyrene and one made of brominated polystyrene.

The results of a “goodness of fit” analysis are shown in Table 4.85 and indicate that, on average, the Weibull distribution was marginally more accurate than the normal distribution in describing both sets of results whereas the Type 1 extreme distribution was, overall, the least accurate.

Weibull plots of both sets of UTS data are illustrated graphically in Figure 4.86 and it can be seen that the Weibull modulus of the plate casting made from a brominated pattern was 25.6, while that of the unbrominated plate was only 10.3.

Cluster design	Analysis	Regression coefficient	Best-fit parameters
Plate made from untreated polystyrene pattern (v = 5 mm/s)	Normal	0.9398	$\mu = 0.8452, \sigma = 0.0881$
	Weibull	0.9393	$\sigma = 0.8760, \lambda = 10.3172$
	Type 1 extreme	0.9406	$\mu = 0.8848, \sigma = 0.0687$
Plate made from Br-untreated polystyrene pattern (v = 5 mm/s)	Normal	0.9441	$\mu = 0.9379, \sigma = 0.0394$
	Weibull	0.9476	$\sigma = 0.9531, \lambda = 25.5988$
	Type 1 extreme	0.9127	$\mu = 0.9556, \sigma = 0.0307$

Table 4.85: ‘Goodness of fit’ of normal, Weibull and type 1 maximum extreme value distributions to the UTS data from plates made from untreated and Br-treated polystyrene patterns. (Approximate metal velocity = 5 mm.s<sup>-1</sup> in both cases).

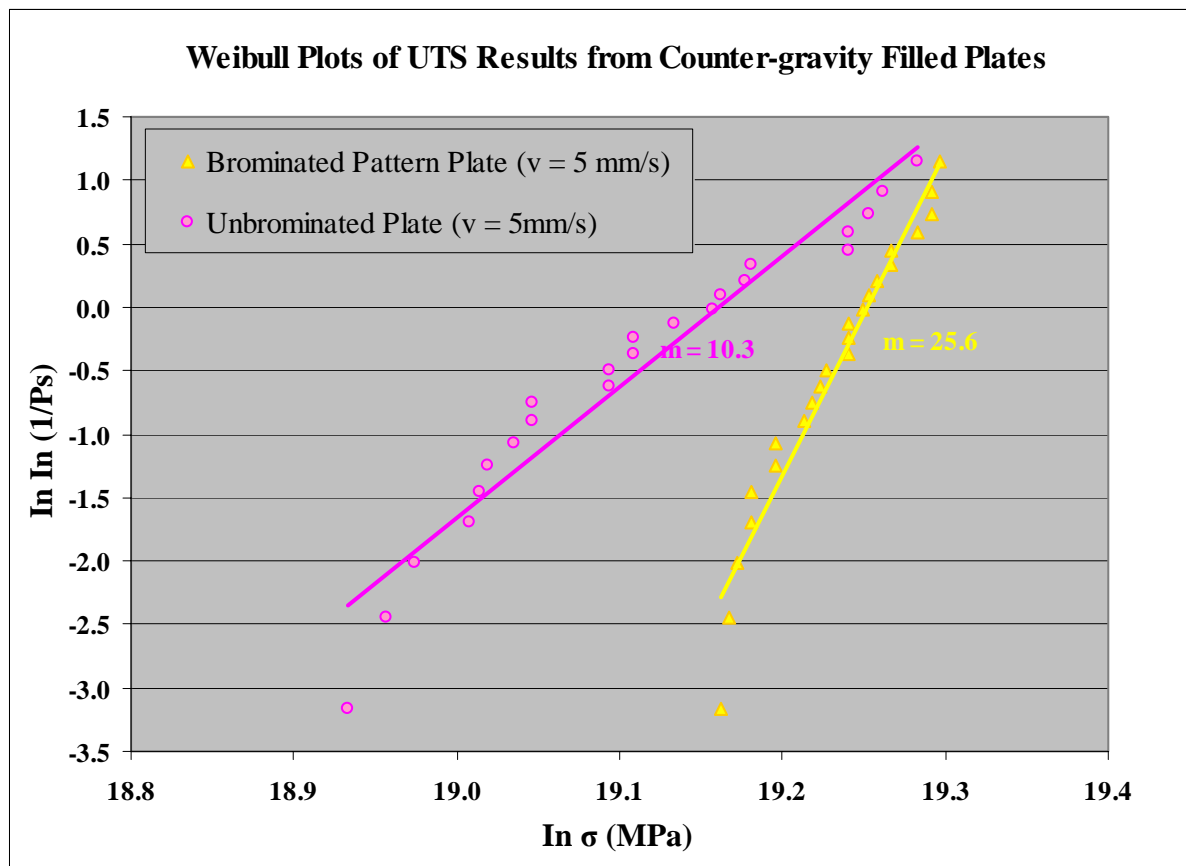


Figure 4.86: Weibull plots of UTS results taken from two counter-gravity cast plates (one from an untreated polystyrene pattern and the other from a Br-treated polystyrene pattern) where the metal velocity in each case had been measured at 5 mm.s<sup>-1</sup>.

Interestingly, the plots are very similar to those shown in Figure 4.49 and Figure 4.51 where 15 mm thick, untreated polystyrene plates were cast at various filling speeds. In these earlier experiments, front speeds of 4 – 5 mm.s<sup>-1</sup> gave rise to planar fronts during mould filling and produced castings with Weibull moduli of 22.4 and 23.2. When similar plates were cast at slightly higher speeds, i.e. 6 – 8 mm.s<sup>-1</sup>, instabilities were observed at the interfaces between the patterns and the metal fronts and the corresponding Weibull moduli were only around 10.

In this series of experiments, the casting with the highest UTS Weibull modulus was made by filling a brominated pattern plate in a planar fashion. However, this slight improvement in modulus compared with those of the other two counter-gravity plates where the metal – foam interface had been stable during mould filling (i.e. 25.6 against 22.4 and 23.2 – see previous paragraph) was likely to have been influenced heavily by a decrease in the plate thickness from 15 mm to 10 mm where a greater surface area to volume ratio reduced the length of the path along which degradation products needed to travel in order to escape into the moulding sand.

## **4.9 SUMMARY**

When Lost Foam moulds were cast in a gravity fashion, filling velocities of around 12 mm.s<sup>-1</sup> were observed. These were not only much smaller than would have been expected if the mould cavity had been open but were also unaffected by the location of the ingate. During the casting of plates, a number of fingers were observed on all metal fronts irrespective of ingate location. However, these were more pronounced where the casting had been gated from the top. Frames filled at an even slower rate than the plates and none of them filled fully. This resulted in the presence of misrun defects on each casting which was most severe where top-gating had been used. Glue joints between the runner bar and pattern were seen to degrade more slowly than the surrounding polystyrene and this caused a temporary reduction in the speed of the metal front. None of these joints degraded evenly, probably because they were not uniform in thickness, and encouraged the metal to flow in a preferential direction as it entered into the pattern. Whilst no significant difference was found between the UTS data sets obtained from three top-gated and three bottom-gated plates, there were significant differences between each of the data sets related to frame castings. This is thought to have been due to the

uncontrolled variation of one or more parameters such as coating thickness or glue joint uniformity. The design of the frame pattern made it much more susceptible to variations because once the metal had been directed preferentially in one direction along a leg of the frame it had limited freedom to change the way it travelled through the mould. Although the distribution of the individual values in each UTS data set was most accurately described by means of the Weibull distribution, the associated modulus for each data set was very low. The best result was 9.2 and was obtained in respect of the three plates that had been bottom-gated. The worst, corresponding to a value of 2.5, was related to the bottom-gated frames. Although pores were found on all fracture surfaces, aluminium oxide, film-type defects were only found on fracture surfaces of test bars that had been taken from frame castings. The oxide films were generally much larger than the pores and would have been responsible not only for the very low UTS values but also for the extremely low Weibull moduli that were associated with the frames.

Casting in a counter-gravity fashion provided more control over the rate that the mould was filled. At metal velocities approaching those observed during gravity casting, the metal front was seen to take on a similar profile where fingers of around 20 mm in both length and spacing were present. As the filling speed was reduced so did the length and distance between the fingers. For example, at a metal velocity of  $8 \text{ mm.s}^{-1}$ , the finger length was around 5 mm and the distance between two adjacent tips was also about 5 mm. These small, closely packed fingers were referred to as perturbations and were associated with a slightly convex curvature of the front across the field of view. When the velocity of the metal front was reduced to  $5 \text{ mm.s}^{-1}$  the perturbations disappeared and the front took on a smooth, planar profile which was horizontally oriented. The associated Weibull modulus was 23.2 and this was significantly greater than the nearest value of 10.7 where the filling velocity had been  $8 \text{ mm.s}^{-1}$  and irregularities had been seen on the metal front. In a second experiment, the Weibull modulus of a plate cast at  $4 \text{ mm.s}^{-1}$ , where the metal front had been planar, was 22.4 whereas plates cast at  $6 \text{ mm.s}^{-1}$  and  $7 \text{ mm.s}^{-1}$ , in which irregular metal fronts were observed, had Weibull moduli of only 10.1 and 5.1 respectively. This strongly suggested that the filling velocity had a large effect on the metal front profile which, in turn, influenced the Weibull modulus that was achieved. Although low filling speeds resulted in the highest reliabilities,

they were also associated with misrun defects which reduced the length of the castings by up to 20%.

The defects found on the fracture surfaces of the tensile specimens taken from a counter-gravity cast plate, where the filling speed had been  $8 \text{ mm.s}^{-1}$  and the metal front had been non-planar, were much more severe than when the metal velocity had been lower and the front had been smooth. Not only was the defect area fraction greater but individual defects were larger and many of them were almost spherical, resembling gas pores. Although a large increase in the hydrogen level was detected in the lower and central regions of the plate compared to the original melt, the values obtained were much higher than aluminium could retain in the liquid state. EDX analysis revealed that carbon was present on the surface of every defect that was analysed and hence it was concluded that they were caused by entrapment of polystyrene pattern material rather than by hydrogen gas pick-up. Hydrogen levels in the plate that had been filled with a planar metal front were essentially the same as the levels detected in the melt before it was cast and, as some carbon was found in each of the defects that were analysed, it is reasonable to conclude that these were also formed as a result of polystyrene entrapment, albeit at a much reduced level. Both the shape of the metal front and the speed with which it travelled through the mould were considered to have been heavily influential in this improvement.

The room temperature analogue, which accelerated a Hg-glucose interface vertically upwards, was constructed to understand the mechanisms that might have controlled the shape of the metal-foam interface and the entrapment of polystyrene degradation products when high density, low viscosity aluminium was pushed upwards into low density, high viscosity liquid polymer. As the velocity of the interface was increased it became unstable and Hg fingers protruded into the overlying glucose syrup. When the viscosity of the glucose syrup was reduced, the velocity required to bring about an unstable interface increased, thereby confirming that the instability observed was of the Saffman Taylor type.

In order to determine whether the perturbations and fingers that had been seen at the metal-foam interface during the casting of Lost Foam were the result of a Saffman Taylor instability, the viscosity of the liquid polystyrene that was reported to be present immediately ahead of

the advancing front was approximated from its molecular weight. It was found that the amount of heat used to transform the polystyrene from a solid to a liquid was much more influential in reducing the viscosity than the peak temperature. Treating the polystyrene with a bromine compound also had a viscosity reducing effect but this was only small in comparison to the influence of the other two parameters.

When an untreated polystyrene plate and a Br-treated plate were cast at a filling speed of  $5 \text{ mm.s}^{-1}$  immediately after one another, an interfacial instability was only observed in the mould containing the untreated plate. Analysis of the UTS data from each plate showed that the Weibull modulus of the plate where an untreated pattern had been used was only 10.3 whereas that of the Br-treated plate was 25.6.

## 5 DISCUSSION

One of the unique features of the Lost Foam casting process is that the pattern remains in the mould at the start of the filling sequence. This allows great flexibility in casting design. Despite this, Lost Foam castings are plagued by a number of defects resulting from the entrapment of pattern degradation products and premature freezing of the metal front. Whilst published literature stresses the importance of controlled mould filling in preventing these defects, the mechanisms used to regulate it have, up to now, almost always been passive. The two most widely used mechanisms have been coating permeability and pattern density.

The effectiveness of these passive systems is somewhat limited because they cannot react to the dynamics of mould filling. For example, where a mould contains a pattern that is oriented in the vertical plane and is bottom-gated and cast by means of gravity, the metallostatic head reduces throughout the filling sequence. This means that, in the initial stages of filling, the pattern is in direct contact with the liquid metal and decomposes by means of ablation [17]. However, as filling progresses and the head pressure decreases, the speed of the metal front also decreases. This suggests that a gap may form between the foam and the metal and the mechanism by which the foam degrades may change to one of melting. The formation of a gap also exposes a larger area of the coating through which degradation products can pass and this reduces any back pressure that restricts the forward movement of the front. On the face of it these two conditions counter each other but the gap cannot grow indefinitely because the advancing liquid metal temperature also has an effect. If this temperature is high, the gap will also be large but as the front slows down due to loss in metallostatic head and loses some of its initial heat energy in decomposing the foam in front of it, the temperature falls and the gap diminishes once again. Thus coating permeability or pattern density can only be truly effective in controlling the front speed at any one point during the casting of the mould.

In the current work a form of controlled, counter-gravity filling was compared with conventional gravity casting to determine if there was any benefit in adopting this technique. Assessment was carried out in terms of tensile strength variation in the resultant castings, as well as from observations concerning metal front velocity, metal front morphology and fracture surface appearance. Vertically oriented plate patterns were used in most of the casting

experiments but limited use was also made of a frame-type pattern that forced the liquid metal to split into a number of fronts that later recombined. This provided data on the influence of converging metal streams with respect to casting quality. Finally, the interfacial interaction between metal and pattern was studied to determine how this influenced the quality of the castings produced, and the filling speed at which castings would show a marked reduction in strength. The mechanism that caused this decrease in reliability was also explored and was used to predict filling speed limitations for the manufacture of quality castings.

## **5.1 MECHANICAL PROPERTIES OF GRAVITY FILLED CASTINGS**

The tensile strength of the gravity filled plates was very low, and individual results ranged from 73 MPa to 155 MPa. Overall, castings that had been filled from the bottom produced the better results in terms of average value, range and Weibull modulus. However, comparison of this set of results with that obtained from top-gated castings suggested that the difference was not statistically significant. There was only a small difference of  $< 1 \text{ mm.s}^{-1}$  in the filling speed when the ingate was located at the top of the plate rather than the bottom. As expected, the speed of filling was slightly slower when the plate was cast from the bottom because the front was travelling against the gravity vector and continued to lose metallostatic head pressure throughout the filling sequence. However, when a top gate was used the liquid metal flowed counter to the flow of degradation products as they escaped out of the mould. This interaction had the effect of reducing the influence of the growing metallostatic head that was trying to drive the metal forward as mould filling proceeded.

The similarity in the overall rate that bottom- and top-gated plates filled can be seen by comparison of Figure 4.10 and Figure 4.13. In Figure 4.10, where the metal entered a plate through an ingate that was located directly above it, the front profile developed into a number of small perturbations that had a wavelength of 12 mm and a height of 4 mm. This can be seen clearly in Frame 3 where the metallostatic head was around 300 mm. A comparable front profile was observed in the latter stages of the filling of a bottom-gated plate as shown in Frame 4 of Figure 4.13. Here the head differential was also about 300 mm and the perturbations were similar in terms of height and wavelength. Hence, the location of the ingate in gravity casting of Lost Foam moulds has little influence on the filling rate of the mould and,

at any given metallostatic head, has no influence on the profile of the metal front. However, the results indicated that the metallostatic head influenced the shape of the metal front and that ingate location determined the position in the mould where a certain front profile would occur. In other words, the change in the shape of the metal front as it progressed through the plate from top to bottom, as in the case of a top-gated plate, was essentially the opposite of that observed when the gate was placed at the bottom.

The presence of an irregular metal front profile throughout the filling of the plates encouraged the entrapment of some of the degradation products between the perturbations or, at higher filling speeds, between the distinct fingers that were observed along the liquid metal front. Any of this material that was subsequently unable to escape to the mould wall became entrapped in the solidified metal. Even if it travelled as a bubble of gas or globule of liquid polystyrene through to the mould wall, any oxygen present in the bubble would have reacted with the liquid metal to leave behind a thin oxide film known as a bubble trail [87] and this would have been associated with carbon residues deposited as a result of polystyrene degradation. The fracture surfaces of tensile test specimens taken from the plates revealed randomly dispersed pore-type defects which contained carbon deposits. This indicated that they were formed as a result of pattern degradation products being trapped within the final structure of the casting, reducing its inherent strength by acting either as a stress raiser or as a non-wetting discontinuity in the matrix.

Frame castings exhibited a much wider range of tensile strength values than the equivalent plate castings and their Weibull moduli were also much lower. A value of only 2.5 was recorded in respect of the bottom-gated frames and where top gating had been used this value was only 2.7. Although the range of results was much greater, 14 out of the total population of 45 results (i.e. 31%) exceeded 155 MPa, the highest value obtained from a specimen taken from a plate casting. This may be because the frame patterns had a lower casting modulus than the plates and therefore solidified more rapidly.

The frame castings not only produced some of the highest tensile strength values, but also yielded the lowest. The lowest value recorded in a plate casting was 73 MPa but this was higher than 9 results obtained from frame specimens, the lowest having a value of 47 MPa. A

statistical analysis of the results indicated that there was a significant difference between the tensile results of one casting to another, even though they had been made in the same way, from the same batch of metal and with the same running system design. This is likely to have been caused by the different ways that individual castings filled, and specifically the horizontal bars of each. For example, Figure 4.22 shows two distinct metal fronts, produced as a consequence of the pattern configuration, recombining in the central region of one of the horizontal bars. However, in the next illustration (Figure 4.23), only one of the fronts was observed filling the horizontal and vertical bars. Additionally, in Frame 2 of the same figure, a small lighter region can be made out at the intersection between a vertical and a horizontal bar. This was created by entrapment of some degrading polystyrene and its location in Frame 2 was at the point that the liquid metal front split into two distinct streams. One of the streams began to travel down the horizontal bar and the other continued to flow upwards along the vertical bar. Therefore, the entrapped material could have proceeded in either direction but, as Frames 3 and 4 of Figure 4.23 show, it actually continued to move with the metal in the vertical leg of the pattern until it reached the coating interface where it was seen to disappear, presumably through the coating and into the sand. Tensile testing was only carried out on specimens machined from horizontal bars and therefore the consequences of entrapping material in the vertical legs of the casting were not recorded. However, if the entrapped material had favoured the other metal stream and entered a horizontal bar, the effect on the tensile strength results could have been significant. Therefore, diverging and recombining metal streams encouraged greater variability in the location that defects were found in the solidified castings.

The frame pattern was intentionally used in order to encourage the liquid metal to split into two distinct streams as it emerged through the ingate into the adjacent, horizontal bar and then recombine as it filled subsequent bars from both ends. Any oxide films or pattern degradation products that were immediately ahead of the two opposing fronts would be entrapped at the point along the bar where these fronts met. Obviously, no metal fronts recombined in the bar attached to the ingate and tensile strengths recorded here were relatively high, although not the highest. This was because all the liquid metal that flowed into the pattern did so through a single ingate and would have caused this region of the frame to become hotter than the rest.

Subsequently, it would have cooled more slowly than other parts of the casting and, therefore would have been associated with a coarser structure.

The only other bar in the frame that produced consistently high results was the fully formed bar furthest away from the ingate. Datalogger results as shown in Figure 4.16 and the real-time X-ray images in Figure 4.23 clearly showed that filling was not uniform in the vertical plane and that one front sometimes travelled half way along a horizontal bar before the other front even entered it from the other end. This meant that the two fronts met much nearer to one end of the bar, possibly in the head portion of the test bar rather than within the gauge length. Additionally, the profile of the opposing metal fronts travelling down the bar furthest from the ingate was different to that seen in the other bars. Here it was much more elongated and tended to spread out across the lower region of the bar rather than filling the complete cross section. Although this gave rise to a larger surface area that could be oxidised, it allowed the degradation products to escape through the coating above it and would tend to push and deposit the liquid metal oxide film against the coating. Without oxides or degradation products entrapped across the cross section of the bar the strength would not have been severely reduced.

The bars situated between these two extremes exhibited the greatest variability in strength which was related to how uniformly each bar filled from both ends and the shape of each of the two metal fronts as they travelled towards each other.

Irrespective of pattern type or ingate location, the Weibull moduli were extremely low in comparison with values reported for castings made by open cavity methods. For example, Green and Campbell [89] cast a number of test bars in Al-7Si-0.4Mg aluminium alloy using the open cavity method and reported a Weibull modulus of 10.8 when the ingate was at the top of the casting and 19.7 when it was located at the bottom. The highest value of 50.3 was obtained when the researchers modified and filtered the alloy before it entered the mould cavity through bottom ingates. Frame casting results even compared poorly with those obtained from ceramic materials where a Weibull modulus of 5 has been commonly regarded as describing the least reliable of this class of materials [158].

Microscopic study of some of the fracture surfaces revealed that all of them contained interdendritic porosity as shown in Figure 4.37. The size and morphology of this defect was responsible for reducing the strength of the material in relation to the area of the fracture surface that it occupied and this accounts for the lower strength values found in the frame samples. Large oxide film defects, such as the one shown in Figure 4.38, were found on some of the fracture surfaces that originated in frame castings and these were thought to have been responsible for the lowest values recorded.

## **5.2 MECHANICAL PROPERTIES OF COUNTER-GRAVITY FILLED CASTINGS**

In the counter-gravity casting experiments two sizes of plate were cast in a pre-modified Al-7wt.%Si0.3%Mg alloy. Tensile testing was carried out on machined samples that had been cut from one of seven separately made castings in the as-cast condition. In contrast to the gravity cast plates, only one specimen failed at a UTS value below 100 MPa and over 60% of the total 152 specimens reached a strength of over 200 MPa prior to failure.

Plates filled at a low velocity (i.e., 4 mm.s<sup>-1</sup> to 5 mm.s<sup>-1</sup>), where a planar front had been observed during casting, produced the highest tensile strength values with a location parameter (i.e. the strength below which no specimens failed) value of 190 MPa. However, where the velocity had been 8 mm.s<sup>-1</sup> and the metal front had been associated with a number of perturbations, this value fell to 94 MPa. These perturbations on the metal fronts were very similar, in terms of length and spacing, to those observed in the upper region of a bottom-gated, gravity cast plate and this can be seen by comparison of the frames in Figure 4.13 with those from Figure 4.43. The filling velocity in each case was similar and was measured to be approximately 6.5 mm.s<sup>-1</sup>. This suggests that the velocity at which the metal proceeded through the mould has a direct influence on its front profile which, in the non-planar condition, resulted in a significant reduction in tensile strength.

Interestingly, a low filling velocity on its own was not sufficient to ensure high average tensile strength results. When casting a 10 mm thick plate at a filling velocity of 5 mm.s<sup>-1</sup> the orientation of the front was almost diagonal across the plate. This encouraged a wave to propagate along the front as it ran from the bottom to the top (see Figure 4.81 and the

associated video contained on a CD in Appendix I of this thesis). This disturbance was thought to have been responsible for the reduction in tensile strength values when compared to the other castings that were filled at  $5 \text{ mm.s}^{-1}$ . Also, apart from the plates that exhibited a planar metal front during filling, the only other one that had an average tensile strength of over 200 MPa was cast at a velocity of  $6 \text{ mm.s}^{-1}$ . This plate was associated with a front that had a few minor perturbations along its length which had a life cycle of only about 2 s. It is thought that the filling of this plate was carried out a velocity at which the metal – foam interface was at its limit of stability and was beginning to show signs of disruption.

Pores were found on the fracture surfaces of all tensile test pieces examined. Where the plate had been cast at a velocity of  $8 \text{ mm.s}^{-1}$  they were more spherical in shape, generally larger in size (up to  $2500 \mu\text{m}$  in diameter) and occupied approximately 10% of the total fracture area. This was in contrast to the smaller, more irregular pores that occupied about 5% of the fracture surface and were found in plates where a planar front had been present during casting. Irrespective of the speed of fill and the morphology of the defects on the fracture surfaces, carbon deposits were found in every pore that was subject to EDX analysis. However, sound regions of the same fracture surfaces contained much lower levels of carbon and on one specimen no carbon was found at all. This indicates that these defects were formed as a result of foam entrapment rather than by hydrogen diffusion into the liquid aluminium from the pattern decomposition layer.

Fracture surfaces containing the largest area of defects originated from the plate that had been filled at  $8 \text{ mm.s}^{-1}$  and in which the metal front had been unstable. This suggests that an irregular metal front, promoted by a higher filling speed, entraps more degrading foam material and results in a higher fraction of defects in the solidified casting. The difference in the hydrogen content in each of the two castings and their associated melts supports this statement. Whereas the hydrogen found in the plate that had been filled at  $5 \text{ mm.s}^{-1}$ , under planar front conditions, was slightly lower than in the original melt, the opposite was found in the plate cast at  $8 \text{ mm.s}^{-1}$ . Because each pore defect contained carbon and therefore was formed as a result of foam entrapment, any increase in hydrogen above that in the original melt would have also originated from the same source. An increase in foam entrapment and therefore severity of defects within the casting caused by an increase in filling velocity concurs with work carried

out by Caulk [20] who proposed that foam engulfment takes place when the metal front is concave and is encouraged by increasing filling velocity.

### **5.3 INTERFACIAL INSTABILITY DURING MOULD FILLING**

#### **5.3.1 The Nature of the Liquid Metal – Pattern Interface**

During the counter-gravity mould filling experiments, metal front velocities ranging from between  $2 \text{ mm.s}^{-1}$  to  $22 \text{ mm.s}^{-1}$  were observed. At velocities below  $5 \text{ mm.s}^{-1}$  the liquid metal front appeared smooth and planar although castings produced at these filling speeds failed to fill completely on their uppermost surfaces. At  $5 \text{ mm.s}^{-1}$  the metal fronts retained their generally smooth, planar profiles but filled the moulds completely. The only exception to this was observed during the counter-gravity casting of a 10 mm thick, conventional polystyrene plate. In this case a large region of the front was oriented almost in the vertical plane, as shown in Frame 1 of Figure 4.81, and a wave-like disturbance was seen running up it, (see relevant video on CD contained in the appendices to this thesis).

At high filling velocities,  $> 8 \text{ mm.s}^{-1}$ , the liquid metal front began to show signs of perturbation on its hitherto smooth profile. At around  $8 \text{ mm.s}^{-1}$ , small perturbations were observed along the length of the interface between the metal and the degrading pattern. These disturbances had a wavelength of approximately 5 mm and a length that varied from between 4 mm to 7 mm. At speeds higher than  $10 \text{ mm.s}^{-1}$  the fronts were seen to split into a number of distinct fingers that became more elongated as the velocity increased. This is illustrated by comparison of Figure 4.11 and Figure 4.41 respectively. In the first of these figures the front velocity was about  $12 \text{ mm.s}^{-1}$  and the fingers that were present had a length of around 20 mm. In Frames 1 to 3 of Figure 4.41 the fingers were about 30 mm in length and these were associated with a liquid metal front that was travelling at approximately  $16 \text{ mm.s}^{-1}$ . These results indicated that an increase in the velocity of the metal front was associated with the onset and growth of disturbances normal to its profile, suggesting that an instability was present at the metal – pattern interface when the liquid metal front travelled at velocities in excess of  $5 \text{ mm.s}^{-1}$ .

A number of authors have reported that unsound regions in the pattern [21-23] or inter-bead porosity that extended to the pattern surface [17,19] encouraged the formation of fingers on the front of the advancing metal. Unsound regions in the pattern have been associated with low density but no such density variations were detected in any of the patterns used in the casting experiments. The lowest density of  $23.5 \text{ kg.m}^{-3}$  was measured in the central region of a 10 mm thick brominated plate and this was well within the range of  $20 \text{ kg.m}^{-3}$  to  $25 \text{ kg.m}^{-3}$  that published literature suggests is acceptable [16,19]. Inter-bead porosity, which has been shown to be the result of poor bead fusion [21], is associated with pattern permeability [19]. However, Davies [54] found that polystyrene plate patterns, similar to those used in these experiments, had zero permeability, even when the denser, well fused surface layer of the pattern had been removed. Also, expanded polystyrene beads in the plate and frame patterns had a diameter of about 1 mm and any poor fusion between them would have resulted initially in finger wavelengths of approximately the same pitch. However, the smallest finger wavelength observed during the casting experiments was 5 mm (see Figures 4.42 and 4.43). Therefore, the physical characteristics of the patterns were not responsible for the formation of fingers at the metal front during casting.

Davies [54] showed that polystyrene pattern material degrades into a viscous liquid at temperatures between  $300 \text{ }^\circ\text{C}$  to  $400 \text{ }^\circ\text{C}$ , and begins to boil at a temperature about  $40 \text{ }^\circ\text{C}$  higher. He also found that by increasing the heating rate of the foam sample from  $10 \text{ }^\circ\text{C.min}^{-1}$  to  $50 \text{ }^\circ\text{C.min}^{-1}$ , boiling was delayed by approximately  $60 \text{ }^\circ\text{C}$ . The interface between liquid aluminium and the foam pattern probably comprises a mixture of liquid polystyrene degradation products, gaseous degradation products and air that had been previously entrapped within the cellular structure during pattern manufacture. It is considered that the temperature range in which aluminium is cast is not sufficient to generate high levels of gaseous degradation products ahead of the metal front, although some might occur. It is more likely that the majority of polystyrene degradation products are in the liquid form [6,8,10,19].

Liquid aluminium at  $750 \text{ }^\circ\text{C}$  has a density of  $2350 \text{ kg.m}^{-3}$  and a viscosity of  $1.07 \text{ mPa.s}$  [102,155]. Liquid polystyrene, on the other hand, has a density of around  $1040 \text{ kg.m}^{-3}$  at  $200 \text{ }^\circ\text{C}$  and its viscosity can vary from  $39 \text{ Pa.s}$  to well over  $1000 \text{ Pa.s}$ , depending upon the rate of shear applied during the viscosity measurement [103, 120]. From this data, it is to be

expected that the liquid polystyrene-gas mixture created just ahead of an advancing metal front would be significantly less dense, but significantly more viscous than the liquid metal advancing to displace it.

### 5.3.2 Saffman-Taylor Instability and Lost Foam Casting

It is known that an interface between a dense, low viscosity liquid and a less dense, higher viscosity liquid lying above it can become unstable if accelerated perpendicularly. This is known as Saffman-Taylor instability [112]. The room temperature analogue, which was built to mimic the interface between liquid polystyrene and the underlying liquid aluminium, revealed that, (i) accelerating such an interface produces an instability (see Figure 4.65 to Figure 4.67), and (ii) as the viscosity of the upper fluid in the cell increased, the velocity at which the underlying metal front became unstable decreased. These effects are characteristic of the Saffman-Taylor instability and are described by Equation 2.20.

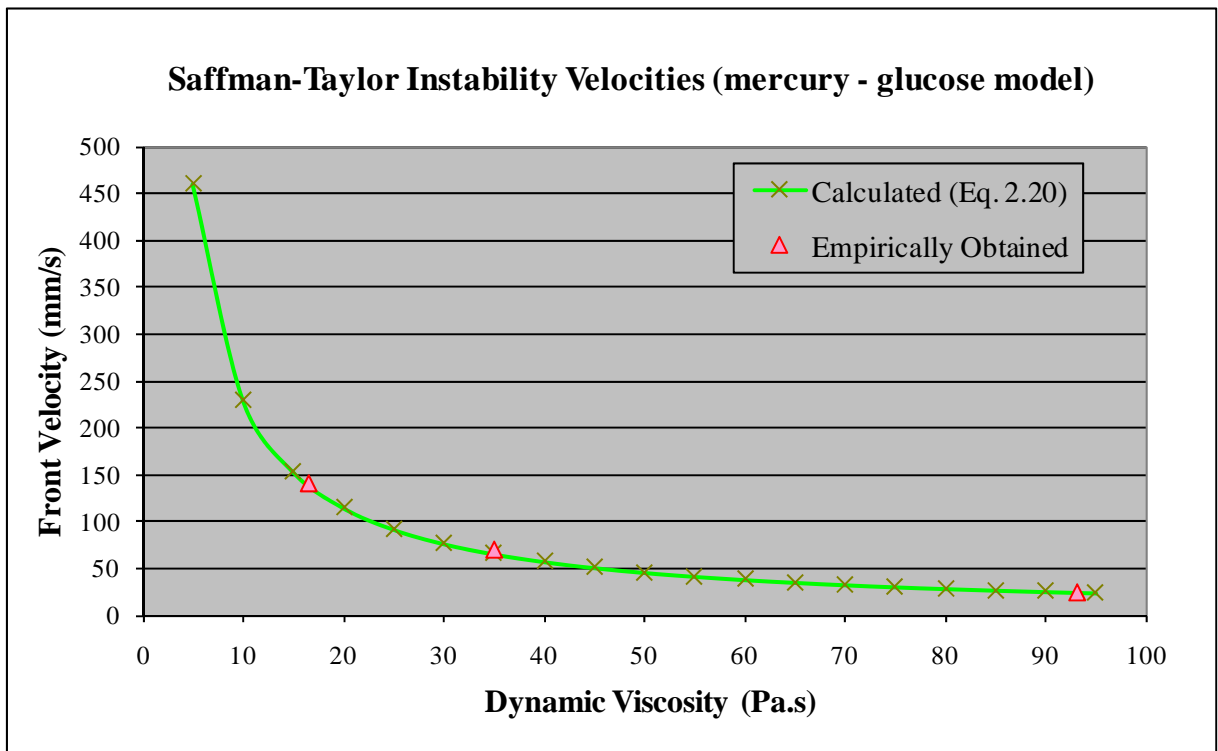


Figure 5.1: Relationship between modelled values observed at the onset of interfacial instability and values derived mathematically using the Saffman-Taylor equation.

The line in Figure 5.1 has been plotted using the Saffman-Taylor equation (Equation 2.20) to predict the velocity at which the Hg-glucose interface in the analogue becomes unstable as the viscosity of the glucose increases. The triangular shaped points on the graph represent the interfacial velocities that were observed during the analogue experiments at three different levels of glucose viscosity. The empirically derived results were a very good fit with the predicted values showing that the instabilities seen during the analogue experiments were Saffman-Taylor instabilities. Although glucose is a shear-thinning liquid, the good agreement shown in Figure 5.1 suggests that, at the velocities involved in this experiment (between  $25 \text{ mm.s}^{-1}$  and  $140 \text{ mm.s}^{-1}$ ), the effect of shear rate on viscosity was not significant. Furthermore, the morphology of the interfacial instability, as it grew from a single, central finger with a well rounded tip into a small number of stubby fingers with the original one predominating, supported Ladtkow's theory that large differences in viscosity between the two fluids result in a high pressure gradient which suppresses the number of fingers formed and reduces the aspect ratio values that they achieve [113].

Since the Saffman-Taylor equation has been shown to describe the onset of an instability in a low viscosity, high density liquid accelerated upwards into a high viscosity, low density liquid, between two parallel plates, it was considered possible that the advancing liquid aluminium being forced upwards into the degrading polystyrene pattern could be behaving in the same way, accounting for the perturbations in the metal front seen in the X-ray radiography. To demonstrate that this was the case, the Saffman-Taylor equation was again used to try to predict the velocity at which the instability began in the Lost Foam castings. However, to predict this critical velocity requires the use of accurate values for the density and viscosity of both liquid aluminium and liquid polystyrene at the temperatures occurring during filling, which for the liquid polystyrene/gas mixture in the pattern-metal interface is difficult. This was the only parameter for which representative data were not available from published literature, and therefore this was estimated empirically.

Samples of conventional and brominated polystyrene patterns were subjected to a variety of thermal degradation cycles that were intended to mimic the effect of different pouring temperatures in Lost Foam casting. The rapidly cooled residues were analysed using Gel Permeation Chromatography to obtain their molecular weight from which to infer their

viscosities using Equation 4.1 (see Section 4.74) which had been shown by Merz and Colwell [126] to be valid for a liquid polystyrene with a temperature of at least 450 °C. Of the three factors that had an effect in causing molecular weight reductions, the addition of a bromine compound to the polystyrene was the most influential. This was followed closely by the amount of heat that each sample had been subjected to, with the effect of the peak temperature only playing a small role.

The molecular weight of conventional polystyrene samples (labelled with the letter U) and brominated polystyrene samples (labelled with the letter B) fell into two distinct categories. The first consisted of samples U1, U3, U4, B3 and B4 which had been subject to a high  $\Delta T$  for a short time during thermal degradation. These samples all exhibited molecular weight values significantly higher than 100 000 g.mol<sup>-1</sup>. The other category, where much lower molecular weight values were determined, was made up of samples U2, B1 and B2, and these had been exposed to lower  $\Delta T$  values for a longer period of time. Table 5.2 shows the different molecular weights found in the foam heating experiments used to estimate viscosities of the associated liquid polymer at different temperatures in the metal-pattern interface. These ranged from 183 000 (U1) to 40 250 (B2). Temperatures of 300 °C, 400, 500, 600 and 700 °C have been selected so as to bracket the temperatures likely to be found in the interface. The estimated viscosity of the degradation products in the interface ranged from < 0.05 Pa.s up to 774 Pa.s and were used in conjunction with Equation 2.20 to predict the critical velocity for the onset of the Saffman-Taylor instability.

The results of the liquid polystyrene viscosity experiments showed that, in addition to chemistry, molecular structure and temperature, this property was influenced by the time during which thermal degradation took place. While casting a series of 10 mm thick, horizontally oriented polystyrene plates in aluminium, Davies [54] measured the temperature gradient ahead of the advancing metal front and found that, for a metal front velocity of about 15 mm.s<sup>-1</sup>, the time taken for the temperature to rise from ambient to that of the liquid metal was approximately 0.3 s whereas, at the slower front speed of 6 mm.s<sup>-1</sup>, it took around 1 s. He also studied the temperature and the rate at which polystyrene pattern samples decomposed into liquid and gaseous phases. When a heating rate of 10 °C.min<sup>-1</sup> was used, the samples liquified at about 300 °C. However, at 50 °C.min<sup>-1</sup> this transformation was only completed at

400 °C. Both heating rates were significantly lower than those observed during the polystyrene viscosity experiments and whilst filling Lost Foam moulds. Therefore, it is reasonable to assume that the liquid polystyrene in the heat-affected zone immediately ahead of the advancing metal front would have a higher temperature than that of the liquid polystyrene in Davies' experiment. Obviously, the temperature of the liquid polystyrene is heavily influenced by the temperature of the metal front but cannot be hotter than it. The front temperatures measured by Davies fell from about 700 °C to 600 °C as the aluminium travelled through the mould. Under these or similar circumstances it is realistic to assume that the liquid polystyrene temperature in the metal-foam interface in these experiments should be between 500 °C and 600 °C.

<b>Liquid Polystyrene Viscosity &amp; Critical Velocity of Metal Front at Various Temp.s</b>											
Sample Ref.	Mol. Wt. (gmol <sup>-1</sup> )	300 °C		400 °C		500 °C		600 °C		700 °C	
		$\eta_0$	V <sub>crit.</sub>								
U1	183000	774.3	0.000	92.9	0.001	27.6	0.004	12.6	0.008	7.3	0.015
U2	67200	25.7	0.004	3.1	0.035	0.9	0.117	0.4	0.256	0.2	0.443
U3	177500	698.0	0.000	83.7	0.001	24.9	0.004	11.4	0.009	6.6	0.016
U4	157500	464.9	0.000	55.8	0.002	16.6	0.006	7.6	0.014	4.4	0.024
B1	55070	13.1	0.008	1.6	0.068	0.5	0.230	0.2	0.503	0.1	0.871
B2	40250	4.5	0.024	0.5	0.199	0.2	0.667	0.1	1.461	0.0	2.530
B3	166000	555.9	0.000	66.7	0.002	19.8	0.005	9.1	0.012	5.2	0.020
B4	136500	285.8	0.000	34.3	0.003	10.2	0.010	4.7	0.023	2.7	0.040

Table 5.2: Velocities, determined by means of Equation 2.20, at which a liquid Al-liquid polystyrene interface becomes unstable as the temperature and viscosity of the polystyrene at the interface changes (assuming that the instability is Saffman-Taylor in nature. (U = unbrominated samples and B = brominated samples).

$$\begin{array}{llll}
 \text{where } g = & 9.81 \text{ m.s}^{-2} & \mu_{Al} = & 0.00107 \text{ Pa.s [159]} & \eta_0 = & \text{in Pa.s} \\
 \rho_{Al} = & 2350 \text{ kg.m}^{-3} \text{ [159]} & b = & 0.01 \text{ m} & V_{crit.} = & \text{in m.s}^{-1} \\
 \rho_{poly.} = & 1040 \text{ kg.m}^{-3} \text{ [136]} & & & & 
 \end{array}$$

Based upon the arguments that liquid polystyrene degradation products just ahead of the metal front (i) have only been subject to short heat exposure times, and would have molecular weights  $> 10^4$ , (see Table 5.2), and (ii) have a temperature of between 500 °C and 600 °C,

predictions were made of the interfacial velocity range in which an instability would arise if it was of the Saffman-Taylor type.

Figure 5.3 considers a 10 mm thick, unbrominated plate that is cast in aluminium and predicts the velocity at which a liquid aluminium – liquid polystyrene interface becomes unstable over a range of interfacial degradation product temperatures of between 300 °C and 700 °C. The lower limit of instability on the graph has been constructed using the critical velocity values for sample U1 in Table 5.2. This sample was chosen because it had the highest molecular weight of all the unbrominated samples and was considered to probably represent the highest liquid polystyrene viscosity that would be found in the mould during the casting experiments. Therefore, any velocity lower than the calculated critical values for this sample would always result in the presence of a stable interface.

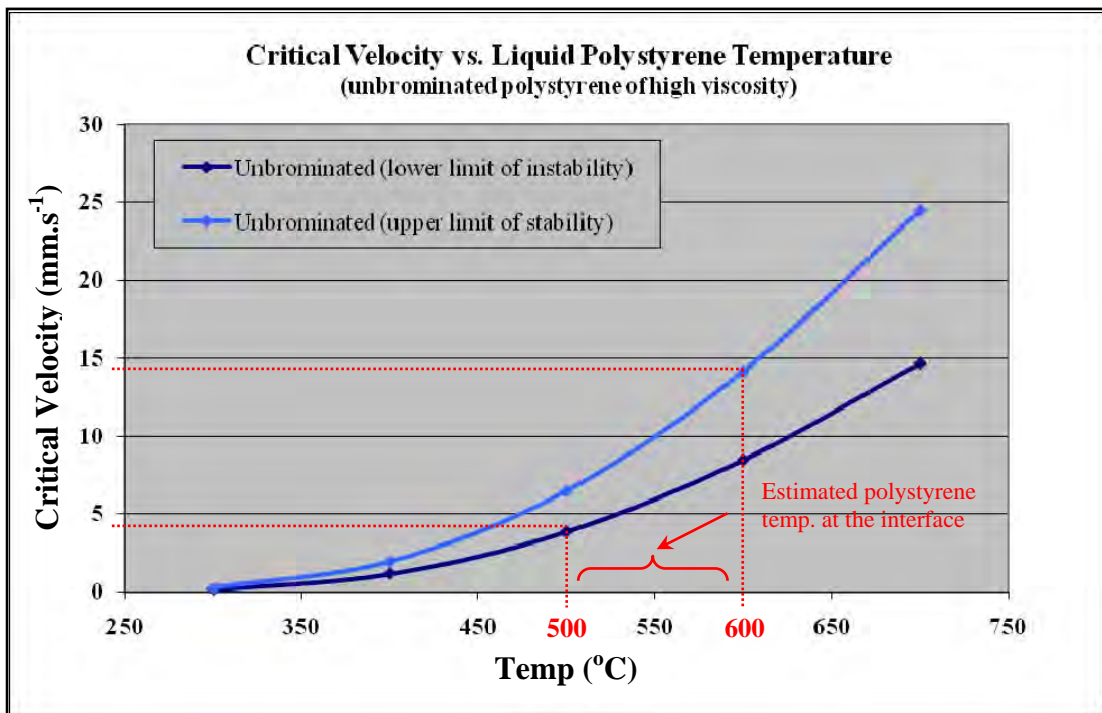


Figure 5.3: Prediction of the metal front velocity that would cause an instability to occur at the interface between the liquid aluminium and liquid products of degradation of a conventional polystyrene pattern.

The upper limit of stability was constructed using the calculated critical velocity values for sample U4 in Table 5.2, because this had the lowest molecular weight of the unbrominated samples that had been exposed to heat for only a short time during their transformation from

solid to liquid. This molecular weight was considered to be probably the lowest that would be encountered under similar filling conditions to those that had been observed during the casting experiments. Hence, for any interfacial velocity laying above this line an instability would be present at the metal – foam interface.

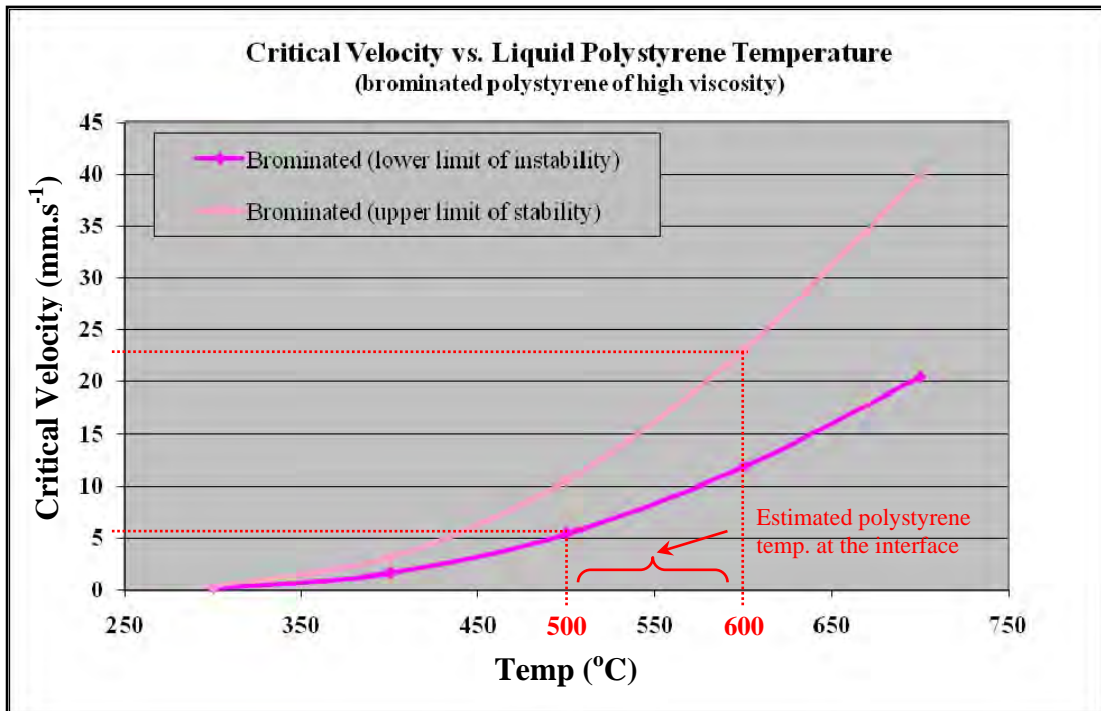


Figure 5.4: Prediction of the metal front velocity that would cause an instability to occur at the interface between the liquid aluminium and liquid products of degradation of a brominated polystyrene pattern.

Figure 5.3 therefore suggests that for a 10 mm thick, plate-type pattern made from untreated polystyrene (i) a stable front should always be present when its speed is  $4 \text{ mm.s}^{-1}$  or less, and (ii) an unstable front will always be present when its speed is greater than  $14 \text{ mm.s}^{-1}$ . A transitional condition will occur when the front is moving at a velocity between the two. The actual point of onset of the instability is heavily dependant upon the actual temperature of the liquid polystyrene and the degree of thermal degradation that has occurred within it.

Figure 5.4 contains similar predictions related to a brominated plate, based on the molecular weights of samples B3 and B4 (see Table 5.2). The limits of stability and instability have been shifted both upwards and apart, (relative to the unbrominated plate shown in Figure 5.3), so that a stable front is predicted to occur at velocities of below about  $6 \text{ mm.s}^{-1}$ , and an unstable

front from  $23 \text{ mm.s}^{-1}$  and above. The range of velocities in which such an instability would be transitional has now risen to a gap of  $18 \text{ mm.s}^{-1}$ , compared to  $11 \text{ mm.s}^{-1}$  in respect of an unbrominated plate. Observations made during the casting experiments supported the predictions made by the two figures. For example, whilst filling an unbrominated polystyrene plate at a velocity of  $5 \text{ mm.s}^{-1}$  disturbances were observed on the metal front (see Figures 4.80 and 4.81) whereas the front observed during the filling of a brominated plate at the same velocity was planar (see Figures 4.82 and 4.83).

Two graphs have been constructed from Table 5.2 in order to illustrate how the velocity of the metal – foam interface must change as the temperature of the liquid polystyrene degradation products increases in order to bring about the onset of a Saffman-Taylor instability, (Figures 5.5 and 5.6).

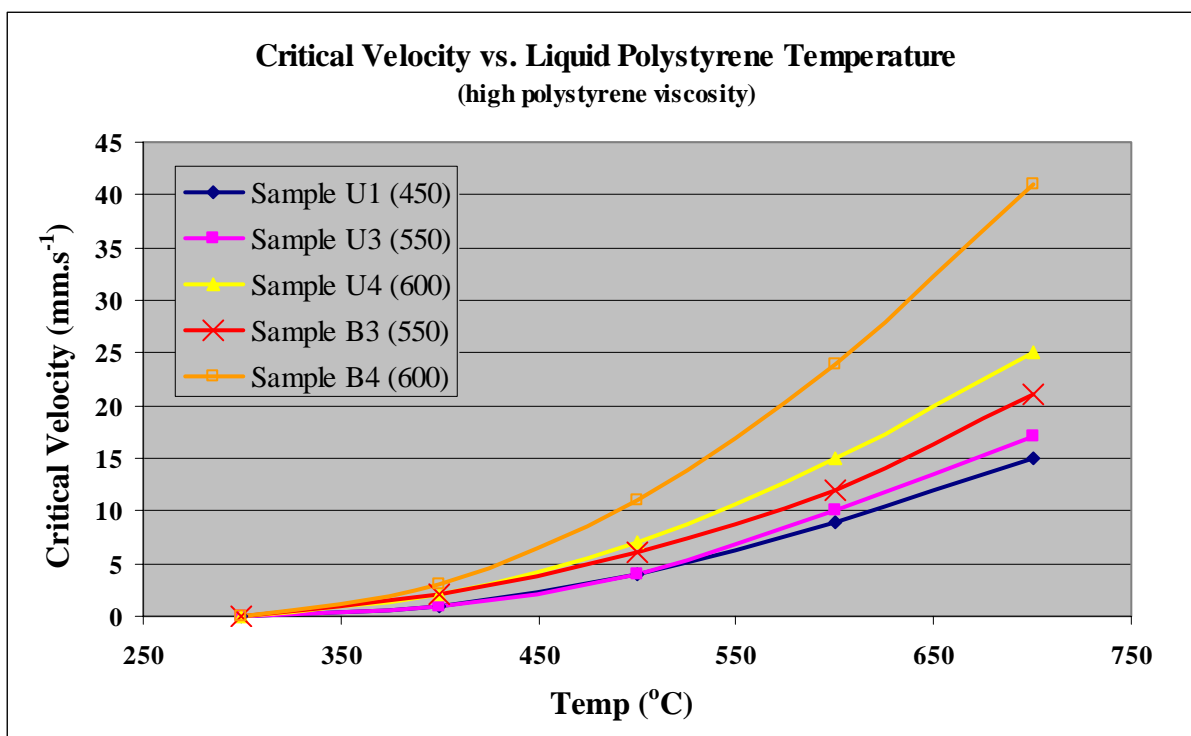


Figure 5.5: Critical velocity of interfacial instability,  $V_{crit.}$ , as a function of the temperature of liquid polystyrene samples with high molecular weights and viscosities.

Figure 5.5, which relates to the higher molecular weight, higher viscosity group of samples, shows that additions of a bromine compound have a positive effect in preventing an instability occurring during counter-gravity filling of a Lost Foam mould, and that this effect becomes

much greater as the temperature of the pattern degradation products increases. A similar trend can be seen in Figure 5.6 where the effects of critical velocity over a range of temperatures were also plotted for the lower molecular weight, lower viscosity group of samples. (The results shown in Figure 5.5 are much more representative of the conditions experienced during the casting of thin plates in the Lost Foam process than those in Figure 5.6).

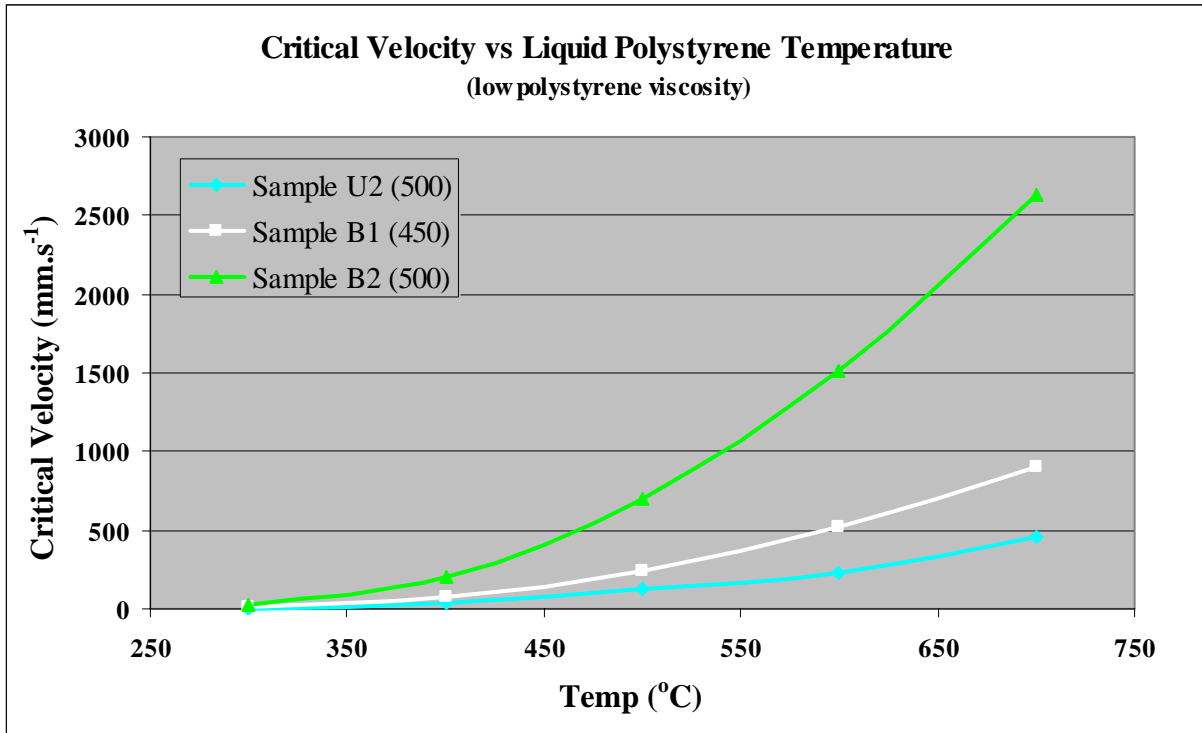


Figure 5.6: Critical velocity of interfacial instability,  $V_{crit.}$ , as a function of the temperature of liquid polystyrene samples with low molecular weights and viscosities.

The perturbations observed at the metal – foam interface during the filling of bottom-gated plate castings were probably due to Saffman-Taylor Instability because, not only did they occur when high density, low viscosity aluminium was being pushed upwards into low density, high viscosity polymer degradation products in a plate pattern, producing a metal front profile which was analogous to the profile found in a Hele-Shaw cell used in the original experiments carried out by Saffman and Taylor [112], but also the interfacial velocity at which they appeared, determined by real-time X-ray imaging, (about  $5 \text{ mm.s}^{-1}$  for an untreated plate and  $6 \text{ mm.s}^{-1}$  for a brominated plate) correlated well with the predictions made, using the Saffman-Taylor equation (Equation 2.20), (see Figures 5.3 and Figures 5.4). However, these predictions were based on liquid polymer viscosities between  $500 \text{ }^{\circ}\text{C}$  and  $600 \text{ }^{\circ}\text{C}$  in samples

that had only been exposed to heat for a short time. A change to any parameter that might influence either of these conditions, e.g., a reduction in the casting temperature, would require the critical velocity predictions to be recalculated.

The ratio of finger width to plate width, i.e., the  $\lambda$  value, observed during the mould filling experiments, was always significantly lower than the value of 0.5 that Saffman and Taylor reported during their experiments using a Hele-Shaw cell [112]. However, the researchers also found that at low interfacial velocities this correlation was not true and that the  $\lambda$  value increased up to 1.0 as the velocity reduced to zero. This general trend was observed in the real-time X-ray imaging during the counter-gravity casting experiments. At an interface velocity of about  $16 \text{ mm.s}^{-1}$  distinct fingers with a width of approximately 30 mm were observed (see Figure 4.41). When the filling velocity was reduced by half to  $8 \text{ mm.s}^{-1}$  the front took on a convex profile along which a series of closely packed perturbations or small, closely packed fingers were seen (as shown in Figure 4.42 and Figure 4.43). The convex metal front could be considered as the start of a single finger with a  $\lambda$  value of 1.0 which was brought about by a reduction in interface velocity from  $16 \text{ mm.s}^{-1}$  to  $8 \text{ mm.s}^{-1}$ .

An alternative explanation for the formation of the small perturbations at the metal – foam interface could be as follows. Molibog [16] and Davies [54] observed that the liquid in the degradation zone contained many gas bubbles which Davies suggested was primarily air that had been trapped within the polystyrene cells. This air would expand as the temperature increased and this would have produced small pockets of lower viscosity gas within the liquid degradation products at the interface. These sites would have been less restrictive to the flow of the advancing metal front and could have been responsible for the presence of the small perturbations on the liquid metal front. When the filling velocity was reduced even further, it is possible that a distinct gas layer formed immediately ahead of the metal front because the rate of decomposition of liquid polystyrene was greater than the rate of advancement of the metal. Because the viscosity of this gas layer was relatively uniform and the interfacial velocity was very slow it follows that the perturbations would subside. This was observed when the filling velocity was only  $5 \text{ mm.s}^{-1}$  as shown in Figure 4.44 and Figure 4.45.

Although the Saffman-Taylor Instability occurred during the mould filling experiments, a different instability was probably observed when part of the advancing metal front was inclined much more towards the vertical rather than the horizontal plane. Under these conditions, shown in Figure 4.75, Figure 4.76 and Figure 4.81, the wave-like instability seen travelling along the inclined region of the front was of the Kelvin-Helmholtz type (see Section 2.4.1.3) and caused by the rapid, upward flow of gaseous degradation products in the small interfacial zone between the liquid metal and solid polystyrene (see CD in Appendix I of this thesis). Interestingly, this phenomenon was only observed during the casting of conventional polystyrene plates that were 10 mm thick.

### 5.3.3 Mechanical Properties and the Metal – Pattern Interfacial Instability

The Weibull distribution plots and Weibull moduli that were obtained from the UTS values of specific castings were placed into 3 distinct categories as summarised in Table 5.7, in which the behaviour of the liquid metal front was also noted.

UTS Results Categorised by Weibull Modulus Value						
Cat.	Pattern		Gating	Front Speed	Front Profile	Weibull Modulus
	Design	Additive				
1	Frame	none	bottom-gated	13 mms <sup>-1</sup>	rounded with occasional small perturbation	2.5
	Frame	none	top-gated	8 mms <sup>-1</sup>	rounded with occasional small perturbation	2.7
2	Plate (15 mm)	none	top-gated	10-12 mms <sup>-1</sup>	irregular with large protruding fingers	6.2
	Plate (15 mm)	none	bottom-gated	10-12 mms <sup>-1</sup>	generally horizontal with small perturbations	9.2
	Plate (15 mm)	none	counter-gravity	8 mms <sup>-1</sup>	slightly convex with small perturbations	10.7
	Plate (15 mm)	none	counter-gravity	7 mms <sup>-1</sup>	generally horizontal with small perturbations	5.1
	Plate (15 mm)	none	counter-gravity	6 mms <sup>-1</sup>	generally horizontal with small perturbations	10.1
	Plate (10 mm)	none	counter-gravity	5 mms <sup>-1</sup>	45° inclination with wave running up across it	10.3
3	Plate (15 mm)	none	counter-gravity	3-4 mms <sup>-1</sup>	horizontal, planar, no perturbations	22.2
	Plate (15 mm)	none	counter-gravity	5 mms <sup>-1</sup>	horizontal, planar, no perturbations	23.2
	Plate (10 mm)	bromine compound	counter-gravity	5 mms <sup>-1</sup>	generally horizontal and planar, no perturbations	25.6

Table 5.7: Categorisation of the Weibull distribution data obtained from castings made during mould filling experiments.

The first category contained two frames that had Weibull moduli of 2.5 and 2.7. The second category was made up of six plate castings that had been made from conventional polystyrene

patterns of 10 mm and 15 mm thick. These patterns had been cast either in a gravity fashion, with the ingate located on the upper or lower face, or by means of the counter-gravity casting apparatus through an ingate situated at the bottom. Weibull moduli for the castings in this group ranged from 5.1 to 10.7. The last of the three categories consisted of two 15 mm thick plates and one of 10 mm thick. The 10 mm thick casting had been made from a brominated pattern whereas the other two had used patterns of conventional polystyrene. The Weibull results for this category were 22.2, 23.2 and 25.6.

The absence of castings from category 3 which had been associated with an interfacial instability during mould filling and the difference between the highest Weibull modulus in category 2 and the lowest of category 3 suggest strongly that interfacial instability during casting is very detrimental to casting quality. Interestingly, the severity of the instability was almost irrelevant to the modulus value, its presence in one form or another being sufficient to cause a marked decline in tensile properties. This suggests that once the filling velocity has reached or exceeded the critical value that triggers the onset of an interfacial instability, the quality of the resultant casting will almost certainly be poor.

#### **5.4 PRACTICAL IMPLICATIONS**

The experimental results have shown that interfacial instability can exist between an advancing liquid metal front and the decomposition products of a pattern in vertical, counter-gravity Lost Foam casting. The onset and propagation of this instability are heavily dependant upon the velocity at which the metal front travels through the mould and the nature and viscosity of the polystyrene degradation products immediately ahead of it. The instability has been shown to be of the Saffman-Taylor type, in which the interface between a dense, low viscosity liquid and a less dense, higher viscosity liquid lying above it becomes unstable when accelerated perpendicularly, and this has allowed predictions to be made, for brominated as well as conventional polystyrene pattern materials, about the front velocity required to bring about its onset. This has provided the foundryman with a tool to determine the velocity threshold for filling of a particular Lost Foam mould, vertically upwards. If this filling speed is exceeded it can be expected that the resultant casting would have severely reduced and more scattered mechanical properties. If an untreated polystyrene pattern material is used and

the maximum filling velocity that could be used without disruption to the metal front might result in a misrun defect, due to a slow filling rate, a brominated pattern material would permit a slightly higher filling speed without detriment to casting integrity.

By application of controlled, counter-gravity filling, the metal front can be maintained below, but close to, the maximum speed permitted thereby creating the best possible conditions for production of sound castings of high reliability. Up until now, most Lost Foam castings have been made using gravity filling techniques and metal velocities have been controlled primarily by variation in coating permeability [40,42]. This has meant that the foundry had to stock as well as control the use of a variety of coatings, each with its own permeability, and effectively carry out a balancing act for every casting. Now, using controlled counter-gravity filling, the coating no longer has to control the fill and it can be of high permeability. This not only reduces the number of different coatings required in the plant to one but also encourages a more rapid removal of pattern degradation products from the mould cavity and into the sand.

Even though the entrapment of polystyrene degradation products can be prevented by the application of a suitably permeable coating in conjunction with controlled counter-gravity filling, the viscosity of the liquid polymer just ahead of the metal front limits the velocity at which the interface can proceed without it becoming unstable. The casting experiments showed that the maximum filling velocity at which the metal – foam interface remained stable was only  $5 \text{ mm.s}^{-1}$  which, in some cases, resulted in the presence of misrun defects on the casting surfaces. To overcome this, the viscosity of the liquid degradation products needs to be reduced and published literature suggests that this may be achieved by using a co-polymer of polystyrene and polymethyl acrylate [160] where the tertiary hydrogen ions in the chain of polystyrene molecules are attacked by polymethyl acrylate macroradicals which results in scission at an adjacent bond and unzipping of the molecular chain. Alternatively, inclusion of a small amount of spherical, nanoparticles, such as fullerenes ( $\text{C}_{60}$ ), that are well dispersed within the polystyrene pattern material, have been reported to bring about substantial reductions in the viscosity of polystyrene melts [161]. These nanoparticles are not thought to participate in the entanglement dynamics within the melt but only to have a dilution effect which translates into a viscosity reduction.

The Lost Foam process relies upon energy from the liquid metal to decompose the pattern material that lies immediately ahead of it and misrun and cold lap defects are relatively common, especially when filling velocities are low. In fact, of the four plates that were filled with a metal velocity of  $\leq 5 \text{ mm.s}^{-1}$ , only two were fully filled. Therefore, the foundryman is encouraged to cast very close to the transition speed where an interface begins to show signs of instability. However, the limits of stability shown in Figures 5.3 and 5.4 are heavily dependant upon the molecular weight of the polystyrene degradation products. This value is in turn affected significantly by the amount of heat that these substances have been exposed to. For example, in Figure 5.3, if the temperature of the degradation products decreases by only 20 K from 500 °C to 480 °C, the limit of stability drops from  $4 \text{ mm.s}^{-1}$  to  $3 \text{ mm.s}^{-1}$ . Although this reduction is not large in absolute terms, it amounts to a 25% decrease and could easily result in an instability at the metal – foam interface. Conversely, if the filling velocity is reduced slightly, it follows that the time required to fill the mould increases and this extends the time that the polystyrene degradation products are exposed to the heat of the liquid metal. Under these conditions and based on the results shown in Table 4.70, the polystyrene degradation products would undergo a reduction in molecular weight which would also reduce their viscosity. This would have the effect of shifting the limit of stability of the interface upwards in terms of filling velocity. Therefore, two distinct mechanisms discourage the propagation of an interfacial instability when the filling velocity is reduced.

A limitation of the casting experiments was that they used simple pattern shapes of uniform thickness that were all oriented in the vertical plane during mould filling. This is generally not the case in production foundries where cast parts usually have a variety of cross sections and are shaped in such a way that the metal does not travel vertically upwards as it proceeds through the mould. This can result in a much more complicated filling pattern with the liquid metal dividing into a number of fronts, each one travelling through a different cross section of the pattern at a different velocity, and only recombining at a later stage in the filling sequence.

It is likely that the decomposition zone in a thin section is significantly different to that in a thicker section. The metal front temperature in the thinner section would be lower because heat loss into the surrounding mould would be higher. This would have the effect of lowering the temperature and increasing the viscosity of the polystyrene degradation products at the

metal – foam interface. As a result, an instability would occur at a lower velocity than in a thicker section. Pattern geometry or orientation could also influence the plane in which the metal front travels through the mould. A change in the cross section of a pattern from one side to the other, even where there is no divergence of the front into more than one stream, may cause it to travel faster in the thicker section because of variations in heat loss, degradation product viscosity and surface tension. Under these circumstances, the front may move forward at a steep angle tending towards the vertical plane and, although moving at a velocity lower than that required to generate a Saffman-Taylor instability, may encourage a Kelvin-Helmholtz instability to occur.

Research into the Lost Foam casting process has now reached a point where most authors recognise that the velocity of the metal, as it travels through the mould, is critical in determining whether the viscous pattern degradation products ahead of the metal front are entrapped or not. This has led to a few researchers applying simple methods of counter-gravity casting to the process to control the filling velocity to improve casting quality [72,74,99,100]. Whilst improvements in the density and dimensional repeatability of castings made in this way have been reported [75,110], most authors have focused on the level of filling velocity control that was achievable. Additionally, a number of authors have put forward explanations for the mechanisms by which foam entrapment takes place [19,20,25,42] but none have offered predictions of the filling velocities at which these mechanisms take place. This research has shown that an unstable metal – foam interface of the Saffman-Taylor type can lead to entrapment of pattern degradation products thereby reducing the quality of the castings produced. This has allowed predictions to be made of the velocity at which an interface becomes unstable and, by means of controlled counter-gravity casting, to ensure that it is not exceeded. Finally, in order to overcome misrun defects the filling velocity can be maximised, without causing an interfacial instability, by inclusion of a bromine additive in the polystyrene pattern material which reduces the viscosity of the degradation products ahead of the advancing metal stream.

## 6 CONCLUSIONS

1. The location of the ingate in gravity casting of Lost Foam plates had no significant influence on the rate that the mould filled and, in all cases, produced castings with tensile strengths of low reproducibility as characterized by the Weibull modulus.
2. None of the gravity cast frame patterns filled completely but, when gated from the bottom, the filling speed was slightly increased and the misrun defect reduced in severity from over half the casting to the third furthest away from the ingate.
3. The range of tensile strength values found in frame castings was much larger than that observed in gravity cast plates. The large film-type defects found only in the frame castings were probably responsible for this phenomenon.
4. Filling of Lost Foam plates from the bottom, under controlled, counter-gravity filling conditions, showed that only very slow filling conditions were associated with reproducible mechanical properties. Counter-gravity filling at a velocity of about  $5 \text{ mm.s}^{-1}$  was associated with a Weibull modulus of up to 25, (still much less than can be obtained with open cavity shape casting).
5. Examination of the filling process using real-time X-ray equipment showed that liquid aluminium front velocities of above  $5 \text{ mm.s}^{-1}$  were associated with a destabilization of the metal – foam interface into small perturbations and fingers, which would lead inevitably to the entrapment of pattern degradation products.
6. The real-time X-ray images showed that the uniform tensile strengths and higher Weibull modulus associated with the slower metal front velocity of  $5 \text{ mm.s}^{-1}$  were the result of a planar advancing metal front, which would be associated with a reduction in the trapped degradation products.
7. As carbon was found in every defect that was analysed by means of EDX, the increased level of hydrogen detected in plates when compared to their melts indicates that it

originated from entrapped degradation products rather than by diffusion through the metal front from the pattern decomposition zone.

8. Modelling the effect of velocity on the metal front profile with a mercury-glucose analogue of the Lost Foam casting process revealed similarities to the filling of Lost Foam moulds with aluminium and suggested that the irregular advancing liquid metal fronts in Lost Foam casting were a case of Saffman-Taylor instability.
9. At 500 °C (the minimum temperature expected in the zone immediately ahead of the advancing liquid metal front) liquid polystyrene from an untreated pattern was estimated to have a viscosity of between 16 Pa.s and 27 Pa.s which, according to the Saffman-Taylor equation, caused the metal – foam interface to become unstable at a velocity of between 4 mm.s<sup>-1</sup> and 6 mm.s<sup>-1</sup>.
10. The addition of an organic brominated additive to the polystyrene pattern material reduced the viscosity of the liquid degradation products at 500 °C to between 10 Pa.s and 19 Pa.s. This had the effect of raising the critical velocity at which the metal – foam interface became unstable to between 5 mm.s<sup>-1</sup> and 10 mm.s<sup>-1</sup>.
11. The filling velocity at which an interfacial instability occurred during the counter-gravity casting of plates in the brominated and unbrominated forms concurred with filling predictions based on the Saffman-Taylor equation and a liquid polystyrene temperature just ahead of the metal front of between 500 °C and 600 °C.
12. A non-horizontal interface, flowing upwards through a vertically oriented plate pattern, has been shown to exhibit a wave-type instability that travelled along the front in the same direction as the metal flow. Its characteristics are similar to those of Kelvin-Helmholtz instability which suggests that the metal – foam interface in Lost Foam casting can become unstable in more than one fashion.

## 7 FURTHER WORK

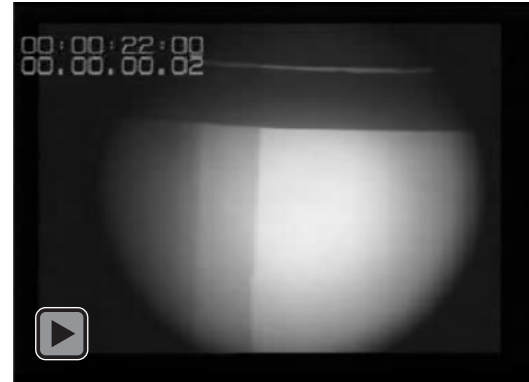
Considerable progress has been made in understanding the mechanisms that are responsible for casting defects specific to the Lost Foam process, the influence of these defects on mechanical properties and the application of a number of techniques to improve casting quality. Nonetheless, further research is needed in the following areas:

1. The quality of Lost Foam castings improves when filled in a counter-gravity fashion. However, further counter-gravity casting experiments should be performed by means of a more sophisticated casting apparatus that monitors and controls the velocity of the metal front throughout the complete filling operation in order to quantify accurately the benefits of this technique.
2. The temperature of the liquid degradation products plays a critical role in determining the velocity at which the metal – foam interface becomes unstable. Further work needs to be carried out not only to determine this temperature more accurately but also how it varies throughout the filling operation and what parameters influence it the most.
3. Some researchers have reported that the pattern degradation products ahead of the aluminium metal front resemble more of a foam than a liquid. Therefore, it is necessary to determine to what extent a foam is more likely to be present than a liquid and what consequences this might have on the stability of the interface.
4. This research only considered the metal – foam interface in simple plate and frame-type patterns. Even so, there were substantial differences between the two. Engineering castings are almost always more complex and have varying section sizes and orientations in the mould. Hence, there is a need to study these variables in more detail.
5. Addition of a bromine compound to a polystyrene pattern has been shown to reduce the molecular weight and hence viscosity of the liquid degradation products that it forms during casting. Investigation into alternative, viscosity reducing additives is needed to determine if there is a more suitable or more potent one available.

**APPENDIX I: VIDEO RECORDINGS OF THE MOULD FILLING & LIQUID-LIQUID  
INTERFACE EXPERIMENTS**



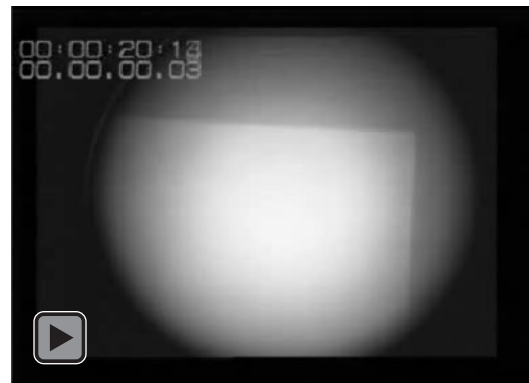
Video Relating to Figure 4.10



Video Relating to Figure 4.11



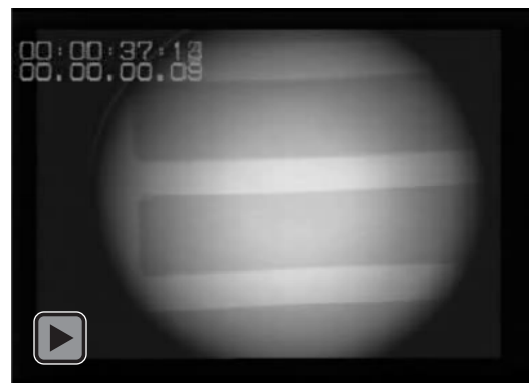
Video Relating to Figure 4.12



Video Relating to Figure 4.13



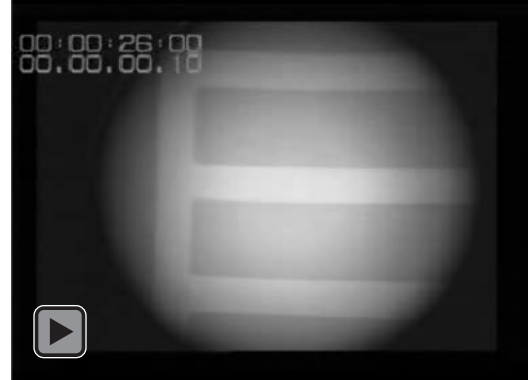
Video Relating to Figure 4.20



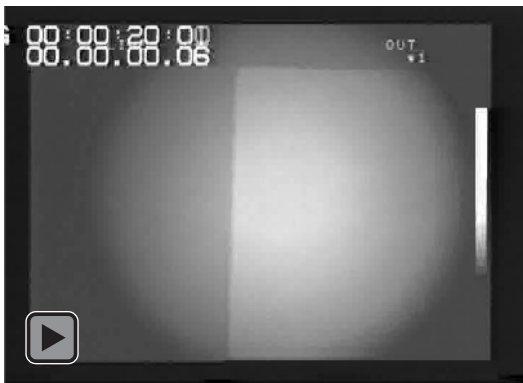
Video Relating to Figure 4.21



Video Relating to Figure 4.22



Video Relating to Figure 4.23



Video Relating to Figure 4.41



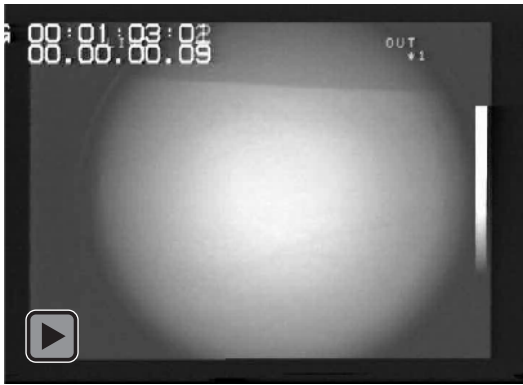
Video Relating to Figure 4.42



Video Relating to Figure 4.43



Video Relating to Figure 4.44



Video Relating to Figure 4.45



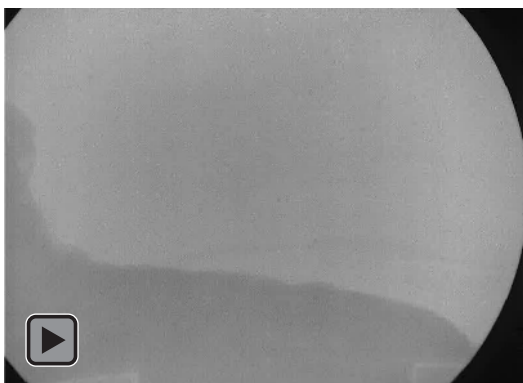
Video Relating to Figure 4.65



Video Relating to Figure 4.66



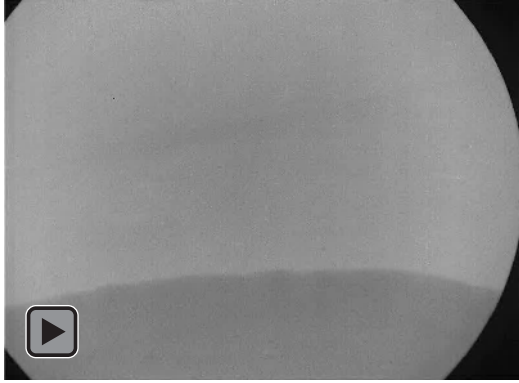
Video Relating to Figure 4.67



Video Relating to Figure 4.75



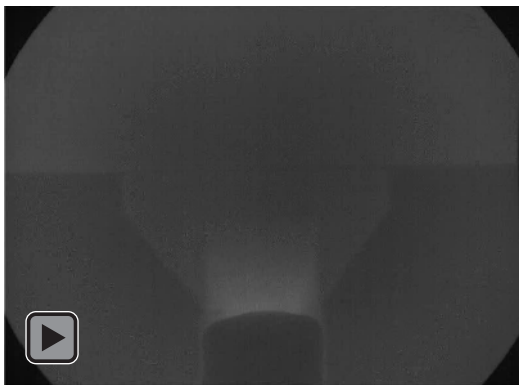
Video Relating to Figure 4.76



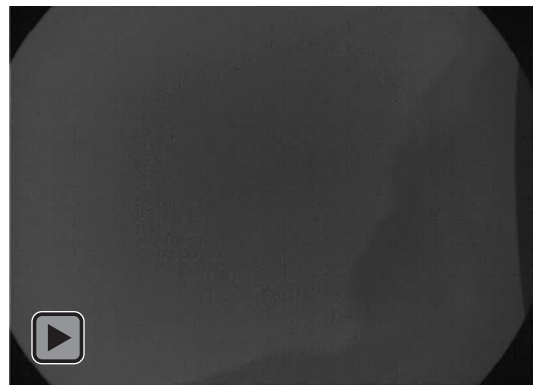
Video Relating to Figure 4.77



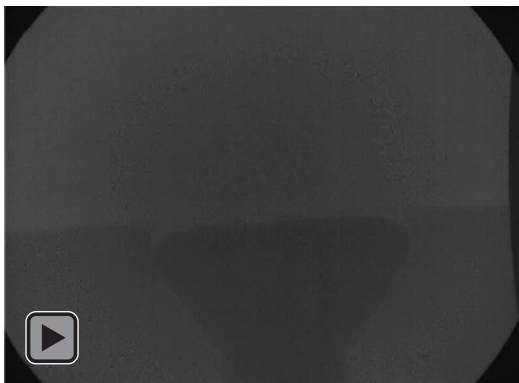
Video Relating to Figure 4.78



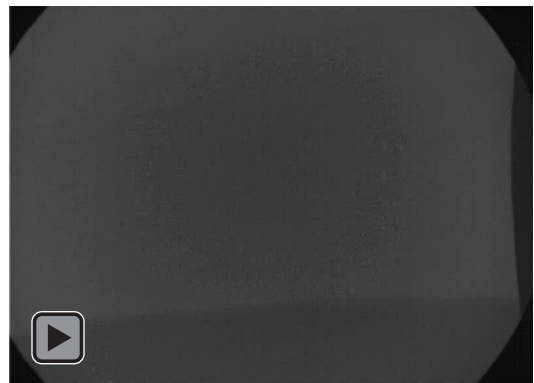
Video Relating to Figure 4.80



Video Relating to Figure 4.81



Video Relating to Figure 4.82



Video Relating to Figure 4.83

## APPENDIX II: CONFERENCE PAPERS

### AI.1. AFS 110<sup>th</sup> Metalcasting Congress, April 18-21 2006, Columbus, Ohio.

#### **Real-time X-ray Study of the Filling Profile in Al Alloy Lost Foam Castings**

M. J. Ainsworth

Gemco Cast Metal Technology, Science Park 5053, Eindhoven, The Netherlands.

W. D. Griffiths

Dept. of Metallurgy and Materials Science, School of Engineering, University of Birmingham, United Kingdom.  
B15 2TT

Copyright 2006 American Foundry Society

#### **ABSTRACT**

To understand better the filling of molds in the Lost Foam casting process, the filling of vertically oriented plates was viewed using a real-time X-ray technique, to examine the interaction of the cast Al alloy with the polystyrene foam pattern and the resulting profile of the metal front. The plates were filled from the bottom, using both gravity and counter-gravity techniques.

The real-time X-ray images from gravity-filled castings showed that the advancing metal front was associated with the development of a number of finger-like protrusions as filling of the mold progressed. These protrusions inevitably led to the entrapment of the degradation products of the polystyrene pattern. Mechanical properties of these castings were characterised by low and variable tensile strength and elongation. Examination of the tensile test bar fracture surfaces revealed pores due to entrapment of the pattern degradation products and oxide films, in all of the castings produced.

Counter-gravity filling was applied by means of a pressurised chamber containing a crucible of the liquid alloy into which was inserted a riser tube leading to the mold. As the filling velocity was reduced below that possible using gravity-filling techniques the metal front became planar, without any finger-like perturbations.

The tensile properties of castings made by counter-gravity filling were significantly improved over the gravity-filled castings, with a corresponding reduction in the number of defects found on the fracture surfaces. In addition, the tensile properties of the counter-gravity filled molds with the planar front were improved by up to 50% in comparison to the counter-gravity filled molds filled at a velocity such as to produce an irregular metal front.

#### **INTRODUCTION**

The Lost Foam casting process is characterized by the use of a polystyrene pattern that is placed within an unbonded silica sand mold and vaporized during casting. This technique allows the production of complex shapes and, in some cases, the unification into one casting of a number of components that were previously made separately and then joined together. This casting method is associated with defects that are specific to this process.

Three major defects associated with the production of aluminum castings in the Lost Foam process have been recognized (Bennett, 1999); internal pores, folds and blisters. All originated from the degradation of the pattern by the liquid metal during mold filling. Internal pores were caused by entrapment of liquid polymer within the

molten metal as it filled the mold, whereas the formation of folds was influenced by a number of factors such as low pouring temperature, metallic oxides, high or variable density patterns and metal turbulence. Blisters, apparent on the surface of the casting, consisted of a thin layer of aluminum that was separated from the main body by a thin layer of entrapped degradation products and oxide.

Experiments were carried out to determine the mechanisms responsible for fold and blister defects in aluminum Lost Foam castings by Ramsay et al. (Ramsay et al., 2000). It was determined that increased velocity of filling was the predominant factor in the formation of blisters, and that the use of a high permeability coating contributed to the incidence of this defect. The authors concluded that increasing liquid metal velocity generated higher surface turbulence thereby trapping higher amounts of pyrolysis products. The higher velocity also meant that the coating was not as hot when the metal front passed, thereby promoting a more rapid formation of a solid aluminum skin at the metal-coating interface. The deleterious effect of a high permeability coating, (Warner, 1998), has been attributed to its higher thermal conductivity.

In conventional gravity casting processes the running system is designed to control the filling rate of the mold and hence, in conjunction with the gravity vector, the metal front velocity. However, experiments conducted using bottom-gated polystyrene plate patterns with varying gate sizes and two pattern coatings of different permeabilities indicated that gate size, number of gates and gate position were not significant in Lost Foam casting (Hill et al., 1997).

The published literature concurs that metal front velocity in Lost Foam casting production is a significant factor in determining the quality of the final casting, and the main focus of control of this variable has been pattern composition, coating composition and coating thickness (Wang, 1997). It was further proposed that the “process choke” could either be the metal-foam interface or the metal-foam-coating interface depending on whether the decomposition of the foam or removal of the products was the most influential (Lawrence, 1998).

A more detailed study of this zone suggested that foam degradation, back pressure, and wetting and wicking were the control mechanisms by which the filling of a Lost Foam mold took place (Liu et al, 1997). In this work it was shown that, with the use of a high permeability coating, the gap between the advancing metal front and the pattern was small and it was deduced that all degradation products could therefore leave the mold without hindrance. This mechanism was defined as foam-degradation control and was associated with a relatively high filling velocity. In contrast, low permeability coating trials exhibited significantly larger gaps between the metal front and pattern material and it was argued that the larger gap reduced the rate of degradation of the pattern and generation of gaseous products. It was argued that the pattern and the liquid metal reached a dynamic pressure balance with a large gap between them. This mechanism was named the back-pressure effect and was characterized by a relatively low filling velocity.

It is quite reasonable to assume that the velocity of the metal front should closely follow the rate of pattern decomposition and its subsequent removal from the mold in order to prevent any entrapment. A number of authors (Hill, 1997; Ramsay, 2000) have put forward critical metal velocity windows with which fully filled castings, with a low incidence of defects, could be produced. The velocity windows reported all fell between 12.5 and 22.9 mm.s<sup>-1</sup> with misrun and sand collapse being observed below the minimum figure and inclusions encountered above the upper limit. The liquid degradation products at the foam-metal interface are viscous in nature and it was suggested that they could only be transported to the pattern coating by a convex metal front (Mobilog, 2001). In patterns oriented vertically, this could only be achieved by top gating. This stance was supported by a set of experiments in which the occurrence of a concave metal front profile was reported in conjunction with vertically oriented patterns that had been filled from the bottom. (Davies, 2002).

The reduction of the metallostatic pressure during gravity filling has a significant effect upon the metal front velocity throughout the filling of the mold. As a vertically oriented, bottom gated, gravity cast mold is filled the reducing metallostatic head reduces the velocity of metal flowing into the mold. For a pattern with uniform cross section throughout its length, such as a plate, this reduction in the metal velocity leads to a reduction in the flow rate and hence the speed of the advancing front.

In an attempt to overcome this limitation a simple, vacuum-assisted, counter-gravity casting apparatus was employed to fill Lost Foam molds with ductile iron (Bakhtiyarov, 2000). A number of molds containing vertically oriented plate patterns were cast and mold filling characteristics monitored by a set of thermocouples inserted at pre-determined locations in the pattern. Isochronal contour maps suggested that the metal flowed into

and through the mold cavity as one continuous convex metal front at an average flow rate of approximately  $120 \text{ mm}\cdot\text{s}^{-1}$ .

A modification of this simple casting procedure was also evaluated in which the mold was rotated immediately after casting. This permitted feeding of hot liquid metal from a reservoir in the mold to the casting during solidification. The density of samples produced by the modified casting technique was higher than those where mold rotation was absent after casting. The author concluded that the modified procedure assisted the removal of gaseous products from the liquid metal and eliminated internal porosity defects.

Therefore the published literature indicates that the velocity of filling of Lost Foam molds has a significant effect on the level of pattern degradation products found in the final casting but the influence on the shape of the advancing metal front and its associated relationship with the level of entrapped degradation products is not completely understood. Almost all metal front morphology studies conducted in conjunction with the Lost Foam casting process have made use of a series of thermocouples or timing probes that have been placed in a pre-determined array in the pattern prior to casting. This method of profile morphology examination has a number of constraints that means that results can only be approximations even in the best cases.

The main focus of this work has been to determine the effect of metal front profile morphology on the quality of the castings produced. Using real time X-ray techniques to monitor the front profile, gravity, and controlled counter-gravity filling techniques, were applied to the filling of simple plate patterns. Profile differences were characterized in terms of the mechanical properties of the castings produced and the types of defects found on the fracture surfaces of the samples.

## EXPERIMENTAL PROCEDURE

The casting experiments described in this study were designed so that pressure (exerted as a result of metallostatic head in the case of gravity filling and by means of a pump when counter-gravity filling) was the only parameter used to effect changes to the fill profile observed. All other factors known to influence this element (i.e. pattern thickness, bead fusion, coating permeability, coating thickness and gating orientation) were maintained at a constant level during the complete set of experiments.

### PATTERNS

A simple plate pattern geometry was employed to evaluate the metal front profile behavior and resultant mechanical properties of castings filled by gravity and counter-gravity techniques. The patterns were made from pre-expanded, T-grade polystyrene beads on an industrial pattern molding machine that was equipped with horizontally split aluminum tooling. All patterns were produced in one batch, and had a bead size of approximately 1 mm and a nominal pattern density of  $29.9 \text{ kg}/\text{m}^3$ .

After ageing for 1 day each pattern was attached to its own running system to form a cluster. The running system for the gravity cast plates consisted of a pre-formed ceramic pouring basin, a 40 mm diameter, expanded polystyrene downsprue with a 10 mm diameter hollow centre, an expanded polystyrene runner bar with a  $6.0 \text{ cm}^2$  cross section and a single ingate of  $10.4 \text{ cm}^2$  cross section (Fig. 1a). In contrast, the simpler counter-gravity system was made up of a short expanded polystyrene upsprue with a 10 mm hollow centre and a single, expanded polystyrene ingate of  $10.4 \text{ cm}^2$  cross section (Fig. 1b).

Pattern and running system components were manually assembled using proprietary hot-melt glue. An aluminosilicate refractory casting, suspended in water, was applied by manually dipping each pattern until all but the pouring basin or, in the case of the counter-gravity filled clusters, the bottom face of the upsprue, was immersed. Each cluster was maintained in the fully immersed position for a period of 5 s and then placed on a rack to dry in a circulating air oven at  $55 \text{ }^\circ\text{C}$  ( $131 \text{ }^\circ\text{F}$ ) for a period of 4 hours. Coating adherence was measured by immersing a stainless steel plate of  $100 \text{ mm} \times 100 \text{ mm} \times 2 \text{ mm}$  thick into the coating bath and then measuring the weight of the coating on the plate after removal. This value was maintained at  $4.5 \text{ g} \pm 0.5 \text{ g}$  for the duration of the operation and resulted in coating thicknesses ranging from  $200 - 275 \text{ }\mu\text{m}$ .

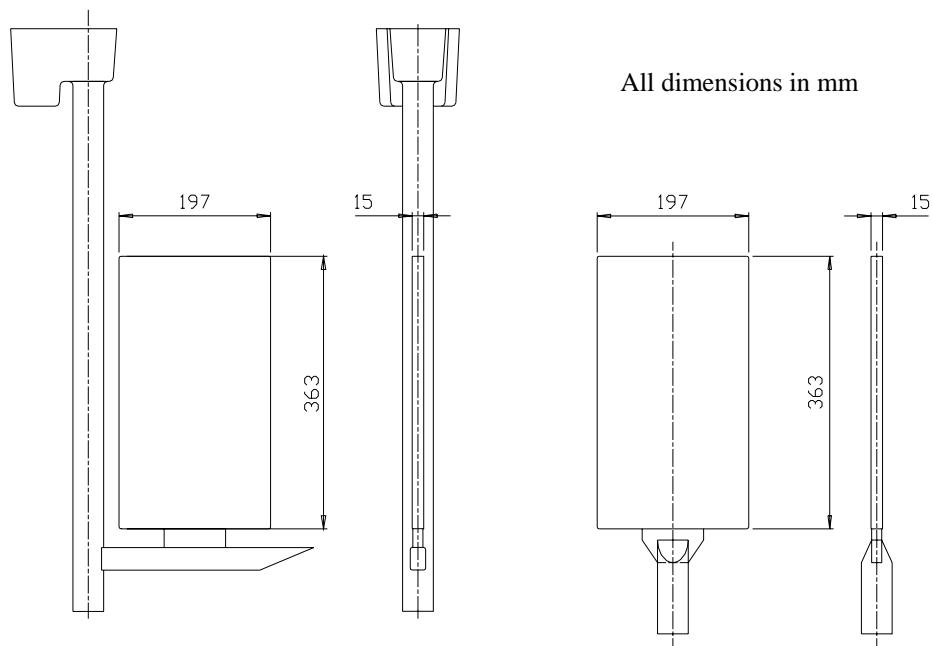


*Fig. 1a Sketch of the gravity-filled plate*

*Fig. 1b Sketch of the counter-gravity filled plate.*

## MOLDING

Loose, dry, silica sand with an average grain size of  $370\ \mu\text{m}$  was used to support the pattern in a flask that had internal dimensions of 0.45 m in length x 0.11 m width x 0.83 m depth. This design produced the best image resolution in the real time X-ray used to study the mold filling. For the gravity filled molds, each flask was filled initially with a bedding layer of sand approximately 150 mm deep. A single cluster was placed on the sand base and located centrally by hand. The flask was then filled with sand while being subjected to vertical vibration to bring about sand compaction. Filling of the flasks took approximately 30 s and maximum sand grain compaction was considered to have been achieved when there was no longer any reduction in the bulk density of the sand within the flask. This situation was always achieved within 10 seconds of completion of filling of the mold.

The same materials, basic flask design and molding procedure, was adopted for the counter-gravity cast plates. However, in this case the flask was modified to incorporate a centrally located, 70 mm diameter hole in the base. This hole contained a compressible ceramic sleeve that had an internal diameter and height of 40 mm, fitted into the hole so that one face of the sleeve was flush with the flask surface. The pattern cluster was positioned in the flask by locating its upsprue into the sleeve so that the face of the upsprue was also flush with the base of the flask.

## MOLD FILLING

The gravity casting process was performed by means of a conventional, joystick controlled autoladle which carried a crucible containing a strontium modified Al-10wt.%Si alloy. Counter-gravity filling was achieved by using a pressure chamber of welded steel construction that housed a similar crucible to that used for the gravity casting (Figs 2a and 2b).

In the case of the counter-gravity filling experiments a pre-modified LM25 (Al-7wt.%Si) alloy was used. One end of a refractory coated "riser tube" was inserted into the crucible in the pressure chamber while the other end of the tube was placed against the mold, and fitted with a flange that located into a recess on the lid of the chamber so that its upper face was flush with the top face of the pressurized chamber. All mating faces of the chamber were made pressure tight by means of gaskets. The chamber was fitted with a coupling to allow connection of a compressed air supply, a pressure gauge, a pressure relief valve and thermocouple for monitoring the metal temperature in the crucible.

Immediately after sealing of the chamber with the crucible of metal in place, a gasket was placed on the rim of the riser tube in line with the upper face of the pressure chamber and the mold placed on the chamber lid. The

bottom inlet to the mold was located over the riser tube and the complete mold clamped to the chamber by means of an A frame arrangement. Compressed air was used to pressurize the chamber, regulated by a pressure control valve, and the chamber was pressurized using a manually operated valve between the pressure regulator and the inlet to the chamber.

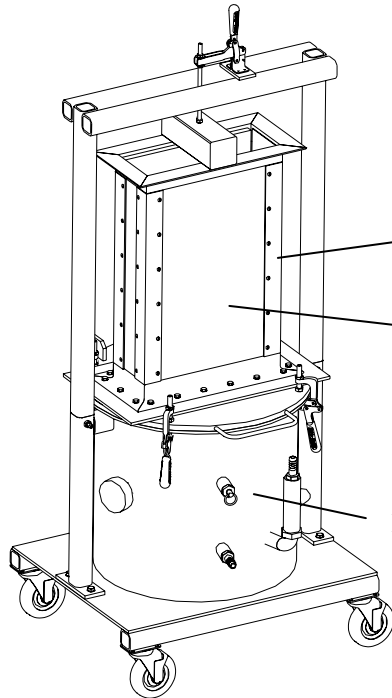


*Fig 2a Isometric View of the Counter-gravity Casting Machine with Mold in Position*

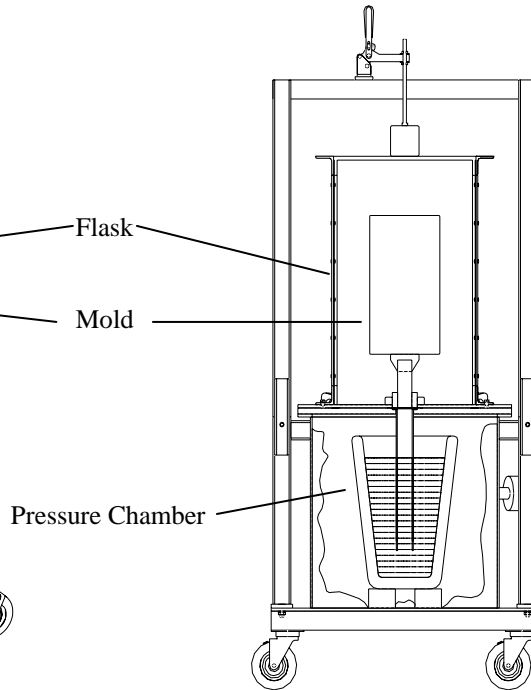


*Fig 2b Section View of the Counter-gravity Casting Machine with Mold in Position*

All castings were filled at a temperature of 785 °C (1445 °F), and the filling process monitored using a 160 kV real-time X-ray with the image captured using a S-VHS 50 Hz video recorder.

#### MECHANICAL PROPERTIES AND FRACTURE SURFACES

Specimens for tensile strength determination were taken from locations in each plate as shown in Fig. 3. In one experiment a counter-gravity cast plate did not fill completely and exhibited a misrun defect along its upper edge. In this case samples were only obtained from locations A – T.

#### Weibull Analysis

The tensile values obtained from the test bars were subject to a Weibull analysis. This technique (Rezvani, 1999) more accurately described the distribution of the tensile strength results of Al-7Si-Mg alloy castings when compared with the Gaussian distribution.

Essentially, when a relationship between the risk of rupture  $RR$  and the probability of survival  $P_s$  is such that  $P_s=0$  at  $RR=\infty$  and  $P_s=1$  at  $RR=0$ , then it was proposed (Weibull, 1951) that the exponential function that best describes this situation is:

$$P_s = \exp(-R_R) \quad \text{or} \quad R_R = -\ln(P_s) \quad \text{Eq. 1}$$

The risk of rupture  $R$  of a given component is a function of the applied stress and also proportional to the volume of the material under stress  $\sigma$ . For a volume  $V$  under uniformly distributed stress  $\sigma$ , the risk of rupture function  $R_R$  is written as :

$$R_R = (V/V_0) \cdot ([\sigma - \sigma_u] / \sigma_0)^M \quad \text{Eq. 2}$$

Similarly, for a non-uniformly distributed stress  $\sigma = \sigma(V)$ :

$$R_R = \int_0^V (\sigma - \sigma_u/\sigma_0)^M dV/V_0 \quad \text{Eq. 3}$$

where  $\sigma_u$  is a threshold stress below which the risk of rupture is zero. Practically, the threshold value is unknown and it is therefore assumed that  $\sigma_u=0$ .  $\sigma_0$  and  $V_0$  are constant normalizing parameters and  $M$  is defined as the Weibull Modulus. Equating the two expressions 1 and 2 for  $R_R$  gives the survival probability  $P_S$  as a function of the volume of material  $V$  under stress and of the parameter  $M$  (=Weibull Modulus) that reflects the statistical distribution of the sizes of fracture-initiating flaws;

$$P_S(V) = \exp \{-(V/V_0) \cdot [\sigma/\sigma_0]^M\} \quad \text{Eq. 4}$$

$$\ln\{\ln[1/P_S]\} = \ln(V/V_0) + M \cdot \ln(\sigma) - M \cdot \ln(\sigma_0) \quad \text{Eq. 5}$$

The linear plot of  $\ln\{\ln[1/P_S]\}$  vs  $\ln(\sigma)$  has a slope equal to the Weibull Modulus  $M$ .

One fracture surface from each test bar was observed using a scanning electron microscope to determine the morphology and distribution of the different types of defect present. Additionally, each fracture surface was subject to chemical analysis in the SEM, of sound as well as defective regions.

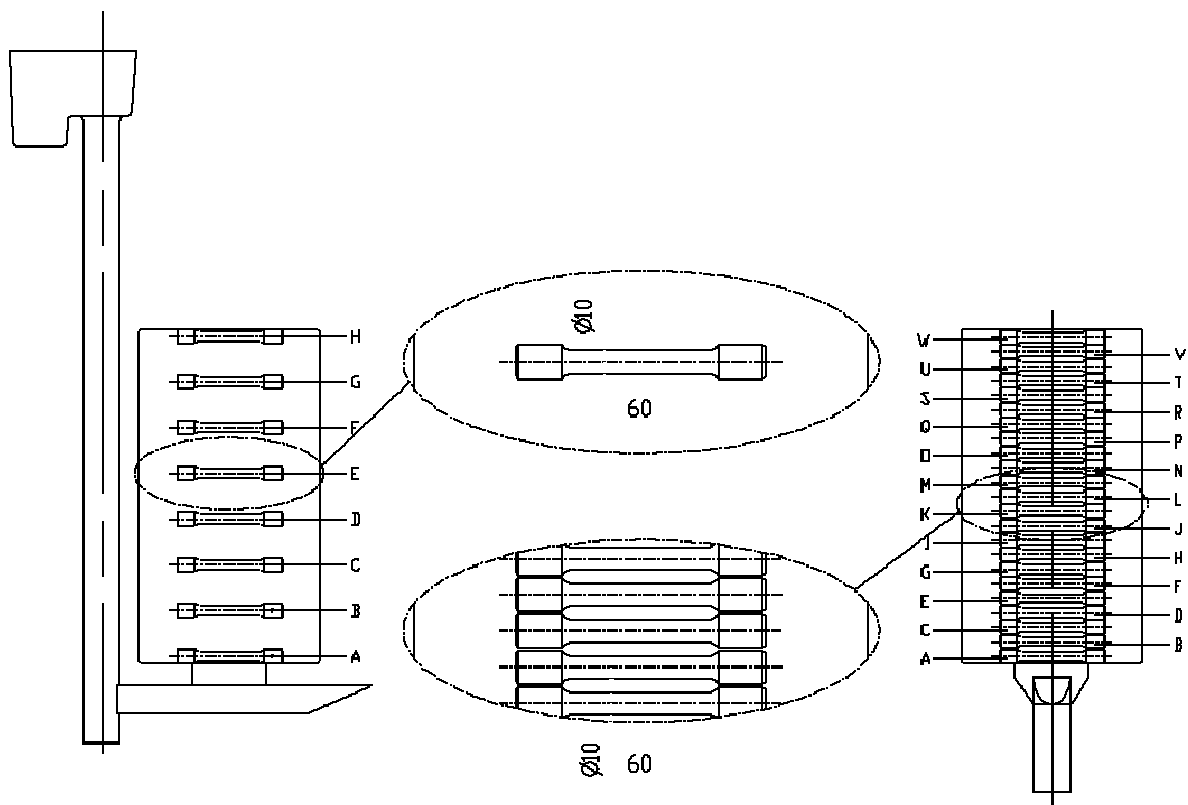


*Fig. 3 Positions from which the mechanical test piece samples were obtained.*

## RESULTS

### MOLD FILLING

#### Gravity Filled Plates

Gravity filled plates exhibited an average metal fill velocity of  $12 \text{ mm.s}^{-1}$ . However, there was significant variation of the actual value across the casting during the fill with a maximum flow rate of  $25 \text{ mm.s}^{-1}$  occurring in the lower part of the plate. The ingate was attached to the runner bar and pattern by means of hot melt glue that did not degrade uniformly. This gave rise to a non-uniform flow of metal into the ingate and the lower pattern region (Fig. 4, Frame 1). The liquid metal began its path into the plate as a single, convex metal front that originated from the downsprue side of the ingate. As the ingate filled, this metal front split into five distinct fingers (Fig 4, Frames 2 and 3).

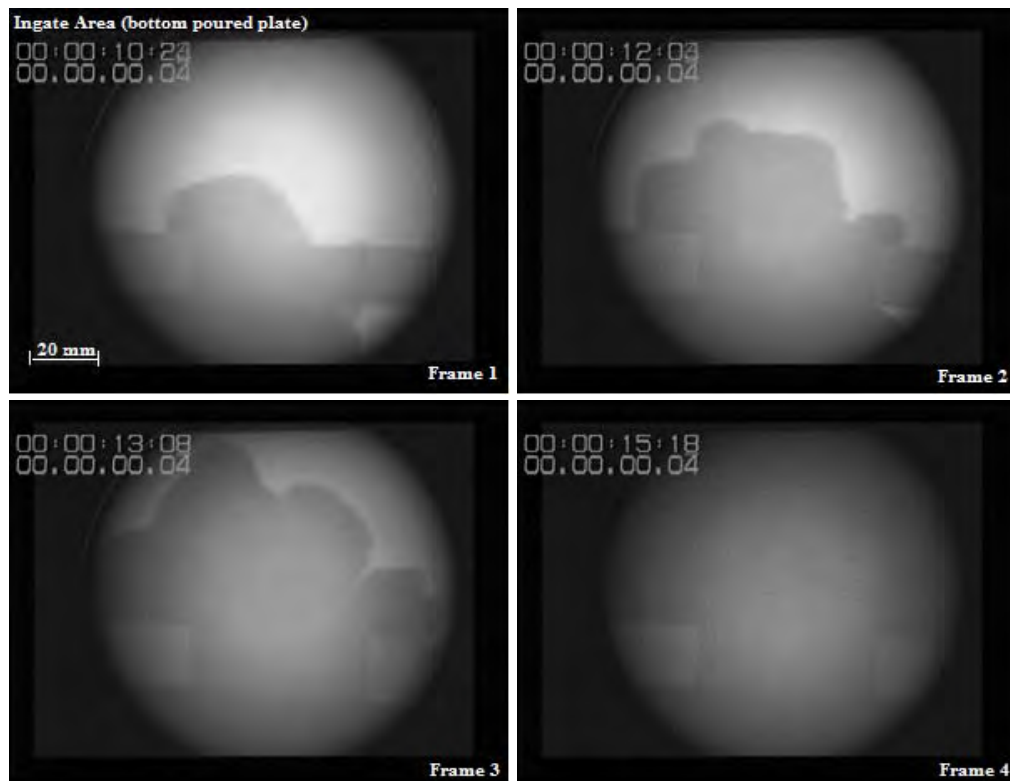


*Fig. 4 Finger Formation of the Metal Front on Entering the Ingate Area of a Gravity Filled Mold.*

After approximately 150 mm of vertical travel the speed of these fingers began to decrease. The flow of metal in the vertical plane in the central region was accelerated towards the side of the plate furthest away from the downsprue. Individual fingers merged after approximately 250 mm of vertical travel to form one metal front. This assumed a slightly concave shape across the complete width of the plate that was slightly advanced at the side furthest from the downsprue (Fig. 5, Frames 3 and 4). The front profile was characterized by a series of small protrusions, approximately 5 mm in height (Fig. 5). The first point of contact with the top of the mold was at the corner opposite the downsprue. From that point filling took place in a horizontal fashion. The duration of filling of the mold with this method of casting was 41 s.

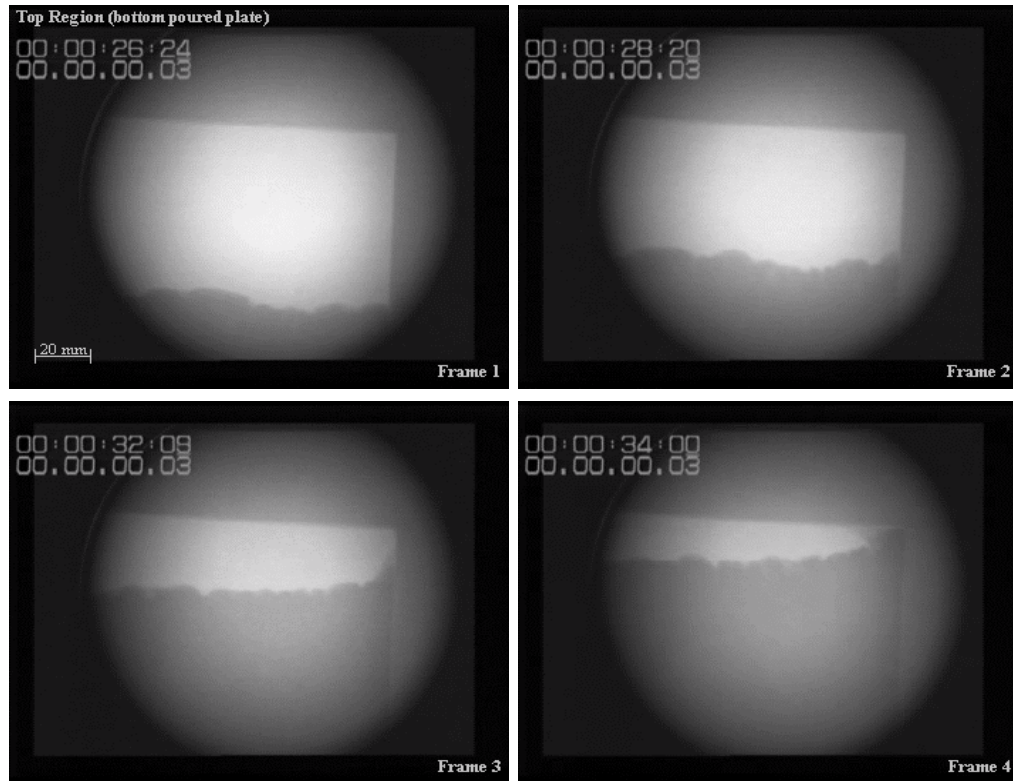


*Fig. 5 Unstable Single Metal Front Profile Observed in the Top Region of a Gravity Filled Plate*

#### Counter-gravity Filled Plates

The application of pressures of 5 psi (34.5 kPa) and above within the casting unit gave rise to metal fronts with long finger-like protrusions that were present throughout the filling of the plate. These fingers had a spiked appearance and were more numerous than those encountered in the gravity filled plates (see Fig. 6). The average filling speed, captured from the real time X-ray image of a plate filled using a chamber pressure of 10 psi (68.9 kPa) was  $24 \text{ mm.s}^{-1}$ , twice the velocity associated with the gravity-filled plate. The rate of fill was such that the liquid metal reached the top of the plate in 21 s. However, the liquid and gaseous pattern degradation products preceding the front could not escape through the mold coating at the same rate and became temporarily trapped in this region. It took a further 7 s for this trapped material to leave the mold cavity and pass into the surrounding sand.

The average filling velocity of plates cast in a counter-gravity fashion at chamber pressures of between 4 - 4.5 psi (27.6 – 31.0 kPa) was  $13 \text{ mm.s}^{-1}$  (see Figure 7). This speed was comparable to that recorded in the upper region of the gravity filled mold. The metal front profile was also similar with small protrusions present along the complete length of the front. An interesting difference was that, rather than being concave, the metal front was slightly convex in shape with the leading region being situated towards the centre of the plate.

A reduction of the chamber pressure by only 0.5 psi (3.4 kPa) to 3.5 psi (24.1 kPa), reduced the average fill velocity to approximately  $5 \text{ mm.s}^{-1}$ . This produced an almost horizontal metal front that had a profile devoid of any protrusions. This was classified as a planar type front. The filling velocity was, however, so slow that it resulted in an arrest of the metal front approximately 30 mm from the top of the plate, resulting in a short run defect on the casting.

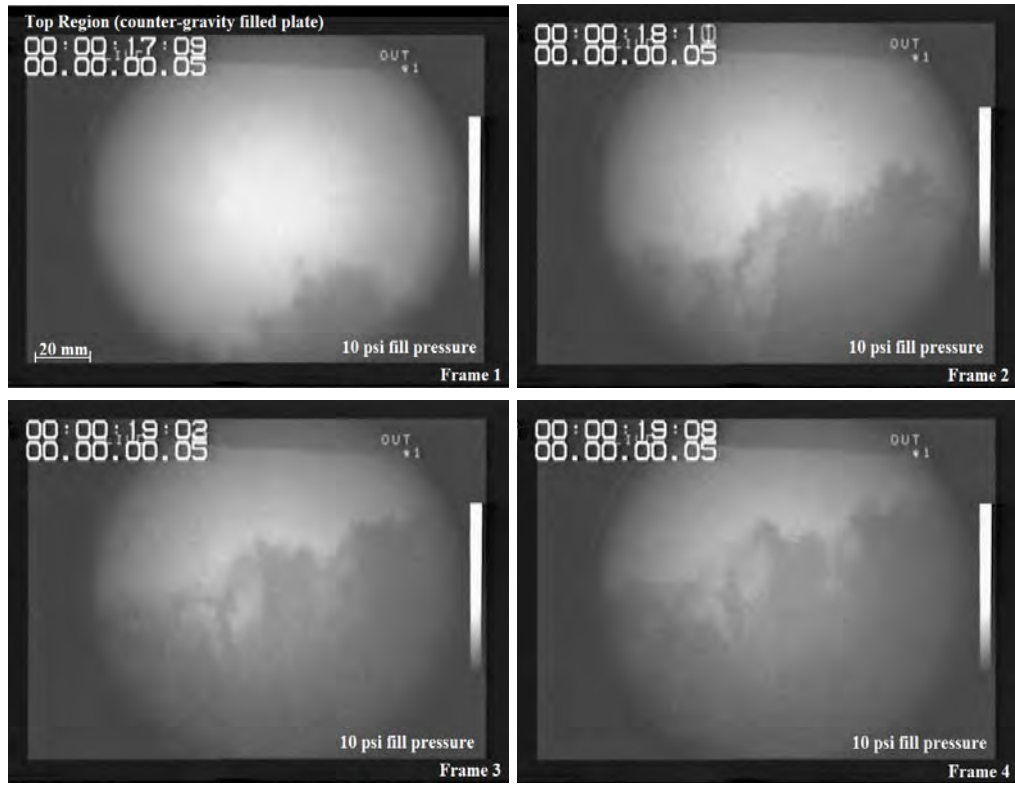


*Fig. 6. Finger-type Front in the Upper Region of a Counter-gravity Filled Plate (10 psi chamber pressure)*

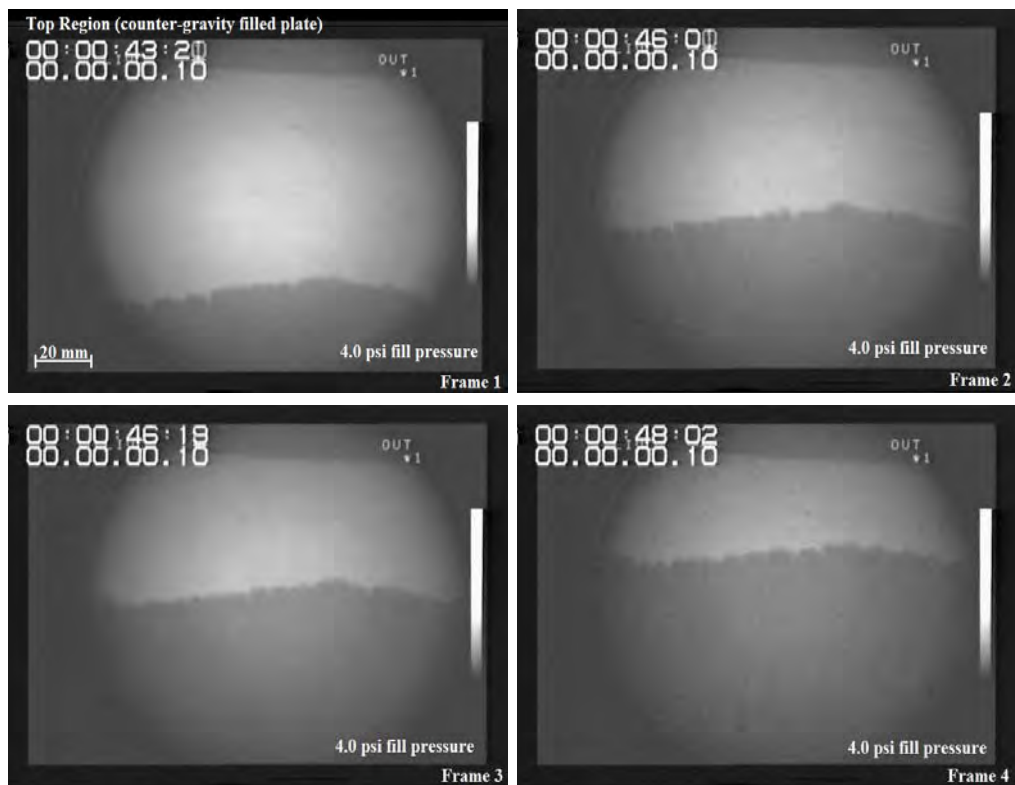


*Fig. 7. Irregular Metal Front in the Top Region of a Counter-gravity Filled Plate (4 psi chamber pressure)*

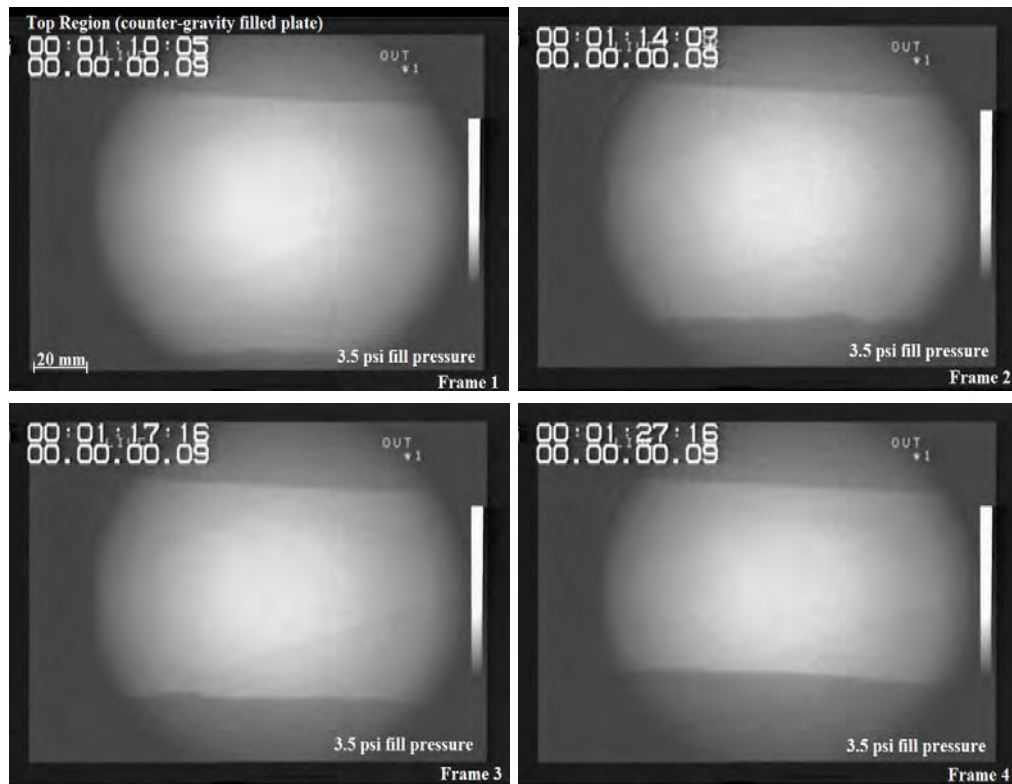


*Fig. 8 Planar-type Metal Front Profile Observed in the Top Region of a Counter-gravity Filled Plate (3.5 psi chamber pressure).*

#### MECHANICAL PROPERTIES

Table 1 contains the complete set of Ultimate Tensile Strength results obtained from three gravity cast plates and two counter-gravity filled plates. All plates filled using gravity, as well as the one made by counter-gravity means at 4.0 psi (27.6 kPa), displayed non-planar fronts during mold filling (Figs. 4, 5 and 7) and yielded similar, low results. In some cases fracture occurred before the 0.2% proof stress value had been reached. In contrast, the tensile results obtained from the counter-gravity cast plate, filled at 3.5 psi (24.1 kPa) and in which a planar metal front was observed (Fig. 8), were significantly higher.

To obtain realistic sample sizes for conducting the Weibull analysis the tensile results from the three plates that were cast in a gravity fashion were combined to form a single set of data whereas those from each of the counter-gravity cast plates were treated separately. The Weibull moduli obtained from the UTS of the combined gravity casting results and the results from counter-gravity filling at a pressure of 4.0 psi (27.6 kPa), were 9 and 11 respectively. In comparison, the counter-gravity cast plate in which a planar metal front had been observed during filling yielded a significantly higher result of 23 (Fig. 9).

Table 1. Ultimate Tensile Strength Results From Gravity and Counter-gravity Filled Plates

Ultimate Tensile Strength (MPa)					
Test Piece Position	Gravity Filled Plates			Counter-gravity Filled Plates	
	No. 1	No. 2	No. 3	4.0 psi	3.5 psi
A	145	149	155	106	227
B	141	135	136	133	196
C	136	123	127	126	205
D	124	130	123	126	197
E	111	116	101	109	203
F	104	111	121	108	212
G	114	113	101	117	199
H	130	130	127	119	198
I				126	206
J				121	209
K				123	205
L				135	207
M				130	215
N				140	222
O				128	211
P				94	190
Q				128	220
R				134	202
S				131	217
T				137	212
U				140	unavailable
V				144	unavailable
W	124	unavailable			

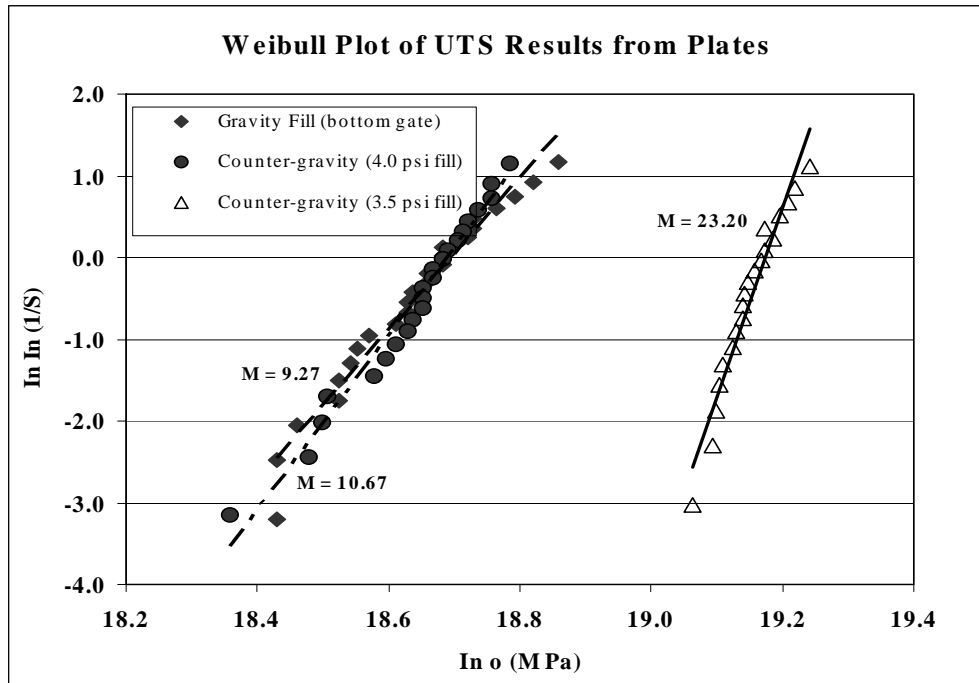
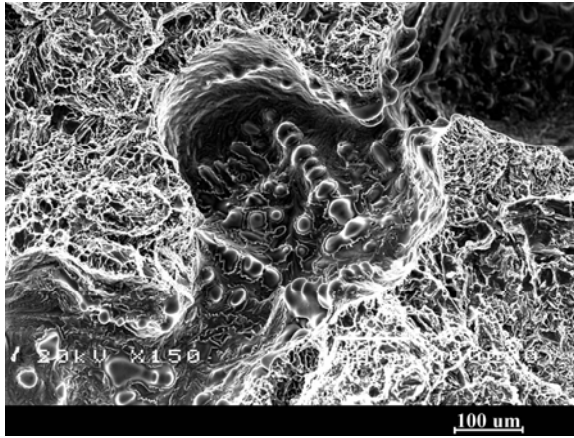


Fig. 9 Weibull Plots of the Ultimate Tensile Strength of Samples Taken from Gravity and Counter-gravity Filled Plates.

## FRACTURE SURFACES

All test bar fracture surfaces were examined using an SEM. Two types of defect were detected and are illustrated in Figs. 10 and 11, namely, a pore, and a film-type defect, respectively.



*Fig. 10 Pore Defect Detected on the Fracture Surfaces of all Samples*

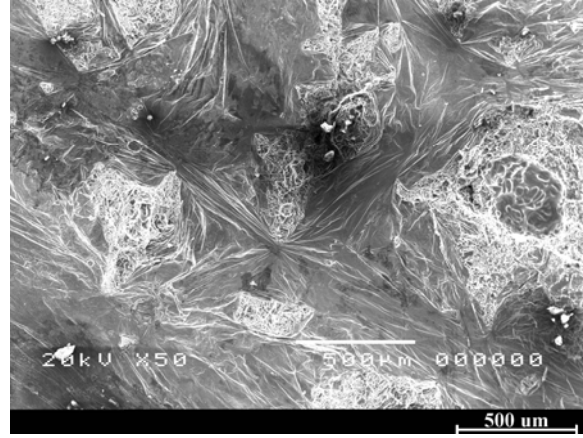


*Fig. 11 Film Type Defect Found on the Fracture Surfaces of Samples Cast with a Non-planar Metal Front*

All fracture surfaces, including those taken from the plate where a planar front was observed during filling, contained interdendritic pore-type defects as shown in Fig. 10. These pores varied in size from approximately 400 μm up to 2 500 μm and were located randomly across the surface. The smaller pore defects were spherical in shape as in Fig. 10 but the larger ones were flatter and more irregular. The film type defect (Fig. 11) was detected on all fracture surfaces originating from the gravity cast plates but on only one of the fracture surfaces from the plate cast by counter-gravity means at 4.0 psi (27.6 kPa) chamber pressure. The location of this defect was seen in specimen G that had been taken from the central region of the casting. No films were observed in the counter-gravity cast plate that exhibited a planar metal front on filling. Observation of film type defects showed that they were at least as large in cross-section as the largest pore defects and had a two-dimensional, wrinkled appearance. EDX analysis indicated that carbon and oxygen were present, as well as the expected alloy constituents, in the defective regions of all fracture surfaces, (see Fig. 12).

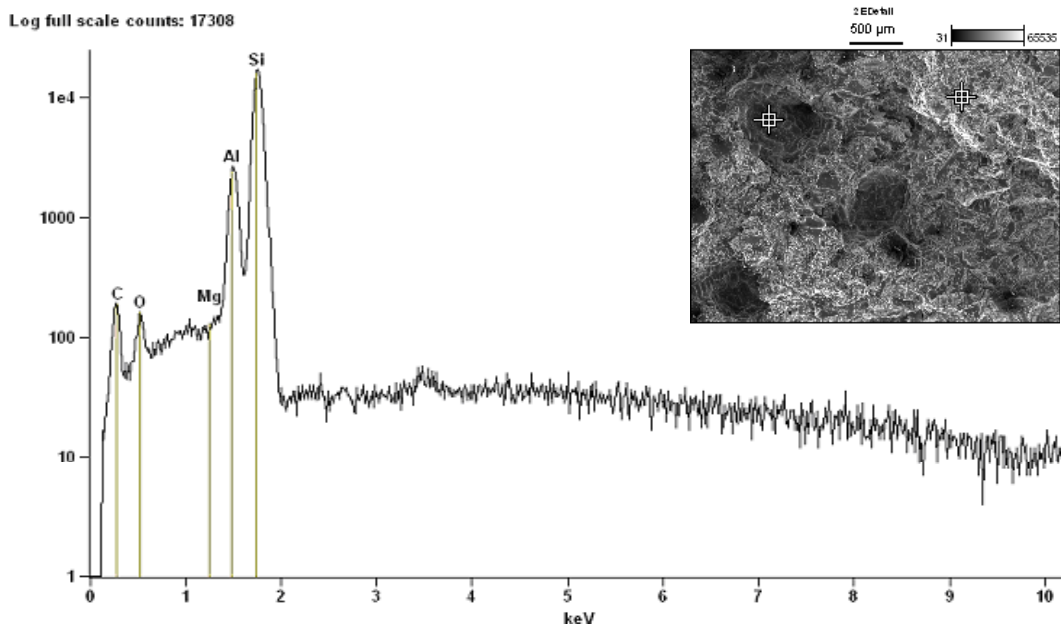


*Fig. 12 EDX Results from a Pore Defect Observed on a Fracture Surface Originating from the plate filled using a chamber pressure of 4.0 psi. (The EDX sample location is shown in the inset micrograph).*

## DISCUSSION

The main aim of the experiments was to determine the level of benefit, in terms of casting quality improvement, that could be achieved by application of counter-gravity filling to Lost Foam molds.

### MOLD FILLING

Plates filled by gravity means exhibited the largest variation in metal front velocity throughout the filling of the mold and this is thought to have been a contributory factor to the change in metal front profile from a series of large, well defined fingers to a single, essentially horizontal front that was associated with a number of small protrusions. At the higher metal front velocities ( $24 \text{ mm.s}^{-1}$  to  $25 \text{ mm.s}^{-1}$ ), recorded in the lower regions of the gravity-cast plates and during application of 10 psi (68.9 kPa) pressure to the chamber when counter-gravity filling, the metal front profile consisted of a number of distinct fingers. However, the well-rounded profile of the fingers associated with gravity casting contrasted sharply with the more pointed nature of those seen in the counter-gravity filled plate, with the latter being obviously more deleterious, and leading to greater entrapment of the pattern degradation products.

In the upper region of the plate a similar metal front profile was observed with both gravity filling and counter-gravity filling with a pressure applied to the chamber of 4.0 psi (27.6 kPa). The filling velocities recorded were also very similar with the metal front in the gravity filled plate closely following the average filling speed of  $12 \text{ mm.s}^{-1}$  and that of the counter-gravity filled plate being about  $13 \text{ mm}^{-1}$ . Although front speeds of  $12 \text{ mm.s}^{-1}$  and  $13 \text{ mm}^{-1}$  produced the same general morphology, characterized by a single, principally horizontal front with small protrusions of approximately 5 mm in height, the overall curvature of the front tended to be slightly concave during gravity filling and convex when associated with counter-gravity filling.

The mechanical property results show that the plate made by the counter-gravity technique that exhibited a planar metal front during mold filling had the greatest and most uniform UTS. However, a large misrun defect was also present which limited the number of samples available for tensile testing to 20 instead of the normal 23 that could be obtained from a fully filled plate.

The observations made during the experiments suggest that there is a direct relationship between metal front morphology and its velocity although the mechanism of the transition from a stable, planar front into an unstable, finger-like front with increasing metal front velocity is, at present, not fully understood. One explanation may be that this is a case of a fluid flow instability, leading to an uneven liquid metal front. Saffman and Taylor described a case where a low viscosity fluid, driven into one of much higher viscosity whilst contained within parallel planes, resulted in an unstable interface, (Saffman and Taylor, 1958), leading to the formation of fingers of the lower viscosity fluid reaching into the higher viscosity one. In the experiments described in this paper the liquid aluminum would represent the low viscosity fluid, while the polystyrene pattern degradation products would represent the high viscosity fluid, respectively.

A second possible explanation for the onset of an unstable metal front is connected with film boiling. The interaction of the liquid metal and the polystyrene pattern produces both liquid and gaseous degradation products and it has been suggested that a gaseous layer of these products would lie immediately above the metal front with a (cooler) liquid layer beyond that. A thin vapor film lying over a horizontal heat source has long been recognized as unstable (Bromley, 1950) and has been associated with the formation of large bubbles that break away. If these gas bubbles pass through the high viscosity liquid polystyrene above, they could lead to localized breakdown of the foam, and create paths in which the liquid metal could follow more easily, leading to the development of the fingers of liquid metal that were observed.

### MECHANICAL PROPERTIES & FRACTURE SURFACES

Published literature has shown that castings manufactured in open molds, under controlled conditions and with well designed running systems, have resulted in Weibull moduli of up to about 38. This contrasted strongly with the results obtained in this set of experiments that yielded Weibull moduli of between 9 and 23. The results obtained were influenced by the presence of pore defects and in some cases film defects in the fracture surfaces.

Gravity casting, where widely varying metal front velocities were observed throughout the filling process, did not provide sufficient control over filling to prevent the formation of these defects. The resultant properties therefore yielded the lowest Weibull modulus figure recorded and indicated that a convex metal front profile was needed to remove polystyrene degradation products effectively from the mold without entrapment.

Although the rates of filling in the bottom region of the plates made in a gravity-filled fashion greatly exceeded those suggested as a maximum to ensure that degradation products could escape from the mold, there was no correlation in the mechanical test results, or from observations of the fracture surfaces, to suggest that the casting quality was worse in this region than in any other area of the casting. To summarize, the mechanical property results clearly indicated that any type of non-planar metal fill profile had a serious, deleterious effect on the reproducibility of the casting properties.

## CONCLUSIONS

1. Filling of Lost Foam plates from the bottom under the influence of gravity, and with controlled counter-gravity conditions, showed that only very slow filling conditions were associated with reproducible properties, as characterized by the Weibull Modulus approach.
2. Counter-gravity filling with a velocity of about  $5 \text{ mm.s}^{-1}$  was associated with a Weibull Modulus of 23, a value below that obtained with an open cavity shape casting.
3. Examination of the filling process using real-time X-ray equipment showed that metal front velocities of around  $12 \text{ mm.s}^{-1}$  were associated with a break-up of the advancing liquid metal front into short fingers, which would lead inevitably to the entrapment of pattern degradation products.
4. Real-time X-ray images of the mold filling process showed that the uniform tensile strengths and higher Weibull Modulus associated with the slower metal front velocity of  $5 \text{ mm.s}^{-1}$  were the result of a planar advancing liquid metal front, which would be associated with a reduction in trapped pattern degradation products.

## REFERENCES

- Bakhtiyarov, S.I., Overfelt, R.A., Alagarsamy, A. and Vatankhah, B., "Study of Molten Metal – Polymeric Interface Dynamics in Counter Gravity Casting Process", Materials Processing Section, 20<sup>th</sup> Southeastern Conference on Theoretical and Applied Mechanics, Pine Mountain, GA, Paper No. MP7, p. 1 – 9, (2000).
- Bennett, S., Moody, T., Vrieze, A., Jackson, M., Ramsay, C.W. and Askeland, D., "Pyrolysis Defects in Aluminum Lost Foam Castings", *AFS Transactions*, vol. 107, p. 795 – 803, (1999).
- Bromley, L.A., "Heat Transfer in Stable Film Boiling", *Chemical Engineering Progress*, vol. 46, p. 221, (1950).
- Davies, P., "The Effect of Orientation on Mould Filling in Lost Foam Casting", MRes. thesis, School of Engineering, Dept. of Metallurgy and Materials, University of Birmingham, United Kingdom, (2002).
- Hill, M.W., Lawrence, M., Ramsay, C.W. and Askeland, D.R., "Influence of Gating and Other Processing Parameters on Mold Filling in the LFC Process", *AFS Transactions*, vol. 105, p. 443 – 450, (1997).
- Lawrence, M., Ramsay, C.W. and Askeland, D.R., "Some Observations and Principles for Gating of Lost Foam Castings", *AFS Transactions*, vol. 106, p. 345 – 356, (1998).
- Liu, J., Ramsay, C.W. and Askeland, D.R., "A Study of Foam-Metal-Coating Interaction in the LFC Process", *AFS Transactions*, vol. 105, p.419 – 425, (1997).
- Molibog, T.V. and Littleton, H., "Experimental Simulation of Pattern Degradation in Lost Foam", *AFS Transactions*, vol. 104, p. 1523 – 1554, (2001).
- Ramsay, C.W., Askeland, D.R. and Tschopp, M.A., "Mechanisms of Formation of Pyrolysis Defects in Aluminum Lost Foam Castings", *AFS Transactions*, vol. 108, p. 609 - 614 (2000).
- Rezvani, M., Yang, X. and Campbell, J., "Effect of Ingate Design on Strength and Reliability of Al Castings", *AFS Transactions* vol. 107, p. 181 – 188, (1999).
- Saffman, P.G. and Taylor, G., "The Penetration of a Fluid into a Porous Medium or Hele-Shaw Cell Containing a More Viscous Liquid", *Proceedings of the Royal Society A*, 245, p. 312 – 329, (1958).
- Wang, C., Ramsay, C.W. and Askeland, D.R., "Process Variable Significance on Filling Thin Plates in the LFC Process – The Staggered, Nested Factorial Experiment", *AFS Transactions*, vol. 105, p. 427 – 434, (1997).
- Warner, M., Miller, B.A. and Littleton, H., "Pattern Pyrolysis Defect Reduction in Lost Foam Castings", *AFS Transactions*, vol. 104, p. 777 – 785, (1998).
- Weibull, W., "A Statistical Distribution Function of Wide Applicability", *Journal of Applied Mechanics*, vol. 18, p. 293 – 297, (1951).

**AIL2. WFO World Foundry Congress, 4-7 June 2006, Harrogate, UK.**

**Mould Filling in the Lost Foam Casting of Al Alloys**

M J Ainsworth \* and W D Griffiths \*\*.

\* Gemco Cast Metal Technology, The Netherlands \*\* IRC, University of Birmingham, United Kingdom.

***Abstract***

The filling of vertically oriented plates was viewed using a real-time X-ray technique to examine the interaction of the cast Al with the polystyrene foam pattern. The plates were cast by means of a counter-gravity technique and bottom-gated running system.

Real-time X-ray images showed that the advancing metal front was associated with the development of finger-like protrusions as mould-filling velocity was increased. This inevitably led to the entrapment of the degradation products of the polystyrene pattern. Tensile properties of the plates showed a significant reduction when an unstable metal front was present during filling.

A similar type of instability was encountered during the displacement of liquid glucose by mercury in a Hele-Shaw cell. The empirically derived displacement velocity required to generate an interface instability concurred with the published mathematical model.

***Key words*** Finger-like, Planar, Viscosity, Instability.

## **Introduction**

Although the metal front velocity in Lost Foam casting is an important factor in determining the quality of the final product, the size, number and position of the gates are not significant in controlling the metal fill velocity [1]. The main focus of control of this variable has been on pattern composition, coating composition and coating thickness [2]. The “process choke” has been determined to be either the metal-foam interface or the metal-foam-coating interface depending on whether the decomposition of the foam or removal of the products was the most influential [3].

It is quite reasonable to assume that the velocity of the metal front should closely follow the rate of pattern decomposition and its subsequent removal from the mould in order to prevent any entrapment. This aspect has been studied by a number of authors [1,2,4] who reported that critical metal velocity windows between 12 and 23  $\text{mm}\cdot\text{s}^{-1}$  have produced fully filled castings with a low incidence of defects. Misrun and sand collapse was observed below the minimum figure and inclusions encountered above the upper limit.

Casting of aluminium into Lost Foam moulds is performed at significantly lower temperatures than those applied for ferrous alloys such as cast irons and steels. This has the effect of heating and melting the foam with little associated gasification and creates a two-phase system behind the advancing metal front [5]. The liquid degradation products at the foam–metal interface are much more viscous in nature than the molten metal that generates them [6] and it has been suggested that they can only be transported to the pattern coating by a convex metal front [7]. This front morphology is most easily achieved, when gravity casting, by means of a top gated running system [7,8] However, this system has a number of specific limitations; (i) mould fill in the direction of the gravity vector is almost totally uncontrolled and, (ii) the flow of foam degradation products in the opposite direction to that of the advancing front results in entrapment of liquid and gaseous polystyrene as well as surface turbulence within of metal.

In an attempt to overcome these limitations Bakhtiyarov [9] used a simple, vacuum-assisted, counter-gravity casting apparatus. A number of moulds containing vertically oriented plate patterns were cast and mould filling characteristics monitored. The observations suggested that metal flowed into and through the mould cavity as one continuous convex metal front and resulted in castings with improved properties.

Although the published literature indicates that the velocity of filling of Lost Foam moulds has a significant effect on the level of pattern degradation products found in the final casting, its influence on the shape of the advancing metal front and its associated relationship with the level of entrapped degradation products is less well reported. Almost all metal front morphology studies conducted in conjunction with the Lost Foam process have made use of a series of thermocouple or timing probes that have been placed in a pre-determined array in the pattern prior to casting. This method of profile morphology examination has a number of constraints that means that results can only be approximations even in the best cases.

Real-time X-ray imaging and data capture overcome many of the above limitations and, when applied to filling of Lost Foam moulds, have revealed that the metal front profile was planar at very low velocities and “finger-like” as velocities were increased [10]. The incidence of pyrolysis product entrapment defects in the resultant castings was also higher when unstable metal fronts were observed.

Aluminium castings made today have relatively thin walls of 15mm or less and are generally bottom gated. When produced by means of the Lost Foam process in this manner, the interaction of the relatively flowable liquid metal underneath a layer highly viscous liquid polystyrene is analogous to that demonstrated by Saffman and Taylor in a Hele-Shaw cell [11]. In the original experiment glycerine, confined between closely spaced, parallel sheets of glass, was driven out by significantly less viscous air. During this action, an instability occurred at the interface between the two fluids. This manifested itself as a series of round-ended fingers of the lower viscosity fluid penetrating into the denser one.

The main focus of this work has been to investigate (i) the effects of various metal front morphologies on the quality of the castings produced and, (ii) the mechanism of metal front morphology variation during the filling of the mould. To achieve this a counter-gravity filling technique was applied to filling simple plate patterns oriented in the vertical plane and the front profile monitored and recorded by means of a real time X-ray data capture device. Profile differences were characterized in terms of the mechanical properties of the castings produced and the type of defects found on the fracture surfaces of the samples.

Further, a physical model was constructed to simulate, at room temperature, the effects of velocity variation on the interface morphology of the metal front and the superimposed pattern degradation products. In this case front profile morphologies were captured by means of digital video recording medium.

## ***Experimental***

### **Casting Manufacture**

A simple plate pattern geometry was employed to evaluate the metal front profile behaviour and resultant mechanical properties of castings filled by counter-gravity techniques. The patterns were made from pre-expanded, T-grade polystyrene beads on an industrial pattern-moulding machine that was equipped with horizontally split aluminium tooling. All patterns were produced in one batch, and had a bead size of approximately 1 mm and a nominal pattern density of 29.9 kg/m<sup>3</sup>.

After ageing for 1 day each pattern was attached to its own running system to form a cluster. The system was made up of a short expanded polystyrene upsprue with a 10 mm hollow centre and a single, expanded polystyrene ingate of 10.4 cm<sup>2</sup> cross section.

Pattern and running system components were manually assembled using a proprietary hot-melt glue. An aluminium-silicate refractory, suspended in water, was applied by manually dipping each pattern until all but the bottom face of the upsprue was immersed. Each cluster was maintained in the fully immersed position for a

period of 5 s. and then placed on a rack prior to drying in a circulating air oven at 55 °C for a period of 4 hours. Coating capacity was measured by immersing a stainless steel plate of 100 mm x 100 mm x 2 mm thick into the coating bath and then measuring the weight of coating that adhered to the plate after removal. This value was maintained at 4.5 g  $\pm$  0.5 g for the duration of the operation and resulted in coating thicknesses ranging from 200 – 275  $\mu$ m.

A modified flask, that had internal dimensions of 0.45 m in length x 0.11 m width x 0.83 m depth and a centrally located, 70 mm diameter hole in the base, was used for making the moulds. This design produced the best image resolution in the real time X-ray unit. The hole in the base of the flask was fitted with a compressible ceramic sleeve that had an internal diameter and height of 40 mm so that one face of the sleeve was flush with the bottom of the flask. The pattern cluster was positioned in the flask by locating its upsprue into the sleeve so that the face of the upsprue was also flush with the base of the flask. Loose, dry, silica sand with an average grain size of 370  $\mu$ m was used to support the pattern in the flask. The flask was then filled with sand whilst being subjected to vertical vibration to bring about sand compaction. Filling took approximately 30 s. and maximum sand grain compaction was considered to have been achieved when there was no longer any reduction in the bulk density of the sand mass. This situation was always achieved within 10 seconds of completion of the filling cycle.

Counter-gravity filling was achieved by using a pressure vessel of welded steel construction that housed a silicon carbide crucible (Fig. 1). This crucible held a pre-modified LM25 (Al-7wt.%Si) alloy into which one end of a refractory coated “riser tube” was inserted. The other end of the tube was fitted with a flange that located into a recess on the lid of the vessel so that its upper face was flush with the top face of the vessel. All mating faces were made pressure tight by means of gaskets. The vessel was fitted with a coupling to allow connection of a compressed air supply, a pressure gauge, a pressure relief valve and thermocouple for monitoring the metal temperature in the crucible.

Immediately after sealing of the vessel with the crucible of liquid Al in place, a gasket was placed on the rim of the riser tube in line with the upper face of the pressure vessel and the mould placed on the vessel lid. The bottom inlet to the mould was located over the riser tube and the complete mould clamped to the vessel by means of an A frame arrangement. Compressed air was used to pressurize the chamber and regulated by a pressure control valve. The chamber was pressurized using a manually operated valve between the pressure regulator and the inlet to the chamber.

All castings were filled at a temperature of 785 °C, and the filling process monitored using a 160 kV real-time X-ray with the image captured using a S-VHS 50 Hz video recorder.

### Mechanical Properties

Specimens for tensile strength determination were taken from locations throughout two plate castings (Fig 2). One of the samples had been filled in association with a cellular metal front and the other where a planar front had been observed. The plate

that filled by means of a planar metal front did not fill completely and exhibited a misrun defect along its upper edge. In this case samples were only obtained from locations A – T.

The tensile values obtained from the test bars were subject to a Weibull analysis [12]. This technique more accurately describes the distribution of the tensile strength results of Al-7Si-Mg alloy castings when compared with the Gaussian distribution.

#### Metal – Foam Interface Modelling

A physical model was constructed to simulate the interaction of molten metal and liquid polystyrene observed during counter-gravity casting of the plates made in the first experiment (Fig. 3). The model consisted of a steel profile base that supported a simple air cylinder in the horizontal plane. The outlet from this cylinder was connected to a vertically positioned mould by a set of steel pipe-work. Both the displacement side of the cylinder and the pipe-work were filled with mercury at a viscosity of 1.55 mPa.s at 20°C [13]. This material was chosen to simulate liquid aluminium because it (i) was a liquid metal at room temperature, (ii) eliminated any density conflicts that might have arisen in the choice of the substitute for liquid polystyrene and (iii) was relatively close to the viscosity as liquid Al (1.220 mPa.s at 20°C) [14].

The mould cavity had the same dimensions as the polystyrene patterns in Fig. 1 with the two large opposing mould sides being constructed from glass plates that permitted observations to be recorded via a high-speed video camera. The complete mould assembly was bolted to a steel base plate in which the ingate was located and a neoprene gasket of 3 mm thickness was used between both parts of the assembly to prevent fluid leakage.

The upper face of the mould was left open to atmosphere which permitted the mould cavity to be filled with a clear glucose syrup of viscosity 95 000 mPa.s. This material was chosen because it had a similar density and as high a viscosity as could be effectively applied.

After filling the model with the two substitute materials, the piston in the air cylinder was actuated, by means of an oil-over-air cylinder that was positioned in line with the main air cylinder and coupled to it by a shaft-to-shaft connection. The secondary drive cylinder was connected to the mains air supply (at 8 bar pressure) and its piston speed, and associated mercury displacement speed into the mould, were controlled via a flow regulator situated on the oil outlet side of the unit.

### **Results**

#### Mould Filling

The application of pressures of 34.5 kPa and above within the casting unit gave rise to metal fronts with long finger-like protrusions that were present throughout the filling of the plate (Fig. 4). The average filling speed, captured from the real time X-ray image of a plate filled using a chamber pressure of 68.9 kPa was 24 mm.s<sup>-1</sup> and the rate of fill was such that the liquid metal reached the top of the plate in 21 s. However, the liquid and gaseous pattern degradation products preceding the front could not escape through the mould coating at the same rate and became temporarily trapped

in this region. It took a further 7 s. for this trapped material to leave the mould cavity and pass into the surrounding sand.

The average filling velocity of plates cast with chamber pressures of between 27.6 – 31.0 kPa was  $13 \text{ mm.s}^{-1}$ . The metal front profile assumed a slightly convex shape across the complete width of the plate with the leading region being situated towards the centre of the plate (Fig. 5). It was characterized by a series of small protrusions, approximately 5 mm in height that gave it a cellular appearance.

A reduction of the chamber pressure by only 3.4 kPa to 24.1 kPa reduced the average fill velocity to approximately  $5 \text{ mm.s}^{-1}$ . This produced an almost horizontal metal front that had a profile devoid of any protrusions (Fig. 6) and was classified as a planar type front. However, the filling velocity was so slow that it resulted in an arrest of the metal front approximately 30 mm from the top of the plate. This gave rise to a short run defect that was visible along the upper edge of the casting.

### Mechanical Properties

Ultimate tensile strength results were obtained from samples taken from one plate in which a cellular front was observed and from one in which a planar front was observed during the filling cycle (Table 1). The results related to filling with a cellular metal front were significantly lower than those where a planar metal front was present during filling.

The Weibull distribution was plotted for each of the two sets of UTS results (Fig. 7). The modulus value related to mould filling with a cellular metal front was only 10.6 whereas that related to a planar metal front was significantly higher at 23.2.

### Metal – Foam Interface Modelling

The interaction of mercury and glucose syrup within the physical casting model produced a planar interface up to a vertical displacement velocity of  $0.020 \text{ m.s}^{-1}$ . As the speed of the metal front increased above this value, the interface became unstable. This was apparent by the formation of a series of fingers (Fig. 8) that were observed across the length of the interface. The displacement speed had a direct effect on the number and length of these fingers.

At  $0.022 \text{ m.s}^{-1}$  one finger was seen emerging from the central area of the metal front. Its length grew to a maximum of 15 mm ahead of the main front during the filling cycle. In contrast, a displacement velocity of  $0.039 \text{ m.s}^{-1}$  caused the initially planar metal front to break up completely into 5 distinct fingers. These fingers were relatively long in comparison to their width and also increased in length during the displacement cycle. The predominant finger was situated centrally along the metal front, directly above the ingate and protruded at its maximum to about 70 mm ahead of the tip of the nearest trailing finger. The maximum distance between the tips of the leading and lagging fingers was measured at 105 mm.

### **Discussion**

The main aims of these experiments were to determine the level of benefit, in terms of casting quality improvement that could be achieved by application of counter-

gravity filling to Lost Foam moulds and to simulate the interaction of the metal front and liquid polystyrene during the filling process in a room temperature model.

### Mould Filling

The results show that as the velocity of the metal front increased above a critical speed, it became unstable and began to break up into a number of fingers that preceded the main body of flow. These fingers are thought to have been associated with oxide films covering their surface. As the fingers grew in size, and because of the physical constraints of the mould walls, they remerged together. The recombining of these individual metal streams is likely to have caused entrainment of oxide films. Additionally, when very high velocities were observed during filling (Fig. 4), some fingers were seen to travel in an upwardly diagonal direction across the mould that recombined initially at their tips. The area of the product directly below was, at that time, unfilled and would have been rich in liquid and gaseous polystyrene degradation products. Although these regions were seen to fill shortly afterwards, presumably as a result of gaseous degradation product escape through the walls of the mould and because of the dynamic pressures in the liquid metal, it is reasonable to conclude that some pyrolysis products did not escape and became entrapped in the body of the final casting.

Although neither of the above phenomena were observed when a fill speed of  $5 \text{ mm}^{-1}$  was applied, the metal front was arrested approximately 30 mm short of the top of the mould cavity. This resulted in a short run defect being apparent in the final casting which was the result of lack of metal fluidity in the final stages of filling caused by excessive heat loss to the mould. It is interesting to note that where the metal front was relatively stable, ie. in planar or cellular form, its profile was convex. The location of the ingate and the relatively controlled and constant flow achieved through counter-gravity filling were considered to be primary factors in achieving this.

### Mechanical Properties

Published literature has shown that castings manufactured in open moulds, under controlled conditions and with well designed running systems have resulted in Weibull moduli of up to about 38. This contrasted strongly to the results obtained in this set of experiments where a Weibull moduli of 10.6 was obtained from a plate associated with cellular filling and a corresponding value of 23.2 achieved by planar filling.

No degassing of the melt was carried out prior to casting and it is possible that some hydrogen gas porosity was present in the castings produced. It is therefore reasonable to assume that that, in these experiments, the factor limiting the value of this statistic changed from metal front stability at a fill speed of  $13 \text{ mm}^{-1}$  to hydrogen porosity at a fill speed of  $5 \text{ mm}^{-1}$ . However, the results clearly indicate that any type of non-planar metal fill profile has a serious, deleterious effect on the reproducibility of the casting properties.

### Metal – Foam Interface Modelling

The room temperature model used to simulate the interaction of liquid aluminium and liquid polystyrene clearly demonstrated that displacement of a viscous fluid by a

significantly more flowable one caused an instability to occur above a specific displacement velocity.

The criterion for the development of this phenomenon between two fluids of different viscosity passing through a porous medium is given by;

$$\left( \frac{\mu_2}{k_2} - \frac{\mu_1}{k_1} \right) V + (\rho_2 - \rho_1) g \leq 0$$

where  $\mu$  = dynamic viscosity,  $k$  = permeability,  $V$  = velocity and  $\rho$  = density. Subscripts 1 and 2 refer to the upper and lower fluids respectively, for a case where fluid 1 is less viscous than fluid 2, and fluid 1 is driven upwards into fluid 2.

For a Hele-Shaw cell consisting of two plane parallel plates,  $k_1$  and  $k_2$  can be replaced by  $b^2/12$ , where  $b$  = the distance between the two plates. The critical velocity for the onset of the instability can therefore be determined from;

$$V = \frac{-g(\rho_2 - \rho_1)}{\frac{\mu_2}{b^2/12} - \frac{\mu_1}{b^2/12}}$$

For all experiments  $b$  was fixed at 15 mm and the applied density and viscosity of mercury were  $13\,570 \text{ kg.m}^{-3}$  and  $1.55 \text{ mPa.s}$  respectively. The corresponding values for glucose were  $1\,050 \text{ kg.m}^{-3}$  and  $95\,000 \text{ mPa.s}$ . Therefore, for liquid Hg driven upwards against glucose,  $V = 0.0242 \text{ m.s}^{-1}$ .

This value concurs well with the results obtained and in order for a liquid aluminium front to become unstable when driven upwards against liquid polystyrene at a velocity of  $0.005 \text{ m.s}^{-1}$ , the viscosity of the liquid polymer would need to be in the order of  $50 \text{ Pa.s}$ . The viscosity of a polystyrene melt is affected dramatically by molecular weight, temperature and shear rate and further work is needed to verify that this viscosity is apparent during the production of Lost Foam castings.

### **Conclusions**

1. Filling of Lost Foam plates from the bottom under the influence of controlled counter-gravity conditions, showed that only very slow filling conditions were associated with reproducible properties, as characterized by the Weibull Modulus approach.
2. Counter-gravity filling with a velocity of about  $5 \text{ mm.s}^{-1}$  was associated with a Weibull Modulus of 23, still much less than can be obtained with an open cavity shape casting.
3. Examination of the filling process using real-time X-ray equipment showed that metal front velocities of around  $13 \text{ mm.s}^{-1}$  were associated a break-up of the advancing liquid metal front into short fingers, which would lead inevitably to the entrapment of pattern degradation products.

4. The real-time X-ray images showed that the uniform tensile strengths and higher Weibull Modulus associated with the slower metal front velocity of  $5 \text{ mm.s}^{-1}$  were the result of a planar advancing liquid metal front, which would be associated with a reduction in the trapped degradation products.
5. Room temperature modelling of the effects of displacement velocity on the metal front profile and interface stability exhibited similarities to observations recorded during filling of Lost Foam moulds with aluminium and the empirically determined critical velocity at which an instability occurred was consistent with that mathematically derived.

### References

1. Hill M W, Lawrence M, Ramsay C W and Askeland D R, *Influence of Gating and Other Processing Parameters on Mold Filling in the LFC Process*, AFS Transactions, vol. 105, p. 443 – 450, (1997).
2. Wang C, Ramsay C W and Askeland D R, *Process Variable Significance on Filling Thin Plates in the LFC Process – The Staggered, Nested Factorial Experiment*, AFS Transactions, vol. 105, p. 427 – 434, (1997).
3. Lawrence M, Ramsay C W and Askeland D R, *Some Observations and Principles for Gating of Lost Foam Castings*, AFS Casting Conference, May 1998, Pre-print No. 98-112.
4. Ramsay C W, Askeland D R and Tschopp M A, *Mechanisms of Formation of Pyrolysis Defects in Aluminium Lost Foam Castings*, AFS Casting Conference, April 2000, Pre-print 00-131.
5. Zhao Q, Burke J T and Gustafson T W, *Foam Removal Mechanism in Aluminum Lost Foam Casting*, AFS Transactions, vol. 110, p. 1399 – 1414, (2002).
6. Cox W P and Ballam R L, *Calculation of the Apparent Viscosity of Polystyrene Melts*, Journal of Applied Polymer Science, vol. 4 Issue 10, p. 121, (1960).
7. Molbilog T V and Littleton H, *Experimental Simulation of Pattern Degradation in Lost Foam*, AFS Transactions, vol. 109, p. 1523 – 1554, (2001).
8. Davies P, *The Effect of Orientation on Mould Filling in Lost Foam Casting*, MRes. Thesis, School of Engineering, Metallurgy and Materials, University of Birmingham, 2002.
9. Bakhtiyarov S I, Overfelt R A, Alagarsamy A and Vatankhah B, *Study of Molten Metal – Polymeric Interface Dynamics in Counter Gravity Casting Process*, Proceedings of the SECTAM-XX, April 2000.
10. Sun W L, Littleton H E and Bates C E, *Real-Time X-ray Investigations on Lost Foam Mold Filling*, AFS Transactions, vol. 110, p. 1347 – 1356, (2002).
11. Saffman P G and Taylor G, *The Penetration of a Fluid into a Porous Medium or Hele-Shaw Cell Containing a More Viscous Liquid*, Proc. Royal Society, 245, p. 312 – 329, (1958).
12. Weibull W, *A Statistical Distribution Function of Wide Applicability*, Journal of Applied Mechanics, vol. 18, p. 293 – 297, (1951).
13. Elert G, *The Physics Hypertextbook*, 1998.
14. Dinsdale A T and Quested P N, *The Viscosity of Aluminium and Its Alloys – A Review of data and Models*, Journal of Materials Science, vol. 39, p. 7221 – 7228, (2004).

**Tables**

Ultimate Tensile Strength (MPa)												
Fill Pressure	Test Piece Position											
	A	B	C	D	E	F	G	H	I	J	K	L
24.1 kPa	227	196	205	197	203	212	199	198	206	209	205	207
27.6 kPa	106	133	126	126	109	108	117	119	126	121	123	135
	M	N	O	P	Q	R	S	T	U	V	W	
24.1 kPa	215	222	211	190	220	202	217	212	n/a	n/a	n/a	-
27.6 kPa	130	140	128	94	128	134	131	137	140	144	124	-

Table 1 Ultimate Tensile Strength Results Achieved at Various Locations in Plates Cast in a Counter-gravity Fashion at Two Different Fill Press

**Figures**

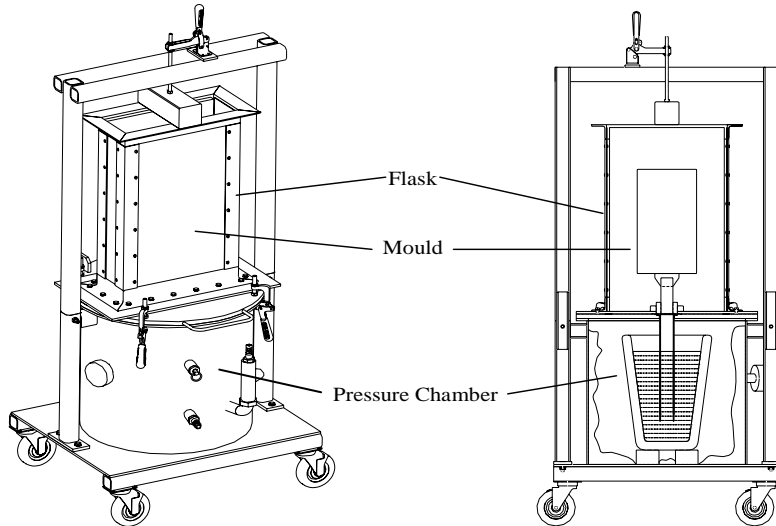


Fig 1a Isometric View of the Counter-gravity Casting Machine with Mould in Position

Fig 1b Section View of the Counter-gravity Casting Machine with Mould in Position

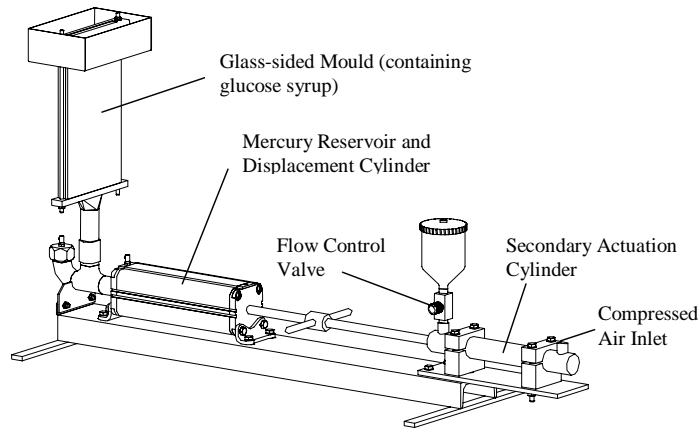


Fig 3 Isometric View of the Physical Model Used to Observe Fluid Interface Morphologies at Varying Displacement Velocities

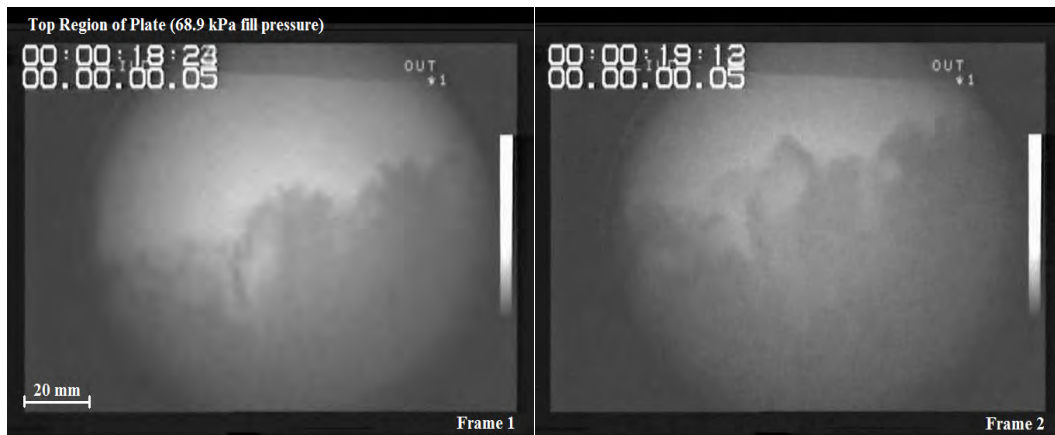


Fig 4 Finger-type Front in the Upper Region of a Plate (Fill Pressure = 68.9 kPa)



Fig 5 Irregular Metal Front in the Upper Region of a Plate (Fill Pressure = 27.6 kPa)

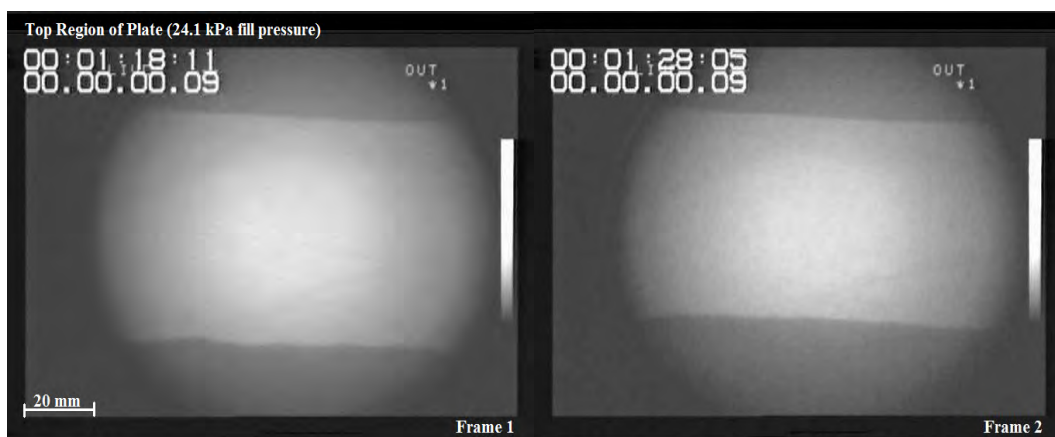


Fig 6 Planar-type Metal Front in the Upper Region of a Plate (Fill Pressure = 24.1 kPa)

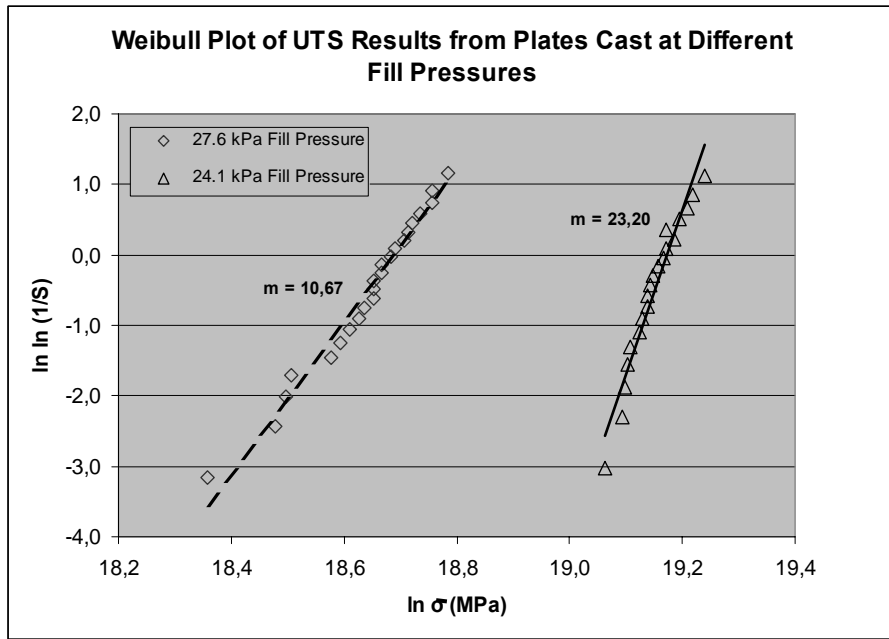


Fig 7 Weibull Plots of the Ultimate Tensile Strength of Samples Taken from Plates Filled in a Counter-gravity Fashion at Two Different Fill Pressures.

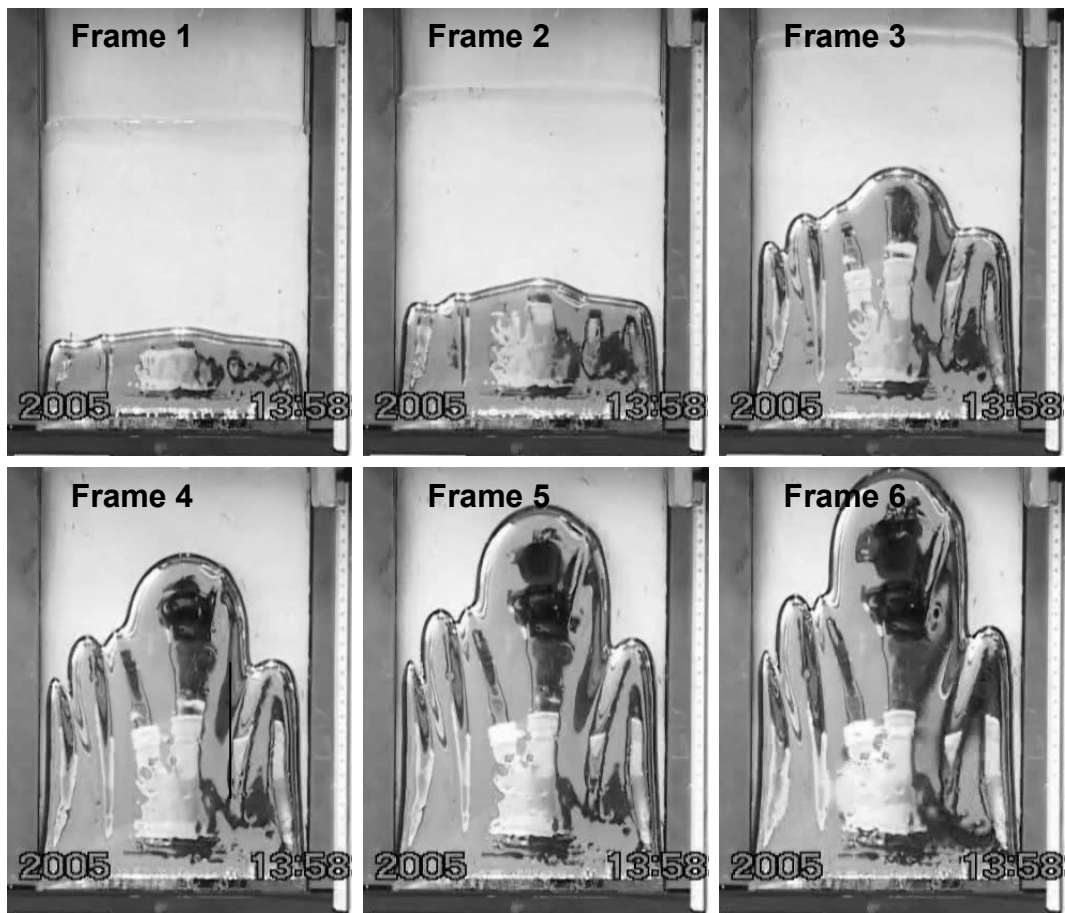


Fig 8 Saffman-Taylor Instability Observed during the Displacement of Glucose Syrup (viscosity 95 000 mPa.s) by Liquid Mercury (viscosity 1.55 mPa.s) in a Hele-Shaw Cell.

**AII.3. VDG Lost Foam Council Conference, 11-12 October 2006,  
Paderborn, Germany.**

**Mould Filling in the Lost Foam Casting Process for  
Aluminium Alloys**

**<sup>1</sup>W. D. Griffiths, <sup>2</sup>M. J. Ainsworth and <sup>3</sup>P. J. Davies**

1. Department of Metallurgy and Materials, School of Engineering,  
University of Birmingham, Edgbaston, Birmingham, UK. B15 2TT.

2. Gemco Cast Metal Technology B.V., Science Park Eindhoven 5053, Eindhoven, The  
Netherlands.

3. Honda of the UK Manufacturing Ltd., Highworth Road,  
South Marston, Swindon, UK. SN3 4TZ

**Abstract**

Recent research has been aimed at investigating the factors that determine the quality of the final product during the casting of Al alloys using the Lost Foam process. Research has been carried out on the role of the coating in removing liquid pattern degradation products, and experiments suggest that absorption of the liquid polystyrene can occur by the coating, but this is dependant upon the degradation of the polystyrene to a sufficiently low molecular weight liquid. In addition, the filling of vertically oriented plates, imaged with real-time X-ray equipment, has shown that in gravity casting experiments the advancing metal front developed finger-like protrusions whether the metal entered the pattern from above or below. In countergravity filling experiments it has been shown that, as the velocity with which the mould was filled was decreased, the nonuniformity of the metal front was also decreased, reducing the entrapment of the degradation products of the polystyrene pattern. An approximate value for the maximum velocity of mould filling associated with a smooth advancing metal front was found to be about  $5 \text{ mm.s}^{-1}$ .

**Introduction**

The Lost Foam casting process is well known for its versatility and holds the promise of producing complex castings more economically than conventional casting processes. However, in the case of casting of Al alloys, the degradation of the expanded polystyrene pattern is associated with large numbers of defects that result in castings with high porosity and high rejection rates during production, particularly when production of the casting is first attempted [1-3].

The liquid metal fills the mould by causing the polystyrene pattern to degrade as it is heated. Firstly there is a collapse of the expanded polystyrene bead structure, then melting, followed by a reduction in molecular weight of the liquid polystyrene, which finally breaks down to

vapour byproducts. It has been suggested that the behaviour of the pattern coating in controlling the passage of these liquid and vapour degradation products is an important factor in controlling the final casting quality [4,5].

Since this is a new casting process the factors that control successful casting production are not well understood. Consequently there is considerable need for further research and in the work reported here the behaviour of the coating in removing the degradation products of the polystyrene pattern has been examined, together with the effect on casting quality and properties of using a counter-gravity filling method.

## **Experimental Procedure**

To examine the possibility of wicking of liquid polystyrene degradation products into the pattern coating an experiment was carried out that involved the degradation of an expanded polystyrene foam sample in contact with a typical pattern coating, (characterised as a low permeability coating). A sketch of the experiment has been shown in Figure 1. A small sample of polystyrene pattern material, (of 20 mm diameter x 10 mm thick and of density  $23.4 \text{ kg.m}^{-3}$ ), was placed in a resistance-heated tube furnace, set to varying temperatures of between  $400^{\circ}\text{C}$  to  $1000^{\circ}\text{C}$ . The temperature of the sample was then allowed to rise to between  $300^{\circ}\text{C}$  and  $500^{\circ}\text{C}$ , (determined by an  $80 \mu\text{m}$  diameter thermocouple embedded in the coating attached to the sample). In this way polystyrene samples that had experienced different amounts of thermal degradation were obtained. When the required temperature was reached the sample was rapidly quenched using a water-cooled chill to minimise any further degradation of the polymer, thus preserving the characteristics of the polymer at that temperature and time. Gel Permeation Chromatography was then used to determine the average molecular weight of the polymer remaining on or in each coating after being heated, as well as being used to characterise the starting pattern material. This experiment was carried out on both typical expanded polystyrene foam pattern material, and Br-treated expanded polystyrene foam.

In addition, expanded polystyrene plate patterns of  $440 \text{ mm} \times 180 \text{ mm} \times 10 \text{ mm}$ , coated with  $\sim 500 \mu\text{m}$  thickness high- and low-permeability coatings, were cast in a flat, horizontal orientation at  $850^{\circ}\text{C}$  using A319 aluminium alloy, (Al-6wt.%Si-3.5wt.%Cu). Pattern and coating temperatures experienced during filling were measured by the same  $80 \mu\text{m}$  diameter type K thermocouples, which were embedded within the pattern at its centre, and within the pattern coating at the same positions, along the centre line of the plate, (see Figure 2). The filling of these castings was also examined using real-time X-ray radiography.

Real-time X-ray radiography was also applied to study the filling of a foam pattern plate in a vertical orientation. These were of two types; in one case a liquid Al alloy was cast into a conventional running system, (that is, conventional for Lost Foam casting), which led to an ingate at either the top or bottom of a vertically oriented pattern plate, thereby filling the plate from either the top or the bottom. This was intended to be a reflection of the practice in open cavity casting processes where it would be expected that filling a mould from the top would produce a casting with more variable (and lower) mechanical properties than if the mould cavity was filled from the bottom.

The second type of mould filling used the equipment shown in Figure 3. In this experiment the pattern was placed in a mould box placed above a steel chamber that contained a crucible of liquid metal. Applying an overpressure to this chamber forced the liquid metal up a connecting tube to enter the plate pattern from below. By varying the overpressure applied to the chamber, the velocity of the liquid metal passing into the pattern plate was varied, and the real-time X-ray image showed the effect of this variation in velocity on the shape of the liquid metal front, and the entrainment of the pattern degradation products into the liquid metal, as it filled the mould. These experiments were cast in both Al-10wt.%Si-0.3wt.%Mg alloy at 785°C, for the gravity casting experiments, and Al-7wt.%Si-0.3wt.%Mg (A356) alloy at 785°C, for the countergravity casting experiments. The cast plates were subsequently sectioned and machined into tensile test specimens so that the effect of filling velocity on mechanical properties could be assessed.

## Results

Table 1 shows the molecular weight of polystyrene foam samples held for different times at different temperatures in the experiment shown in Figure 1. The original molecular weight of the foam was about 290,000. As the furnace temperature was increased, but the sample removed when it reached the same temperature, (for example, 300°C), the molecular weight of the degraded sample tended to increase. In other words, as the sample was heated more quickly, but to the same temperature, less degradation of the polymer took place. For samples placed in the same furnace temperature, (for example, 800°C), but heated to higher temperatures, (and therefore heated for longer times), increased degradation of the polymer occurred.

After each experiment was completed the coating was examined to determine if the degraded (liquid) polymer had wetted the coating surface and had been wicked into the coating interior. The results showed that the degraded polystyrene wetted the low permeability coating once its molecular weight was reduced to about 100,000, but that wicking of the liquid polymer degradation products into the coating occurred when the molecular weight had been reduced to about 13,000, about 5% of the original molecular weight.

The same experiment was carried out for a high permeability coating[6] and the same effects were found. Increasing time and temperature resulted in a reduction in molecular weight, until wetting of the coating occurred. As the molecular weight reduced still further the liquid polymer was wicked into the coating. However, in the case of the high permeability coating, wicking occurred when the molecular weight was reduced to about 70,000, about 24% of the original molecular weight.

Table 2 shows the change in molecular weight found with the Br-treated polystyrene foam. This showed wicking behaviour at a molecular weight of below about 23,000, a reduction in molecular weight to about 7% of the original molecular weight. The Br-treated pattern material therefore behaved in a similar way to the untreated foam, but with the low molecular weight liquid polymer residue occurring at lower temperatures in the experiment, more readily than in the case of the untreated polystyrene.

Figure 4 shows temperature-time curves obtained from the coating and from within the foam pattern during filling of the mould, for the locations shown in the sketch in Figure 2. All four thermocouples within the horizontal plate showed a steep temperature gradient ahead of the advancing metal front, but the thermocouples within the coating showed that here the temperature rose only slowly. For example, by the time the liquid metal had reached thermocouple 4, closest to the end of the plate, the thermocouple embedded in the coating at location 1, closest to the ingate, (and 300 mm away), had risen to only about 430°C. The thermocouples at locations 2 and 3 at this time were at still lower temperatures, (about 390° and 180°C respectively). The thermocouples in the coatings were only an indication of the temperature at the coating-pattern interface but suggested that the temperature at this point should be much lower than the metal temperatures within the filling casting.

In the real-time X-ray studies of filling of the vertically oriented plates the gravity cast experiments showed an irregular metal-foam interface, whether the mould was filled from above or from below, (see Figures 5 and 6 respectively). The mean UTS values shown in Table 3 indicate similar, low values in each case, and the Weibull modulus values, used here as an indication of the scatter of the tensile properties of the castings, were also low. Values of 6 and 9 were found, whereas values of more than 20 have been typically reported for open cavity castings. In the counter-gravity filled castings, the nature of the advancing metal front was quite different. At a velocity of 24 mm.s<sup>-1</sup>, a highly irregular metal front was observed, (see Figure 7). When the castings were filled more slowly, at 13 mm.s<sup>-1</sup>, the advancing metal front lost its highly irregular appearance and became what may be termed “cellular”, (see Figure 8). This is similar in appearance to the metal front seen in Figure 6. Despite the apparent improvement in the filling of the mould the mean UTS value (see Table 3) was still low, and the Weibull modulus of 11 again indicated a poor quality casting. (These castings were made in a slightly different alloy to the gravity cast plates, but the comparison should not be misleading.) When the mould filling velocity was decreased to only about 5 mm.s<sup>-1</sup> a smooth metal-pattern interface was obtained, (see Figure 9). The mean UTS values from this casting were significantly improved, (by 66% compared to the casting shown in Figure 8), and the Weibull modulus improved to 23, a value associated with open cavity castings. However it should be noted that this casting, was filled so slowly that the metal solidified prematurely before the casting was complete.

## Discussion

The experiments involving the thermally degraded polystyrene in contact with the coating suggested that wicking of liquid polymer into the coating can occur once the liquid has reached a sufficiently low molecular weight, and therefore viscosity. The molecular weight at which this occurred depended upon coating permeability.

A comparison between the temperatures recorded in a casting being filled, (shown in Figure 4), and the temperatures and heating times necessary for the wicking to take place in the experiment shown in Figure 1, (the results of which have been shown in Table 1), suggest that, in a casting, any wicking of liquid polymer into the coating must occur after the metal front has passed. For example, in Table 1 wicking occurred with a sample placed in a furnace temperature of 600°C and heated to 450°C, resulting in a molecular weight of about 11,900. The time taken for this reduction in molecular weight was 590 s. When the polystyrene was

heated to 450°C with a furnace temperature of 800°C, resulting in a molecular weight of about 96,400, (which took 205 s), no wicking occurred because of the high molecular weight of the liquid residue. In the case of the Br-treated polystyrene, wicking occurred when the molecular weight was reduced to 19,700 (see Table 2), a process that took 830 s in the experiment. The heating curves shown in Figure 4 for the coating, where filling of the mould took place in less than 60 s, although only a guide to the temperature of the polystyrene degradation products displaced to the coating-pattern interface, suggest that insufficient time and heating would have occurred for the polymer residue to break down to a sufficiently low molecular weight liquid to be absorbed by the coating, at least until after the metal front had passed.

These experiments therefore clarify the role of the pattern coating in removing liquid polymer degradation products in the Lost Foam casting process. It was proposed by Sun et al. [4] that the liquid polymer was wicked into the coating at a critical temperature. Conversely, Zhao et al. [5] proposed that liquid polymer degradation products were instead pushed to the coating-casting interface and were not absorbed by the coating, but remained there as the metal front passed by and eventually vaporised with only the vapour passing through the coating. These results suggest instead that both theories are partly true. The liquid polymer degradation products displaced to the coating-casting interface should remain there while the casting is filling. At the coating surface they continue to break down into lower molecular weight products until their viscosity is reduced sufficiently and they are then wicked into the coating, but this should occur after the passage of the liquid metal front. This behaviour may not therefore have a great effect on the filling of the mould, although it would affect the area of the coating through which vapour pattern degradation products can pass, but it would certainly strongly affect surface quality.

The appearance of the liquid metal front advancing up through the pattern in the countergravity filling experiments shown in Figures 7 to 9, show that it is possible for the Lost Foam casting process to produce well-filled castings with good and uniform mechanical properties, (as shown in Table 3). A comparison of the appearance of the metal fronts in Figures 8 and 9 and the tensile properties of the castings given in Table 3 suggest that only a completely smooth advancing metal front can give good casting properties. This poses a problem, if such a smooth metal front can only be obtained by such slow filling rates that misrun castings can occur.

One explanation for the transition in the shape of the metal fronts shown in Figures 7 to 9 may be that the countergravity filling of the pattern was preceded by a volume of hot air, originally in the connecting tube between the liquid metal and the pattern, which would be displaced up into the pattern once filling had begun. Rapid injection of this volume of hot air into the base of the pattern could lead to some initial degradation and partial collapse of the pattern structure and give rise to the highly irregular metal front seen in Figure 7. However, the transition from the “cellular” to the planar front in Figures 8 and 9 suggests other mechanisms that may control the shape of the metal-pattern interface and the entrainment of pattern degradation products into the casting.

## Conclusions

1. Liquid polymer degradation products from an expanded polystyrene pattern can be absorbed (wicked) into the pattern coating once they have degraded to a sufficiently low molecular weight. This molecular weight needed for wicking to take place depends upon the permeability of the pattern coating.
2. Real-time X-ray examination of countergravity filling of a vertical pattern plate showed that smooth filling of the mould can be achieved at a velocity of about  $5 \text{ mm.s}^{-1}$ , producing a sounder casting with good mechanical properties.

## References

1. S. Shivkumar, L. Wang and D. Apelian, JOM, 1990, 38-44.
2. M. H. Warner, B.A. Miller and H.E. Littleton, AFS Trans., 1998, 777-785.
3. S. Bennett, T. Moody, A. Vrieze, M. Jackson, D.R. Askeland, C.W. Ramsay, AFS Trans., 1999, 795-803.
4. Y. Sun, H.L. Tsai and D.R. Askeland, AFS Trans., 1992, 297-308.
5. Q. Zhao, J.T. Burke and T.W. Gustafson, AFS Trans., 2002, 1399-1414.
6. P. J. Davies and W. D. Griffiths, proc. conf., 67<sup>th</sup> World Foundry Congress, Harrogate, UK, Jun. 5-6, 2006, paper no. 23.

## TABLES

		Sample Temperature (°C)				
		300	350	400	450	500
Furnace Temperature (°C)	400	156,000				
	450	138,000	93,500			
	500	167,000	128,000	31,700		
	600	179,000	170,000	117,000	<b><i>11,900</i></b>	<b><i>no signal</i></b>
	800	221,000	182,000	168,000	96,400	<b><i>13,100</i></b>
	1000	211,000	191,000	193,000	169,000	52,000

Table 1. Molecular weights of expanded polystyrene foam samples having undergone differing amounts of thermal degradation. The values in italics are from the samples that showed that the polymer had wicked into the low permeability coating. (Original molecular weight about 290,000).

		Sample Temperature (°C)				
		300	350	400	450	500
Furnace Temperature (°C)	400	118,000				
	450	86,000	40,200			
	500	64,500	43,400	<b><i>19,700</i></b>		
	600	134,000	59,500	29,500	<b><i>8,210</i></b>	<b><i>no signal</i></b>
	800	217,000	98,600	49,200	<b><i>22,800</i></b>	<b><i>no signal</i></b>
	1000	247,000	162,000	69,300	41,200	13,700

Table 2. Molecular weights of Br-treated expanded polystyrene foam samples having undergone differing amounts of thermal degradation. The values in italics are from the samples that showed that the polymer had wicked into the low permeability coating. (Original molecular weight about 340,000).

Mould filling method	Mean UTS (Mpa)	Weibull Modulus
Gravity cast; (Al-10wt.%Si)		
Top-filled	122	6
Bottom-filled	125	9
Counter-gravity cast; (Al-7wt.%Si)		
Filling velocity of ~ 24 mm/s	not determined	not determined
Filling velocity of ~ 13 mm/s	125	11
Filling velocity of ~ 5 mm/s	208	23

Table 3. Summary of tensile properties of Al test bars taken from cast Lost Foam plates produced by different mould filling methods.

**FIGURES**

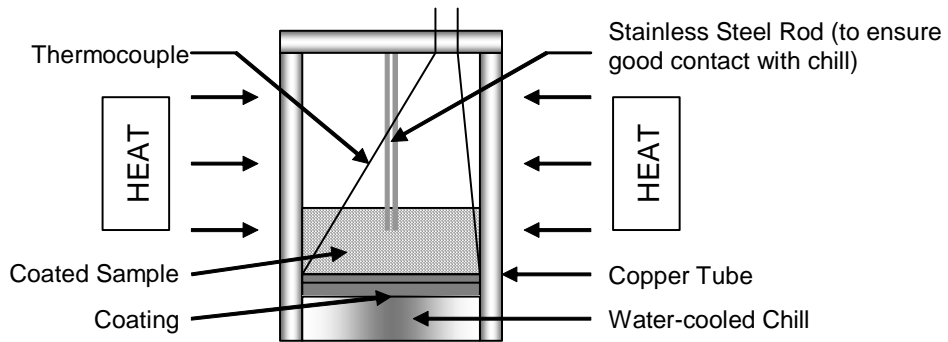


Figure 1. Diagram of experimental arrangement for the controlled thermal degradation of coated expanded polystyrene samples.

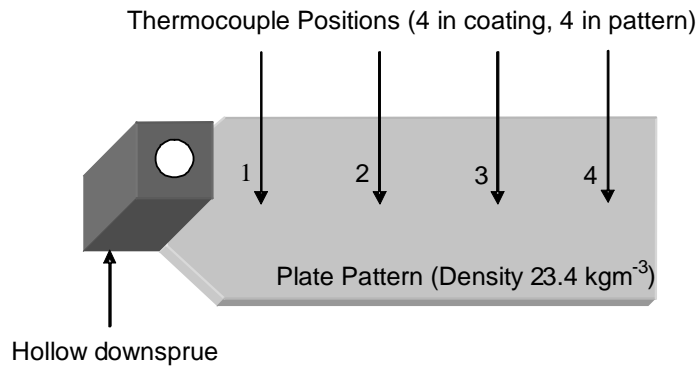


Figure 2. Location of thermocouples in the coating and the pattern for the horizontal pattern plate casting experiments, (seen from above).

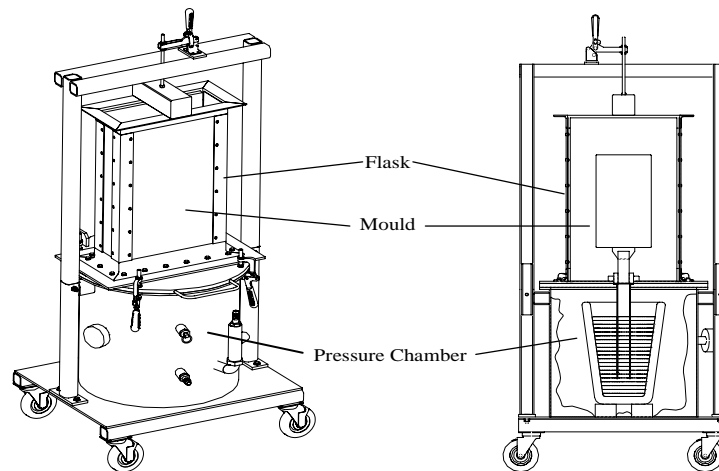


Figure 3. Diagram of the experimental arrangement used for the counter-gravity casting of Lost Foam plate patterns from below.

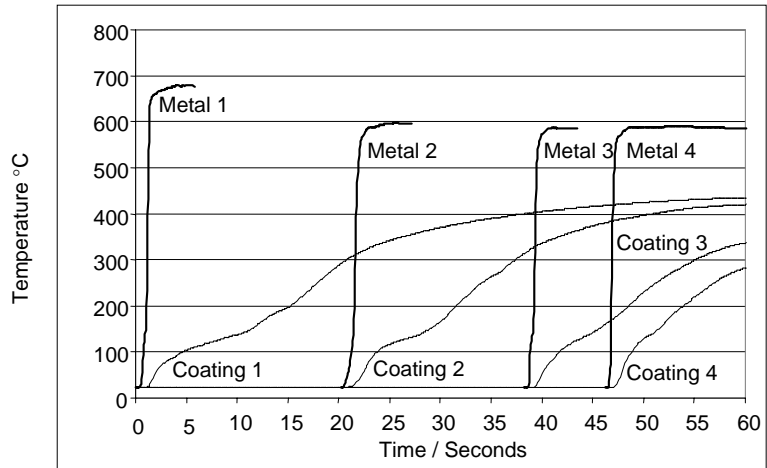


Figure 4. The temperatures recorded in the coating and in the pattern during the filling of a horizontally oriented pattern, (using a low permeability coating).



Figure 5. Real-time X-ray image of the filling of a Lost Foam plate pattern with a top-gated running system.

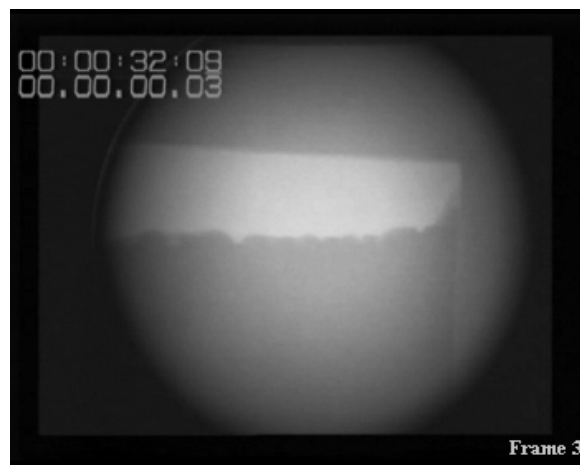


Figure 6. Real-time X-ray image of the filling of a Lost Foam plate pattern with a bottom-gated running system.

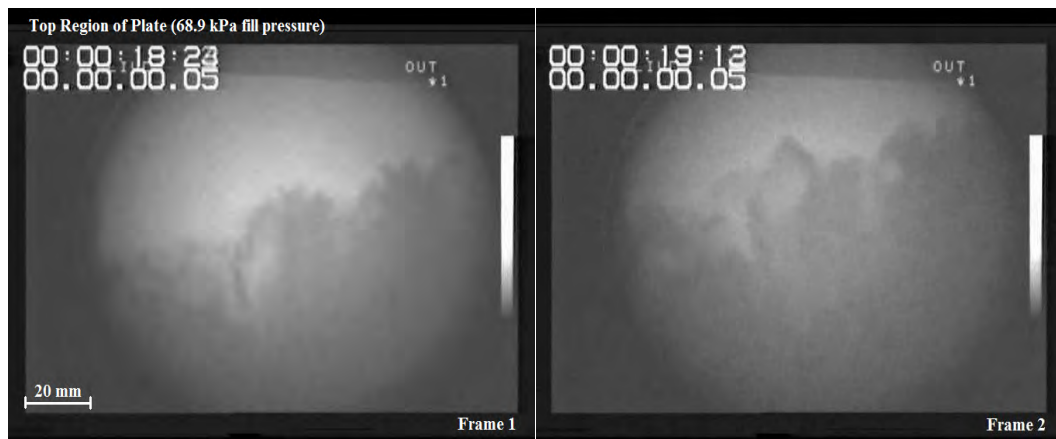


Figure 7. Real-time X-ray image of the filling of a Lost Foam plate pattern at a velocity of about  $24 \text{ mm.s}^{-1}$ .



Figure 8. Real-time X-ray image of the filling of a Lost Foam plate pattern at a velocity of about  $13 \text{ mm.s}^{-1}$ .

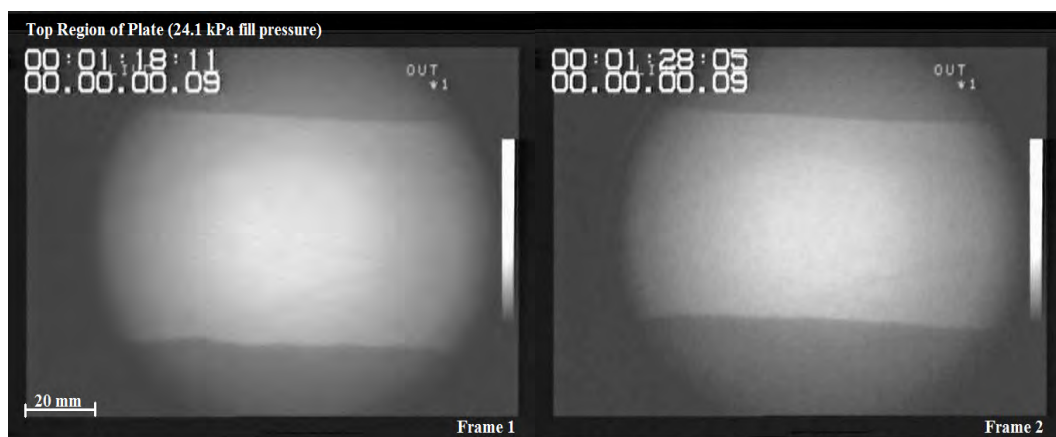


Figure 9. Real-time X-ray image of the filling of a Lost Foam plate pattern at a velocity of about  $5 \text{ mm.s}^{-1}$ .

## LIST OF REFERENCES

1. Shroyer, H.F., *Cavityless Casting Mold and Method of Making Same*. 1958: U.S. Patent No. 2,830,343.
2. Smith, T.R., *Method of Casting*. 1964: U.S. Patent No. 3,157,924.
3. Butler, R.D. and R.J. Pope, *Some Factors Involved in Full Mould Casting with Unbonded Sand Moulds*. The British Foundryman, 1964. **April**: p. 178-191.
4. Hess, D.R., B. Durham, C.W. Ramsay and D.R. Askeland, *Observations on the Effect of Pattern and Coating Properties on Metal Flow and Defect Formation in Aluminum Lost Foam Castings*. Transactions of the American Foundrymen's Society, 2002. **110**: p. 1435-1448.
5. Gorla, C.A., G. Serramoglia, G. Caironi and G. Tosi, *Coating Permeability: A Critical Parameter of the Evaporative Pattern Process*. Transactions of the American Foundrymen's Society, 1986. **94**: p. 589-600.
6. Sun, Y., H.L. Tsai, and D.R. Askeland, *Investigation of Wetting and Wicking Properties of Refractory Coating in the EPC Process*. Transactions of the American Foundrymen's Society, 1992. **100**: p. 297-308.
7. Gowariker, V.R., N.V. Viswanathan and J. Sreedhar, *Polymer Science*, New York: Halstead Press (John Wiley & Sons), 1986.
8. Shivkumar, S., X. Yao, and M. Makhlof, *Polymer-Melt Interactions during Casting Formation in the Lost Foam Process*. Scripta Metallurgica et Materialia, 1995. **33**: p. 39-46.
9. Cai, M., J. Siak, B.R. Powell, G. Nouaime and S.J. Swarin, *Physical and Chemical Analysis of the Thermal Degradation Products of Expanded Polystyrene Patterns with Short Thermal Exposures*. Transactions of the American Foundrymen's Society, 2002. **110**: p. 1463-1481.
10. Kannan, P., J.J. Biernacki and D.P. Visco Jr., *A Review of Physical and Kinetic Models of Thermal Degradation of Expanded Polystyrene Foam and their Application to the Lost Foam Casting Process*. Journal of Analytical and Applied Pyrolysis, 2006. **78**: p. 162-171.
11. Shivkumar, S. and B. Gallois, *Physico-Chemical Aspects of the Full Mold Casting of Aluminum Alloys, Part 1: The Degradation of Polystyrene*. Transactions of the American Foundrymen's Society, 1987. **95**: p. 791-800.
12. Mehta, S., S. Biederman and S. Shivkumar, *Thermal Degradation of Foamed Polystyrene*. Journal of Materials Science, 1995. **30**: p. 2944-2949.

13. Madorsky, S.L., *Thermal Degradation of Organic Polymers*. New York: Interscience Publishers, 1964.
14. Yang, J., T. Huang and J. Fu, *Study of Gas Pressure in EPC (LFC) Molds*. Transactions of the American Foundrymen's Society, 1998. **106**: p. 21-26.
15. Zhao, Q., T.W. Gustafson, M. Hoover and M.C. Flemings, *Folds Formation and Prevention in the Lost Foam Aluminium Process*. Transactions of the American Foundrymen's Society, 2004. **112**: p. 1145-1159.
16. Molibog, T. and H. Littleton, *Experimental Simulation of Pattern Degradation in Lost Foam*. Transactions of the American Foundrymen's Society, 2001. **109**: p. 1523-1554.
17. Barone, M.R. and D.A. Caulk, *A Foam Ablation Model for Lost Foam Casting of Aluminum*. International Journal of Heat and Mass Transfer, 2005. **48**: p. 4132-4149.
18. Caulk, D.A., *A Foam Melting Model for Lost Foam Casting of Aluminum*. International Journal of Heat and Mass Transfer, 2006. **49**: p. 2124-2136.
19. Caulk, D.A., *A Pattern Decomposition Model for Lost Foam Casting of Aluminum: Part III-Collapse Mode*. Transactions of the American Foundrymen's Society, 2007. **115**: p. 833-844.
20. Caulk, D.A., *A Pattern Decomposition Model for Lost Foam Casting of Aluminum: Part IV-Engulf Mode*. Transactions of the American Foundrymen's Society, 2007. **115**: p. 845-860.
21. Sun, W.L., H.E. Littleton and C.E. Bates, *Real-Time X-Ray Investigations on Lost Foam Mold Filling*. Transactions of the American Foundrymen's Society, 2002. **110**: p. 1347-1356.
22. Sun, W., H.E. Littleton and C.E. Bates, *Effects of Foam Pattern Fusion on the Quality of Lost Foam Aluminum Castings: Real Time and Digital X-ray Observations*. Transactions of the American Foundrymen's Society, 2003. **111**: p. 1245-1253.
23. Littleton, H.E., T. Molibog and W. Sun, *The Role of Pattern Permeability in Lost Foam Casting*. Transactions of the American Foundrymen's Society, 2003. **111**: p. 1265-1277.
24. Rossacci, J. and S. Shivkumar, *Influence of EPS Bead Fusion on Pattern Degradation and Casting Formation in the Lost Foam Process*. Journal of Materials Science, 2003. **38**: p. 2321-2330.
25. Wang, C., C.W. Ramsay and D.R. Askeland, *Processing Variable Significance on Filling Thin Plates in the LFC Process - The Staggered, Nested Factorial Experiment*. Transactions of the American Foundrymen's Society, 1997. **105**: p. 427-434.

26. Bex, T., *Coating Chemistry Key to FPC Consistency*. Modern Casting, 1989. **October**: p. 34-35.
27. Martinez, O.A., *A Supplier's Overview of Lost Foam Refractory Coatings*. Transactions of the American Foundrymen's Society, 1990. **98**: p. 241-244.
28. Liu, J., C.W. Ramsay, and D.R. Askeland, *A Study of Foam-Metal-Coating Interaction in the LFC Process*. Transactions of the American Foundrymen's Society, 1997. **105**: p. 419-425.
29. Walling, R.P. and J.A. Dantzig, *Mechanisms of Mold Filling in the EPC Process*. Transactions of the American Foundrymen's Society, 1994. **102**: p. 849-854.
30. Dieter, H.B. and A.J. Paoli, *Sand Without Binder for Making Full Mold Castings*. Transactions of the American Foundrymen's Society, 1967. **75**: p. 147-160.
31. Shivkumar, S., *Modelling of Temperature Losses in Liquid Metal during Casting Formation in Expendable Pattern Casting Process*. Materials Science and Technology, 1994. **10**: p. 986-992.
32. Warner, M.H., B.A. Miller, and H.E. Littleton, *Pattern Pyrolysis Defect Reduction in Lost Foam Castings*. Transactions of the American Foundrymen's Society, 1998. **106**: p. 777-785.
33. Rossacci, J. and S. Shivkumar, *Bead Fusion in Polystyrene Foams*. Journal of Materials Science, 2003. **38**: p. 201-206.
34. Bennett, S., T. Moody, A. Vrieze, M. Jackson, D.R. Askeland and C.W. Ramsay, *Pyrolysis Defects in Aluminum Lost Foam Castings*. Transactions of the American Foundrymen's Society, 2000. **108**: p. 795-803.
35. Pan, E.N. and G.L. Sheu, *The Filling Phenomena of Lost Foam Cast Irons and Aluminium Alloys*. Transactions of the American Foundrymen's Society, 2003. **111**: p. 1255-1263.
36. Fu, J., H.L. Tsai and D.R. Askeland, *Transport of Foam Decomposition Products into the Sand in the Lost Foam Casting Process*. Transactions of the American Foundrymen's Society, 1996. **104**: p. 263-270.
37. Tseng, C.H.E. and D.R. Askeland, *Thermal and Chemical Analysis of the Foam, Refractory Coating and Sand in the EPC Process*. Transactions of the American Foundrymen's Society, 1992. **100**: p. 509-518.
38. Zhao, Q., J.T. Burke and T.W. Gustafson, *Foam Removal Mechanism in Aluminum Lost Foam Casting*. Transactions of the American Foundrymen's Society, 2002. **110**: p. 1399-1414.

39. Cox, W.P. and R.I. Ballmann, *Calculation of the Apparent Viscosity of Polystyrene Melts*. Journal of Applied Polymer Science, 1960. **4**: p. 121.
40. Hill, M., A.E. Vrieze, T.L. Moody, C.W. Ramsay and D.R. Askeland, *Effect of Metal Velocity on Defect Formation in Al LFCs*. Transactions of the American Foundrymen's Society, 1998. **106**: p. 365-374.
41. Tschopp, M.A., Q.G. Wang and M.J. DeWyse, *Mechanisms of Misrun Formation in Aluminum Lost Foam Castings*. Transactions of the American Foundrymen's Society, 2002. **110**: p. 1371-1386.
42. Liu, J., C.W. Ramsay and D.R. Askeland, *Effects of Foam Density and Density Gradients on Metal Fill in the LFC Process*. Transactions of the American Foundrymen's Society, 1997. **105**: p. 435-442.
43. Monroe, R.W., *Expendable Pattern Casting*. Des Plaines: American Foundrymen's Society, 1992.
44. Hess, D.R., *Comparison of Aluminum Alloys and EPS Foams for Use in the Lost Foam Casting Process*. Transactions of the American Foundrymen's Society, 2004. **112**: p. 1161-1174.
45. Sands M. and S. Shivkumar, *Influence of Coating Thickness and Sand Fineness on Mold Filling in the Lost Foam Casting Process*. Journal of Materials Science, 2003. **38**: p. 667-673.
46. Littleton, H.E., B.A. Miller, D. Sheldon and C.E. Bates, *Lost Foam Casting - Process Control for Precision*. Transactions of the American Foundrymen's Society, 1996. **104**: p. 335-346.
47. Kocan, G.H., *Incorporating Permeability into Lost Foam Coating Controls*. Transactions of the American Foundrymen's Society, 1996. **104**: p. 565-569.
48. Zhao, Q., H. Wang, S. Biederman, D. Jason and J.S. Parish, *Lost Foam Casting Coating Characterization: Heat and Mass Transfer*. Transactions of the American Foundrymen's Society, 2005. **113**: p. 1013-1027.
49. Philipse, A.P. and H.L. Schram, *Non-Darcian Airflow through Ceramic Foams*. Journal of the American Ceramic Society, 1991. **74**: p. 728-732.
50. Massey, B.S., *Laminar Flow between Solid Boundaries*, in Mechanics of Fluids. London: Chapman & Hall, 1995.
51. Darcy, H., *Les Fontaines Publiques de la Ville de Dijon*. Paris: Victor Dalmont, 1856.
52. Liu, Y., S.I. Bakhtiyarov and R.A. Overfelt, *Numerical Modeling and Experimental Verification of Mold Filling and Evolved Gas Pressure in Lost Foam Casting Process*. Journal of Materials Science, 2002. **37**: p. 2997-3003.

53. Innocentini, M.D.M., V.R. Salvini, V.C. Pandolfelli and J.R. Coury, *Assessment of Forchheimer's Equation to Predict the Permeability of Ceramic Foams*. Journal of the American Ceramic Society, 1999. **82**: p. 1945-1948.
54. Davies, P., *The Role of the Pattern Coating in Lost Foam Casting of Aluminium*. Ph.D. Thesis, 2006, University of Birmingham, England.
55. Tan, L.S., R.A. Bambauer, T.A. DeLong, R.B. Dinwiddie and H. Wang, *The Effect of Thermal Conductivity on Metal Fill in Lost Foam Casting of Aluminum*. Paper presented at the 101<sup>st</sup> AFS Casting Congress, April 1997, Seattle, WA.
56. Molibog, T., R.B. Dinwiddie, W.D. Porter, H. Wang and H.E. Littleton, *Thermal Properties of Lost Foam Casting Coatings*. Transactions of the American Foundrymen's Society, 2000. **108**: p. 471-478.
57. Hill, M.W., M. Lawrence, C.W. Ramsay and D.R. Askeland, *Influence of Gating and Other Processing Parameters on Mold Filling in the LFC Process*. Transactions of the American Foundrymen's Society, 1997. **105**: p. 443-450.
58. Liu, X., C.W. Ramsay and D.R. Askeland, *A Study on Mold Filling Control Mechanisms in the Expendable Pattern Casting Process*. Transactions of the American Foundrymen's Society, 1994. **102**: p. 903-914.
59. Lawrence, M.D., C.W. Ramsay and D.R. Askeland, *Some Observations and Principles for Gating of Lost Foam Castings*. Transactions of the American Foundrymen's Society, 1998. **106**: p. 349-356.
60. Sun, Y., H.L. Tsai and D.R. Askeland, *Effects of Silicon Content, Coating Materials and Gating Design on Casting Defects in the Aluminum Lost Foam Process*. Transactions of the American Foundrymen's Society, 1996. **104**: p. 271-279.
61. Vinarcik, E.J., *Thermo Gravimetric Analysis of Expendable Pattern Casting Adhesives*. Transactions of the American Foundrymen's Society, 1997. **105**: p. 355-357.
62. Bates, C.E., J. Griffin and H.E. Littleton, *Expandable Pattern Casting, Process Manual*. Des Plaines, American Foundrymen's Society, 1994.
63. Sun, W. and H.E. Littleton, *Real-Time X-Ray Visualization of Effects of Glue Joints on Metal Filling and Defect Formation of Lost Foam Castings*. Transactions of the American Foundrymen's Society, 2005. **113**: p. 1099-1107.
64. Shivkumar, S., *Casting Characteristics of Aluminum Alloys in the EPC*. Transactions of the American Foundrymen's Society, 1993. **101**: p. 513-518.
65. Buesch, A., C. Carney, T. Moody, C. Wang, C.W. Ramsay and D.R. Askeland, *Influence of Sand Temperature on Formation of Pyrolysis Defects in Aluminum Lost*

- Foam Castings*. Transactions of the American Foundrymen's Society, 2000. **108**: p. 615-621.
66. Fu, J., H.-L. Tsai and D.R. Askeland, *Mold Filling in Thin-Section Castings Produced by the EPC Process*. Transactions of the American Foundrymen's Society, 1995. **103**: p. 817-828.
  67. Bennett, S., C.W. Ramsay and D.R. Askeland., *Temperature Gradients during Fill and Solidification of Al LFCs*. Transactions of the American Foundrymen's Society, 1998. **106**: p. 357-363.
  68. Bennett, S., M. Tschopp, A. Vrieze, E. Zelkovich, C.W. Ramsay and D.R. Askeland, *Observations on the Effect of Gating Design on Metal Flow and Defect Formation in Aluminum Lost Foam Castings: Part I*. Paper presented at the 105<sup>th</sup> AFS Casting Congress, April 2001, Dallas, TX.
  69. Tschopp, M., C.W. Ramsay and D.R. Askeland, *Mechanisms of Formation of Pyrolysis Defects in Aluminum Lost Foam Castings*. Transactions of the American Foundrymen's Society, 2000. **108**: p. 609-614.
  70. Shin, S.R., Z.H. Lee, G.S. Cho and K.W. Lee, *Hydrogen gas pick-up mechanism of Al-alloy melt during Lost Foam Casting*. Journal of Materials Science, 2004. **39**: p. 1563-1569.
  71. Chintalapati, P.P., J.A. Griffin and R.D. Griffin, *Improved Mechanical Properties of Lost Foam Cast A356 and A319 Aluminum Solidified under Pressure*. Transactions of the American Foundrymen's Society, 2007. **115**: p. 881-898.
  72. Bakhtiyarov S.I., R. Overfelt and A. Alagarsamy, *Advances in Counter Gravity Lost Foam Casting Process*. Transactions of the American Foundrymen's Society, 2000. **108**: p. 137-145.
  73. Fan Z-T., S. Ji, *Low Pressure Lost Foam Process for Casting Magnesium Alloys*. Materials Science and Technology, 2005, **21**: p. 727-734.
  74. Penumadu, D., M. Kant, R. Michaels and E. Lichner, *Lost Foam Casting Using Electromagnetic Pump Avoiding Downsprue With Feedback Control*. Transactions of the American Foundrymen's Society, 2005. **113**: p. 1047-1057.
  75. Chen, Q. and C. Ravindran, *Effects of Hydrogen Content and Solidification Time on Porosity Formation in Lost Foam Casting of A356 Alloy – A Semi-Empirical Model*. Paper presented at the 104<sup>th</sup> AFS Casting Congress, April 2000, Pittsburgh, PA.
  76. Khan, S., C. Ravindran, D. Naylor and D. Sharma, *Measurement of Interfacial Heat Transfer Coefficient in LFC of A356 Al Alloy*. Transactions of the American Foundrymen's Society, 2000. **108**: p. 445-452.

77. Khan, S., D. Naylor and C. Ravindran, *Effect of Casting Section Thickness and Coating Thickness on the Interfacial Heat Transfer Coefficient in Lost Foam Casting*. Transactions of the American Foundrymen's Society, 2001. **109**: p. 1495-1501.
78. Zhao, Q., S. Biederman and M. Flemings, *The Effects of Coating on Heat Transfer in Lost Foam Aluminum Process*. Transactions of the American Foundrymen's Society, 2006. **114**: p. 899-912.
79. Moore, A.R., T.C. Pederson and A.K. Sachdev, *New Pattern Coating for Improved Metal Fill in Low-Pressure Lost Foam Aluminum Castings*. Transactions of the American Foundrymen's Society, 2006. **114**: p. 875-886.
80. Shivkumar, S., L. Wang and D. Apelian, *The Lost-Foam Casting of Aluminum Alloy Components*. Journal of the Minerals, Metals and Materials Society, 1990. **November**: p. 38-44.
81. Hess, D.R., B. Durham, C.W. Ramsay and D.R. Askeland, *Observations on the Effect of Gating Design on Metal Flow and Defect Formation in Aluminum Lost Foam Castings : Part II*. Transactions of the American Foundrymen's Society, 2001. **109**: p. 19-34.
82. Batchelor, G.K., *An Introduction to Fluid Dynamics*, 1<sup>st</sup> ed. New York: Cambridge University Press, 2000.
83. Sands, M. and S. Shivkumar, *EPS Bead Fusion Effects on Fold Defect Formation in Lost Foam Casting of Aluminum Alloys*. Journal of Materials Science, 2006. **41**: p. 2373-2379.
84. Pedersen, T.C., *New Brominated Additives for Expanded Polystyrene Patterns to Reduce Fold Defects in Lost Foam Aluminum Castings*. Transactions of the American Foundrymen's Society, 2006. **114**: p. 887-898.
85. Jagoo, S., C. Ravindran and D. Nolan, *Minimizing Fold Defects in Aluminum Alloy A356 Lost Foam Casting*. Transactions of the American Foundrymen's Society, 2007. **115**: p. 899-910.
86. Nyahumwa, C., N.R. Green and J. Campbell, *The Concept of the Fatigue Potential of Cast Alloys*. Journal of the Mechanical Behaviour of Materials, 1998. **9**: p. 227-235.
87. Campbell, J., *Entrainment Defects*. Materials Science and Technology, 2006. **22**: p. 127-145.
88. Campbell, J., *Castings*. 2<sup>nd</sup> ed. Oxford: Butterworth-Heinemann, 2003.
89. Green, N. and J. Campbell, *Influence of Oxide Film Filling Defects on the Strength of Al-7Si-Mg Alloy Castings*. Transactions of the American Foundrymen's Society, 1994. **102**: p. 341-347.

90. Weibull, W., *Statistical Distribution Function of Wide Applicability*. Journal of Applied Mechanics, 1951. **18**: p. 293-297.
91. Nyahumwa, C., N.R. Green and J. Campbell, *Effect of Mold-Filling Turbulence on Fatigue Properties of Cast Aluminium Alloys*, Transactions of the American Foundrymen's Society, 1998. **106**: p. 215-223.
92. Ammar, H.R., A.M. Samuel and F.H. Samuel, *Effect of Casting Imperfections on the Fatigue Life of 319-F and A356-T6 Al-Si Casting Alloys*. Materials Science & Engineering A, 2008. **473**: p. 65-75.
93. Kang, B., Y. Kim, K. Kim, G. Cho, K. Choe and K. Lee, *Density and Mechanical Properties of Aluminum Lost Foam Casting by Pressurisation During Solidification*. Journal of Materials Science and Technology, 2007. **23**: p. 828-832.
94. Edelson, B.I. and W.M. Baldwin Jr., *The Effect of Second Phases on the Mechanical Properties of Alloys*. Transactions of the American Society for Metals, 1962. **55**: p. 230-250.
95. Hedjazi, D., G.H.J. Bennett and V. Kondik, *Effects of Non-metallic Inclusions on the Tensile Characteristics of Al4.5Cu1.5Mg Aluminium Alloy*. Metals Technology, 1976. **December**: p. 537-541.
96. Wang, Q.G., P.N. Crepeau, D. Gloria and S. Valtierra, *Advances in Aluminium Casting Technology*. 2<sup>nd</sup> International Aluminum Casting Technology Symposium, October 2002, Columbus, OH.
97. Smith, R.A. and P.S.A. Wilkins, *Low Pressure Sand Casting: Current Experience with a New Process*. Transactions of the American Foundrymen's Society, 1986. **94**: p. 785-792.
98. Lavington, M.H., *The Cosworth Process – A New Concept in Aluminium Alloy Casting Production*. Metals and Materials, 1986. **November**: p. 713-719.
99. Bast, J., *Lost Foam Process with Low Pressure Casting*. Foundry Trade Journal, 1997. **November**: p. 446-448.
100. Bakhtiyarov, S.I., R.A. Overfelt and A. Alagarsamy, *Measurements of Decomposed EPS Gases Pressure and Molten Metal-Polymeric Foam Interface Velocity during Counter-Gravity Lost Foam Casting*. Transactions of the American Foundrymen's Society, 2001. **109**: p. 1439-1453.
101. Hirt, C.W. and M.R. Barkhudarov, *Modeling the Lost Foam Process with Defect Prediction-Progress Report: Lost-Foam Model Extensions*, Wicking. Flow Science Inc. Technical Notes TN 45-1, 1999.

102. Dinsdale, A.T. and P.N. Queded, *The Viscosity of Aluminium and Its Alloys – A Review of Data and Models*. Journal of Materials Science, 2004. **39**: p. 7221-7228.
103. Nichetti, D. and I. Manas-Zloczower, *Viscosity Model for Polydisperse Polymer Melts*, Journal of Rheology, 1998. **42**: p. 951-969.
104. Mackay, M.E. and D.J. Henson, *The Effect of Molecular Mass and Temperature on the Slip of Polystyrene Melts at Low Stress Levels*. Journal of Rheology, 1998. **42**: p. 1505-1517.
105. Rayleigh, Lord, *Investigation of the Character of the Equilibrium of an Incompressible Heavy Fluid of Variable Density*. Proceedings of the London Mathematical Society, 1883. **14**: p. 170-177.
106. Taylor, G.I., *The Instability of Liquid Surfaces when Accelerated in a Direction Perpendicular to their Planes*. Proceedings of the Royal Society of London, 1950. **A201**: p. 192-196.
107. Bird, R.B., W.E. Stewart and E.N. Lightfoot, *Transport Phenomena*. 2<sup>nd</sup> ed. New York: John Wiley & Sons, 2002.
108. Joseph, D.D., *Fluid Dynamics of Two Miscible Liquids with Diffusion and Gradient Stresses*. European Journal of Mechanics. B/Fluids, 1990. **9**: p. 565-596.
109. Cook, A.W. and P.E. Dimotakis, *Transition Stages of Rayleigh-Taylor Instability between Miscible Fluids*. Journal of Fluid Mechanics, 2001. **443**: p. 69-99.
110. Chandrasekhar, S., *The Character of the Equilibrium of an Incompressible Heavy Viscous Fluid of Variable Density*. Proceedings of the Cambridge Philosophical Society, 1955. **51**: p. 161-178.
111. Duff, R.E., F.H. Harlow and C.W. Hirt, *Effects of Diffusion on Interface Instability between Gases*. Physics of Fluids, 1962. **5**: p. 417-425.
112. Saffman, P.G. and G.I. Taylor, *The Penetration of a Fluid into a Porous Medium or Hele-Shaw Cell Containing a More Viscous Liquid*. Proceedings of the Royal Society, 1958. **245**: p. 312-329.
113. Ladtkow, T., *Fluorescent Fingers produced using Saffman-Taylor Instability in a Hele-Shaw Cell*, Course in Flow Visualisation, University of Colorado, USA, 2006.
114. Kelvin, Lord, *Hydrokinetic Solutions and Observations*. Philosophical Magazine, 1871. **42**: p. 362-377.
115. Helmholtz, H.L.F. von, *Über discontinuierliche Flüssigkeitsbewegungen [On the discontinuous movement of fluids]*. Monatsberichte der Königlich Preussische Akademie der Wissenschaften zu Berlin [Monthly Reports of the Royal Prussian Academy of Philosophy in Berlin], 1868. **23**: p. 215-228.

116. Thorpe, S.A., *Experiments on the Instability of Stratified Shear Flows: miscible fluids*. Journal of Fluid Mechanics, 1971. **46**: p. 299-319.
117. Cushman-Roisin B., *Kelvin-Helmholtz Instability as a Boundary-value Problem*. Environmental Fluid Mechanics, 2005. **5**: p. 507-525.
118. École Nationale Supérieure d'Electrotechnique, d'Electronique, d'Informatique, d'Hydraulique et des Télécommunications, *Kelvin-Helmholtz Instability* [online]. Available from: [http://hmf.enseciht.fr/travaux/optmfn/hi/01pa/hyb72/kh/kh\\_theo.htm#part1](http://hmf.enseciht.fr/travaux/optmfn/hi/01pa/hyb72/kh/kh_theo.htm#part1). [accessed 29th October 2007].
119. Newton, Sir. I., *Philosophiae Naturalis Principia Mathematica*. New York: Prometheus Books, 1995.
120. Joshi, J., R. Lehman and T. Nosker, *Selected Physical Characteristics of Polystyrene/High Density Polyethylene Composites Prepared from Virgin and Recycled Materials*. Journal of Applied Polymer Science, 2006. **99**: p. 2044 -2051.
121. Kavassalis T.A. and J. Noolandi, *New View of Entanglements in Dense Polymer Systems*. Physical Review Letters, 1987. **59**: p. 2674-2677.
122. Osswald, T.A. and G. Menges, *Materials Science of Polymers for Engineers*. New York: Hanser Gardner Publications, Inc., 2003.
123. Anukulthanakorn, K., S. Limtrakul and T. Vatanatham, *Commercial Polystyrene Melt Behaviour in Rod Capillary Die Extrusion*. Technical Report, Department of Chemical Engineering, Kasetsart University, Bangkok, Thailand, 2005.
124. Williams, M.L., R.F. Landel and J.D. Ferry, *The Temperature Dependence of Relaxation Mechanisms in Amorphous Polymers and Other Glass-forming Liquids*. Journal of the American Chemical Society, 1955. **77**: p. 3701-3707.
125. Diduch, C., R. Dubay and W.G. Li, *Temperature Control of Injection Molding Incorporating Zone Interactions and Back Pressure - Part I: Modeling and Simulation*. Polymer Engineering and Science Journal, 2004. **44**: p. 2308 -2317.
126. Merz, E.H. and R.E. Colwell, *A High Shear Rate Capillary Rheometer for Polymer Melts*. ASTM Bulletin No. 232, Sept. 1958.
127. Lomellini, P., *Williams-Landel-Ferry versus Arrhenius Behaviour: Polystyrene Melt Viscoelasticity Revised*. Polymer, 1992. **33**: p. 4983-4989.
128. Wilkes, C.E., J.W. Summers and C.A. Daniels, *PVC Handbook*. 1<sup>st</sup> ed. Munich: Hanser Gardner, 2005.
129. Berry, G.C. and T.G. Fox, *The Viscosity of Polymers and Their Concentrated Solutions*. Advances in Polymer Science, 1968. **5**: p. 261-357.

130. Colby, R.H., L.J. Fetters and W.W. Graessley, *Melt Viscosity-Molecular Weight Relationship for Linear Polymers*. Macromolecules, 1987. **20**: p. 2226-2237.
131. Fox, T.G. and P.J. Flory, *The Glass Temperature and Related Properties of Polystyrene*. Journal of Polymer Science, 1954. **14**: p. 315-319.
132. Gennes de, P.G., *Reptation of a Polymer Chain in the Presence of Fixed Obstacles*. Journal of Chemical Physics, 1971. **55**: p. 572-579.
133. Curtiss, C.F. and R.B. Bird, *A Kinetic Theory for Polymer Melts, Parts I and II*. Journal of Chemical Physics, 1981. **74**: p. 2016-2033.
134. Bernard, D.A. and J. Noolandi, *Zero-Shear Viscosity Exponent and Polydispersity Effects*. Macromolecules, 1982. **15**: p. 1553-1559.
135. Brown, J.R., *Foseco Ferrous Foundryman's Handbook*. Oxford: Butterworth-Heinemann, 2000.
136. Moll, N. and D. Johnson, *Advanced Moldable Foam Eliminates Carbon Defects in Evaporative Pattern Castings*. Modern Casting, 1987. **June**: p. 37-40.
137. Mehta, S. and S. Shivkumar, *Thermal Degradation of Foamed Polymethyl Methacrylate in the Expendable Pattern Casting Process*. Journal of Materials Engineering and Performance, 1994. **03**: p. 329-333.
138. Dufton, P., *Flame Retardants for Plastics – Market Report*. Rapra Technology Limited, Shrewsbury, 2003.
139. Bertini, F., G. Audisio and J. Kiji, *Thermal Behavior and Degradation Mechanism of Brominated Polystyrenes*. Journal of Analytical and Applied Pyrolysis, 1995. **33**: p. 213-230.
140. Sonnenberg, F., *Recent Innovations with EPS Lost Foam Beads*. Transactions of the American Foundrymen's Society, 2003. **111**: p. 1213-1229.
141. Molibog, T.V. and H. Littleton, *Degradation of Expanded Polystyrene Patterns*. Transactions of the American Foundrymen's Society, 2002. **110**: p. 1483 – 1496.
142. Sonnenberg, F., K.M. Taristo and T.V.J. Johansson, *Treatment for Reducing Residual Carbon in the Lost Foam Process*. 2001: U.S. Patent No. 6,303,664.
143. Hess, D.R., D.R. Askeland and C.W. Ramsay, *Influence of Bead Chemistry on Metal Velocity and Defect Formation in Aluminum Lost Foam Castings*. Transactions of the American Foundrymen's Society, 2003. **111**: p. 1279-1292.
144. Khodai, M. and N. Parvin *Pressure Measurement and Some Observation in Lost Foam Casting*. Journal of Materials Processing Technology, 2008. **206**: p. 1-6.

145. Yao, X. and S. Shivkumar, *Mould Filling Characteristics in Lost Foam Casting Process*. Materials Science and Technology, 1997. **13**: p. 841-846.
146. Fry, S.L., *Preliminary Investigation of Metal Pouring by Cine Radiography*. Proceedings of the Institute of British Foundrymen, 1944. **39**: p. 44-54.
147. Sun, W. and H.E. Littleton, *Real-Time X-ray Study on Formation of Lustrous Carbon in Lost Foam Iron Castings*. Transactions of the American Foundrymen's Society, 2006. **114**: p. 1001-1008.
148. Green, N.R. and J. Campbell, *Statistical Distributions of Fracture Strengths of Cast Al-7Si-Mg Alloy*. Materials Science and Engineering A, 1993. **173**: p. 261-266.
149. Khalili, A. and K. Kromp, *Statistical Properties of Weibull Estimators*. Journal of Materials Science, 1991. **26**: p. 6741-6752.
150. Rezvani, M., X. Yang and J. Campbell, *Effect of Ingate Design on Strength and Reliability of Al Castings*. Transactions of the American Foundrymen's Society, 1999, **107**: p. 181 – 188.
151. British Standards Institution, *Tensile Testing of Metallic Materials. Method of Test at Ambient Temperature*, London: BSI, 2001. (BS EN 10002-1).
152. Sands, S. and S. Shivkumar, *EPS Molecular Weight and Foam Density Effects in the Lost Foam Process*. Journal of Materials Science, 2003. **38**: p. 2233-2239.
153. Roquette UK Limited, *ROCLYS C3078S Specification Sheet*, Reference No. E00-123A40, August 2005.
154. Sommer, K.-D and J. Poziemski, *Density, Thermal Expansion and Compressibility of Mercury*, Metrologia, 1993. **30**: p. 665-668.
155. Assael, M.J., K. Kakosimos, R.M. Banish, J. Brillo, I. Egry, R. Brooks, P.N. Qusted, K.C. Mills, A. Nagashima, Y. Sato and W.A. Wakeham, *Reference Data for the Density and Viscosity of Liquid Aluminium and Liquid Iron*. Journal of Physical and Chemical Reference Data, 2006. **35**: p. 285-300.
156. Beer, S.Z., *Liquid Metals – Chemistry and Physics*. New York: Marcel Dekker Inc., 1972.
157. Holland, F.A. and E.V. Zaretsky, *Investigation of Weibull Statistics in Fracture Analysis of Cast Aluminum*. Failure Prevention and Reliability Conference, September 1989, Montreal, Canada.
158. Carter, C.B. and M.G. Norton, *Ceramic Materials – Science and Engineering*. New York: Springer Science + Business Media, 2007.

159. Kaufmann, J.G. and E.L. Rooy, *Aluminum Alloy Castings – Properties, Processes and Applications*. Ohio: ASM International, 2004.
160. Gardner, P., R. Lehrle and D. Turner, *Polymer Degradation Modified by Blending with Polymers Chosen on the Basis of Their  $\Phi$ -factors*, *Journal of Analytical and Applied Pyrolysis*, 1993. **25**: p. 11-24.
161. Tuteja, A., P.M. Duxbury and M.E. Mackay, *Multifunctional Nanocomposites with Reduced Viscosity*, *Macromolecules*, 2007. **40**: p. 9427-9434.